2011

GROWTH MECHANISMS OF COMPLEX ORGANICS IN THE GAS PHASE AND ON METAL NANOPARTICLES GENERATED BY A LASER VAPORIZATION PROCESS

Abdel Rahman Soliman
Virginia Commonwealth University

www.manaraa.com

College of Humanities and Sciences
Virginia Commonwealth University

This is to certify that the dissertation prepared by Abdel Rahman Ibrahim Mohamed Soliman entitled GROWTH MECHANISMS OF COMPLEX ORGANICS IN THE GAS PHASE AND ON METAL NANOPARTICLES GENERATED BY A LASER VAPORIZATION PROCESS has been approved by his or her committee as satisfactory completion of the thesis or dissertation requirement for the degree of Doctor of Philosophy

M. Samy El-Shall, Ph.D., Professor, Department of Chemistry, Research Adviser

James Terner, Ph.D., Professor, Department of Chemistry

Alenka Luzar, Ph.D., Professor, Department of Chemistry

Hani El-Kaderi, Ph.D., Assistant Professor, Department of Chemistry

Puru Jena, Ph.D., Professor, Department of Physics

Scott Gronert, Ph.D., Professor, Chair, Department of Chemistry

Fred Hawkridge, Ph.D., Dean, College of Humanities and Sciences

Dr. F. Douglas Boudinot, Dean of the School of Graduate Studies

May,11th, 2011

GROWTH MECHANISMS OF COMPLEX ORGANICS IN THE GAS PHASE AND
ON METAL NANOPARTICLES GAENERATED BY A LASER VAPORIZATION
PROCESS

A dissertation submitted in partial fulfillment of the requirements for the degree of doctor
of philosophy at Virginia Commonwealth University.

by

ABDEL RAHMAN IBRAHIM MOHAMED SOLIMAN
B.Sc., Cairo University, Egypt, 1997
M.Sc., Cairo University, Egypt, 2005

Director: M. SAMY EL-SHALL
PROFESSOR, DEPARTMENT OF CHEMSITRY

Virginia, Commonwealth University

Richmond, Virginia

May, 2011

Acknowledgement

I would like to thank my father, *Ibrahim M. Soliman*, and my mother for their support, help and guidance to be a better person. My bigger family of uncles and aunts. Also, my dedications to my father-in-low. The support and patience of my wife, *Manal*, I really appreciate your help and encouragement. I cannot forget my brother, *Mohamed*, for his encouragement and support to pursue the best level of education. I am very thankful to my advisor Prof. Samy El-Shall for all his patience, guidance and all the help he offered to get this work done. I am also grateful to Dr. Ridha Mabrouki and Dr. Paul Momoh, whom they guide my steps in understanding and learning new techniques and they always offered their help. I am thankful to Mrs. Enli Xie for training me on the IMS system. At last, I am thankful to all members of El-Shall's research group for the good time we spent together working in the lab, with special thanks to Ahmed Hamid.

Table of Contents

List of Tables

List of Figures

Abstract

GROWTH MECHANISMS OF COMPLEX ORGANICS IN THE GAS PHASE AND ON METAL NANOPARTICLES GENERATED BY A LASER VAPORIZATION PROCESS

By Abdel Rahman Ibrahim Mohamed Soliman, Ph.D.

A Dissertation submitted in partial fulfillment of the requirements for the degree of Doctor of Philosophy at Virginia Commonwealth University.

Virginia Commonwealth University, 2011

Major Director: M. Samy El-Shall
Professor, Department of Chemistry

In this dissertation, the ion mobility mass spectrometry technique is used to study the possible mechanisms of formation of polyaromatic hydrocarbons (PAHs) and polyaromatic nitrogen-containing hydrocarbons (PANHs) via the ion-molecule reactions of acetylene neutrals with different aromatic cations, in order to infer the possible mechanisms of formation of PAHs and PANHs in different environments such

as interstellar media under different ionizing conditions. Furthermore, this technique is used to probe structures, address the thermochemistry, and measure the kinetics of the product ions originated from these reactions.

Reactions of benzene radical cations with acetylene produce styrene and naphthalene-type cations at high temperatures. The second order rate constant of this reaction is found to be in the order of 10^{-14} cm^3.s^{-1} with a barrier of 3.5 kcal.mol^{-1}. Under low temperature regime, benzene radical cation acts as a catalyst to initiate the formation of higher complex hydrocarbons through the associative charge transfer to the acetylene clusters, $(C_2H_2)_n^+$, n= 6-10. Phenylium cation reactions with acetylene is found to be four orders of magnitudes faster than those of benzene radical cation, as predicted theoretically. In these systems the second addition of acetylene molecule is found to follow the Bittner-Howard mechanism. Phenylacetylene and styrene radical cations reactions with acetylene are also studied and the addition of one acetylene molecule to the radical cation is observed. The second order rate constant of the product ions is found to be in the order of 10^{-13} and 10^{-14} cm^3.s^{-1} for the phenylacetylene and styrene radical cations respectively.

Ion molecule reactions of pyridine cation, benzonitrile cation and pyrimidine radical cation with acetylene are studied. Formation of complex organics with fused nitrogen atom in an aromatic ring is reported. Condensation products of acetylene via the ion-molecule reactions are observed with pyridine cation of up to five acetylene molecules onto the pyridine cation at room temperature. Meanwhile, condensation of only two acetylene molecules is observed for benzonitrile cation and pyrimidine radical cation respectively. In the later case, these condensation reactions are observed with hydrogen abstraction. Ion

mobility measurements, collisional induced dissociation (CID) and ab initio calculations are combined to probe the possible structures of the reaction products.

Formation of PAHs over nanoparticle surfaces is carried out by studying polymerization of acetylene over Pd nanocatalyst and supported Pd nanocatalyst over MgO and CeO_2 prepared by the LVCC technique under different temperature conditions. C_8H_{10} species are formed at 400 ^{o}C. However, at 600 ^{o}C, production of $C_{16}H_{10}$ (pyrene isomer) is found to be the major catalytic product. Self polymerization of acetylene at different temperatures is presented as well.

Our results of the ion-molecule reactions, associative charge transfer (ACT) and catalytic polymerization over catalysts surfaces' of acetylene interacting with different aromatic and heterocyclic cations could explain the different possible pathways of formation of complex organics in different ionizing environments in carbon-rich interstellar media in space.

Chapter 1 Introduction

Polycyclic aromatic hydrocarbons, PAHs, are produced as a result of incomplete combustion processes, especially from anthropogenic activities. They are formed during pyrolysis and grow to high molecular weight complex organics.[1] The hydrocarbon flames are very complicated systems due to the many chemical and physical processes simultaneously involved in high temperature reactions. Many different carbon-containing molecular and supramolecular species have been identified during combustion processes. Among them are very short-lived species, such as radicals and ions.[2] The high level of PAHs in an urban atmosphere is considered as one of the pollution hazards affecting human health, typically in highly populated areas in the western hemisphere.[3] Understanding the mechanisms of PAHs formation is one of the hottest topics in the field of hydrocarbon fuel combustion and pyrolysis. The importance of investigating different reaction mechanisms of PAH formation is not only limited to the combustion and flame processes, but also for the determination of PAHs and complex organics found in vast areas in space as well. PAHs have been first identified in space and are believed to play an important role in the interstellar chemistry of solar planets and their moons.[4-12] Astronomical observations of Cassini-thermal infrared spectroscopy experiment result in the detection of methyl radical, acetylene, diacetylene, ethane and polar species such as carbon monoxide and hydrogen cyanide.[13-14] PAH vibrationally excited ions are believed to be responsible for the mid-infrared (mid-IR) interstellar emission features, known as

unidentified infrared bands (UIB).[8,15-17] These observations, accompanied by the discoveries of vast number of organic molecules in space, with special interest in acetylene[18] and benzene[9] which are critical building blocks for the formation of PAHs compounds, are of special interest in the interstellar reactions. The presence of these organic molecules under the cosmic UV irradiation in interstellar media supports the role of these molecules in the formation of large PAHs in space. In addition, the presence of interstellar dust, produced by the wind of evolving stars and supernovae that contributes to the chemistry and physics of interstellar medium, allows the formation of PAHs and polyaromatic nitrogen-containing hydrocarbons (PANHs) as well, and can act as a catalyst favoring several reactions to occur on their surfaces which facilitate the formation of complex organics in the interstellar medium.[19]

Acetylene is the fundamental building block of larger carbon-rich structures such as PAHs.[20] Observation of acetylene in space is of a great significance, as it would be the first step in producing larger PAHs through different reaction protocols such as ion-molecule reactions, self polymerization under high temperatures or via polymerization on the surface of dust grains.[15-16,21-29] Understanding the mechanisms of formation of PAHs starting from acetylene, the simplest organic molecule to be polymerized, has been the subject to many experimental and theoretical investigations.[18,23,30-49] One of the early experiments that has been conducted to study the ion-molecule reactions in high pressure acetylene was conducted by Derwish et al.[50] In that study, long chain ionic reactions have been recognized leading to the formation of high order ions. The ion-molecule reactions of acetylene were believed to proceed through the formation of a collision complex, which in

turn, lead to the formation of the major products $C_4H_2^+$, $C_4H_3^+$, $C_6H_4^+$ and $C_6H_5^+$. It was concluded that the $C_2H_2^+$ cation has two energetic states, the low energy state and the high energy one, leading to different reaction products, which were explained through the ionic mechanism. Interestingly, the formation of $C_6H_6^+$ radical cation from those reactions was in very low yield and was explained to be formed through the radical mechanism. To explain the role of acetylene in the formation of higher PAHs in ionizing environments such as space, the polymerization of ionized C_2H_2 into the C_6H_6 cation was the subject of many investigations in the last two decades, as benzene is considered the missing link between the linear molecules and aromatic ones.[15-16,21,23,27,51] Ion-molecule reactions of diacetylene radical cation with ethylene in a flowing after-glow triple quadrupole experiment has been reported as the first example of aromatic ring formation from the diacetylene radical cation.[52] It was believed that the acetylene trimer ion, $(C_2H_2)_3^+$, was considered as a stable benzene cation, $C_6H_6^+$,[53] provided the fragmentation patterns of both species are identical under the unimolecular decomposition of both ions produce $C_6H_5^+$, $C_6H_4^+$, $C_4H_4^+$, $C_4H_3^+$, $C_4H_2^+$ and $C_3H_3^+$ ions.[51] This belief was not supported by structure elucidation of the acetylene trimer ions, until the pioneering work done by Momoh et al.[54] in which the polymerization of ionized acetylene trimer ions, produced from acetylene clusters, into covalent bonded benzene cations had been reported. In that study, a combination of mass-selected ion mobility, collisional induced dissociation (CID), and theoretical calculations provided the most conclusive evidence for the formation of benzene ions from the largest ever reported ionized acetylene clusters. The distribution of the formed cluster ions revealed some features corresponding to the enhanced intensities

"magic numbers" for the $(C_2H_2)_n^+$ ions with n = 3, 6, 14, 33, 36, and 54-56. The strong magic number at n = 3 is consistent with the previously reported work.[40,51,55] Fragmentation study shows large stability of the ionized acetylene cluster $(C_2H_2)_n^+$, with n=3. The measurements of the mobility and the corresponding collision cross section of the $(C_2H_2)_3^+$ ions are similar to those reported for the benzene cation. These results were further confirmed by studying the hydration of acetylene trimer ions utilizing the drift tube technique. The binding energies of the addition of 1-7 water molecules to the acetylene trimer ion were identical to those corresponding to the hydration of benzene radical cation, providing further evidence for the formation of benzene radical cation form the ionized acetylene trimer.[56-57] Observation of benzene in Titan's atmosphere at high altitude (~1000 km) was reported by Waite et al.[9] and was considered as an astonishing result from the Cassini spacecraft flyby Titan. Also, the optically thick haze layer in the lower Titan's atmosphere is composed of higher precursors of PAHs such as naphthalene and anthracene. Laboratory simulations of Titan organic products suggested that the PAHs and PANHs are plausible ones.[58] The production of PAHs, specifically the fused-ring types such as naphthalene and anthracene, is thought to start with the addition of unsaturated molecules such as acetylene to a benzene ring. A sequence of additions can create larger ring structures. PAHs production on Titan would differ from PAH production on Earth because of the absence of oxygen, making the classical combustion mechanism of organic molecules an unlikely mechanism for PAHs and PANHs formation in Titan's atmosphere. The classic PAH formation mechanism is usually referred as the hydrogen abstraction acetylene addition, HACA, mechanism. In this mechanism, benzene ring loses a hydrogen

atom by some process and then has an unpaired electron. If acetylene or vinylacetylene is present, it will add to the carbon with the unpaired electron and close another ring onto the benzene ring to form naphthalene. Similar mechanisms will cause the production of higher-order PAHs.[4] This mechanism was predicted theoretically by Bauschlicher et al.[59] and Ricca et al.[60] to model the growth of second aromatic ring upon reactions of acetylene with benzene radical cation and the incorporation of nitrogen atom in the second ring upon reacting benzene radical cation with acetylene and hydrogen cyanide respectively. In both cases, the formation of the second aromatic ring was calculated to be feasible and exothermic reaction, following the HACA mechanism. However, in case of incorporating the nitrogen atom to model of the PANHs formation, the highest barrier was calculated to be 15 kcal.mol^{-1}, though the presence of the nitrogen atom facilitates the second ring formation. Generation of PAHs and their corresponding PANHs has been subject to numerous theoretical and experimental investigations.[2,61-72] Reactions of benzene radical cation with pyridine and of pyridine radical cation with benzene have been recently reported to afford a covalently bound adduct via a C–N bond forming process. This is quite interesting because it extends the synthetic growth mechanisms to N-containing species.[73] Growth of PAHs molecules via ion-molecule reactions of naphthyl cation with benzene have been reported.[74] Reactions of different ionic precursors with benzene have been reported as well.[75-76] Experimental and theoretical results showed that the ionic route is evident for the growth of polycyclic aromatic species by associations of small building blocks. Reactions of benzene radical cation with diacetylene have been reported by Bohme et al.[77] as a prototype example of the formation of naphthalene cation via ion-molecule

reactions from benzene radical cation. It was reported that the benzene radical cation does not react with acetylene under these conditions. Though, the reaction of benzene radical cation with acetylene is a barrierless and exothermic one as predicted by Bauschlicher's calculations.[59]

In this work, we are utilizing the selected ion-mobility mass spectrometry technique (IMS-MS), collisional induced dissociation studies (CID), thermochemical measurements and density functional theory (DFT) calculations in order to study the mechanisms of the complex organics formation and the chemistry in which a small molecule such as acetylene can react with ionized aromatics to form larger ring structures that may eventually help to understand the formation processes of complex organics and PAHs in different environments. The reactions with acetylene will include, *for the first time*, benzene radical cation, phenylium ion, phenylacetylene radical cation and styrene radical cations.

In the next section of the thesis, formation of PANHs from the reactions of pyridine cation, benzonitrile cation and pyrimidine radical cation with acetylene has also been studied. Chemical kinetics measurements and CID studies have been utilized to investigate the possible structures of the formed adducts from these reactions. Evidence of incorporation of nitrogen atom in a fused ring is provided, *for the first time*, as a result of reactions of acetylene with different heterocyclic precursor ions.

There are several reasons why gas phase and cluster studies can provide detailed information that cannot be obtained by conventional methods. In these systems, one can observe in real time the direct formation of product ions that represent early stages of

polymerization and formation of complex organics. Both kinetics and thermodynamic information on the individual reaction steps can be obtained. The kinetic studies will measure the reaction rate coefficients at different carrier gas pressures and temperatures. The temperature studies will determine the activation energies at higher temperatures or the negative temperature coefficients at lower temperatures depending on the nature of the reaction. In addition, structural information on the growing ions can provide detailed understanding of the formation mechanisms. In this study, structural determination of growing complex organics in clusters has been determined using the ion mobility measurements.

In the last part of the thesis, polymerization of acetylene catalyzed by Pd nanoparticles and Pd nanoparticles supported on MgO and CeO_2 is presented. Acetylene reactions on metal surfaces including the polymerization to form benzene and other cyclic organics are very important not only for the formation mechanisms of complex organics but also for reactions in flames, combustion processes and for the production of numerous chemicals used in industry. Understanding the polymerization processes of acetylene over metal nanoparticles will also help in probing the formed PAHs over dust grain in space. Thermal cyclization of three acetylene molecules was discovered in the late nineteenth century,[78] but this process requires very high temperatures.[79] This situation was changed dramatically by utilizing transition metals [80-82] and supported transition metals as catalysts.[83-84] Theoretical studies of the cyclotrimerization of acetylene on supported size selected Pd clusters showed that the production of benzene can be efficient at room temperature.[80,85] In those studies, the cyclotrimerization of acetylene on size selected Ag,

Rh and Pd atoms and also on metal clusters such as Pd_n, where n is varied between (1≤n≤30) atoms was investigated. DFT calculations support this activation of Pd atom, which is inserted in an F center on the MgO substrate. The interaction of the Pd atom and the F center is strong (3.4 eV). As a result, the Pd atom can be catalytically active towards the acetylene polymerization.[80]

Chapter 2 Experimental setup

The work done in this thesis was conducted on different instruments; the Quadrupole Mass-Selected Ion-Mobility Quadrupole Mass Spectrometer (QMS-IM-QMS) was used to study the formation mechanisms of PAHs and PANHs. A Tube Furnace Quadrupole Mass Spectrometer (TF-QMS) is used to study acetylene polymerization over various metal/metal supported nanocatalysts. Varian Saturn GC/MS/MS instrument was utilized to resolve and detect different polymerization products obtained by flowing purified acetylene over metal nanocatalysts.

2.1 Ion generation

2.1.1 Electron impact (EI) ionization

Neutral clusters are ionized by electron impact using an axial electron-impact ionizer coupled to the first quadrupole mass filter, which are then skimmed through a 3 mm conical skimmer. Details of the cluster formation process will be discussed in details later. The skimmed clusters form a molecular beam, which is then ionized by Extrel axial beam ionizer (model 04-11) coupled to the first quadrupole mass filter. Ionizing electrons are thermionically generated from a tungsten filament and are subsequently accelerated to the ion region where they interact with the neutral cluster beam. Quantum effects between the accelerated electrons and neutral clusters result in electron expulsion from a neutral cluster

9

molecule resulting in ionization of these neutral clusters.[86] Extra energy present in the cluster beam from the ionization process is dispersed by evaporation of cluster molecules. The ionized clusters are subsequently extracted and focused into the quadrupole mass filter by a series of focusing lenses. The electron energy in normal experiments varies between 40-100 eV.

2.2 Cluster formation

The clusters are generated by a supersonic adiabatic expansion, where the vapor of a chemical compound is mixed with a carrier gas, helium or argon, at high pressures of 30-80 psi, then expanded through an orifice to the low pressure cluster chamber ~ 10^{-7} Torr. This expansion is carried out by a pulsed nozzle valve *General Valve* (series 9) operating at a frequency range from 10 to 100 Hz. Orifice of the nozzle flange can vary from 0.1 to 0.5 mm. When the gas is expanded, the thermal energy of the gas in the high-pressure source is converted into a directed velocity V. If C_p and T_S are the heat capacity of the gas and the temperature of the source, respectively, the energy balance of an ideal gas of molecular weight m will be given by the following equation;

$$C_p T_S = C_p T_B + \frac{1}{2} m V^2 \tag{2.1}$$

where T_B is the beam temperature. It is clear that the temperature of the formed beam is lower than the initial temperature of the source, since $\frac{1}{2} m V^2 \geq 0$. This cooling resulting from the adiabatic expansion promotes the formation of clusters.[87]

2.3 Quadrupole Mass Selected-Ion Mobility Spectrometry-Quadrupole Mass spectrometry (QMS-IMS-QMS)

The quadrupole mass selected-ion mobility spectrometry-quadrupole mass spectrometry system composed of four stainless steel chambers, shown in Figure 1. The first chamber is the neutral cluster source and is pumped by a Varian VHS-6 diffusion pump with a pumping speed of 3000 L/s (He) and backed by an Edwards E2M28 rotary vacuum pump. A typical operating pressure in this chamber is $1\text{-}5 \times 10^{-5}$ Torr. The second chamber is separated from the first one by a 3 mm conical skimmer. This chamber houses the electron-impact (EI) ionizer (Extrel model 041-11, tungsten filament) and the first quadrupole mass filter assembly (3/8" $\times$ 7.88", 1-4000 amu). It is pumped by an Edwards Diffstak 160/700 M diffusion pump with a pumping speed of 1300 L/s (H_2). A typical working pressure of $1\text{-}2 \times 10^{-6}$ Torr is maintained during the experiment. The third chamber houses two sets of ions focusing/transport lenses and the drift/reaction cell and is pumped by an Edwards standard Diffstak 250/2000P diffusion pump with a speed of 3000 L/s in H_2. Edwards E2M40 two stages vacuum pump is used to back the diffusion pump. The pressure in this chamber depends mainly on two factors: the size of the orifice of the entrance and exit plates of the drift cell, 1 mm orifice, and the pressure of the gas inside the drift cell 1-5 Torr, which is typically around 10^{-5} Torr. The fourth chamber houses the second quadrupole mass spectrometry assembly and the detector. This chamber has a cylindrical shape, and it is pumped by an Edwards standard Diffstak 150/700 M diffusion pump with a speed of 1300 L/s in H_2 where the pressure is maintained at $5\text{-}9 \times 10^{-7}$. The second and the fourth chambers are connected to the same foreline, and they are backed by an Edwards E2M40

two stage rotary vacuum pump. The pressure in all chambers is monitored by ion gauges (Scientific Instrument Services ion gauge tube 3/4' Pyrex), and the foreline pressure is also monitored by a thermocouple gauge tube (Edwards, type ATC-M D 355 13 000).

The axial electron impact ionizer equipped with the quadrupole mass filter is used to ionize the neutral clusters formed via supersonic adiabatic expansion. Electron energies used in the ionization process range from 40-100 eV. These ionized clusters are focused to the quadrupole mass filter through set of focusing lenses that act as a one-way gate which direct the ions to go through the quadrupole entrance lens without allowing them to return back to the ionization region. Following the ionization step, mass selection is carried out using the quadrupole mass filter, which separates the ions according to their mass to charge ratios, for further studies/reactions of the ion(s) of interest. The quadrupole mass filter can be operated on either mass selection mode (RF-DC) or on RF-only modes of operation. In the first case, mass selection mode (RF-DC), the quad will allow only the selected ion to pass through its poles and rejecting any other formed ions depending on the mass to charge ratio of the selected ion. However, on the RF-only mode a window of mass to charge ratio ions is allowed to be transmitted in this case. The quadrupole housing is floated at ±100 V to either accelerate or decelerate the mass selected ions travelling through the quad poles for better resolution and handling of fast ions. Exiting ions are guided and transported to the drift cell entrance through three sets of Einzel lenses as shown in Figure 2. Two sets of steering lenses are placed after the focusing lenses, these sets are used to steer the ion beam horizontally and vertically, so the intensity of the ion signal entering the drift cell will be at its maximum. These two steering lenses are made of two halves of nickel plates, one half of

each lens is directly connected to the last set of Einzel lenses (Einzel lens # 3), while the other half is connected to an external power supply which is biased as well to the Einzel lens #3. The vertical steering lens is also acting as an ion gate to chop the ion beam into 10-40 µs ion pulses entering the drift cell. The gate is open when the two halves of the vertical steering lenses have the same voltage applied to them (-240 V in our case), but the gate is closed when the applied voltages on each half has the same value with opposite sign (-240V and +240V); this will cause the ions to be deflected under these conditions. The drift cell was designed by P. Kemper [88] and it is composed of two main parts, the cell body and the end cap. The body has the dimensions of (3.5" × 3.5" × 2.14"), while the end cap has the dimensions of (3.5" × 3.5" × 0.40") and they are made of oxygen free high conductivity copper alloy (Alloy 10100 OFHC). The drift cell body is separated from the end cap by a ceramic ring (2.34" OD, 1.97" ID and 0.40" width). The entrance plate is made of stainless steel (SS) with an orifice of 0.254 mm and held inside by a copper retainer. Two lenses are mounted on the entrance of cell's body and are separated from each other and from the body by ceramic spacers. These lenses are used to focus the ion beam into the drift cell entrance and both are controlled by separate DC power supplies. The exit plate (SS, 1.40" OD, 0.60" ID, 0.128" width) with an orifice of 0.254 mm is mounted with its retainer and five copper drift rings on the end cap by six ceramic rods, shown in Figure 3. An exit lens is also mounted on the exterior of the end cap, is controlled by a separate power supply and it is isolated by ceramic spacers from the end cap. The voltage supply to the body and the end cap as well as the three sets of the Einzel lenses prior to the drift cell is provided by the ABB-Extrel QC-150 power supply. Buffer gas (usually He or Ar) and/or reactant gas is

introduced into the drift cell through a stainless steel tube which isolated from the ground by ceramic breaker for insulation, the flow rate is controlled by two mass flow controllers (MKS 1479A), the accuracy of the cell pressure can be reach up to ±1 mTorr. Cell pressure is monitored by a capacitance manometer (MKS Baratron type 626). The maximum pressure that could be reached in the drift cell depends on two factors; the pumping speed of the diffusion pump and the diameter of the drift cell entrance and exit orifice. The cell is heated by two heating cartridges (Watlow 100W/ 120V) connected to the cell body and the end cap. The heating elements are tantalum wires running through ceramic tubes which are inserted in the cell body as well as the end cap. The cell body contains eight ceramic tubes while the end cap has two. The heat is generated from a DC current transferred from the AC current by the use of a combination of isolation transformers and a dynode conversion as a bridge rectifier. This conversion of the applied current is made because the ceramic becomes conductive at high temperature and if the AC current is applied and the voltage applied to the heating wires will interfere with the voltage applied to the cell. The maximum operating temperature for the drift cell is 500 ^{o}C. Cooling of the drift cell is done by flowing liquid nitrogen through an inlet tube located on both the body and the end cap. The liquid nitrogen goes through the drift cell via drilled pores inside the cell body and the end cap and then escapes through an outlet tube. The lowest operating temperature for the drift cell is -195 ^{o}C. Cooling is controlled by two Omega (CNi-3233) temperature controllers coupled to three on/off solenoid valves. This wide range of operating temperatures allows us to carry out many experimental studies. Ions exiting the drift cell are guided through three sets of Einzel lenses to the entrance of the fourth chamber which contains the second quadrupole

mass filter and the electron multiplier detector. The quadrupole mass filter's ionizer is turned off and its lenses act as focusing lenses to guide the ion beam/pulses into the quadrupole mass filter. The quadrupole mass filter can be operated in either single ion mode or scan mode. In the single ion mode the intensity of an ion under interest is monitored and can be optimized through tuning the system optics. However, in the scan mode, all ions exiting from the drift cell are scanned. Arrival time distribution (ATD) is obtained using a multichannel scalar detector with 2 μs resolution. The arrival times represent the ion drift times from the ion-gate to the detector.

2.3.1 Ion Energy and Injection Energies

Ion energy is defined as the voltage applied at cage (ion region) where the ions are born.[89] With this definition, the ion energy is independent of the ionizing electron energy or the potential applied to the extracting lenses. Also, the ion energy considered as the sum of the ion region voltage and the quad housing voltage, since the quad is floated. The quad is floated to slow down the ions with high energy, such those formed from the laser vaporization ionization (LVI) method.[90] Slowing down the speed of these ions allows the quad to have enough time to handle them, so it can resolve them and attain higher resolution. This technique is also applied to the pole bias, where a potential is applied to the poles of the mass filter on the z-axis of the quad rods. The pole bias actually, reduces the ion energy "seen" by the quad, making these ions manageable by the mass filter, thus, enhancing its resolution. Ion energy of the range of 12eV is suitable for quad handling.

Another energy consideration is the injection energy which is defined as the energy of the ions entering the drift cell. The injection energy is difference between the ion energy and the drift cell entrance voltage, so, if the ion region potential is 45 V, the floating quad potential is 45 V and the drift cell entrance voltage is 76 V, the injection energy in this case will be 14 eV. It is of a major importance to inject the ions into the drift cell with appropriate injection energy, low injection energies will result in no signal since the ion will not be capable of entering the drift cell due to the barrier set by the drift/reacting gas molecules escaping through the drift cell entrance orifice. However, excessive injection energy of the ions will result in two drawbacks. The first one is, the ion will penetrate too deep into the drift cell before they are being thermalized, which leads to inaccurate mobility and other experimental measurements. The thermalization of the ion packets should be done at the entrance of the drift cell. The second drawback of the high injection energies is ion fragmentation. This fragmentation will result in the ion signal loss of the selected ion and in some cases secondary reactions involving the fragment ion and the reacting gas present in the drift cell. Injection energies of the range of 10-20 eV are typically used in our experiments.

The energy of the ions exiting the drift cell is controlled by the voltage applied on the drift cell exit. These ions are entering the second mass filter. The ideal ion energy of these ions should be in the range of 3-12 eV, seen by the second quadrupole, so, the pole bias voltage applied on the second quad should be adjusted according to the drift cell exit voltage.
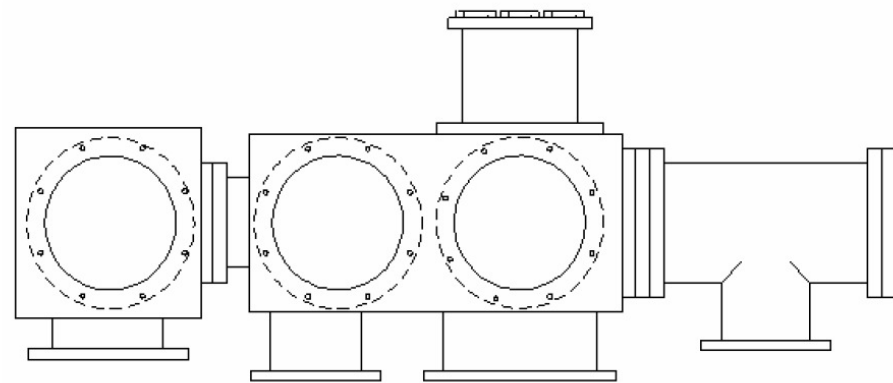
Figure 1. Side view of the ion mobility instrument showing the main chambers of the machine
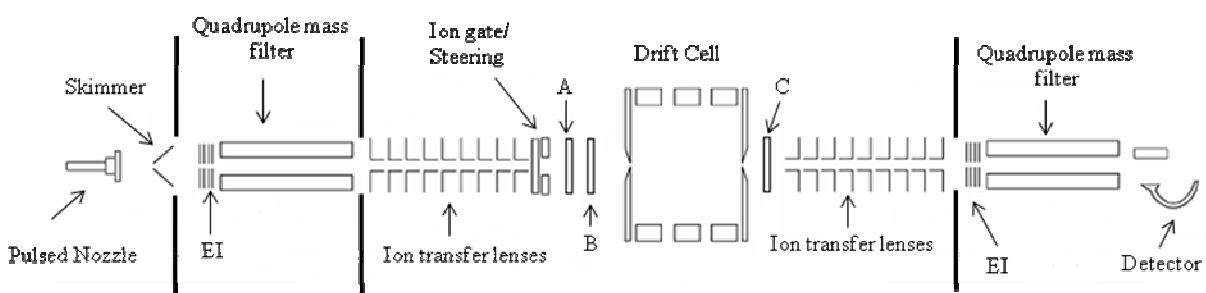
Figure 2. The experimental setup of the mass-selected ion mobility system. pulsed nozzle; 3 mm skimmer; electron-impact ionizer; quadrupole mass filter; ions transport lenses (Einzel Lenses 1, 2 and 3); 6) steering lens/ion gate; focusing lenses A and B, drift cell; lens C; ions transport lenses (Einzel Lenses 4, 5 and 6); quadrupole mass filter; electron multiplier (detector).
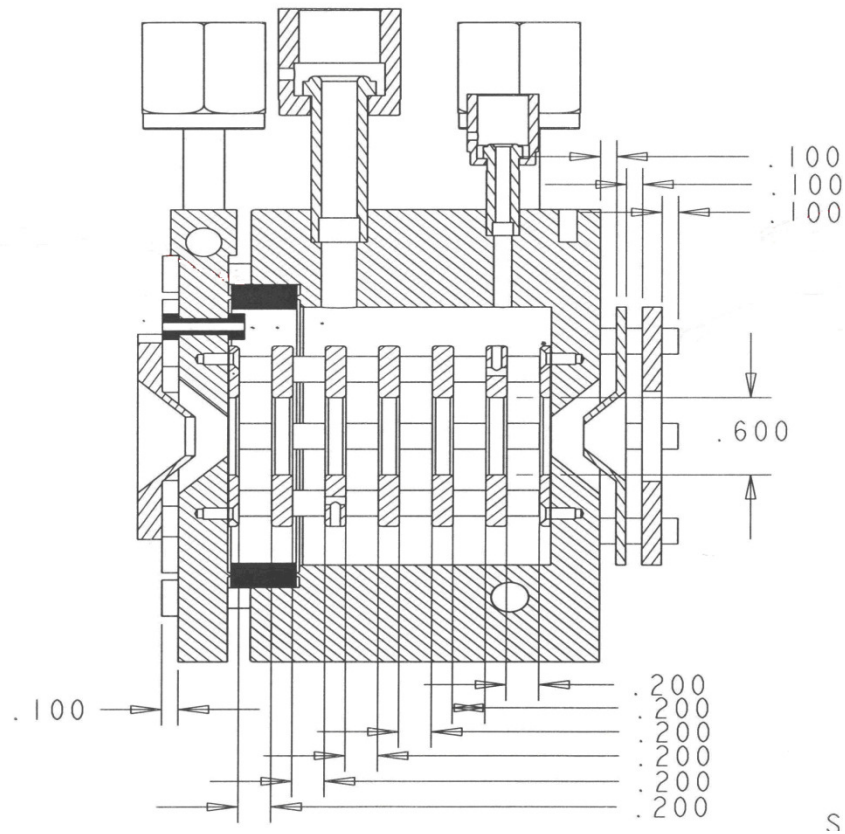
Figure 3. Schematic representation of the drift cell showing the five copper rings forming the cell with the separating ceramic spacers and the set of lenses before and after the cell section.

2.4 Preparation of nanocatalysts utilizing the Laser Vaporization Controlled Condensation (LVCC) method

The LVCC method is based on the formation of nanoparticles by condensation from the vapor phase employing laser ablation. The LVCC process consists of pulsed laser vaporization of a metal target (Pd, Pd/MgO and Pd/CeO$_2$) into a selected gas mixture in a modified diffusion cloud chamber. The laser vaporization produces a high-density vapor within a very short time, typically 10^{-8} s, in a directional jet that allows directed deposition. Desorption is possible from several targets simultaneously, yielding mixed particles. An important feature is the use of an upward diffusion cloud chamber, at well-defined temperature and pressure. A temperature differential between the end plates produces a convection current into which the metal is evaporated. The chamber consists of two horizontal, circular stainless-steel plates, separated by a glass ring. A metal target of interest is set on the lower plate, and the chamber is filled with a pure carrier gas such as helium or Ar (99.99% pure) or a mixture containing a known composition of a reactant gas (e.g., O$_2$ in case of oxides, N$_2$ or NH$_3$, for nitrides, CH$_4$ for carbides, etc.). A schematic representation of the LVCC chamber is given in Figure 4.

The metal target and the lower plate are maintained at a temperature higher than that of the upper one (temperatures are controlled by circulating fluids). The top plate can be cooled to less than 150 K by circulating liquid nitrogen. The large temperature gradient between the bottom and the top plates results in a steady convection current, which can be enhanced by using a heavy carrier gas such as Ar under high-pressure conditions (10^3 Torr). The metal vapor is generated by pulsed laser vaporization using the second harmonic

(532nm) of Nd:YAG laser (Spectra-Physics, Qunta-Ray Pro Series, 15-30 mJ/pulse, 10^{-8} s pulse). The laser beam is moved on the metal surface to expose new surface to the beam.

Following the laser pulse, the ejected pulse of the metal atoms interacts with the gas mixture in the chamber. Both diffusion and convection affect the removal of the small particles away from the nucleation zone (once condensed out of the vapor phase) before they can grow into larger particles.

By controlling the temperature gradient, the total pressure, and the laser power (which determines the number density of the metal atoms released in the vapor phase), it is possible to control the size of the condensing particles.

Purified acetylene was used at a flow rate of 100 SCCM (controlled by MKS flow controller Model 1479A) over the metal nanoparticle catalysts prepared by the LVCC method at different temperatures controlled by the tube furnace (temperatures can vary from 100 ^{o}C to 1200 ^{o}C).

Polymerized products were transferred to be analyzed by Varian Saturn 2000 GC/MS/MS where, these samples were injected and separated by the gas chromatographic column, Restek Rtx-50, 50% methyl-50% phenylpolysiloxane, 30 meter, 0.25mm ID, max. temperature 310 ^{o}C. Detection was carried out utilizing the ion-trap mass spectrometer.
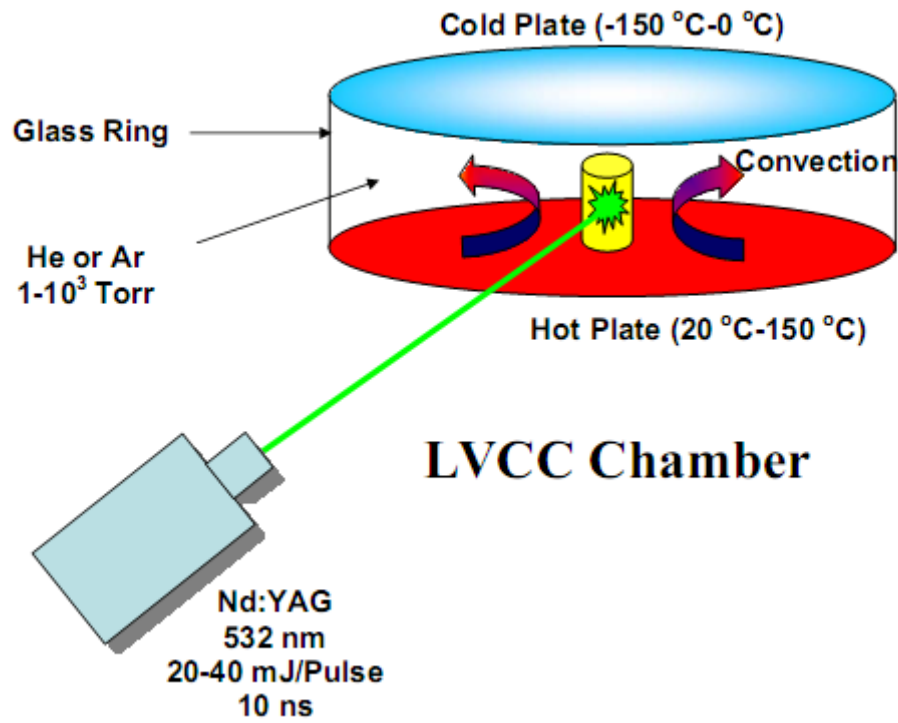
Figure 4. Pulsed Laser Vaporization-Controlled Condensation (LVCC) System.

Chapter 3 Gas phase experimental techniques

3.1 Ion Mobility and structure investigation

The ion mobility is a measure of the velocity of the ion traveling through a buffer gas (He or Ar), under the influence of a weak uniform electric field. The mobility K can be defined as given in equation (3.1):

$$K = \frac{v_d}{E} \qquad (3.1)$$

Where $v_{d=\frac{z}{t_d}}$ is the drift velocity (z is the drift cell length in cm, and td is the drift time in s), $E=\frac{V}{z}$ is the electric field across the drift region (V is drift field in volts). So the units for mobility K are cm^2/V.s. The reduced mobility K_0 can be scaled to the number density at standard temperature and pressure and defined as given in equation (3.2):

$$K_0 = K\left(\frac{273.15}{T}\right)\left(\frac{P}{760}\right) \qquad (3.2)$$

where T is the drift cell temperature in Kelvin and P is the drift cell pressure. By combining equations (2) and (3), and rearrange it, a new equation (3) is obtained:

$$t_d = \left(\frac{z^2 \times 273.15}{T \times 760 \times K_0}\right)\left(\frac{P}{V}\right) + t_0 \qquad (3.3)$$

where t_0 is the time which ions spend outside the drift cell before reaching the detector. Figure 6 represents the arrival time distributions (ATDs) for d- benzene radical cation,

23

$(C_6D_6)^+$ at different voltages. K_0 can be obtained from the slope of the plot of the ion drift time t_d versus P/V, as shown in Figure 5.

$$slope = \left(\frac{z^2 \times 273.15}{T \times 760 \times K_0} \right)$$

(3.4)

The collected ATDs will be fitted to a theoretical ATDs predicted by the transport equation (3.5). For flux of ions ($\phi(t)$) in the drift tube with an aperture of area a and with a length of z. This is given by equation (3.5):

$$\phi(t) = \frac{sae^{-\alpha t}}{4\sqrt{\pi D_L t}} \left(\upsilon_d + \frac{z}{t} \right) \left(1 - exp\left(-\frac{r}{4D_T t} \right) \right) exp\left(-\frac{(z - \upsilon_d t)^2}{4D_L t} \right)$$

(3.5)

The ions are introduced as a delta pulse in the form of an axially thin disk of radius r_0 and uniform surface density s. The term s can be used as a scaling factor for the signal intensity, α is a constant, t is the time spent inside the cell, this time is obtained with subtracting the recorded arrival time (t_d) by the time spent by the ion outside the cell (t_0), and D_L and D_T are the longitudinal and transverse diffusion coefficients, respectively, and under low field conditions are given by the equation (3.6):

$$D = D_L = D_T = K \frac{k_B T}{e}$$

(3.6)

Molecular structure can be obtained by comparing the measured collision cross section, Ω, with the calculated Ω values under the low field limit. The low field limit is

defined as $E/N \leq 6$ Td (N is the buffer gas number density and Td = Townsend = 10^{-17} cm^2 .V), the corresponding collision cross section, $\Omega^{(1,1)}$, can be given by equation (3.7):

$$K = \frac{3qe}{16N}\left(\frac{2\pi}{k_B T_{eff}}\right)^{\frac{1}{2}}\left(\frac{M_i + M_b}{M_i M_b}\right)^{\frac{1}{2}}\frac{1}{\Omega^{(1,1)}(T_{eff})} \qquad (3.7)$$

where qe represents the ion charge, N is the buffer gas number density, M_i is the ion mass, M_b is the buffer gas mass, k_B is the Boltzmann constant and T_{eff} is the effective gas temperature (the second term accounts for temperature perturbation due to the drift field), M_i and M_b are the masses of the ion and buffer gas respectively, and $\Omega_{avg}^{(1,1)}$ is the averaged orientation collision integral, the average of $\Omega^{(1,1)}$ over all possible collision orientations. The superscript, (1,1), refers to the pair-wise collision assumption used in the collision cross sectional calculation. The averaged collision cross section can be obtained by three methods which differ in the most part by the interaction potentials utilized in their computation. The first of these methods is called the hard sphere approximation.[91] As the name suggest, a hard sphere potential is assumed for the interaction between an atomic or molecular ion and the buffer gas. Here, a molecule oriented randomly in space is enclosed in a square plane of area A. A hard sphere radius is drawn around each atom of the molecule and random points are selected within the plane. If a selected point falls within the radius defined by the sum of the atom and He hard sphere radius, a collision is assumed. The product of the ratio of "hits" to number of tries and area, A, represents the cross section of a particular orientation. The process is repeated for different orientations. An average collision cross section over all orientations is then obtained. The second

approach is similar to the first but differs in the method of hard sphere determination. This method utilizes a temperature-dependent collision radius (R_{coll}) obtained from a compilation of collision integrals for atom-atom collision using a 12-6-4 potential.[92] This potential has the form

$$U(r) = \frac{n\varepsilon}{n(3+\gamma) - 12(1+\gamma)}\left[\frac{12}{n}(1+\gamma)\left(\frac{r_m}{r}\right)^n - 4\gamma\left(\frac{r_m}{r}\right)^6 - 3(1-\gamma)\left(\frac{r_m}{r}\right)^4\right] \quad (3.8)$$

where ε is the potential depth, r_m, the distance at the potential minimum, n is an exponent for short range interaction behavior (repulsion) and equal to 12 for this method, and γ is a dimensionless parameter defining the relative strengths of the r^{-6} and r^{-4} terms. The last term (r^{-4} term), $U_4(r)$, represents attractive charge (q) and ion-induced dipole interaction between the ion and buffer gas. This term is given by

$$U_4(r) = -\frac{q^2\alpha}{2R^4} \quad (3.9)$$

where α is the polarizability of the gas. Expressed as a sum of Lennard-Jones (LJ) potential and ion-induced dipole interaction, (3.10) becomes

$$U(r) = \varepsilon_{LJ}\left[\left(\frac{r_{LJ}}{r}\right)^{12} - 2\left(\frac{r_{LJ}}{r}\right)^6\right] - \frac{q^2\alpha}{2r^4} \quad (3.10)$$

here, ε_{LJ} and r_{LJ} are Lennard-Jones parameters, corresponding to well depth and position respectively, α is the polarizability of the neutral gas. γ, r_m, and ε (3.10) can thus be obtained by fitting q, ε_{LJ} and r_{LJ} (3.10) into (3.9). For a given set of γ, r_m, and ε parameters at a particular temperature, T, the momentum-transfer collision integral, $\Omega^{(1,1)}$, can be obtained from a table. From $\Omega^{(1,1)}$, R_{coll} can be obtained using the relationship

$$R_{coll} = \left(\frac{\Omega^{(1,1)}}{\pi} \right)^{\frac{1}{2}} \qquad (3.11)$$

The projection approximation gives better results than the hard sphere method due to the inclusion of long-range potential effects. The sigma program, written by the Bowers group,[91-93] uses both methods described above. The third method is called the trajectory method.[94] In this method the collision integral, $\Omega^{(1,1)}$ is related to the angle defining pre- and post-impact trajectories of ion and buffer gas molecules (scattering angle). It is the average over the impact parameter and relative velocity. The average collision integral, $\Omega_{avg}^{(1,1)}$, is the average over all collision geometries. The same potential (3.10) as that used in the projection approximation is used for the trajectory method, a program, Mobcal, written by Jarrold *et al.,*[86,94-95] is used here. This method is computationally expensive but gives more reliable results when compared to the experimental results. Thus, we used this method for all structural determination.
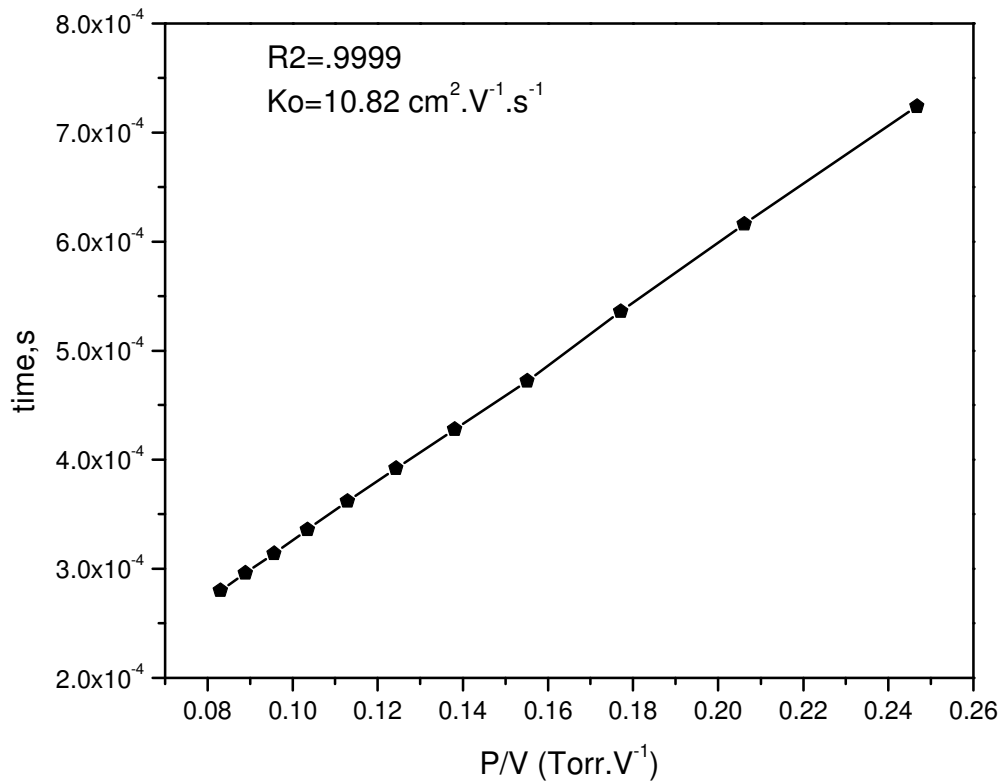
Figure 5. Plot of arrival time vs. P/V for $C_6D_6^+$; 20 μs ion pulse into a drift cell filled with 2.51 Torr He at different cell voltages (28-10 V).
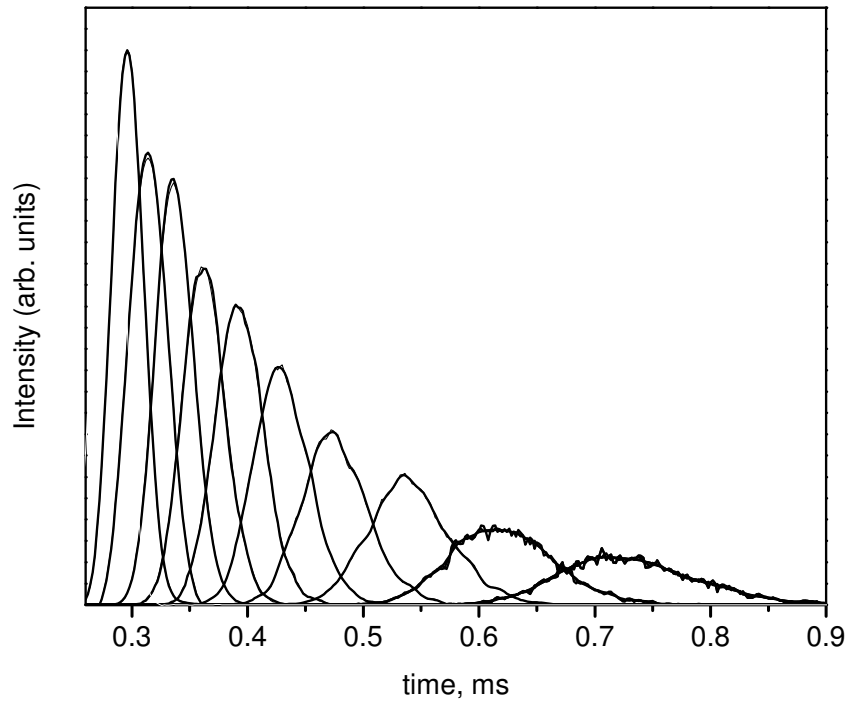
Figure 6. The arrival time distribution (ATDs) of injecting $C_6D_6^+$; 20 μs ion pulse into a drift cell filled with 2.51 Torr He at different cell voltages (28-10 V). The earlier ATD corresponds to drift cell voltage of 28V and the later ATD corresponds to drift cell voltage of 10 V.

3.2 Kinetics Measurements

The variation of the residence time of the injected ions in the drift cell with controlling the temperatures and pressures makes it possible to carry out kinetics measurements using the IM-MS technique.

For an irreversible second-order reaction such as:

$$A^+ + B \rightarrow A + B^+ \tag{3.12}$$

the reaction rate is given by

$$rate = -\frac{d[A^+]}{dt} = k_2[A^+] \times [B] \tag{3.13}$$

where $-\frac{d[A^+]}{dt}$ is the rate of disappearance of A$^+$, k_2 is the second-order rate constant, and [A$^+$] and [B] are the concentrations of A$^+$ and B respectively. With the concentration of reactant in the cell, [B], much greater than the injected ion, [A], the reaction can be considered pseudo-first order and the integrated rate law can be written in the form

$$-\ln\frac{[A^+]}{[A^+]_0} = k_2[B]t \tag{3.14}$$

where $[A^+]_0$ is the initial concentration of A^+, and t is the reaction time. Typically, the concentration of B (reacting gas/vapor) is much more than that of A^+ and as a result, the reaction can be treated as a pseudo-first order reaction and the rate constant of this reaction, k_1, is determined from the plot of $-\ln\frac{[A^+]}{[A^+]_0}$ as a function of residence time in the cell, t_d. Since the concentration of B is known, k_2 can be calculated. In this experiment, the reactant ion is injected into the drift cell containing the neutral vapor, B, and He. As the

reactant ion drifts through the cell, it reacts with the neutral vapor to give products. The initial concentration of the reactant ion, $[A^+]_0$, is the sum of both reactant and product ions, $[A^+] + [B^+]$ and the reaction time is the ion residence time in the cell. The arrival time obtained in this experiment represents the time the ions spend inside and outside the cell. To obtain the true residence time, the intercept (t_o) from a mobility measurement on A^+ is subtracted from the arrival time, resulting in t_d can thus be written as,

$$-\ln \frac{[A^+]}{[A^+]+[B^+]} = k_1 t_d \tag{3.15}$$

where k_1 is the first order rate constant. To obtain t_d for the plot described in, the cell voltage is varied. This varies the resident time of the reactant ion and consequently the relative concentrations of A^+ and B^+. The concentrations of A^+ and B^+ are obtained from the integrated arrival time distribution (ATD) of each species. In a less quantitative technique, $[A^+]$ and $[B^+]$ can be obtained from their individual mass spectrum intensity. As shown in Figure 7, a plot of $-\ln \frac{[A^+]}{[A^+]+[B^+]}$ versus t_d gives a straight line with slope equal to k_1. Knowing k_1, the second order rate constant, k_2, can be obtained from the relation

$$k_2 = k_1[B] \tag{3.16}$$

where $[B]$ is the number density of the neutral reactant gas.
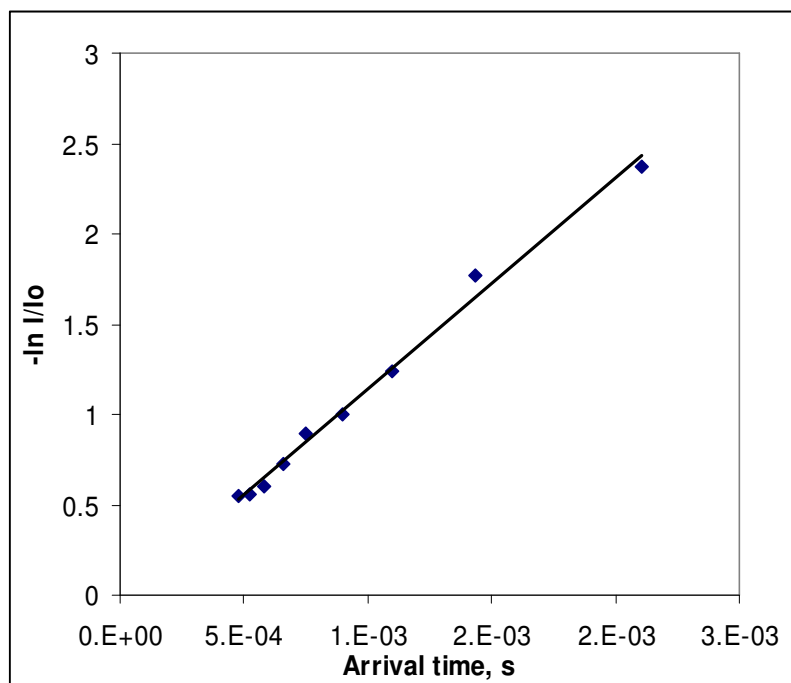
Figure 7. Plot of ln I/I$_o$ vs. arrival time of the reaction of $C_6D_6^+$ with acetylene at 400°C, the least squares linear fit (solid line) gives a first order rate constant of 1170 s^{-1} and R^2=0.9919

3.3 Thermochemical Measurements (van't Hoff Plots)

Information on thermochemical parameters such as ΔH^o and ΔS^o for ion-molecule association reactions can be obtained using the drift cell technique. For a typical association reaction of the form

$$A^+ \cdot (B)_{n-1} + B \Leftrightarrow A^+ \cdot (B)_n \tag{3.17}$$

ΔH^o and ΔS^o for the addition of neutral B can be obtained using the van't Hoff equation

$$\ln K = -\frac{\Delta H^\circ}{RT} + \frac{\Delta S^\circ}{R} \tag{3.18}$$

where R is the gas constant. K, the equilibrium constant, is calculated from the relation

$$K = \frac{I(A^+ \cdot B_n)}{I(A^+ \cdot B_{n-1})P(B)} \tag{3.19}$$

where I is the integrated ion intensity of the arrival time distribution (ATD) and $P(B)$ is the partial pressure of the neutral B in the drift cell.

For the hypothetical reaction above, the ATD of injected $A^+\cdot$ and association complexes, $A^+ \cdot (B)_{n-1}$ and $A^+ \cdot (B)_n$ formed inside the cell, is measured as a function of drift voltage corresponding to different residence (reaction) times. Equilibrium is reached when the ratio of $A^+ \cdot (B)_n / A^+ \cdot (B)_{n-1}$ is constant. Another indication of equilibrium is the observation of the same mean arrival time, t_d, for the injected and association complexes. For Reaction (13) above, true equilibrium means a coupling of the association reactant and products $A^+ \cdot (B)_{n-1}$ and $A^+ \cdot (B)_n$ respectively, hence the same mean arrival time. Figure 8, shows a typical van't Hoff plot for association reaction.
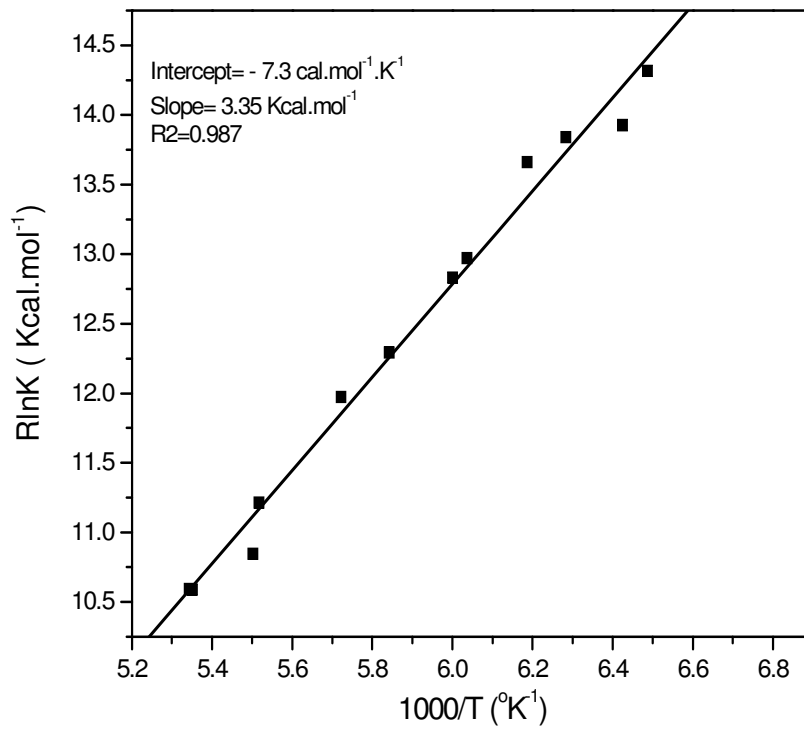
Figure 8. van't Hoff plot of the binding energy and entropy of the first C_2H_2 molecule onto $C_6D_6^{\cdot+}$ radical cation.

Chapter 4 Formation of polyaromatic hydrocarbons in the gas phase

A detailed discussion of the results of the formation of PAHs from the reactions of acetylene with benzene radical cation at different temperature regimes, phenylium cation, phenylacetylene radical cation and styrene radical cation is presented in this chapter. Kinetic measurements and thermochemical measurements are reported as well. Ion mobility measurements of the injected and product ions are reported for each reaction.

4.1 Ion-molecules reactions of benzene radical cation with acetylene utilizing the IMS technique

4.1.1. Introduction

Ion-molecule reactions are believed to be of the most apparent possible mechanisms for the formation of polyaromatic hydrocarbons (PAHs) and carbonaceous materials, which in turn act as catalysts, in envelopes of carbon rich space in the interstellar media (ISM).[96] Observation of acetylene, the smallest organic molecule to be polymerized, and benzene, the smallest cyclic aromatic compound, are of special interest in the formation of PAHs.[9,27,58,97-100] Observation of benzene and other PAHs such as naphthalene, anthracene and higher fused rings in Titan's upper atmosphere has been reported and believed to be responsible for the organic haze layers present in its atmosphere and was considered a very interesting result from the Cassini-Huygens spacecraft mission.[65] Understanding the formation mechanisms of benzene and higher PAHs in different media drew a great attention in the last decades.[39,101-107]

Growth of PAHs ions is believed to proceed in two different pathways; by direct addition to chain-like molecules or by successive build up of aromatic rings starting from

benzene nucleus.[108] Both mechanisms are possible for ionic and neutral species. The formation of $C_6H_6^+$ and $C_6H_7^+$ by successive addition of acetylene to $C_2H_2^+$ and $C_2H_3^+$ respectively has been reported. However, the structures of the formed $C_6H_n^+$ ions in those studies had not been elucidated by ritual means.[108] Recently, ionized clusters of acetylene where the intracluster formation of benzene radical cation occur from large ionized acetylene clusters have been reported by Momoh et al.[54,56] In those studies, the first ion-mobility measurements, collisional induced dissociation (CID) and theoretical calculations were made to provide the most conclusive evidences of the formation of covalent bonded ions, particularly benzene, from large ionized acetylene clusters. The intracluster polymerization of acetylene clusters to benzene ions is of great significance because it provides well-resolved structural information on the $(C_2H_2)_2^+$ and $(C_2H_2)_3^+$ cluster ions and links the simple aliphatic molecule to the formation of PAHs.[15-16,22-24,26-29,109-116] Benzene has been postulated to be the 'missing link' between simple carbonaceous molecules such as acetylene and the complex molecules made of hundreds of carbon atoms that could be responsible for the unidentified infrared bands (UIBs) in the IR spectra of the solar nebulae.[15-16] The presence of benzene,[117] acetylene[118] and other organic molecules such as C_2H,[119] H_2C,[120] CH_3 [121] and C_2H_4 [122] and the likes in ionizing environments in space could lead to the formation of higher PAHs.

Also, in the ionizing radiation media, the presence of cations and neutrals could catalyze the formation of PAHs by associative charge transfer (ACT). An example of such reactions is the polymerization of propene to the covalent bonded ion of propene oligomer $(C_3H_6)_n^+$ catalyzed by benzene radical cation reported by Pithawalla et al.[123] In this

example of the formation of larger hydrocarbons, no direct charge transfer from benzene radical cation to propene monomers took place, as this process is endothermic by 0.45 eV, rather, the charge transfer to the olefin in the activated complex formed through the reactions of benzene radical cation with propene. These types of reactions could lead to the formation of higher PAHs form olefin monomers.

The formation of PAHs starting from benzene as a prototype cyclic aromatic moiety subjected to intense theoretical and experimental investigations.[2,39,124-138] The mechanism of the growth of PAHs starting from benzene was studied by Bauschlicher et al.[59,132] In those studies, the energy barriers and heat of formations of the growth of the second aromatic ring fused to benzene through the reaction of benzene neutral/radical cation with acetylene were calculated. The addition of acetylene molecules to benzene neutral/ion was calculated according to the mechanisms proposed by Frenklach[39,139] and Bittner-Howard.[140] In both mechanisms, a loss of hydrogen atom from the benzene neutral/ion triggers the phenyl radical/radical cation formation, and the additions of acetylene molecules transpire to form the second aromatic ring. The difference between the two mechanisms is as the following; in the Frenklach mechanism the addition of the two acetylene molecules is carried out on the aromatic ring, meanwhile, in the Bittner-Howard mechanism the second acetylene molecule is added to the first one, then for both mechanisms cyclization occur to build up the second fused ring. These calculations predict that these additions of acetylene to benzene are barrierless and exothermic.[59] The reactions of simple carbocations such as CH_4^+ and CH_3^+ with neutral benzene has been studied by triple quadrupole mass spectrometer by Morrison et al.[141] Four types of reactions are

observed in these studies, simple charge exchange, hydrogen transfer, charge transfer with hydrogen-atom scrambling and disproportionation. No observations of any adduct ions were detected in those studies. In another successful attempt of growing large PAHs form benzene, ionized naphthalene from the reaction of diacetylene with benzene radical cation using the selected-ion flow tube (SIFT) and Fourier transform ion cyclotron resonance (FT-ICR) techniques was reported as a prototype model for the growth mechanism of PAHs in the gas phase by ion-molecule reactions.[77] The chemical reactivity and photodissociation techniques were utilized to test the formed $C_{10}H_8^+$ ion produced from this addition reaction. The reactivity of the formed $C_{10}H_8^+$ cation was tested with many reactants such as deuterium, acetylene, diacetylene, styrene, trimethylamine, nitric oxide and p-methylaniline and compared to those obtained from the reaction of naphthalene cation with the same reactants. The identical reactivity for both ions under the same experimental conditions, suggests that naphthalene ion was formed from the reaction of diacetylene with benzene radical cation. The most interesting observation of that study was that acetylene did not react with benzene radical cation at 296±2 K even though it was predicted theoretically to be a feasible reaction.

In this section, we present the addition reactions of acetylene neutrals to benzene radical cation under a wide range of temperatures and pressures. At high temperatures, these addition/elimination reactions led to the formation of styrene-type and naphthalene-type cations. At low temperatures, we present direct evidence for the formation of cyclic/polymerized ions through the association of acetylene onto benzene radical cation according to the ACT mechanisms.

4.1.2 Reactions of d-benzene radical cations with acetylene

4.1.2.1 High temperature regime

Benzene, d-6, (Aldrich, 99.6 atom % D) $C_6D_6^{\bullet+}$ radical cations are generated by electron impact ionization (EI=50-75eV) of the clusters formed by supersonic adiabatic expansion of $C_6D_6^{\bullet+}$/He mixture (2% $C_6D_6^{\bullet+}$) and are mass selected and injected into a drift cell containing pure acetylene (~0.5 Torr purified C_2H_2) at room temperature (300 K). Under these conditions $C_6D_6^{\bullet+}$ does not react with acetylene, in agreement with previously reported work.[142] Upon raising the temperature (423.15 K) the addition of first acetylene molecule to the benzene radical cation and formation of $C_8D_6H_2^{\bullet+}$, (m/z=110), ion starts to occur. Further increase in the drift cell temperature (523.2 K) leads to the formation of the second adduct ion $C_{10}D_6H_4^+$, (m/z=136). At (623.2 K), the relative intensity of the benzene cations decreases while the intensities of the first and second adduct became relatively high. At this temperature (623.2 K), elimination products $C_{10}D_5H_4^+$ (m/z=134) or $C_{10}D_6H_2^+$ (m/z=134) are detected as shown in Figure 9. These results suggest that there is an energy barrier for the addition of acetylene molecules to the benzene radical cation.

The kinetic study for the reaction of $C_6D_6^{\bullet+}$ cation with neutral acetylene at high temperature showed the following products:

$$C_6D_6^{\bullet+} + C_2H_2 \longrightarrow C_8D_6H_2^{\bullet+} \qquad (4.1)$$

$$C_8D_6H_2^{\bullet+} + C_2H_2 \longrightarrow C_{10}D_6H_4^{\bullet+} \qquad (4.2)$$

$$C_8D_6H_2^{\bullet+} + C_2H_2 \longrightarrow C_{10}D_5H_4^{\bullet+} + D \qquad (4.3)$$

$$C_8D_6H_2^{\bullet+} + C_2H_2 \longrightarrow C_{10}D_6H_2^+ + H_2 \qquad (4.4)$$
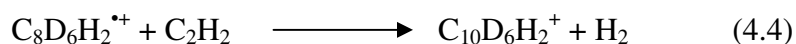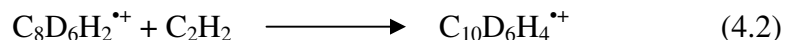
Figure 10 represent the variations in ion intensities by changing the applied field across the drift cell and Figure 11 illustrates the change of ions time profile according to the previous reactions.

Table 1. Summarizes the second order reaction rate for the previous reactions at different acetylene concentrations and different cell temperatures.

Table 1. Second order reaction rate for the reactions of $C_6D_6^{\bullet+}$ with acetylene at different acetylene concentrations and at different cell temperatures.

C_2H_2 Pressure (mTorr)	Temp. K	k_2 (cm^3.s^{-1})
1764	572.8	1.9×10^{-14}
2696	573.2	1.2×10^{-14}
1676	623.5	2.7×10^{-14}
2356	623.7	2.2×10^{-14}
910	623.6	1.8×10^{-14}
1850	623.2	3.7×10^{-14}
1544	648.3	4.1×10^{-14}
1901	672.5	3.4×10^{-14}
2416	673.3	3.3×10^{-14}

Arrhenius parameters can be estimated from the $\ln k_2$ vs. 1/T plots measured at different temperatures of the drift cell. Meanwhile, the activation energy (Ea) and the pre-exponential factor (A) can be obtained according to the following equation;

$$k = A. e^{-Ea/RT} \tag{4.5}$$

where Ea is the activation energy, in kcal.mol^{-1}, R the molar gas constant and A is the pre-collision factor. Equation (4.5) can be rearranged as follows:

$$\ln k = -Ea/RT + \ln A \tag{4.6}$$

Figure 12 shows the plot of $\ln k_2$ as a function of inverse temperature. The resulting overall barrier for the formation of ($C_8D_6H_2^{\bullet+}$ (m/z=110), $C_{10}D_6H_4^{\bullet+}$ (m/z=136) and $C_{10}D_6H_2^{\bullet+}$ or $C_{10}D_5H_4^{\bullet+}$ (m/z=134)) for the reaction of $C_6D_6^{\bullet+}$ with acetylene was found to be 3.5 kcal.mol^{-1}.

The experimental results are completely consistent with the theoretical calculations which show that the formation of $C_{10}H_{10}^{\bullet+}$ cyclic ion by the addition of two acetylene molecules followed by hydrogen elimination to the $C_8H_8^{\bullet+}$ ion is highly exothermic.[59] The first step in any growth mechanism is the loss of an aromatic hydrogen atom from the $C_6H_6^{\bullet+}$. In interstellar space this may took place as a result of UV photon absorption, but in combustion systems this occurs by reaction with reactive species like H or C_2H. This step is followed by the addition of C_2H_2 in a barrierless exothermic reaction leading to the formation of $C_8H_7^+$. The addition of the second C_2H_2 molecule and the ring closure is also found to be exothermic process with a small barrier. The product of equation (4.1) $C_8D_6H_2^{\cdot+}$ is most likely a styrene-type cation. However, the addition of the second

acetylene molecule (4.2) $C_{10}D_6H_4^{\cdot+}$ could be an open chain isomer, and the elimination products (4.3 and 4.4) $C_{10}D_5H_4^{\cdot+}$ or $C_{10}D_6H_2^{\cdot+}$ are most likely to be a naphthalene-type or D-naphthalene radical cations.
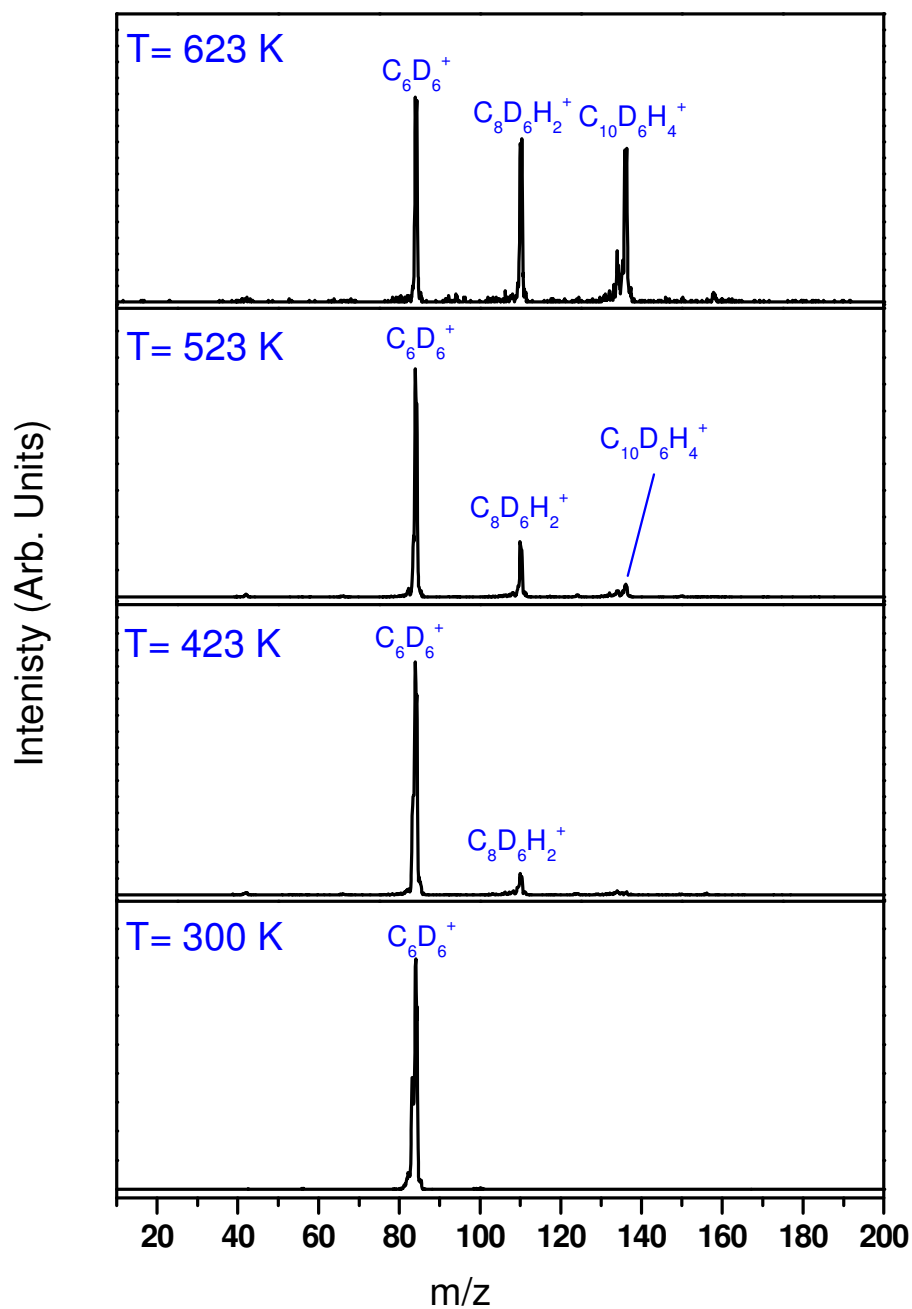
Figure 9. Mass spectra obtained upon injection of mass selected d-Benzene radical cation, $C_6D_6^{\bullet+}$, into the drift cell containing purified acetylene at different temperatures. The cell field was 5.8 V. cm^{-1}, the injection energy (IE) was 15.3 eV (lab) and the cell pressures were 419, 512, 478 and 728 mTorr and the corresponding temperatures were 300 K, 423 K, 523 K and 623 K from bottom to top panel respectively.
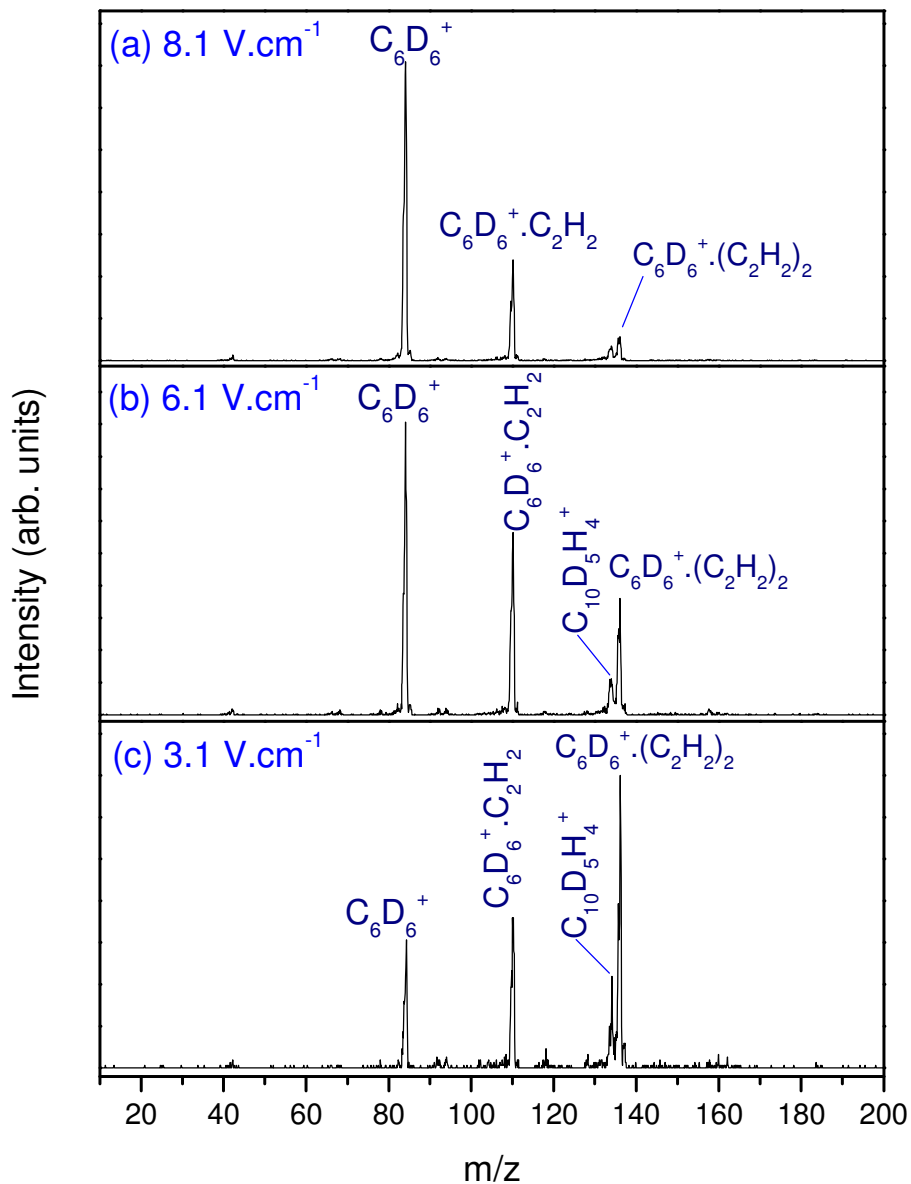
Figure 10. Mass spectra obtained upon injection of mass selected d-Benzene cation $C_6D_6^+$ into the drift cell containing 1.746 Torr purified acetylene. The cell temp was 573 K, injection energy (IE) was 15.3 eV (lab), cell field was 8.1 V.cm^{-1}, 6.1 V.cm^{-1}, and 3.1 V.cm^{-1} from top panel to bottom one respectively.
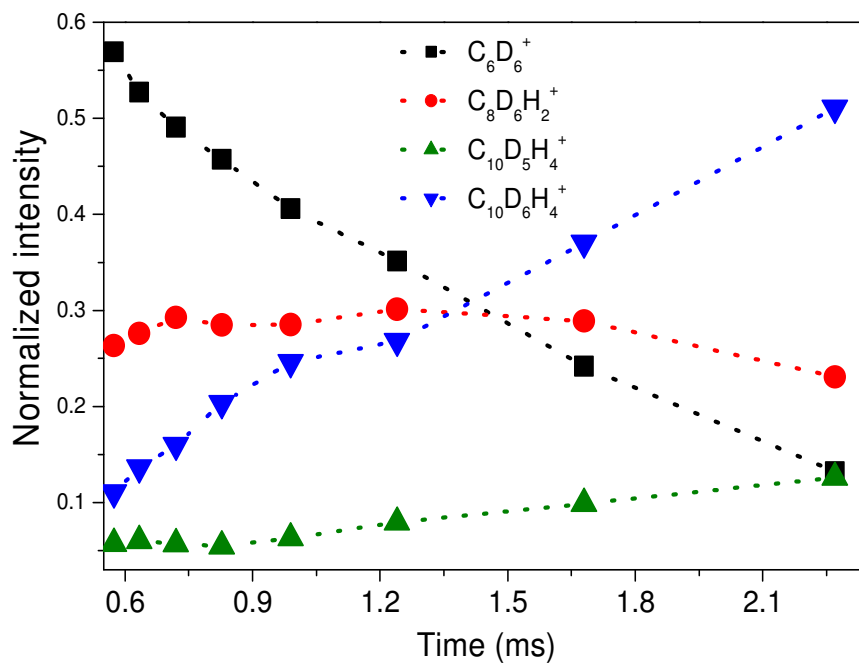
Figure 11. Integrated arrival time distribution of the reactant and product ions as a function of reaction time following the injection of $C_6D_6^{\bullet+}$ into the drift cell containing 2.4 Torr acetylene at 623 K.
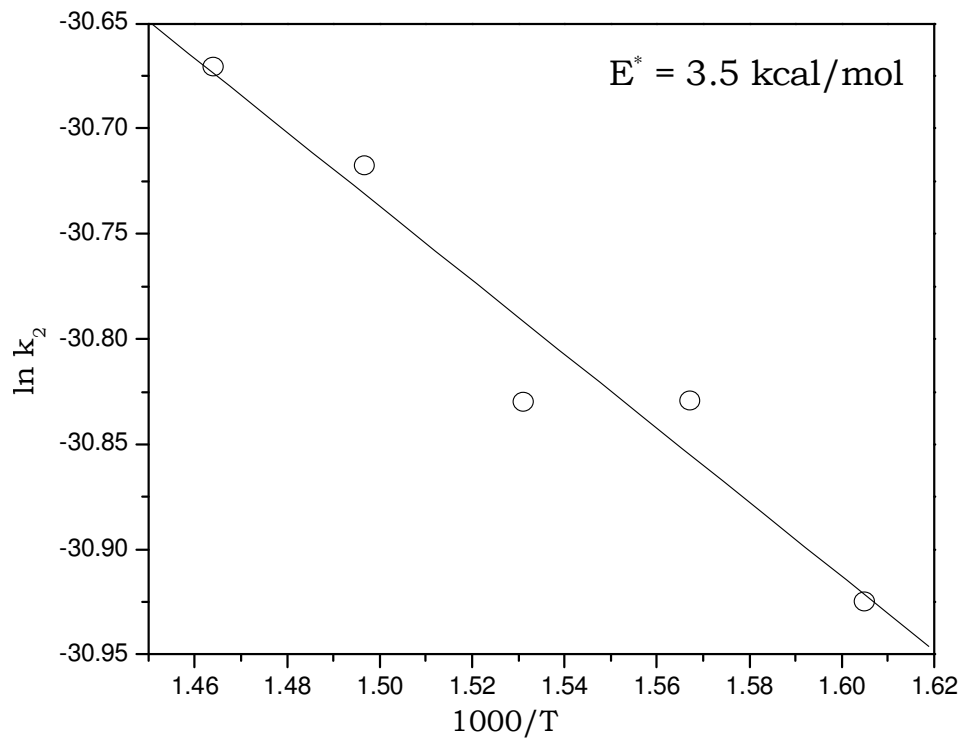
Figure 12. Arrhenius plot obtained by plotting the measured second order rate coefficient as a function of inverse temperature. The resulting barrier for the conversion of the benzene radical cation to the 110, 134, and 136 amu products in the presence of acetylene was 3.5 kcal/mol.

4.1.2.2 Theoretical Calculations of the possible isomers of the first and second additions of (C$_2$H$_2$) to C$_6$H$_6$·+
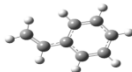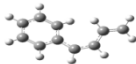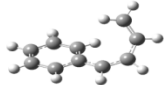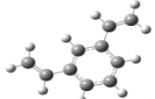
Several possible isomers of the first and second additions of (C$_2$H$_2$) to benzene radical cation have been optimized by the ab initio calculations at the UB3LYP/6-31+G** level. Table 2 represents different possible isomers for the first and second additions of acetylene to C$_6$H$_6$·+. All the examined structures are the covalent ones. For the first acetylene molecule added to benzene radical cation, the lowest energy structure is (Bzac1) in which a covalent bond formed between a carbon of the acetylene molecule with another carbon of the aromatic ring, accompanied with a proton migration to the acetylene molecule, (m/z=104). The binding energy of the (Bzac1) isomer assuming the interaction of C$_6$H$_6$·+ with acetylene was found to be ~65 kcal.mo^{-1}. Other possible isomers have been examined as well where the proton has transferred to the ortho-, meta-, and the para- positions in the benzene ring (only the para- isomer represented in Table 2), have higher relative energies with respect to the (Bzac1) isomer, ~28 kcal.mol^{-1} for isomer (bzac2), with less binding energies as well, ~38 kcal.mol^{-1}. The calculated cross section of (Bzac1) was 57.8Å^2 in good agreement with the measured one 53.1±3 Å^2. The calculated mobility of (bzac1) isomer was 9.4±0.1 cm^2.V^{-1}.s^{-1} also in good agreement with the measured value 9.8±0.6 cm^2.V^{-1}.s^{-1} (will be discussed later).
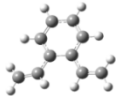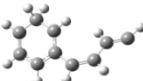
Different possible isomers were calculated for the second addition of acetylene to the formed product (C$_6$H$_6$.C$_2$H$_2$)·+ and represented in Table 2, isomers (Bz2ac1-Bz2ac7). The lowest energy structure of this addition was (bz2ac1) isomer where the second

acetylene was added to the first one as predicted by Bittner-Howard's mechanism. However, the isomers predicted by the Frenklach's mechanism, Isomers (Bz2ac2, Bz2ac4 and Bz2ac5), were found to be higher in their relative energies by 1.3, 8.1 and 9.8 kcal.mol^{-1} respectively. In all previously discussed isomers, the proton migration took place on the acetylene molecule. The calculated isomers where the proton transferred to the benzene ring, isomers (Bz2ac6 and Bz2ac7), showed high relative energies 53.7 and 65.8 kcal.mo^{-1} respectively, and these values suggests that there is a barrier for such transfer.

These results suggest that the Bittner-Howard addition mechanism is the favored route for addition of acetylene to benzene radical cations.

Table 2. Proposed structures of the products of reactions of $C_6H_6^{\bullet+}$ and (C_2H_2)

				B.E.
Isomer	**Structure**	**Method/Basis Set**	**Relative E**	**kcal.mol^{-1}**
$C_6H_6^{\bullet+} + C_2H_2$			
Bzac1		**UB3LYP/6-31+G****	**0**	**-65.2**
Bzac2		**UB3LYP/6-31+G****	**27.5**	**-37.6**
	$C_6H_6^{\bullet+} + 2\ C_2H_2$			
Bz2ac1		**UB3LYP/6-31+G****	**0**	**-121.8**
Bz2ac2		**UB3LYP/6-31+G****	**1.3**	**-120.6**
Bz2ac3		**UB3LYP/6-31+G****	**5.2**	**-116.6**
Bz2ac4		**UB3LYP/6-31+G****	**8.1**	**-113.6**

Bz2ac5		UB3LYP/6-31+G**	9.8	-112
Bz2ac6		UB3LYP/6-31+G**	53.7	-68.1
Bz2ac7		UB3LYP/6-31+G**	65.8	-56

4.1.3 Low temperature regime

The equilibrium studies were carried out as described previously in the experimental section (3.3). Purified acetylene (0.72 Torr) was introduced into the drift cell. The product ions were identified by scanning the second quadrupole mass filter located coaxially beyond the drift cell. The arrival time distributions (ATDs) were collected by monitoring the intensity of each ion as a function of time after the injection. Equilibrium among the ions as demonstrated by the identical ATD peaks of the $C_6D_6^{\bullet+}$ and the cluster products $C_6D_6^{\bullet+}(C_2H_2)_n$ ions.

To further confirm that equilibrium was achieved, the resident times of ions inside the drift cell were varied by varying the drift cell voltage. The ratio of the product ions to reactant ions is independent of the applied voltage. The test experiments were carried out at 136 K confirming that the ion ratios remained constant independent of the reaction time. These results also showed that the measured equilibrium constant is independent of the applied field across the drift cell in the low field region. All the equilibrium experiments were carried out at low drift cell field (5 V.cm^{-1}). Equilibrium constants were calculated from equation (4.7), where the ion intensities were obtained from the integrated peak areas of the ATDs and $P(C_2H_2)$ is the partial pressure of acetylene inside the cell.

$$Keq = \frac{I(C_6D_6^{+}.(C_2H_2)_n)}{I(C_6D_6^{+}.(C_2H_2)_{n-1}) \times P(C_2H_2)} \qquad (4.7)$$

The equilibrium constant measured as a function of temperature yields ΔH^o and ΔS^o from the van't Hoff equation as shown in equation (4.8):

$$\ln K = -\Delta H^\circ / RT + \Delta S^\circ / RT \qquad (4.8)$$

The extent of clustering of the acetylene molecules around the $C_6D_6^{\bullet+}$ radical cations is increased by lowering the temperature of the drift cell (more association observed). Figure 13 and Figure 14 show the mass spectra of the addition of several acetylene molecules on the $C_6D_6^{\bullet+}$ ion (addition of up to n=7 acetylene molecules). Figure 15 shows the arrival time distributions of the observed ions and confirms that equilibrium has been established. Figure 16 shows van't Hoff plots of the sequential additions of acetylene to the benzene radical cation. Table 3 summarizes the ΔH^o and ΔS^o values resulting from the van't Hoff plots and the calculated value of the first association of acetylene molecule to benzene radical cation obtained from Figure 16. Figure 17 represents the optimized structure of the first acetylene addition to benzene radical cation, $(C_6H_6.C_2H_2)^{\cdot+}$, at the UB3LYP/6-31G+** level. The binding energy calculated for the first addition is in excellent agreement with the measured one, 3.8 Kcal.mol^{-1}. The bond length between the acetylene carbons and the hydrogen on the benzene ring is 2.52 Å.
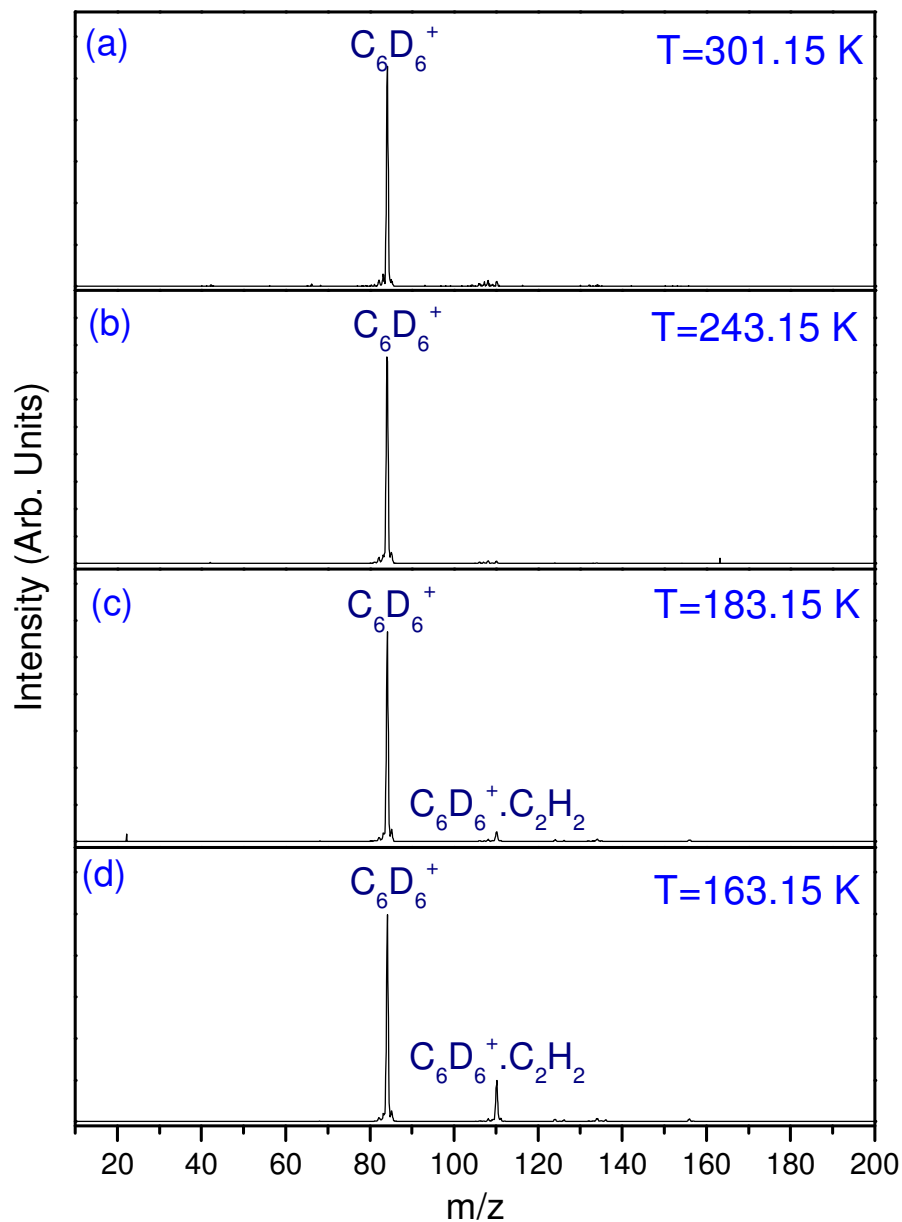
Figure 13. Mass spectra obtained upon injection of mass selected benzene cation $(C_6D_6)^+$ into cell containing purified acetylene at different temperatures. The cell field was 7.4 Vcm^{-1}, the injection energy (IE) was 11.6 eV (lab), and the cell pressure was 419, 590, 552, and 473 mTorr for panel (a) to (d) respectively.
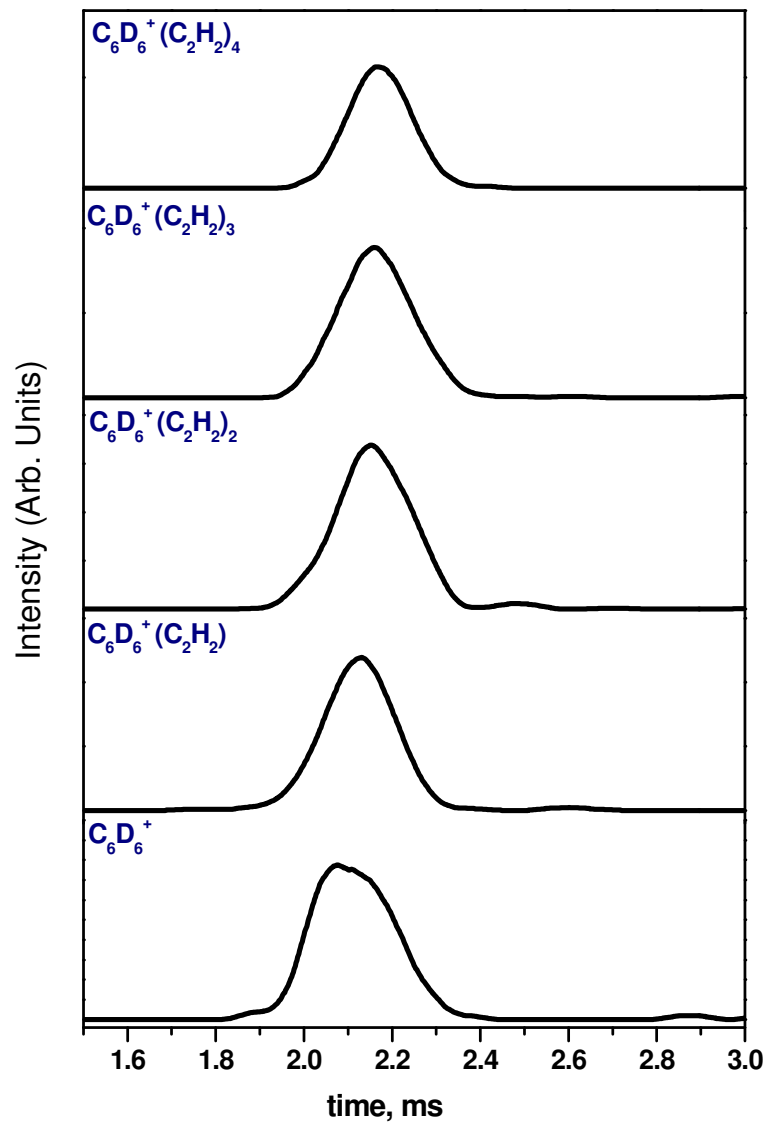
Figure 15. The Arrival time distribution of the reactant $C_6D_6^{.+}$ and products $C_6D_6^{.+}(C_2H_2)_n$, n=1-4, at equilibrium.
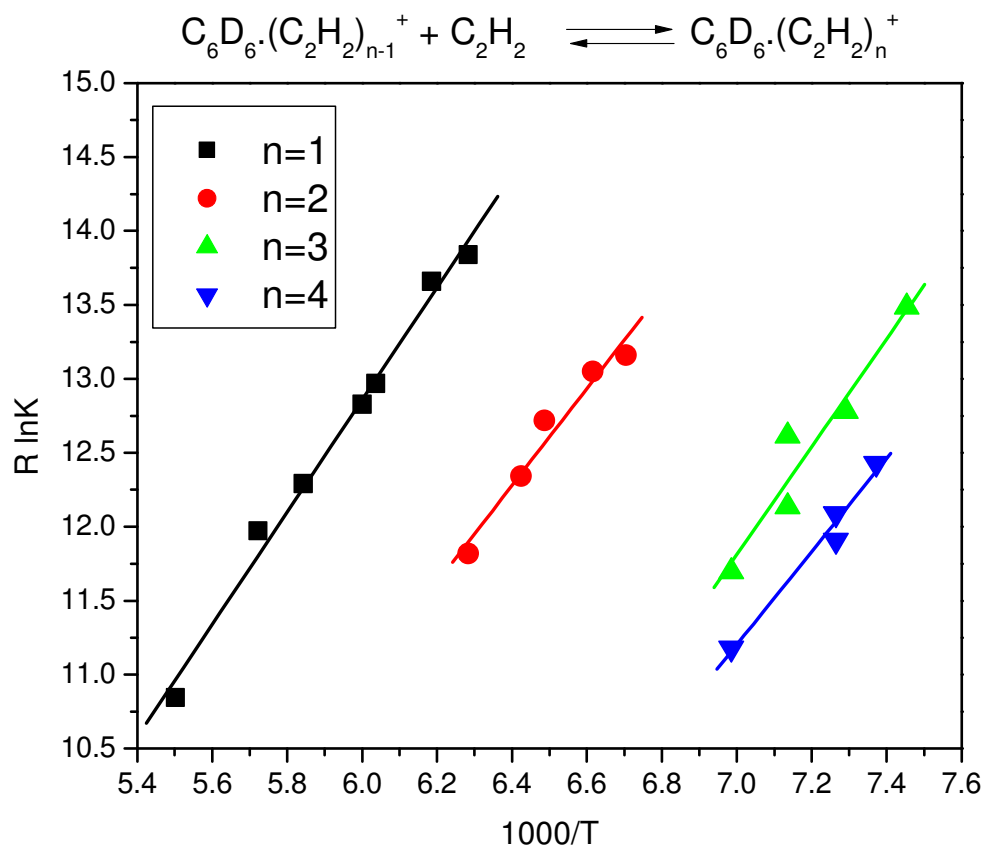
Figure 16. van't Hoff plot of addition of acetylene molecules to $C_6D_6^{\bullet+}$ radical cation. Series1 is the addition of first acetylene molecule, Series 2 is the addition of the second acetylene molecule to the first series, Series 3 is the addition of third acetylene molecule to the second series, and Series four is the addition of fourth acetylene molecule.
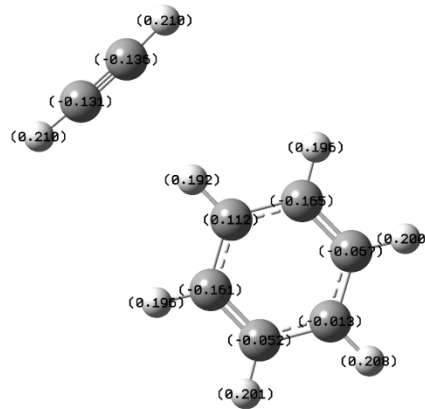
Figure 17. Optimized structure of $(C_6H_6.C_2H_2)^{.+}$ at the UB3LYP/6-31+G** level of theory.

Table 3. Binding energies and entropy changes of association of C_2H_2 on $C_6D_6^+$ ions.

n	$-\Delta H^o$ (kcal.mol^{-1})	$-\Delta S^o$ (cal.mol^{-1}.k^{-1})	$-\Delta H^o$ (kcal.mol^{-1}) Calculated at (UB3LYP/6-31+G**)
1	3.8	9.9	3.8
2	3.3	8.6	N/A
3	3.6	13.7	N/A
4	3.1	10.8	N/A

Moreover, at low temperatures (123.15 K), a series of acetylene clusters is observed corresponding to $(C_2H_2)_n^{+\bullet}$ with n=6-10 as shown in Figure 18 and its inset . This series of cluster ions couldn't result from charge transfer within the $C_6D_6^{+\bullet}(C_2H_2)_n$ cluster ions because of the higher ionization energy (IE) of acetylene (11.4 eV) compared to that of benzene (9.2 eV). The generation of $(C_2H_2)_n^{+\bullet}$ cluster ions with n≥ 6 can be explained by the Associative Charge Transfer (ACT) reactions observed in the benzene$^{+\bullet}$/propene system.[143] For clusters containing few acetylene molecules such as $C_6D_6^{+\bullet}$ $(C_2H_2)_3$, less charge will reside on the acetylene which may not be sufficient to induce cyclization of acetylene trimer, and we do not observe the $C_6H_6^{+\bullet}$ product ion. For larger clusters partial charge transfer (CT) may be assisted by stabilizing effect resulting from the formation of covalent bonds in the adduct ions making the overall process thermodynamically favorable. The polymerized adduct can have lower IEs than benzene that can take up the charge and leave benzene neutral. So, the benzene ion acts here as a catalyst for the cyclization of the acetylene clusters according to the following mechanism:

$$C_6D_6^{+\bullet} + n\ HCCH \xrightarrow{ACT} C_6D_6^{+\bullet} \ldots (HCCH)_n^{\delta+} \qquad (4.9)$$

$$\downarrow$$

$$C_6D_6 + (HCCH)_n^{+} \qquad (4.10)$$
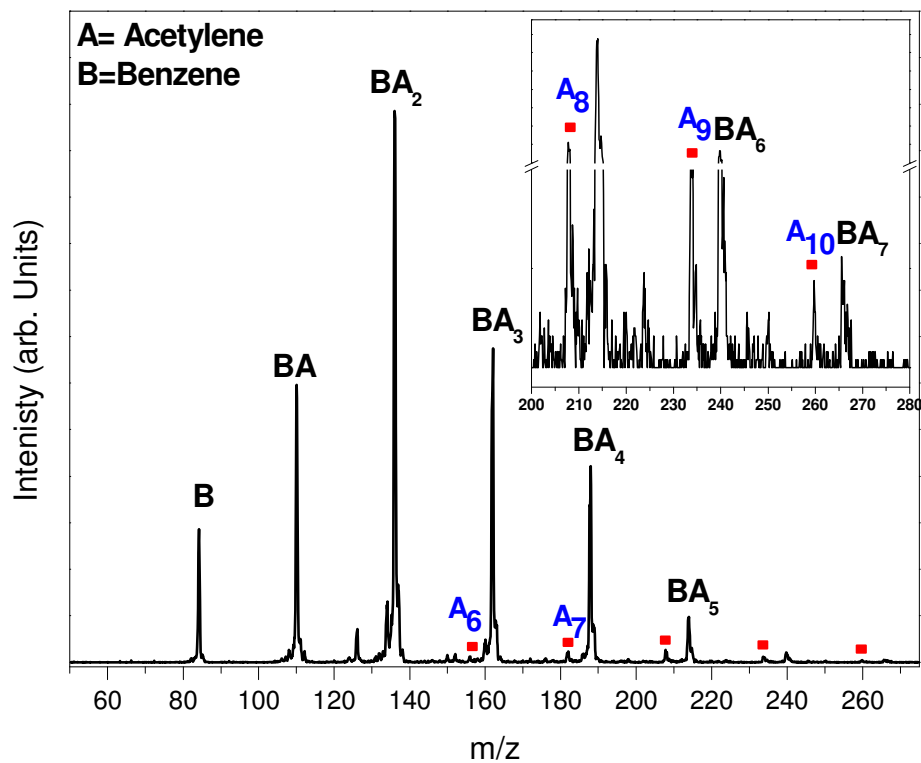
Figure 18. Mass spectrum of mass selected $C_6D_6^+$ injected into the drift cell containing 350 mTorr purified C_2H_2 at 123 K, Injection energy was 11.6 eV.

4.1.4 Mobility measurements

Ion mobilities of the d-benzene radical cation were measured in He, as summarized in Table 4. Fitting the measured ATD of d-benzene radical cation with the one predicted by the transport theory is shown in Figure 19. To obtain the structural information on the first product, the reduced mobility of the $C_6D_6^{\bullet+}C_2H_2$ ion in He was measured, The $C_6D_6^{\bullet+}C_2H_2$ ion was formed by electron impact ionization (EI) of the C_6D_6-C_2H_2 neutral clusters generated by supersonic beam expansion. The reduced mobility of the $C_6D_6^{\bullet+}C_2H_2$ ion was measured as 9.8 ± 0.6 $cm^2.V^{-1}.s^{-1}$ corresponding to $\Omega=53.1\pm3$ $\mathring{A}^2$ (in He at 300 K). The calculated Ω values using the trajectory method [144] for several low energy $C_8D_8^{\bullet+}$ covalent isomers are 52-58 $\mathring{A}^2$. This suggests that the $C_6D_6^{\bullet+}.C_2H_2$ ion has a covalent structure probably similar to the styrene-type cation as reported for isomer (Bzac1) in the calculation section.

Table 4. Measured and calculated mobilities and their corresponding cross sections of d-benzene radical cation.

	T K	K_o cm^2.V^{-1}.s^{-1} measured	Ω Å^2 measured	K_o cm^2.V^{-1}.s^{-1} Calculated	Ω Å^2 Calculated
$C_6D_6^{\bullet+}$	303	10.82	50.4	11.3	48.2
	648	8.7	43.5	8.9	41.8
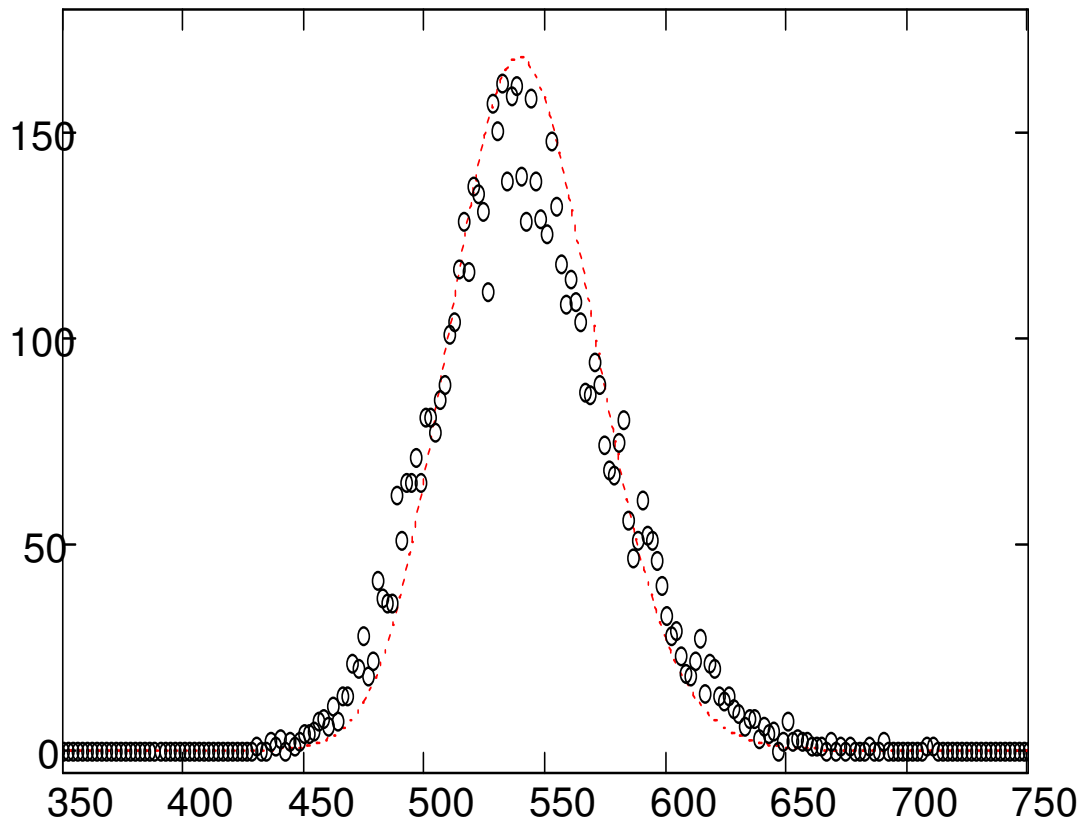
Figure 19. Comparison of measured ATD of the d-benzene radical cation, $C_6D_6^{\bullet+}$, with that predicted by the transport theory equation.

4.2 Phenylium Cation

4.2.1 Phenylium cation/C$_2$H$_2$ system

4.2.1.1 Introduction

Formation of PAHs starting from benzene is one of the prototype models for PAH growing mechanisms. As described in the previous section, we provided evidence of the formation of styrene, naphthalene and complex organic ions through the ion-molecule reactions and associative charge transfer (ACT) mechanisms of the reactions of benzene radical cation with neutral acetylene molecules in the gas phase.[145] The formation of C$_6$H$_5^{\bullet}$ radical is the mainspring to trigger of the formation of the second aromatic ring of PAHs.[146] Moreover, the mechanisms of the formation of PAHs proposed by Frenklach and Bittner-Howard involve the formation of the phenyl radical, C$_6$H$_5^{\bullet}$, that reacts with acetylene as the initiating step of the formation of higher PAHs complexes.[39,139-140] These mechanisms, referred as hydrogen abstraction-acetylene addition (HACA), are widely accepted in explaining PAHs formation in different environments. Numerous spectroscopic and kinetic studies are carried out on the phenyl radical in combustion and extraterrestrial environments. The rate constants of phenyl radical reactions with alkenes and alkynes have been measured using many techniques.[147-155] The measured rate constants are in the range of 10^{-11} and 10^{-12} cm^3.s^{-1} at high temperatures up to 1500 K were reported utilizing the cavity ring-down spectroscopy technique. Also, the addition of the phenyl radical to olefins and alkynes was reported to have activation energy barriers ranging from 5-45 kJ.mol^{-1}.[156] Though the detailed kinetic data were reported, the structural elucidations of the reaction products were rarely probed. Based on the quantum chemical and statistical

calculations, the addition of the phenyl radical to the carbon-carbon double bond in ethylene is carried out through the formation of an activated complex ($C_6H_5.C_2H_4^{\bullet}$), then followed by hydrogen elimination to form styrene according to Lin et al.[156-157] In case of the reactions of phenyl radical with acetylene, the proposed mechanism of the formation of activated complex $C_6H_5C_2H_2^{\bullet}$ is the same as the olefin, and in this case the formed complex is stabilized by either hydrogen elimination and/or collisional stabilization.[157] The main products of this reaction are phenylacetylene and H-atom. The stabilized isomeric $C_8H_7^{\bullet}$ radicals can serve as active agents in the mass growth reactions with C_2H_2, hence, formation of higher PAHs.

The formation of phenylium cation, $C_6H_5^+$, has drawn much interest as source of reactive species that could lead to the formation of PAHs in both combustion environments and interstellar medium.[158-164]

The reaction of phenylium cation with acetylene is of a great interest which could reveal the mechanism of formation of PAHs in combustion flames and interstellar space. These reaction were predicted theoretically according to equation (4.11)[59]
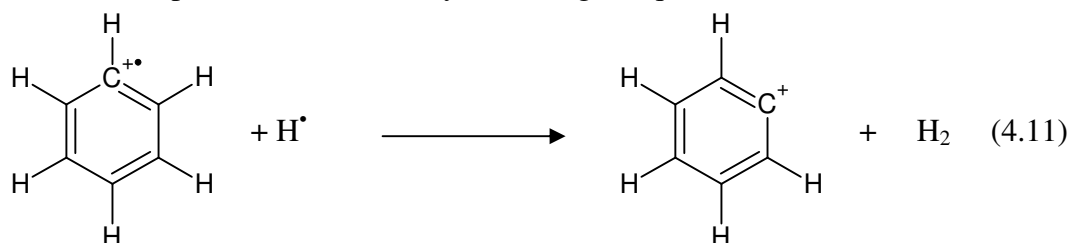
Here, we report the experimental results of the reactions of phenyl cation with acetylene utilizing the drift cell technique, as a mean of understanding the growth mechanisms of PAHs in different ionizing environments. The results are compared with

those obtained from the reactions of benzene with acetylene as discussed in the previous section.

4.2.1.2 Results and Discussion

Benzene, C_6H_6 (Sigma-Aldrich, 99.9+% HPLC grade), and bromobenzene, C_6H_5Br (Fluke 99.5% GC grade), were used to generate the phenylium cation, $C_6H_5^+$, through the EI ionization (90-100 eV) of the clusters formed by supersonic beam expansion of benzene/He or bromobenzene/He mixtures. The $C_6H_5^+$ cations were mass selected by the first quadrupole mass filter and injected into the drift cell containing different acetylene/He mixtures or purified acetylene at different cell pressures (0.1-1.5 Torr). Injection energies of 12-17 eV (laboratory frame) in 10-50 μs pulses were utilized in this case. High ionization energies were utilized to generate the phenylium cation fragment and the choice of bromobenzene was made to avoid the interference of the parent peak of the benzene ion (m/z=78) with that of the $C_6H_5^+$ fragment (m/z=77). Figure 20 represents the mass spectra of the mass selected phenyl cation generated from benzene precursor. It is clear that both $C_6H_6^+$ and $C_6H_5^+$ peaks are present due to the small difference (1 amu) between the parent cation, $C_6H_6^{\bullet+}$, and the phenylium cation. It is clear that upon utilizing high ionization energies on the EI ionization source, we could obtain more than 80% fragmentation of benzene. Figure 21 represents the injection of $C_6H_5^+$ into the drift cell containing different acetylene concentrations. At low acetylene pressure, 37 mTorr C_2H_2, the following reaction is observed.

$$C_6H_5^+ + C_2H_2 \longrightarrow C_8H_7^+ \qquad (4.12)$$

Under these experimental conditions, the phenylium cation, $C_6H_5^+$, did not completely react with acetylene in the drift cell due to the small acetylene concentrations, observation of phenylium, $C_6H_5^+$, cation is shown in Figure 21 (a). Also the addition of acetylene molecules was done only to the phenylium cation, while the benzene radical cation did not react with acetylene under the given experimental conditions in consistent with our reported results of the reactions of benzene cations with acetylene.[145] As the acetylene pressure increases in the drift cell, two more observations were noticed. First observation was that, the peak of the phenylium cation, $C_6H_5^+$, completely disappeared and transformed to the reaction products. Second, the addition of the second acetylene molecule to the phenylium cation starts at higher pressures of acetylene, 428 mTorr, as shown in Figure 21 (d, e), according to the following equation (4.13).

$$C_8H_7^+ + C_2H_2 \longrightarrow C_{10}H_9^+ \qquad (4.13)$$
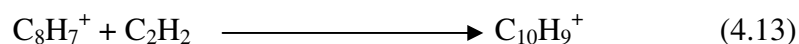
The observed products of the reactions of the phenylium cation with acetylene are in full agreement with the theoretical predictions for these reactions.[59] To further investigate the stability of the product ions; phenylium cations produced from bromobenzene precursor, were injected into the drift cell containing 540 mTorr purified acetylene at different cell temperatures. Temperatures ranging from 383.2 K to 660.2 K were employed as shown in Figure 22 (a) and Figure 23 (g) respectively. Note that the formed adducts show high thermal stability at high temperatures. The addition of the second acetylene molecule to the phenylium cation is enhanced at high temperatures as well. The enhanced stability of the formed adducts at high temperatures could be attributed to their covalent character. At high temperatures, the detection of $C_8H_6^+$ and $C_{10}H_8^+$ ions was evident, which correspond to

phenylacetylene and naphthalene isomers respectively. It could also be explained by hydrogen elimination from the $C_8H_7^+$ and $C_{10}H_9^+$ cations respectively. The addition of acetylene molecules to phenylium cation is limited to two molecules with no further additions observed at high temperatures or by increasing the acetylene pressure in the drift cell as shown in Figure 24. Note that, the temperature of the drift cell is kept at 623.2 K and the acetylene pressure varies from 728 mTorr to 1120 mTorr. These results are in agreement with the theoretical predictions. The observations of $C_8H_8^+$ and $C_{10}H_{10}^+$ cations in Figure 24 is the result of the reaction of benzene radical cations with acetylene.

The kinetics of the addition of acetylene molecules to the phenyl radical have been studied by several groups.[153,165-167] The rate constant of the addition of acetylene to phenyl radical was measured to be 2×10^8 cm^3.mol^{-1}.s^{-1} (2×10^{-15} cm^3.s^{-1}) at high temperatures (850 K-1250 K) by Stein et al.[165] The observed products of this measurement were phenylacetylene radical and hydrogen. The rate coefficient of the reaction of the phenyl radical with acetylene was measured to be 2.5×10^{-11} cm^3.s^{-1} as compared to the literature value of 4.0×10^{-10}.cm^3.s^{-1}. The kinetics measurements of the reaction of phenylium cation with acetylene showed second order rate constant k_2 to be in the range of 1.2×10^{-11}cm^3.s^{-1} to 9.1×10^{-10}cm^3.s^{-1} that is higher than the values reported by Anicich et al. and in good agreement with the literature measurments.[166] Figure 25 represents a voltage study showing the effect of varying the resident times on both the reactants and products across the drift cell. The measured reaction rate coefficients of the reaction of $C_6H_5^+$ with C_2H_2 are reported in Table 5. Figure 26 represents the plots of the normalized intensities of the

reactant and product ions of reaction (4.12) as a function of reaction time at room temperature.

At low temperatures, sequential association reactions of several acetylene molecules onto the $C_6H_5^+$ cation are observed as shown in Figure 27. Also, the associations of acetylene molecules to the benzene cation $C_6H_6^+$ are also observed similar to the results shown in Figure 14.

Our results are in good agreement with the theoretical predictions[62] of the fast addition of the acetylene molecule to the phenyl cation as compared to the slow addition of acetylene to benzene cation ($k_2 =\sim\times10^{-14}$ cm^3.s^{-1} according to our results). There is no barrier for the acetylene addition to the phenyl cation and the reaction is observed at as low temperature as 127 K, see Figure 27.
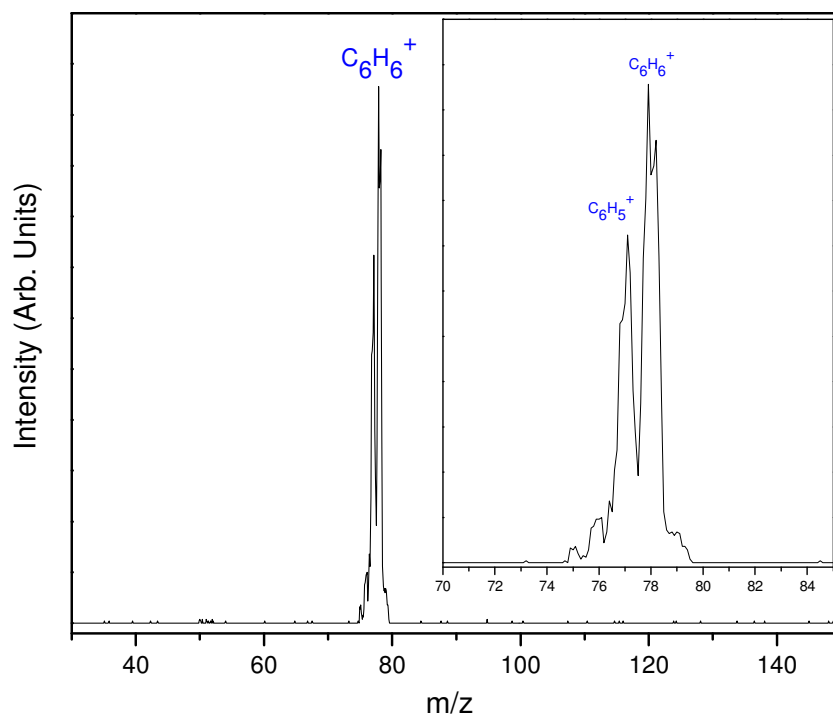
Figure 20. Mass spectra obtained upon injection of mass selected phenyl radical cation $(C_6H_5)^+$ into cell containing Helium. The cell field was 4.2 Vcm^{-1}, the injection energy (IE) was 13 eV (lab), and the cell pressure was 600 mTorr, The cell temperature was 300.15 K. Observation of the parent ion $(C_6H_6)^+$ appears as well in the mass spectra due to the very low mass difference.
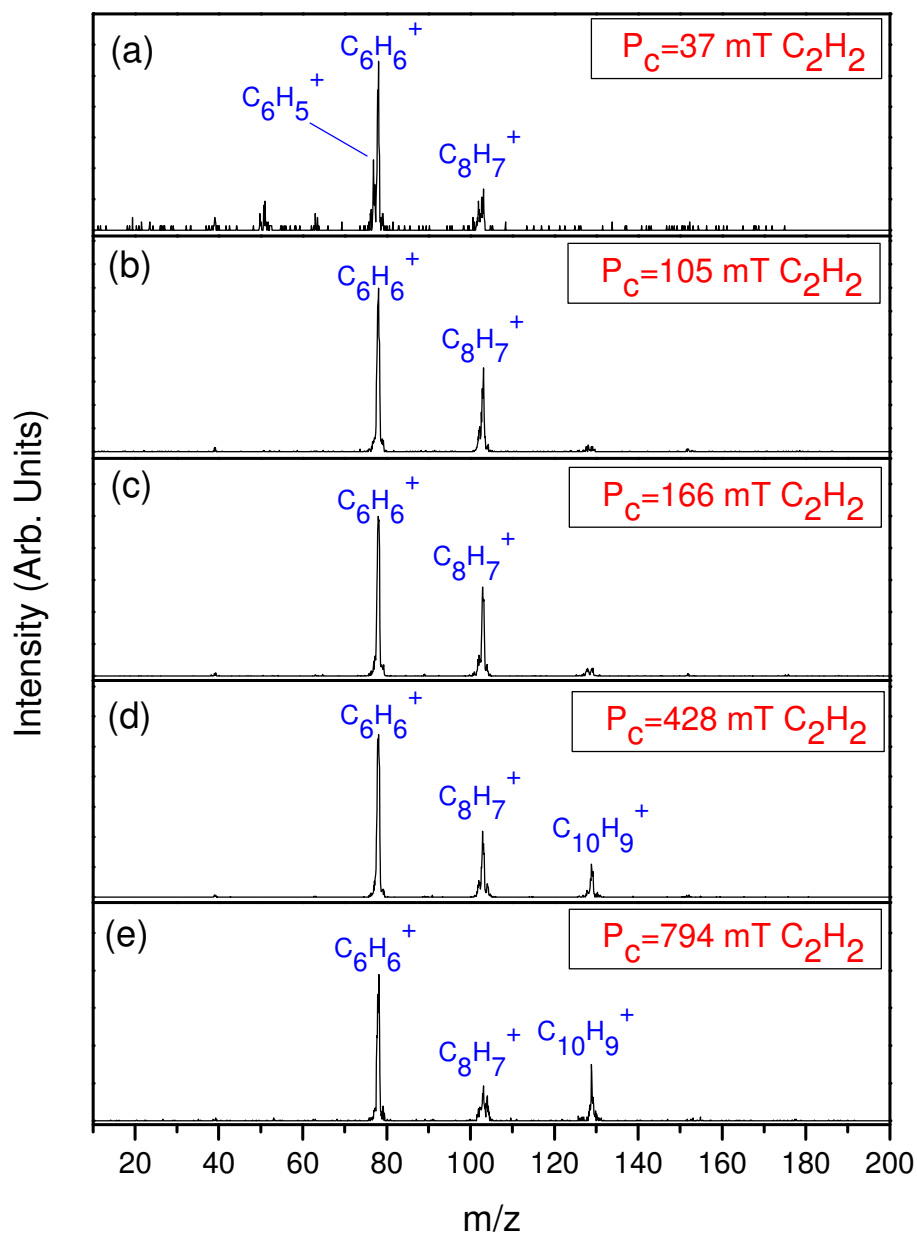
Figure 21. Mass spectra obtained upon injection of mass selected phenyl radical cation $(C_6H_5)^+$ into the drift cell. The cell field was 4.2 Vcm^{-1}, the injection energy (IE) was 13 eV (lab). The cell temperature was 300.15 K. Drift cell contained purified acetylene, the pressure was, 37 mTorr, 105 mTorr, 166 mTorr, 428 mTorr and 794 mTorr on panel (a) to (e) respectively.
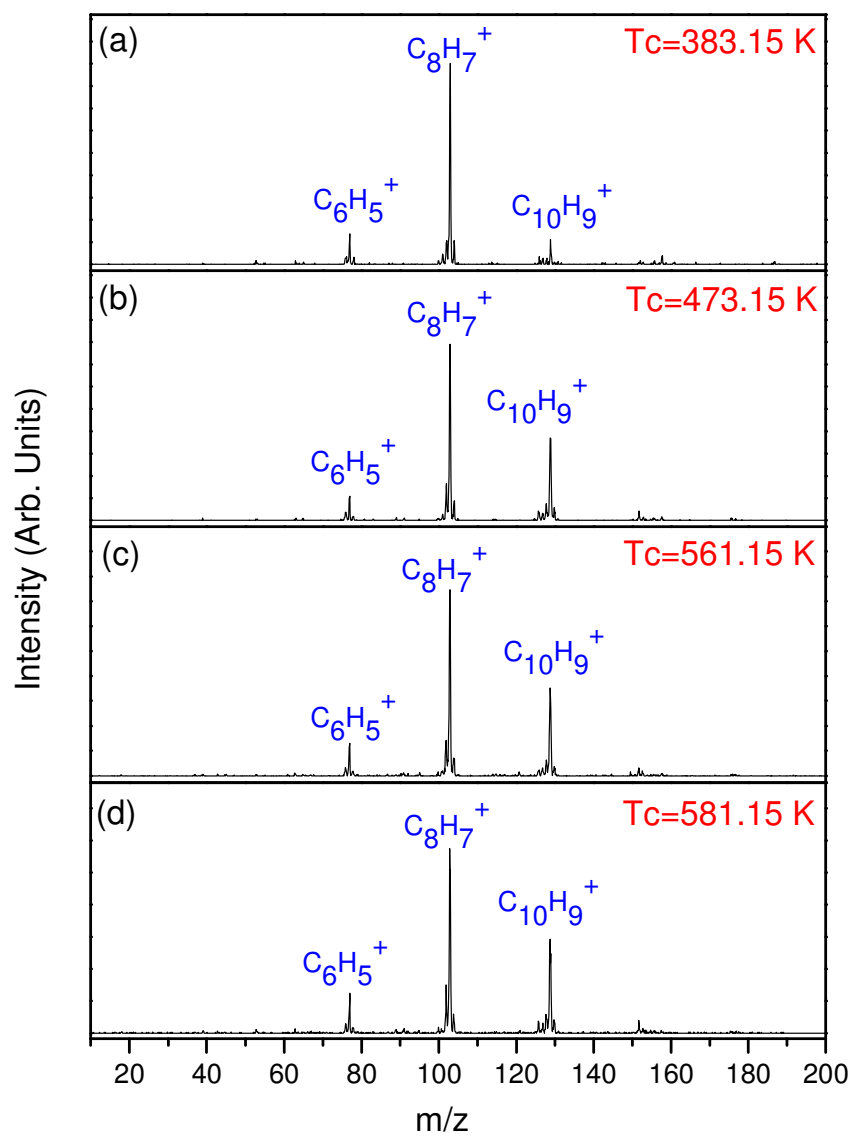
Figure 22. Mass spectra obtained upon injection of mass selected phenyl radical cation $(C_6H_5)^+$ into the drift cell. The cell field was 5.94 Vcm^{-1}, the injection energy (IE) was 13.9 eV (lab). The cell pressure was 540 mTorr purified C_2H_2. The temperatures ranged from383.15 K to 581.15 K on panel (a) to (d) respectively.
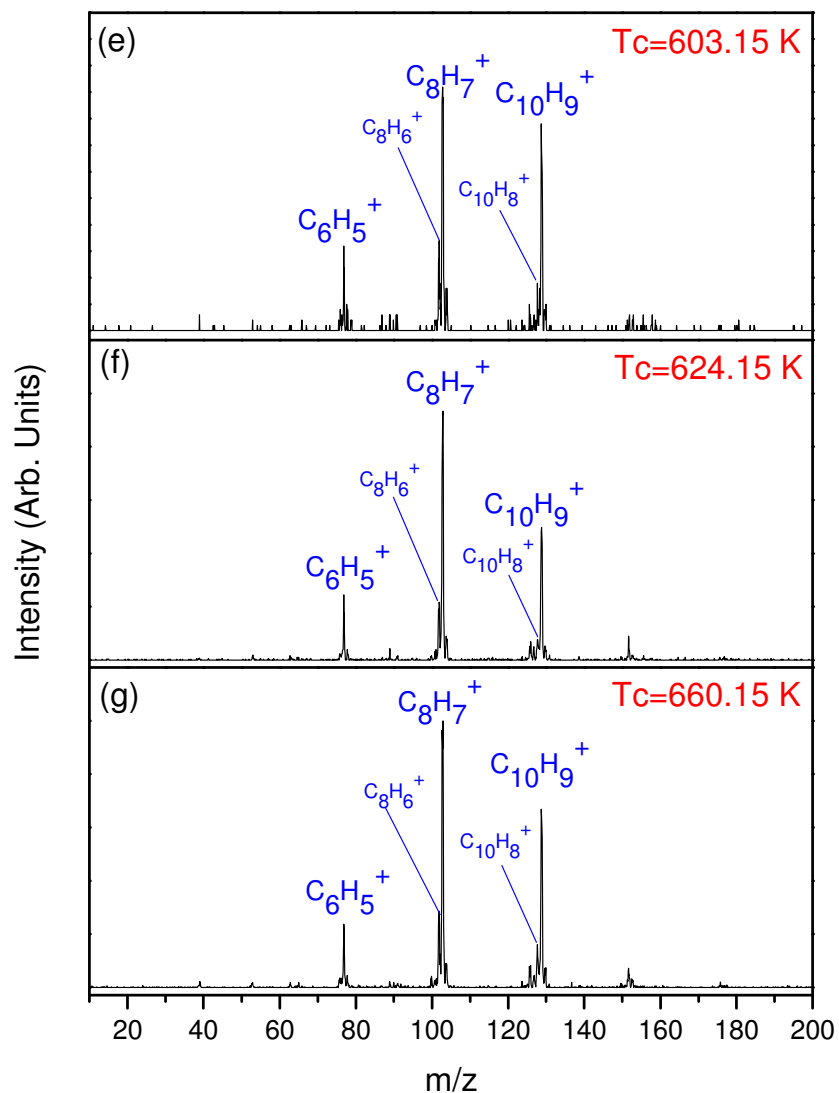
Figure 23. Mass spectra obtained upon injection of mass selected phenyl radical cation $(C_6H_5)^+$ into the drift cell. The cell field was 5.94 Vcm^{-1}, the injection energy (IE) was 13.9 eV (lab). The Cell pressure was 540 mTorr Purified C_2H_2. The temperatures ranged from 603.15 K to 660.15 K on panel (e) to (g) respectively.
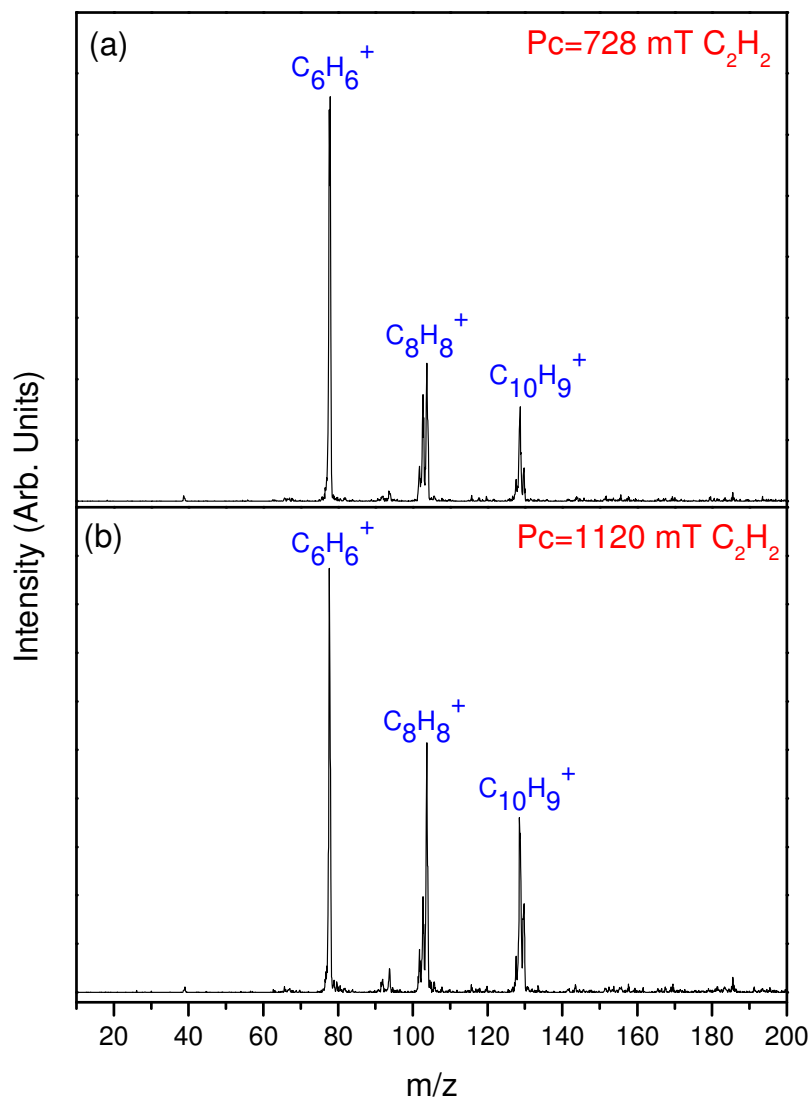
Figure 24. Mass spectrum of mass selected phenylium cation, $C_6H_5^+$, injected into the drift cell containing 728 mTorr of C_2H_2 using an injection energy of 11 eV (lab frame). The temperature of the drift cell was 623.15 K and the cell voltage was 33V.
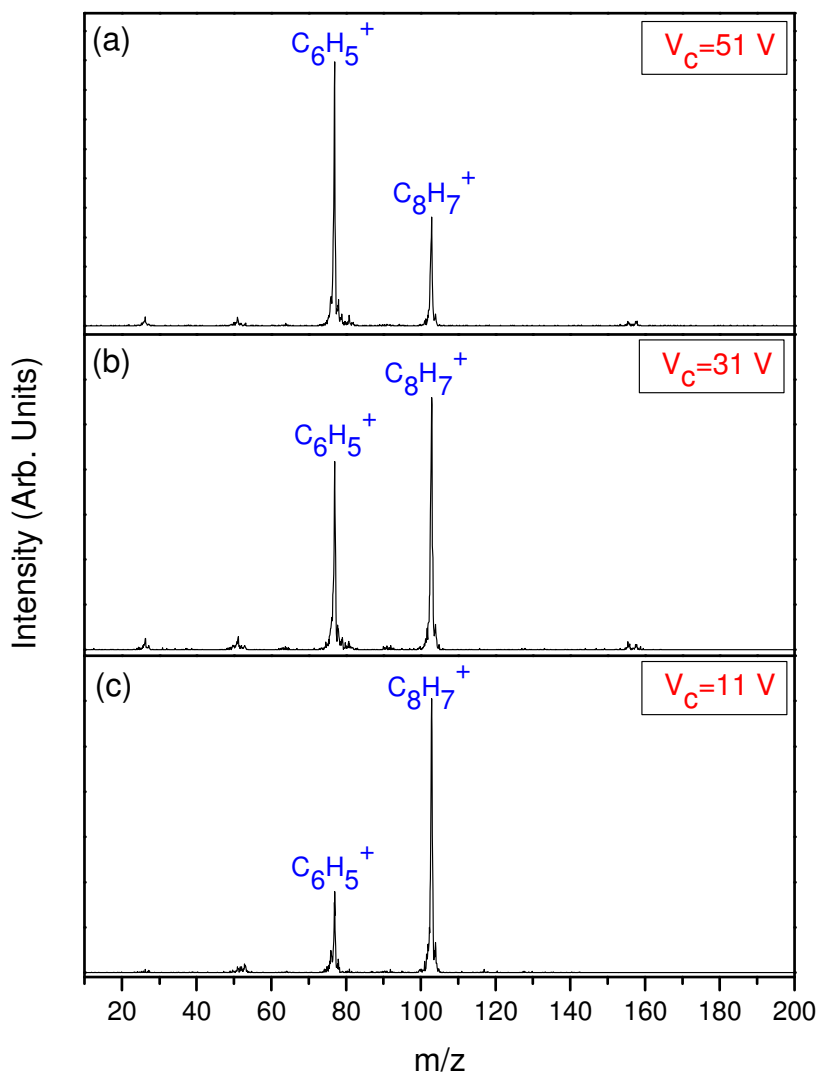
Figure 25. Mass spectrum of mass selected phenylium cation, $C_6H_5^+$, injected into the cell containing 34 mTorr of C_2H_2 and 1093 mTorr He using injection energy of 12.9 eV (lab frame). The temperature of the drift cell was 249.15 K and the cell voltage was a) 51V, b) 31V and c) 11V.
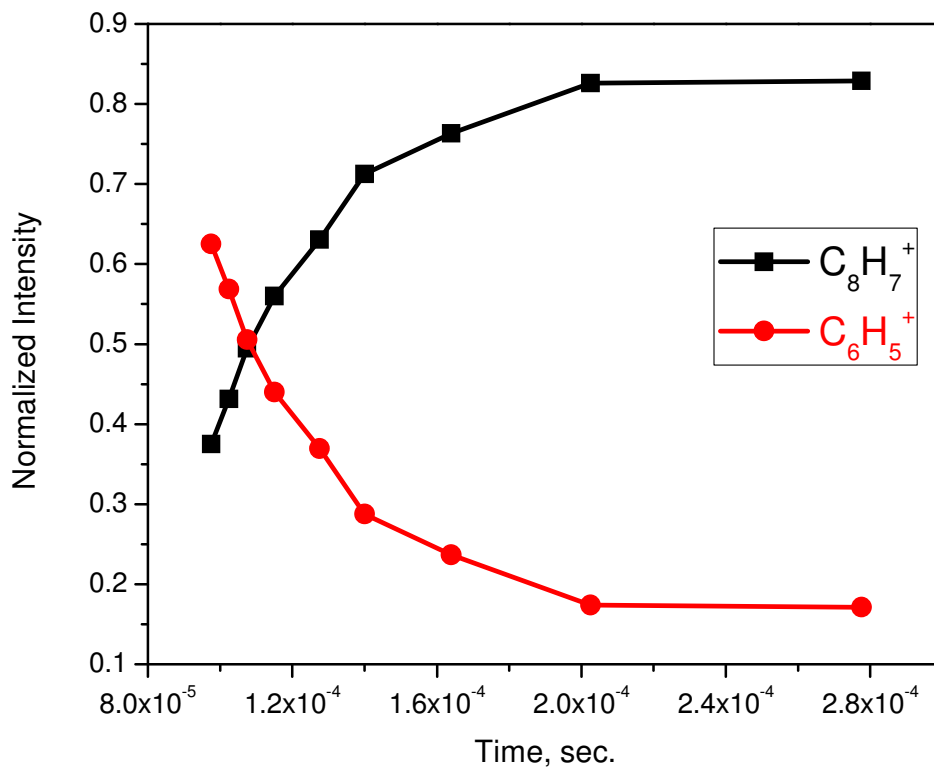
Figure 26. Integrated arrival time distribution of the reactant and product ions as a function of reaction time following the injection of phenylium cation, $C_6H_5^+$, into the drift cell containing 77m Torr acetylene at 304.6 K.

Table 5. Reaction rate coefficients of the reactions between phenylium cation, $C_6H_5^+$, and C_2H_2 using the QMS-IMS-IMS technique.

Temp K	C_2H_2 pressure mTorr	He pressure mTorr	$k_2\,cm^3.s^{-1}$
299.9	8.32	745	1.2×10^{-10}
373.9	8.32	847	8.6×10^{-11}
443.9	8.32	918	1.8×10^{-10}
305.1	6.66	755	1.8×10^{-10}
374.2	9.98	836	1.1×10^{-10}
444.2	11.23	909	1.5×10^{-10}
514.4	11.65	970	1.7×10^{-10}
305.8	9.98	767	1.3×10^{-10}
252.4	8.32	694	8.9×10^{-11}
223	4.99	646	7.0×10^{-11}
162.7	3.33	545	6.6×10^{-11}
133.2	2	486	1.5×10^{-10}
300.3	0.25	818	5.4×10^{-10}
373.5	0.25	906	8.0×10^{-10}
473.2	0.25	1019	8.3×10^{-10}
572.8	0.25	1020	8.2×10^{-10}
298.9	0.35	1215	2.4×10^{-10}
350.5	0.31	1340	5.6×10^{-10}
387.9	0.31	1386	7.5×10^{-10}
322.9	0.30	1248	6.7×10^{-10}

273.9	0.29	1144	6.2×10^{-10}
249.3	0.28	1093	7.1×10^{-10}
224.9	0.28	1029	6.4×10^{-10}
184.9	0.25	920	7.0×10^{-10}
300.7	8.32	554	1.2×10^{-10}
300.5	16.64	553	6.3×10^{-11}
300.8	31.14	553	1.3×10^{-11}
300.1	0.08	886	3.9×10^{-10}
300.1	0.30	886	4.8×10^{-10}
300.2	0.49	886	5.7×10^{-10}
300.2	0.72	889	2.9×10^{-10}
300.3	0.43	884	2.8×10^{-10}
306.8	0.28	822	8.0×10^{-10}
306.1	0.18	822	9.1×10^{-10}
306.3	0.56	822	7.5×10^{-10}
304.5	0.77	822	7.1×10^{-10}
300.5	8.32	547	1.1×10^{-10}
300.5	8.32	1102	9.4×10^{-12}
300.5	8.32	1701	4.8×10^{-12}
300.2	6.66	413	1.9×10^{-10}
300.1	6.66	758	1.3×10^{-10}
300.2	6.66	1614	8.9×10^{-10}
299.7	8.32	1205	1.1×10^{-10}

299.7	8.32	1672	7.1×10^{-11}
299.7	8.32	2074	2.9×10^{-11}
300.2	0.49	886	5.7×10^{-10}
300.2	0.49	1212	5.9×10^{-10}
300.2	0.49	1600	4.4×10^{-10}
300.3	0.23	394	1.0×10^{-9}
300.3	0.23	800	1.0×10^{-9}
300.3	0.26	1600	7.1×10^{-10}
300.4	0.26	2000	7.0×10^{-10}
300.1	0.27	400	4.0×10^{-10}
300.2	0.29	802	4.6×10^{-10}
300.1	0.24	1203	4.6×10^{-10}
300.1	0.24	1597	4.8×10^{-10}
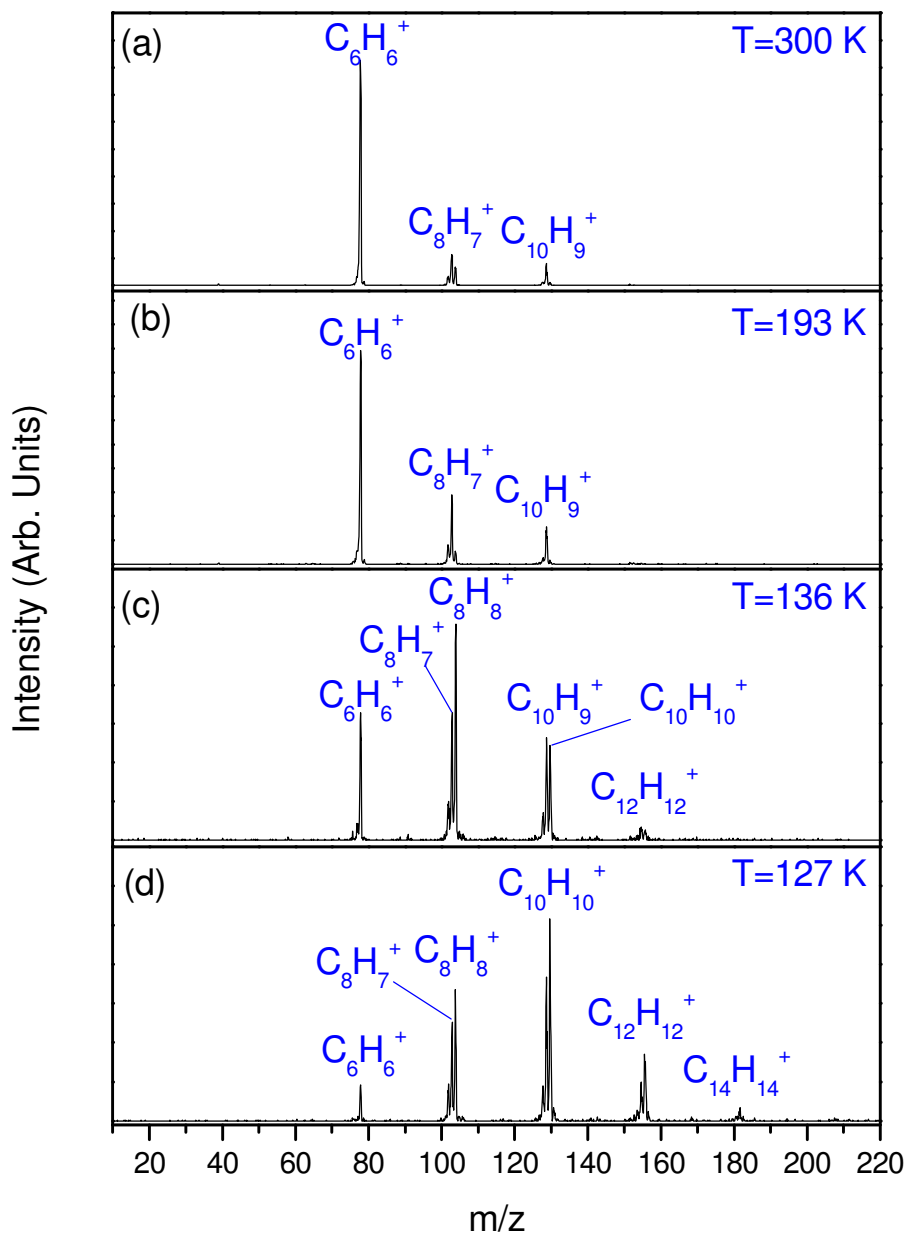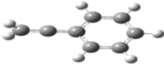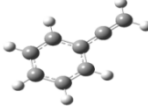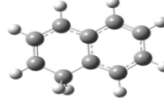
Figure 27. Mass spectra obtained upon injection of mass selected benzene fragment cation $(C_6H_5)^+$ into cell containing purified acetylene at different temperatures. The cell field was 7.4 Vcm^{-1}, the injection energy (IE) was 11.6 eV (lab), and the cell pressure was 300, 193, 136 and 127 K for panel (a) to (d) respectively.
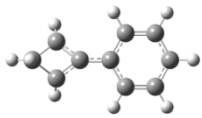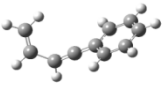
4.2.1.3 Theoretical Calculations of the possible isomers of the first and second additions of (C_2H_2) to $C_6H_5^+$

Several possible isomers of the first and second additions of (C_2H_2) to phenylium cation have been optimized by the ab initio calculations at the B3LYP/6-31+G** level. Table 6 represents different possible isomers for the first and second additions of acetylene to phenylium cation, $C_6H_5^+$. All the examined structures are the covalent structures. For the first acetylene molecule added to the phenylium cation, the lowest energy structure was found to be for the isomer (Phac1) with binding energy of 101 Kcal.mol^{-1} assuming the interaction of $C_6H_5^+$ with C_2H_2. These strong binding (as twice as observed for the benzene radical cation with acetylene) could explain the fast interaction of the phenylium cation with acetylene.

Also, possible isomers for the second addition were calculated at the same level of theory. The Bittner-Howard mechanism was favored as expected to produce the most stable covalent isomers. Isomers (Ph2ac2) and (Ph2ac3) show slightly higher relative energies, 1.8 and 5.1 Kcal.mol^{-1} respectively. The most stable calculated isomer was (Ph2ac1) isomer which is the protonated naphthalene isomer. Cyclization and ring closure was predicted theoretically to be exothermic with a barrier in the range of (7-30 Kcal.mol^{-1}).[59]

Table 6. Proposed structures of the products of the addition of acetylene (1st and 2nd addition) to $C_6H_5^+$

	$C_6H_5^+ + C_2H_2$			
Isomer	Structure	Method/Basis Set	Relative E	B.E. kcal.mol^{-1}
Phac1		B3LYP/6-31+G**	0	-101
Phac2		B3LYP/6-31+G**	61.7	-39.4
	$C_6H_5^+ + 2\ C_2H_2$			
Ph2ac1		B3LYP/6-31+G**	0	-159.2

Ph2ac2		B3LYP/6-31+G**	1.8	-157.5
Ph2ac3		B3LYP/6-31+G**	5.1	-154.1

4.2.1.4 Ion mobility measurement of phenylium cation

Phenylium cations were believed to have many possible isomers, depending on the utilized phenyl cation precursor. Alkyl benzene and alkyl benzene derivatives were used under electron impact ionization to produce $C_6H_5^+$ ions which have been assumed to be cyclic phenyl ions. However, the $C_6H_5^+$ ions produced from alpha-chlorobenzene and ethylbenzene are formed by a process involving ring cleavage.[163-164] The cyclic isomer was unreactive towards the reactions with acetylene, and two higher energy acyclic isomers are reactive towards the acetylene reactions according to Eyler et al.[159] Nevertheless, due to the low pressure in the ICR experiment and consequently the low collisions in this experiment, could be the case, while in the flow tube where there are much more collisions, would favor the lower energy phenylium isomer.[43] The reactions of the phenylium cation $C_6H_5^+$ with acetylene are possible in the flow tube where the pressure was 100 Torr acetylene in presence of methanol and proceed at room temperatures.

In order to investigate the structure of the phenylium cation, the mobility measurements were carried out to get insight about the geometry of the phenylium cation. The phenylium cation was injected into the drift cell, in 20 µs pulses, containing 3.082 Torr He. The voltage of the drift cell varied from 32 V to 20 V with corresponding E/N 6.44 to 4.01 Td which represents weak electric filed required for mobility measurements. The plot of the ATDs of the $C_6H_5^+$ ion pulses at different cell voltage represented in Figure 29. The plot of P/V against the time of $C_6H_5^+$ cation spent in the drift cell represented in Figure 28. The measured and calculated mobility and corresponding collision cross

sections are tabulated in Table 7. The value of the measured mobility was 11.58 $cm^2.V^{-1}.s^{-1}$ and the corresponding measured collision cross section is 47.20 $\mathring{A}^2$. The calculated mobilities of both the singlet and triplet states of the phenylium cation were 11.70 and 11.60 $cm^2.V^{-1}.s^{-1}$ respectively, with the corresponding collision cross sections of 46.69 and 47.11 $\mathring{A}^2$ for the singlet and the triplet states respectively. These results provide an evidence for the existence of the phenylium cation through the course of our experiments in the form of cyclic structure not the open isomer as suggested by Eyler et al.[159]
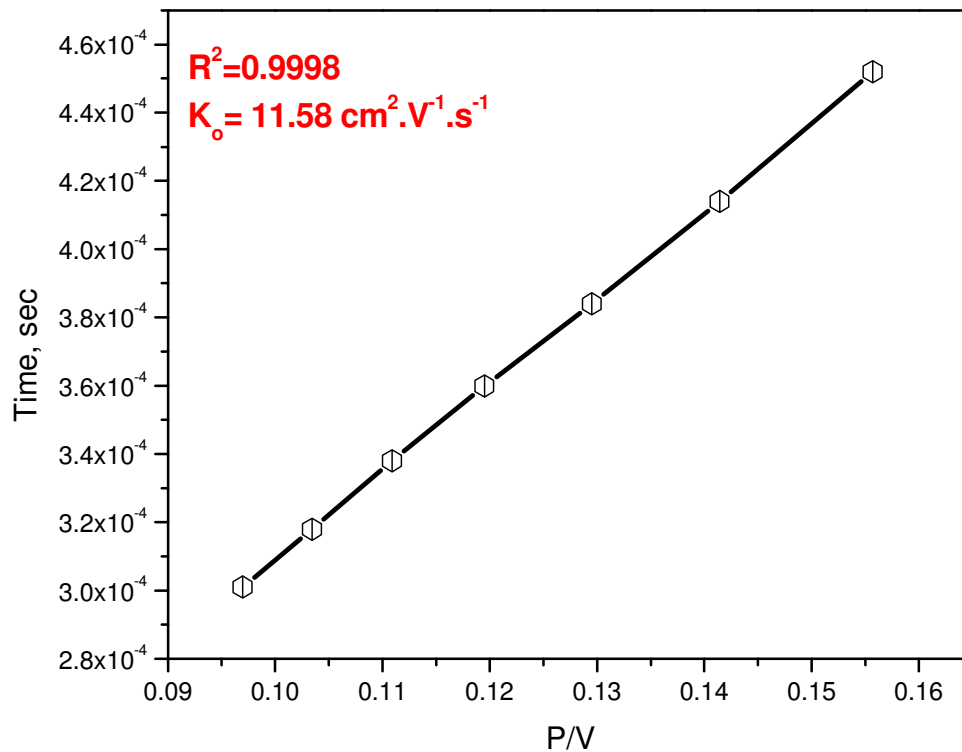
Figure 28. Plot of arrival time vs. P/V for $C_6H_5^+$, 20 μs ion pulse into a drift cell filled with 3.082 Torr He at different cell voltages (32-20 V).
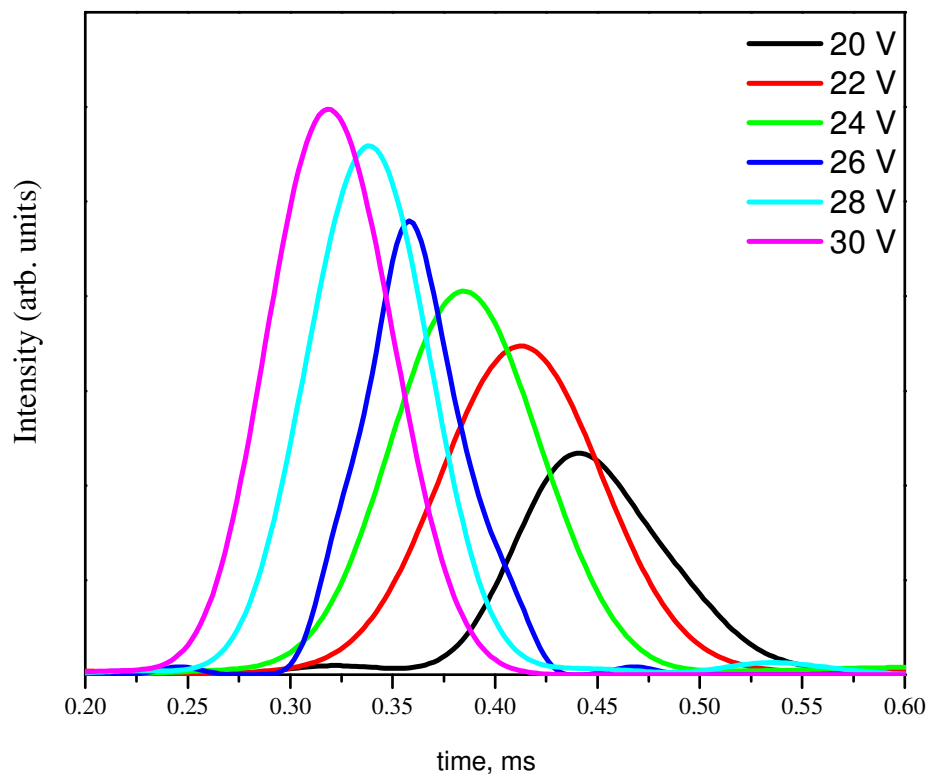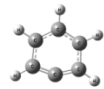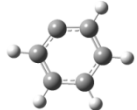
Figure 29. The arrival time distributions (ATDs) of injecting $C_6H_5^+$ (20 μs ion pulses) into the drift cell filled with 3.083Torr He at different cell voltages (30-20 V). Injection energy is 18.8 eV (lab frame). The earlier ATD corresponds to drift cell voltage of 30V and the later ATD corresponds to drift cell voltage of 20 V. The cell temperature was 301.5 K.

Table 7. Measured and calculated mobilities and the corresponding collision cross sections of phenylium cation.

	T K	K_o cm^2.V^{-1}.s^{-1}	Ω Å^2	Structure
Phenylium ion (measured value)	301	11.6	47.2	
Singlet $^1A_1$ (Calc.)	301	11.7	46.7	
Triplet $^3B_1$ (Calc.)	301	11.6	47.1	

4.2.2 Phenylium cation/C_6D_6 ion-molecule reactions

The phenylium cation reactions with other aromatic moieties are of great importance for the formation of PAHs in combustion processes and interstellar clouds. The reactions reported in the previous sections represent the coupling reactions of aryl cation with acetylene for PAHs formation in combustion and interstellar medium. The coupling reaction of aryl-aryl bond formation is of fundamental interest in modern organic chemistry [168] and it is achieved through cross coupling reactions of aryl halides and organometallic complexes.[169-171] Ascenzi et al.[172] reported the reaction mechanism of phenylium ions with benzene. The main product of those reactions was the $C_{12}H_{11}^+$ cation which represents the covalent adduct. Also, $C_{12}H_{10}^+$, $C_{12}H_9^+$, $C_{10}H_9^+$ and $C_9H_7^+$ cations were detected as minor products. The $C_{12}H_{11}^+$ cation was believed to be the protonated biphenyl cation. According to those results, the plasma producing phenylium cation plays the same role of the metal catalysts in the aryl-aryl bond formation. Biphenyl is one of the major products of the radiolysis of benzene.[173-174] The mechanism of formation of the biphenyl subjected to a lot of debate in the literature, and one of these possible mechanisms is the ion-molecule reactions.[173-175] The ionic mechanism is supported over the radical one as the overall rate constant for the later one is very small $\sim 8.4 \times 10^{-16}$ $cm^3.s^{-1}$ at 300 K as predicted from equation (4.14).

$$C_6H_5^{\bullet} + C_6H_6 \longrightarrow C_{12}H_{11}^{\bullet} \qquad (4.14)$$
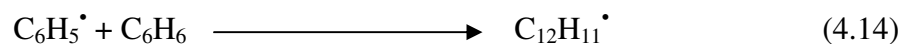
Note also that, it cannot be used for the explanation of the production of the biphenyl in pyrolysis of benzene.[176-177] The formation of $C_{12}H_{11}^{\bullet}$ and the biphenyl like compounds could also be produced from the addition of C_6H_7 to C_6H_4 as predicted from the high

temperature quantum chemical molecular dynamics simulations on the PAHs formation during combustion of benzene with varying H/C ratios.[2]

In this part, we present the reactions of the phenylium cation with benzene-d_6 as an example of the aryl-aryl reactions that could produce PAHs.

4.2.2.1 Results and discussions

The fragmentation of benzene is carried out using high electron energy in the EI source in order to obtain the phenylium cation as shown in Figure 30 and as described in the previous section. Upon the injection of phenylium cation into very low C_6D_6 pressure, Figure 31 (a), the following products are observed,

$$C_6H_5^+ + C_6D_6 \longrightarrow C_6H_5.C_6D_6^+ \qquad (4.15)$$
$$\longrightarrow C_6D_6^+ + C_6H_5 \qquad (4.16)$$
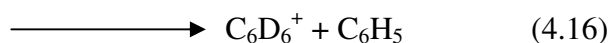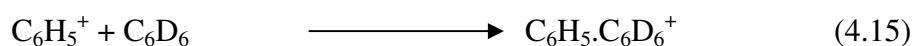
The phenylium cation reacts with C_6D_6 to form the d-biphenyl adduct, $C_6H_5.C_6D_6^+$ as shown in equation (4.15). At higher pressure of C_6D_6, the formation of the $(C_6D_6)_2^+$ dimer cation becomes the major peak as shown in Figure 31 (c to e). The detection of $C_6D_6^+$ cation could be explained by direct charge transfer from the benzene cation or the phenylium cation injected into the drift cell as represented by equation (4.16). The formed $C_6D_6^+$ cation could further reacts with another C_6D_6 molecule to produce the benzene dimer cation, $(C_6D_6)_2^+$ as shown in equation (4.17).

$$C_6D_6^+ + C_6D_6 \longrightarrow (C_6D_6)_2^+ \qquad (4.17)$$
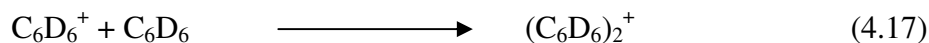
The reactions of phenylium cation with C_6D_6 were followed at wide range of temperatures, 239.2 K to 623.2 K, as shown in Figure 32. The $(C_6D_6)_2^+$ cation is observed at low temperatures. However, at higher temperatures, the dimer dissociates due to its weak

binding energy, 17 kcal.mol^{-1},[178] compared to the covalent adducts. Meanwhile, the formed adduct, $C_6H_5.C_6D_6^+$, shows high stability at high temperatures as shown in Figure 32 (d-f). The high intensity of the $C_6D_6^+$ cation at high temperatures could be produced from the charge transfer as mentioned before or by partial decompositions of the formed. The appearance of the $C_6H_5.C_4D_5^+$ cation at high temperatures, which could be protonated naphthalene, could be attributed to the following reaction;

$$C_6H_5^+ + C_6D_6 \longrightarrow C_{10}H_4D_5^+ + C_2D \qquad (4.18)$$
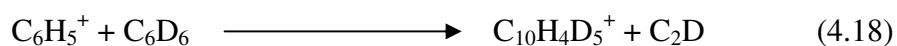
This reaction was predicted previously by Lifshitz et al.[179] The stability of these adducts at high temperatures may be attributed to their covalent character.

The kinetics of the reaction (4.15) was studied and the reaction rate coefficient k_2 was measured and the results are included in Table 8. Figure 33 represents the integrated arrival time distribution of the reactants and products ions of the reaction time following the injection of $C_6H_5^+$ into C_6D_6 in the drift cell.
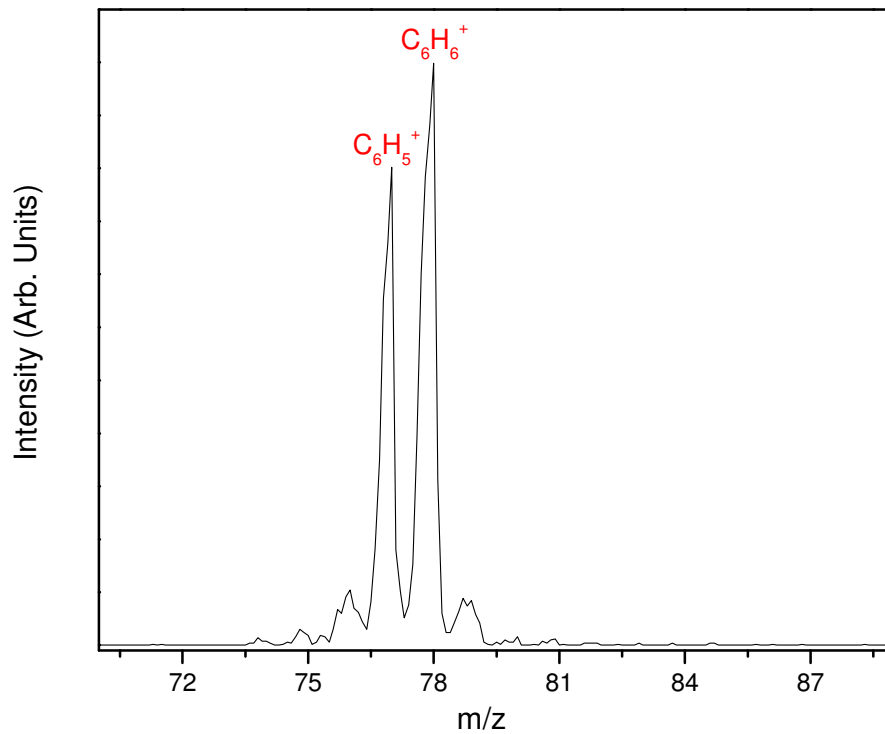
Figure 30. Mass spectra obtained upon injection of mass selected phenylium cation, $C_6H_5^+$, in the drift cell containing 638 mTorr He. Ionization energy was 14 eV (Lab Frame). Voltage across the drift cell was 5.6 V.Cm^{-1}. Temperature of the drift cell was 298.15 K.
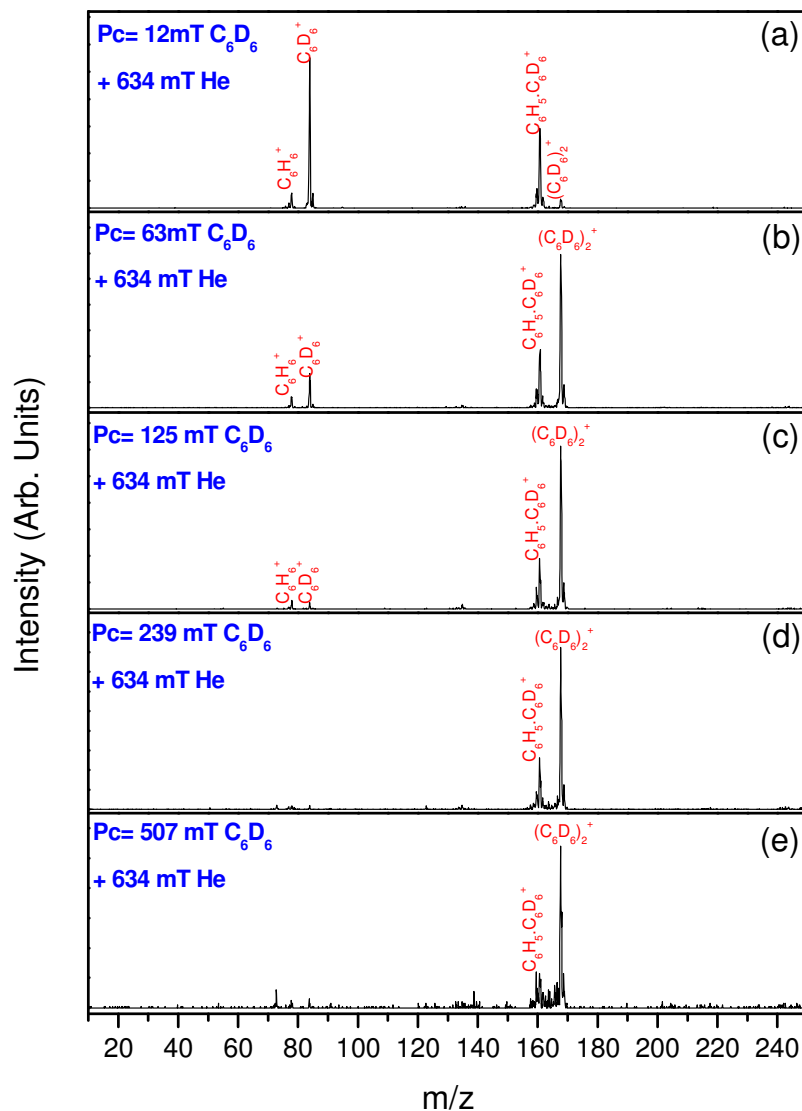
Figure 31. Mass spectra obtained upon injection of phenylium cation, $C_6H_5^+$, into the drift cell . Cell temperature was 299.15 K. IE used was 16.9 eV (Lab frame). Voltage across the cell was 6.4 V.cm-1. Pressure inside the drift cell was mixed He, 634 mTorr, with C_6D_6 as follows: a) 12 mTorr, b) 63 mTorr, c) 125 mTorr, d) 239 mTorr and e) 507 mTorr from up to bottom.
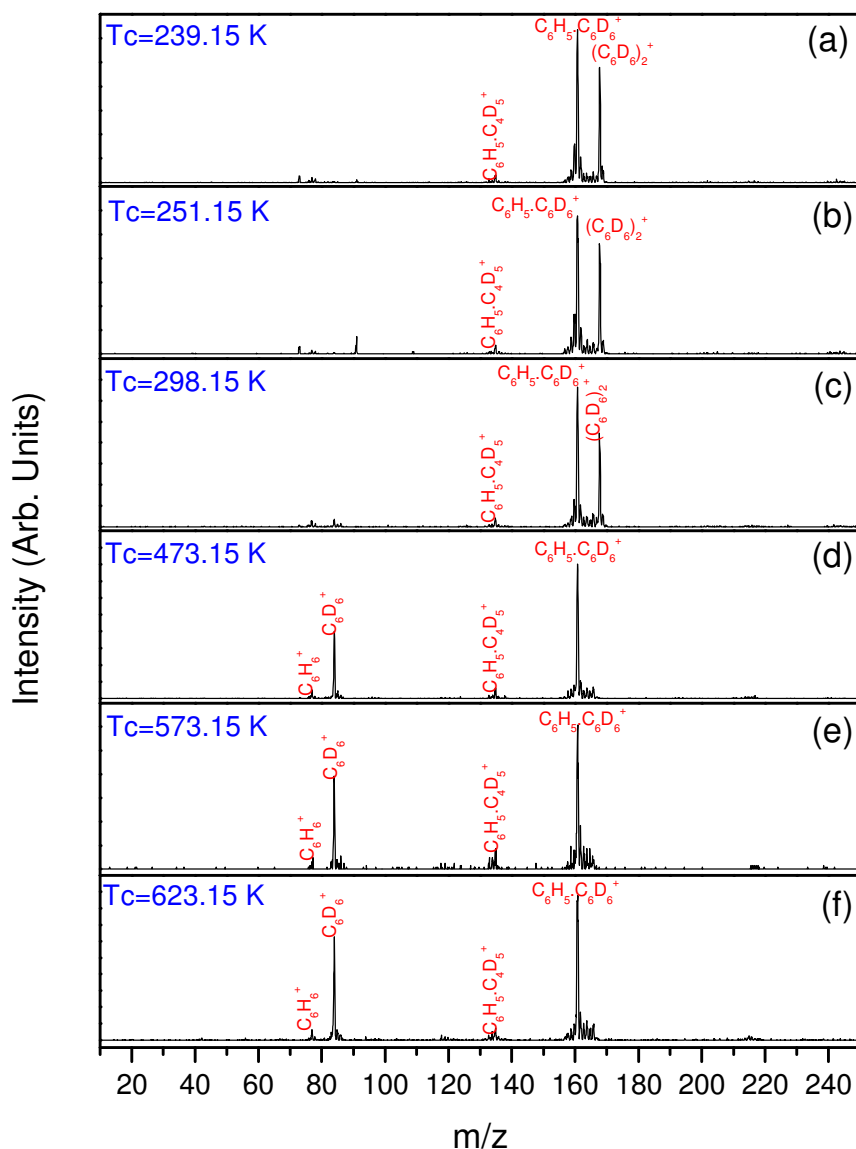
Figure 32. Mass spectra obtained upon injection of phenylium cation, $C_6H_5^+$, into the drift cell . IE used was 14 eV (Lab frame). Voltage across the cell was 5.6 V.cm^{-1}. Pressure inside the drift cell was mixed He/C_6D_6; 104 mTorr/621 mTorr respectively. Cell temperature was; a)239.15 K, b) 251.15 K, c)298.15 K, d)473.15 K, e) 573.15 K and f) 623.15 K from up to bottom respectively.
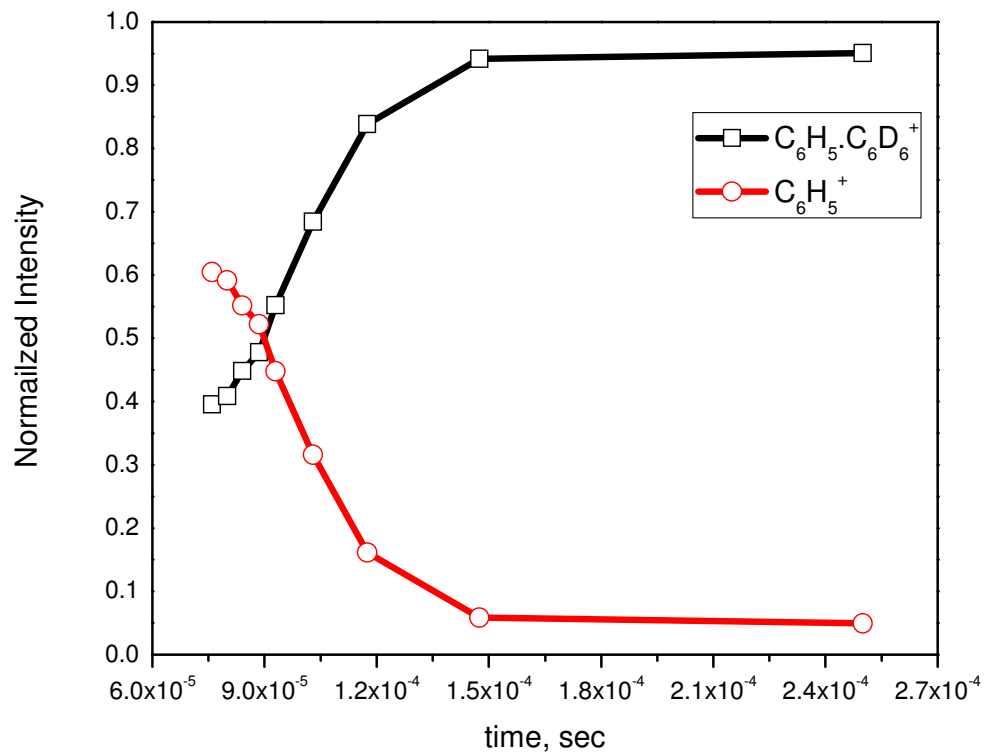
Figure 33. Normalized intensities of the reactions and products ions of the reactions between the phenylium cation, $C_6H_5^+$, with C_6D_6.

Table 8. Reaction rate coefficient of the reaction of $C_6H_5^+$ with C_6D_6

Temp. K	P C_6D_6 mTorr	k_2 $cm^3.s^{-1}$
299	0.462 (1004 mTorr He)	2.0×10^{-9}
299	0.424 (625 mTorr He)	2.7×10^{-9}

4.3 Phenylacetylene radical Cation/C_2H_2 System

4.3.1 Introduction

The chemical kinetics and dynamics of small molecules, such as acetylene, reactions with unsaturated hydrocarbons are of crucial importance in understanding the formation of PAHs in combustion processes,[2] interstellar medium,[10] and the solar system.[16] The reactions of acetylene with different ionic hydrocarbons are of a particular interest to understand the synthesis of complex organics in hydrocarbon-rich atmospheres such as of Saturn's moon Titan.[4,61,180-182] PAHs and their corresponding PANHs are believed to be responsible for the formation of Titan's aerosol-particle based haze layers.[7] Phenylacetylene has been subject to intense studies as a typical precursor for the formation of the PAHs in the gas phase[62,180,183-189] and on metal nanoparticles.[190-194] Phenylacetylene is believed to form naphthalene upon reactions with acetylene.[195] Many studies show the possibility of producing phenylacetylene through a loss of acetylene molecule from naphthalene fragmentation and this route was the most favored one.[196-199] The $C_8H_6^+$ cations produced from the loss of acetylene molecule from naphthalene could be also benzocyclobutadiene as well as phenylacetylene.[200] The energy difference between these two isomers is about 4 kcalmol^{-1}. The benzocyclobutadiene is also observed in the high temperatures molecular beam experiments done by Friedrichs et al.[201] where the o-benzyne radical were reacted with acetylene, ethene and propene in order to investigate the mechanism of soot formation in combustion environments.

Herein, we expand our studies to investigate the formation of PAHs through the ion-molecule reactions of phenylacetylene radical cation with acetylene. The mass selected

phenylacetylene monomer and dimer cations were injected into the drift cell to investigate the possible interactions of the selected cations with acetylene. These experiments will provide information of the possible mechanisms of the formation of PAHs especially in interstellar media and solar nebulae.

4.3.2 Results and Discussions

4.3.2.1 Reactions of $C_8H_6^{\bullet+}$ with C_2H_2

Phenylacetylene radical cations were produced by electron impact ionization technique of a He gas seeded with phenylacetylene vapor. The $C_8H_6^{\bullet+}$ radical cation were mass selected and injected into the drift cell. The mass selection of the $C_8H_6^{\bullet+}$ is shown in Figure 34 where the cell temperature was 302.2 K and the cell pressure was attained at 1 Torr He. Injection of phenylacetylene radical cations into the drift cell containing acetylene, as the only observed product is $C_{10}H_8^+$ corresponding to m/z=128 as shown in Figure 35 (a) which is believed to be naphthalene isomer, as shown in the following equation,

$$C_8H_6^{\bullet+} + C_2H_2 \longrightarrow C_{10}H_8^{\bullet+} \qquad (4.19)$$
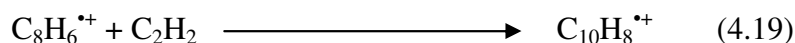
This reaction is independent of acetylene pressure as shown in Figure 35 where, the acetylene pressure increased in the drift cell from ~200 mTorr to ~1600 mTorr from panel (a) to (d) respectively. At high acetylene pressures, the m/z=129 corresponding to the protonated naphthalene isomer is observed as well.

The addition of acetylene to the phenylacetylene cation is limited only to one molecule. The stability of the formed adduct was tested thermally to determine its type

either is it a covalent or van der Waal's adduct. The drift cell was filled with C_2H_2 and the temperature increased from 302.2 K up to 573.2 K as shown in Figure 36. The formed adduct, $C_{10}H_8^+$, is stable at the all temperature range as shown in Figure 36 which is a good indication of its covalent nature. No further additions of acetylene onto the phenylacetylene cation were observed at high temperatures. Interestingly, at very high temperature, 573.15 K, the inset of panel (e) of Figure 36 shows peaks of $(C_2H_2)_n^+$ cations where n=6-11. These interesting ions could be formed through further addition of acetylene molecules to the formed adducts at high temperatures and in the presence of active species such as C_2^+ and C_2H^+ [202-203] under these high temperatures will explain the higher products, up to $(C_2H_2)_{12}^+$, formed under these conditions.

The reaction rate coefficient of the addition of acetylene molecules to phenylacetylene radical cation was measured through the kinetic studies. ATDs intensities of the reactants and products ions were measured as a function of time upon the injection of phenylacetylene radical cation into the drift cell containing 56 mTorr C_2H_2 and 914 mTorr He. Residence time had been changed from 10 ms to 40 ms by varying the applied filed across the drift cell. The ratios of the reactions to the products had been changed by changing the residence time as shown in Figure 37. Figure 38 present the normalized intensities of ion signals as a function of reaction time following the injection of $C_8H_6^{•+}$ radical cation into the drift cell filled with $P(C_2H_2)$=56 mTorr and the He partial pressure was 914 mTorr at 300 K. The rate coefficient for the overall reaction to form products is in the order of $1.3(\pm0.3)\times10^{-12}$ $cm^3.s^{-1}$,which is about 3 orders of magnitude smaller than the collision rate (10^{-9} $cm^3.s^{-1}$), as shown in Table 9. This suggests that the back-dissociation

of the excited complex $(C_8H_6^{\bullet+}\bullet C_2H_2)^*$ occurs at a rate faster by a factor of 1000 than the forward reaction to form products. The rate coefficient of this reaction was found to be independent of temperature and third body as well.
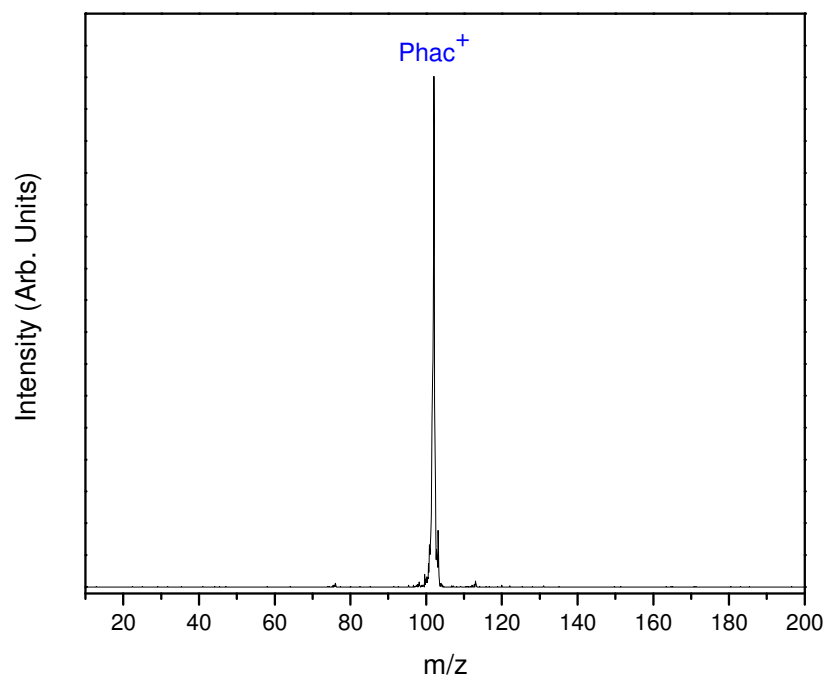
Figure 34. Mass spectra of mass selected phenylacetylene radical cation (m/z=102) injected into the drift cell containing 1 Torr He. Cell voltage was 8.4 V.cm^{-1}. Injection Energy was 20 eV (lab Frame). Cell Temperature was 302.15 K.
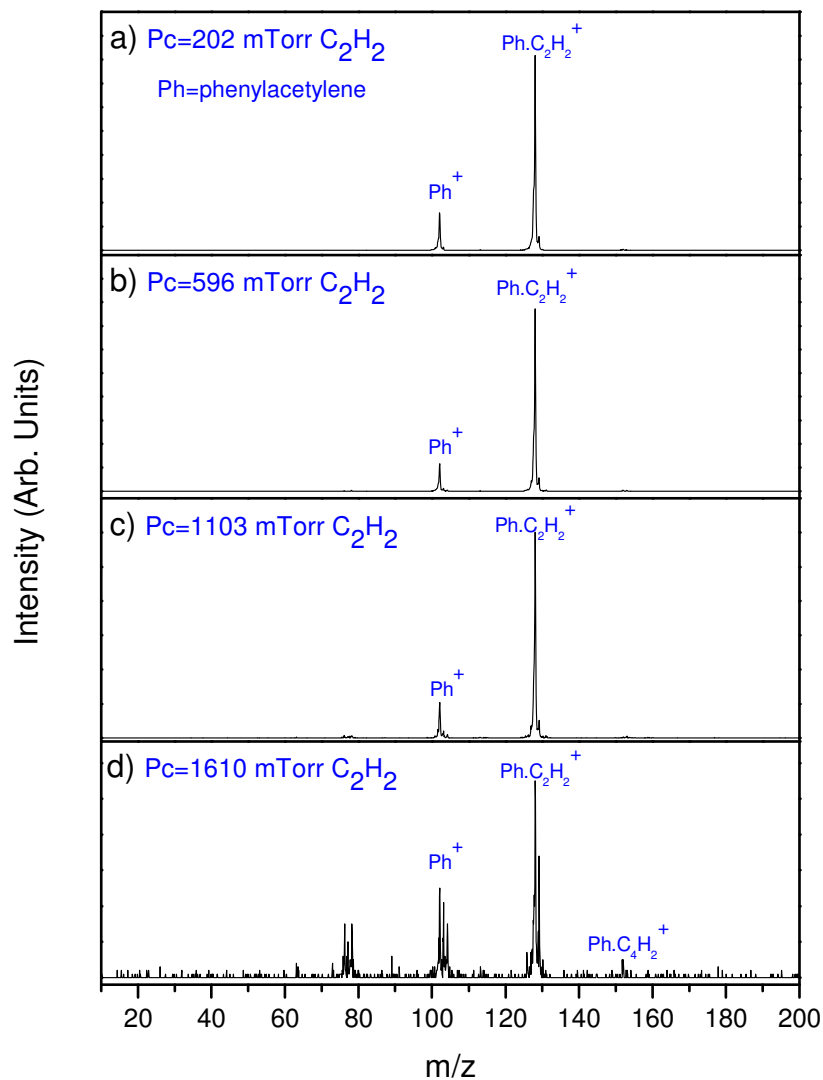
Figure 35. Mass spectra of injected Phenylacetylene radical cations into the drift cell. Cell temperature was 302.15 K. Cell voltage was 8.4 V.cm^{-1}. Injection Energy was 20 eV (lab Frame). Cell pressure varied from 202 mTorr to 1610 mTorr acetylene from panel (a) to (d) respectively.
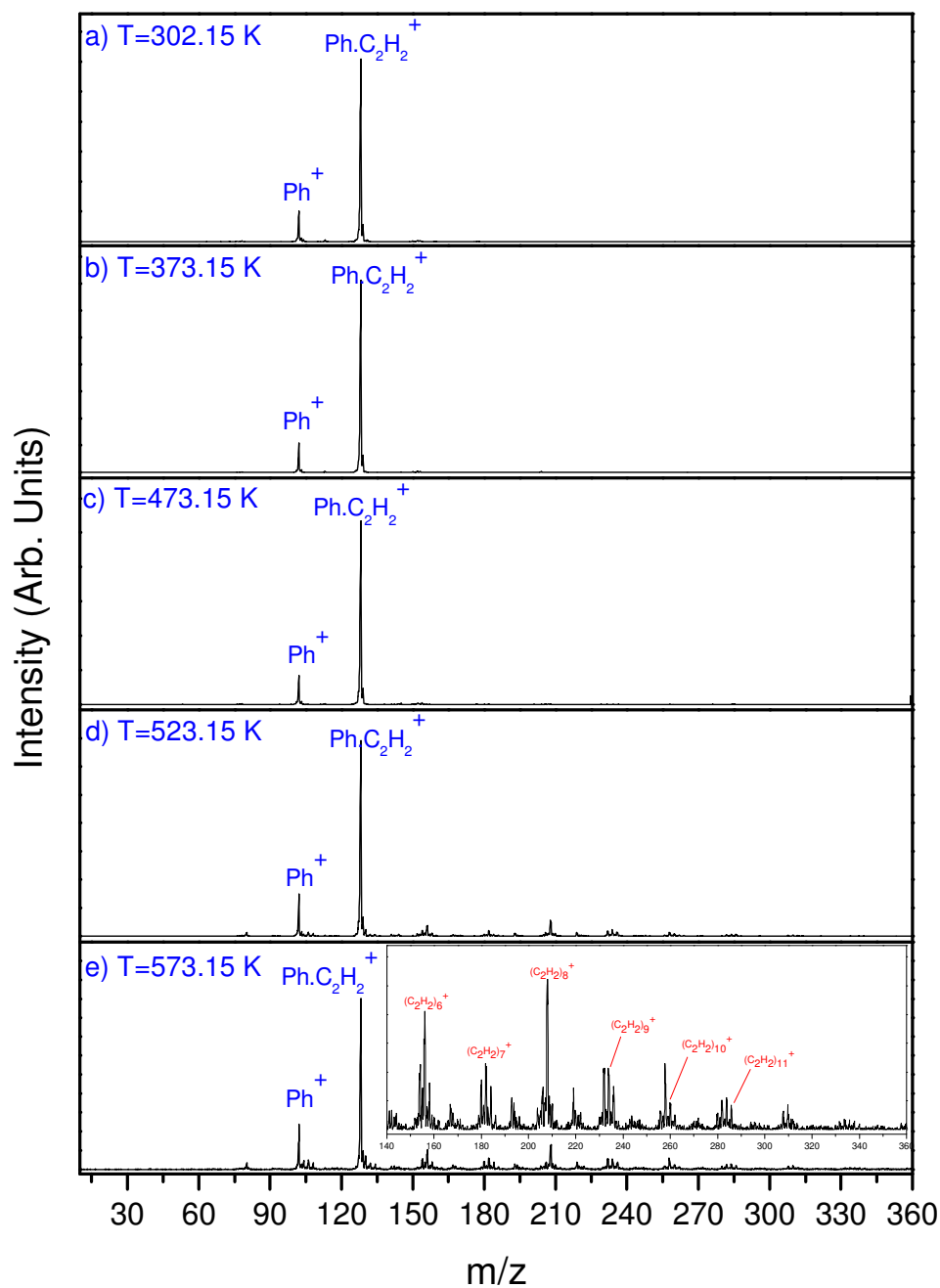
Figure 36. Mass spectra of injected mass selected Phenylacetylene radical cations into the drift cell containing 620 mTorr purified C_2H_2. Cell voltage was 7.6 V.cm^{-1}. Injection Energy was 13 eV (lab Frame). Cell temperature varied from 302.15 K to 573.15 K from panel (a) to (e) respectively.
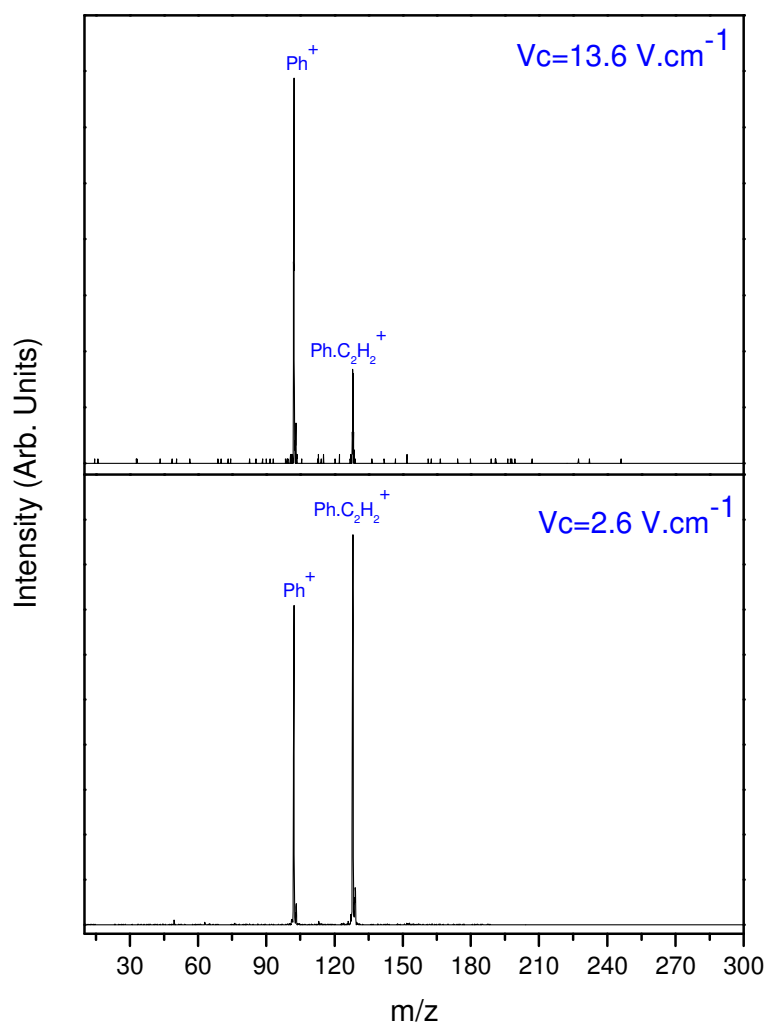
Figure 37. Injection of mass selected phenylacetylene cation into the drift cell containing 56 mTorr C_2H_2 in 914 mT He. IE=14.9 eV (Lab), Tc=300 K.
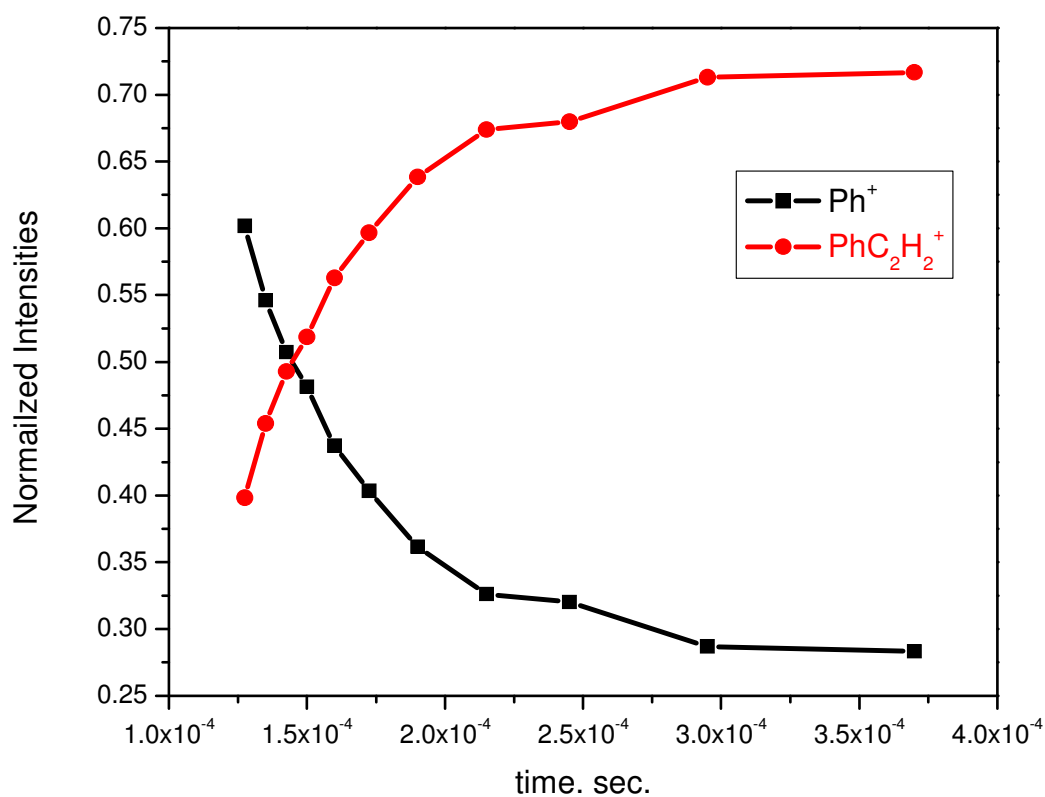
Figure 38. Normalized intensities of ion signals as a function of reaction time following the injection of $C_8H_6^{\bullet+}$ radical cation into the drift cell filled with $P(C_2H_2)$=56 mTorr and the He partial pressure was 914 mTorr at 300K.
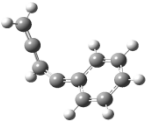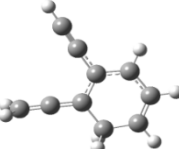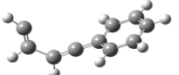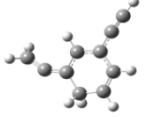
Table 9. Rate coefficients of the reactions between phenylacetylene radical cation with acetylene.

T K	P C_2H_2 mTorr	P He mTorr	k_2 cm^3.s^{-1}
300.3	67	970	1.5×10^{-12}
300	50	1044	1.2×10^{-12}
300	110	1027	1.4×10^{-12}
300	210	1154	1.1×10^{-12}
300.4	102	1780	1.4×10^{-12}
336.2	102	1067	1.3×10^{-12}
223.2	102	869	1.0×10^{-12}

Several possible isomers of the addition of (C_2H_2) to phenylacetylene radical cation have been optimized by the ab initio calculations at the UB3LYP/6-31+G** level. Table 10 represents different possible isomers for the addition of acetylene to $C_8H_6^{.+}$. All the examined structures are the covalent conformers. The lowest energy isomer found was (Phac1) where acetylene molecule added to the phenylacetylene cation following the Bittner-Howard mechanism.

The addition of acetylene was perpendicular to the plane of the phenylacetylene radical cation are shown in Table 10 (Phac1). The calculated structure where both acetylene and phenylacetylene radical cation were in the same plane, (Phac3), has relatively higher energy, 14 Kcal.mol^{-1}. The addition of acetylene to the aromatic ring in the phenylacetylene radical cation was found to have higher relative energies (8 and 17.5 Kcal.mol^{-1} for isomers Phac2 and Phac4 respectively). Cyclization of isomer (Phac1) could occur to produce the naphthalene radical cation as predicted. Calculated mobilities and collision cross sections of isomer (Phac1) will be discussed in the following section.

Table 10. Proposed structures of the products of the addition of acetylene to $C_8H_6^{.+}$

Isomer	Structure	Method/Basis Set	Relative E.	Binding E. kcal.mol^{-1}
Phac1		UB3LYP/6-31+G**	0	-34.8
Phac2		UB3LYP/6-31+G**	8	-26.8
Phac3		UB3LYP/6-31+G**	14	-20.8
Phac4		UB3LYP/6-31+G**	17.5	-17.3

4.3.2.2 Mobility Measurements

Ion mobility measurements of the phenylacetylene radical cation were conducted in He, and the results are tabulated in Table 11. The average measured mobilities of phenylacetylene radical cation were found to be 9.5 $cm^2.V^{-1}.s^{-1}$ and the average calculated mobilities were found to be 8.8 $cm^2.V^{-1}.s^{-1}$. The measured and calculated collision cross sections for the phenylacetylene radical cation were 57.5 and 61.5 $Å^2$ respectively.
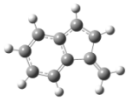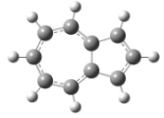
The ion mobilities and collision cross section of the $C_{10}H_8^{.+}$ produced from equation (4.19) were measured and were 7.3 $cm^2.V^{-1}.s^{-1}$ and 74.6 $Å^2$ respectively. The product ion was formed by injecting phenylacetylene radical cation into the drift cell which contain a mixture of acetylene/He (0.142 Torr purified C_2H_2/ 2.878 Torr He). The product ion will be formed at the entrance of the drift cell due to escaping acetylene molecules and then thermalized through the collision with He molecules while moving across the drift cell under the weak electric field regime. The calculated mobilities and collision cross sections for the product ion, (calculated for isomer (Phac1) obtained from the ab initio calculations), were found to be 8.1 $cm^2.V^{-1}.s^{-1}$ and 67.2 $Å^2$ respectively. These results indicate that the proposed structure of the product ion is not the only possible structure. Also, it is not the naphthalene isomer as the average measured mobilities of naphthalene is 8.7 $cm^2.V^{-1}.s^{-1}$ and the average collision cross section of naphthalene radical cation is 62.8 $Å^2$. The mobilities and collision cross sections of different possible isomers were also calculated. The calculated average mobility and collision cross section for azulene were 8.7 $cm^2.V^{-1}.s^{-1}$ and 62.8 $Å^2$ respectively. Calculated mobilities and collision cross section of 1H-indene,1-methylene isomer were also found to be 8.7 $cm^2.V^{-1}.s^{-1}$ and 62.8 $Å^2$

respectively. These results indicate that the formed adduct $C_{10}H_8^{.+}$ has different structure than naphthalene, azulene or 1H-Indene-1-methylene isomers and could be a mixture of different possible isomers of $C_{10}H_8^{.+}$ radial cation.

The measurements of the ion mobilities and their corresponding cross sections were extended to the phenylacetylene dimer radical cation as well. The measured values for the ion mobility and the collision cross section for the phenylacetylene dimer radical cations were 6.1 $cm^2.V^{-1}.s^{-1}$ and 88.5 Å^2 respectively. Two possible isomers of the phenylacetylene dimer radical cation were calculated by the ab initio calculations at the B3LYP/6-31+G** level of theory, the sandwich structure (D1) and the perpendicular structure (D2), their relative and binding energies are given in Table 12. The sandwich structure is the most stable isomer; the difference in energy is 0.33 kcal.mol^{-1} between the two isomers. The calculated binding energies for the sandwich and perpendicular isomers were 13.3 and 12.9 Kcal.mol^{-1} respectively. These energy differences are considered as small difference but due to their great difference in their structures, their mobilities will indicate which isomer is the actual one. The calculated mobility and collision cross section for the sandwich structure (D1) are 5.8 $cm^2.V^{-1}.s^{-1}$ and 93.1 Å^2 respectively. However, the calculated mobility and collision cross section for the perpendicular isomer (D2) were 5.3 $cm^2.V^{-1}.s^{-1}$ and 102 Å^2 respectively. Comparing the measured values with the calculated ones give a conclusion that the phenylacetylene dimer radical cation present in the sandwich structure which gives good results compared with the measured ones.

Table 11. Measured and calculated mobilities and collision cross sections of phenylacetylene radical cation, phenylacetylene dimer radical cations, naphthalene radical cation and different naphthalene isomer radical cations.

m/z	P mTorr	T K	K_o mesu.	Ω meas.	K_o Calc.	Ω Calc.
102	2.795	302.50	9.18	59.07	8.81	61.46
102	1.626	304.65	9.23	58.54	8.79	61.39
102	3.015	303.4	9.45	57.29	8.79	61.42
102	2.612	304.0	9.55	56.64	8.79	61.39
102	2.602	295.65	9.85	55.75	8.87	61.73
204 dim	2.445	303.95	6.06	88.42	5.8 (D1) 5.3(D2)	93.1(D1) 101.7(D2)
204 dim	2.622	304	6.0	89.3	5.8 (D1) 5.3(D2)	93.1 (D1) 101.7 (D2)
204 dim	2.602	295	6.19	87.87	5.8 (D1) 5.3 (D2)	93.6 (D1) 102.1 (D2)
128 our product	2.805	299.85	7.34	73.92	8.1(Phac1)	67.2(Phac1)
128our product	2.878	299.8	7.21	75.26	8.1(Phac1)	67.2(Phac1)
128 (Naph. Old	2.276	303.15	8.67	62.24	8.76	61.57

data)						
128(Naph old data)	2.223	293.55	8.66	63.32	8.85	61.98
Iso1					8.65	62.9
Iso2					8.66	62.8

4.3.2.3 Phenylacetylene dimer cation/C$_2$H$_2$

As shown in Figure 39, the mass selected phenylacetylene dimer cation was injected into the drift cell containing He (panel a) and different acetylene pressures, 100-600 mTorr purified acetylene (panel b to e respectively). No reactions between acetylene and phenylacetylene dimer cation occur under these experimental conditions. Phenylacetylene dimer undergoes dissociation into the phenylacetylene monomer, which in turn reacted with the acetylene according to equation (4.19) to produce C$_8$H$_6^+$ and C$_{10}$H$_8^+$ cations. The small binding energies (13.3 Kcal.mol^{-1}) explain the ease of dissociation of the phenylacetylene dimer radical cation. At low acetylene pressure, (100 mTorr), the intensity of the C$_8$H$_6^+$ is higher than the C$_{10}$H$_8^+$ as shown in Figure 39 (b). Upon further increase in acetylene pressure, the intensity of C$_{10}$H$_8^+$ increases as shown in panel (c and d).
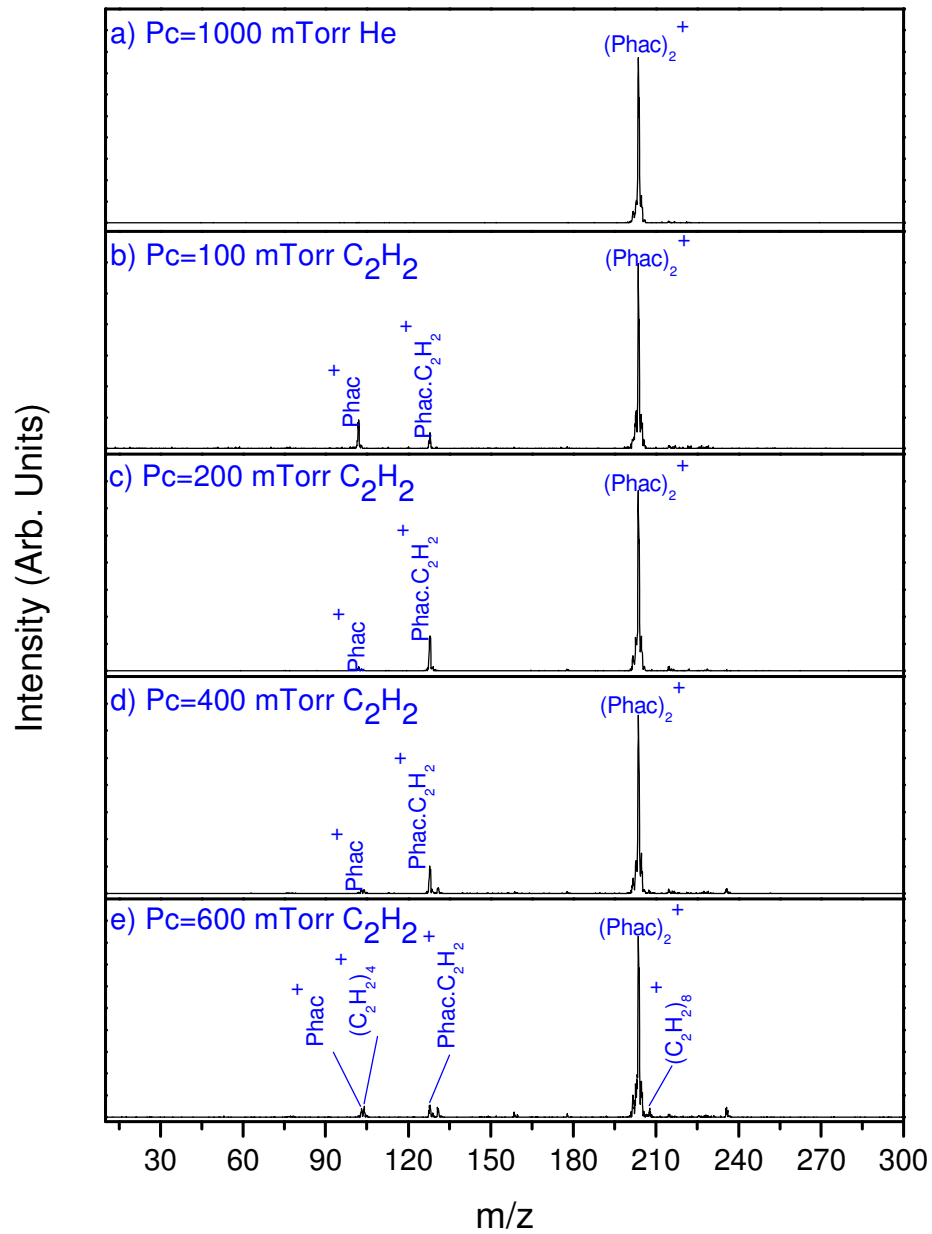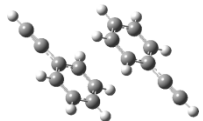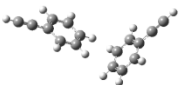
Figure 39. Injection of phenylacetylene dimer into different pressures of C_2H_2.

Table 12. Proposed structure of phenylacetylene dimer radical cations

Isomer	Proposed structure	Method/Basis Set	Relative Energy	B.E. Kcal.mol^{-1}
D1		UB3LYP/6-31+G**	0	-13.3
D2		UB3LYP/6-31+G**	0.33	-12.9

4.4 Styrene Radical Cation/C_2H_2 System

4.4.1 Introduction

Styrene, a crucial precursor to form larger PAHs upon reactions with olefins and ethynes, has gained a considerable attention in many fields, specially, polymer science. The mechanism of self polymerization of styrene in the bulk phase such as liquids and solutions has been a challenging subject of research. The Mayo mechanism was the generally accepted mechanism of the self polymerization in this case.[204-206] The polymerization mechanisms has been elucidated by studying the early stages of polymerization of styrene radical cation in the gas phase utilizing the MSIM technique, that resulted in great similarities in the initiation mechanism of polymerization of styrene in the bulk and the gas phase using the ion mobility technique, supported by DFT calculations of the polymerization products.[31,207] These results are of a great significance as they reveal the structures of the gas phase oligomer which help to understand the polymerization mechanism in the bulk phase. Also, the formation of styrene radical from the reactions of phenyl radical with ethylene in the gas phase has been previously studied.[165,208] Those reactions proceed via complex formation and involved an addition of the phenyl radical to the olefinic bond of the ethylene molecule forming an, $(C_6H_5CH_2CH_2)^{.*}$, intermediate followed by a hydrogen loss. Formation of styrene radical cation in the gas phase were studied by Bohme et al.[77] where benzene radical cation was reacted with diacetylene using the (SIFT) technique. In our group, formation of styrene type cation through reacting benzene radical cation with acetylene at elevated temperatures was also reported in our high temperature measurements in a previous section. The ion-

molecule reactions of styrene radical cation have drawn much attention in the last few decades.[31,209] The reactions of styrene radical cations with styrene and its corresponding isomer cyclooctatetraene (COT) are studied utilizing the ion cyclotron resonance spectrometry. Styrene radical cation reacts with styrene to form the adduct $C_{16}H_{16}^{\bullet+}$ which subsequently loses a benzene to form the $C_{10}H_{10}^{\bullet+}$ adduct. Meanwhile, upon the reactions of styrene radical cation with the (COT), no such observations were determined. These findings show the utility of the ICR as a mean of isomer differentiation in the gas phase. Since the ICR experiments are performed at very low pressures, no products were detected upon reacting styrene radical cations with acetylene.[209] These findings are in contradiction with the theoretical predictions of the barrierless addition of acetylene to styrene type cations.[59] In this section we expand our experiments to study the reactions of styrene radical cation with acetylene utilizing the ion mobility mass spectrometry technique.

4. 4. 2 Results and discussions

4. 4. 2. 1 Styrene radical cation reactions with acetylene

Styrene clusters were produced by supersonic expansion of He seeded with styrene vapor, (0.22 % styrene in He). The cluster beam then skimmed through the skimmer that separates the 2nd chamber from the source chamber in our MSIM system. The styrene clusters were ionized by electron impact ionization technique. Styrene radical cations were mass selected via the 1st quadrupole mass filter and guided through Einzel lenses and introduced into the drift cell.

In contrast to the ICR experiments that resulted in no reactions between styrene radical cations with acetylene,[209] we had observed that styrene radical cation reacts with acetylene, Figure 40, according to the following equations,

$$C_8H_8^{\bullet+} + C_2H_2 \longrightarrow C_{10}H_{10}^{\bullet+} \qquad (4.20)$$

$$\longrightarrow C_{10}H_9^+ + H^{\bullet} \qquad (4.21)$$
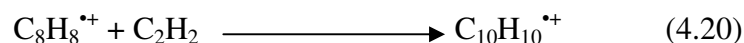
The addition of acetylene molecules to styrene radical cation was limited to one addition only. The cell temperature was increased from 302 K up to 573 K as shown in Figure 40, resulting in an increases in the intensity of the $C_{10}H_{10}^{\bullet+}$ radical cation, with no observations of more acetylene addition to styrene radical cation other than the observed products in equations (4.20 and 4.21). These observations are still valid for the low temperature regimes as shown in Figure 41. When the temperature of the drift cell was lowered to 130.2 K, no association of acetylene molecules were observed on the styrene radical cation.

4. 4. 2. 2 Kinetics measurements

The reaction rate coefficient of the addition of acetylene molecules to styrene cation was measured through the kinetic studies and tabulated in Table 13. ATDs intensities of the reactants and products ions were measured as a function of time upon the injection of styrene radical cation into the drift cell containing 804 mTorr C_2H_2. Residence time had been changed from 0.4 ms to 10 ms by varying the applied filed across the drift

cell. The rate coefficient for the overall reaction to form products is in the order of $1.2(\pm0.3)\times10^{-14}$ $cm^3.s^{-1}$, which is about 5 orders of magnitude smaller than the collision rate ($\sim\times10^{-9}$ $cm^3.s^{-1}$). This suggests that the back-dissociation of the excited complex $(C_8H_8^{\bullet+}\bullet C_2H_2)^*$ occurs at a rate faster by a factor of 10^5 than the forward reaction to form products which indicates low reaction efficiency.
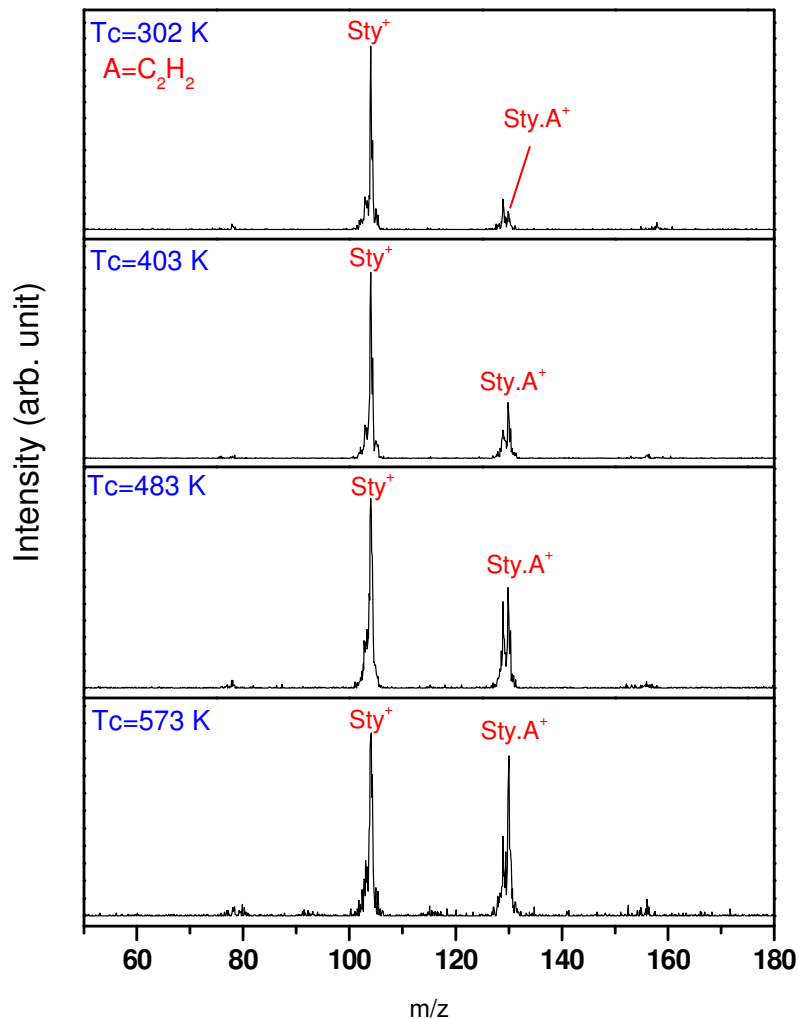
Figure 40. Mass spectra obtained upon injection of mass selected styrene radical cation $(C_8H_6)^{\bullet+}$ into the drift cell. The cell field was 5 Vcm^{-1}, the injection energy (IE) was 12 eV (lab), and the cell pressure was 693 mTorr purified acetylene. Drift cell temperature was 302 K, 403 K, 483 K, and 573 K from top panel to bottom one respectively.
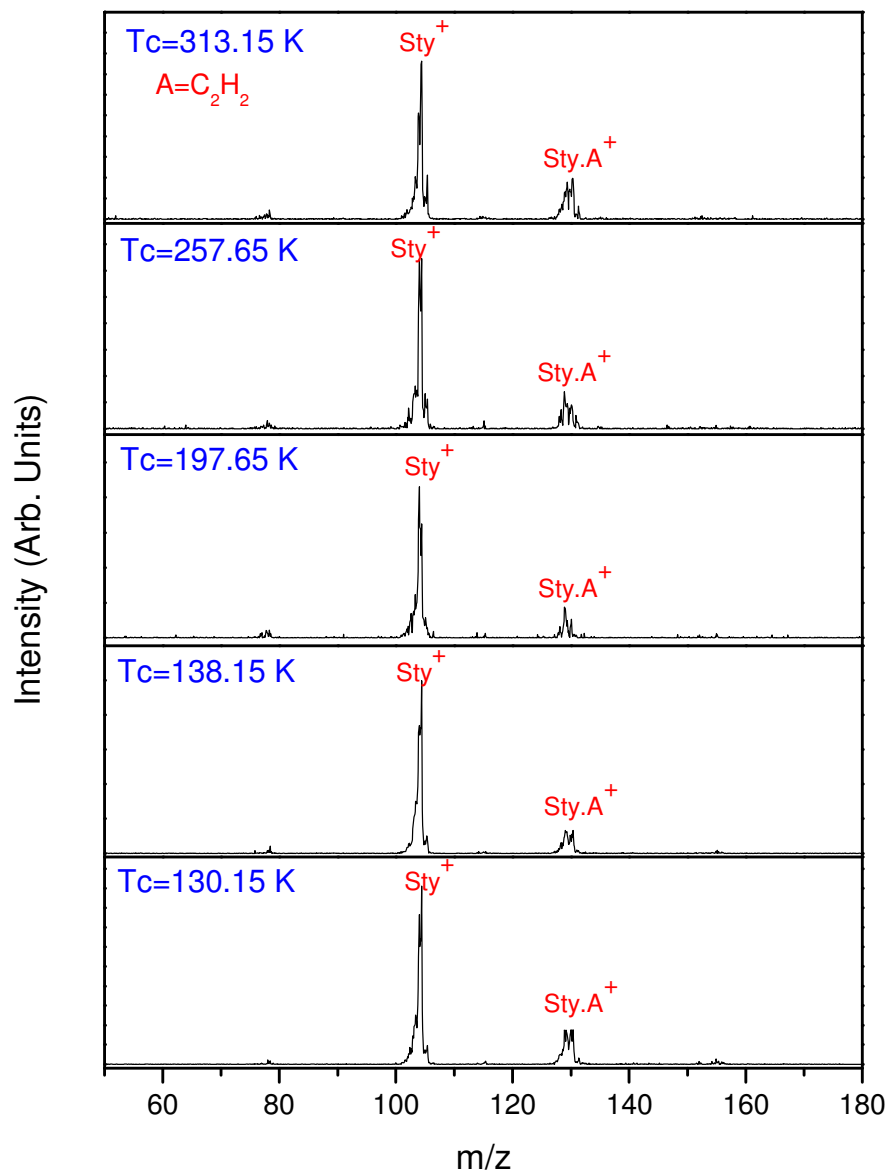
Figure 41. Mass spectra obtained upon injection of mass selected styrene radical cation $(C_8H_6)^{\bullet+}$ into the drift cell. The cell field was 5 Vcm^{-1}, the injection energy (IE) was 12 eV (lab), and the cell pressure was 722 mTorr purified acetylene. Drift cell temperature was 313.15 K, 257.65 K, 197.65 K, 138.15 and 130.15 K from top panel to the bottom one respectively.
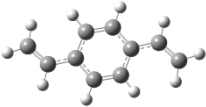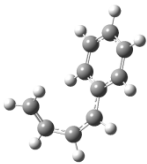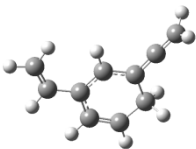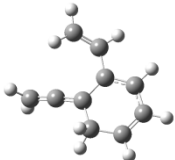
Table 13. Second order reaction rate for the reactions of $C_8H_8^+$ with acetylene at different acetylene concentrations and at different cell temperatures.

T K	P C_2H_2 mTorr	K_2 cm^3.s^{-1}
588.4	848	1.3×10^{-13}
303.5	804	2.1×10^{-14}
373.4	896	4.6×10^{-14}
473.5	1062	6.2×10^{-14}
314.3	830	3.6×10^{-14}
383.1	932	6.1×10^{-14}
454	1033	1.1×10^{-14}

Several possible isomers of the addition of (C_2H_2) to styrene cation have been optimized by the ab initio calculations at the UB3LYP/6-31+G** level. Table 14 represents different possible isomers for the addition of acetylene to $C_8H_8^+$. All the examined structures are the covalent conformers. The lowest energy isomer found was (Sa2), this isomer follows the Bittner-Howard addition mechanism. The second most probable isomer is (Sa1) isomer where acetylene molecule added to the aromatic ring of the styrene cation with a slightly higher energy than (Sa2) isomer by 4 kcal.mol^{-1}..

The other two isomers (Sa3) and (Sa4) have higher energies, ~30 and ~34 Kcal.mol^{-1} respectively. These could be a result from two processes, the hydrogen abstraction according to Frenklach mechanism and hydrogen to the aromatic ring.

Table 14. Proposed structures of (Styrene.C_2H_2)$^{.+}$ adducts

isomer	Structure	Method/Basis Set	R.E.	B.E. kcal.mol^{-1}
Sa1		UB3LYP/6-31+G**	4	-55.4
Sa2		UB3LYP/6-31+G**	0	-51.4
Sa3		UB3LYP/6-31+G**	29.7	-25.7
Sa4		UB3LYP/6-31+G**	33.9	-21.5

4. 4.2.3 Mobility Measurements

Ion mobility measurements of the styrene radical cation were measured in He, representing mass spectra is shown in Figure 42. The measured and calculated mobilities are 9.44 $cm^2.V^{-1}.s^{-1}$ and 9.39 $cm^2.V^{-1}.s^{-1}$ respectively. The corresponding measured and calculated cross sections are 57.23 and 57.82 $Å^2$ respectively which is in excellent agreement. These values also in very good agreements with the values obtained from the reactions of benzene radical cation with acetylene providing further evidence for formation of styrene type cation from those reactions. Figure 43 represents the plot of P/V with the arrival time distribution of the styrene radical cation under different applied filed, and the corresponding ATDs of the measured mobility is given in Figure 44. Fitting the measured ATD of styrene radical cation with the one predicted by the transport theory is shown in Figure 45.
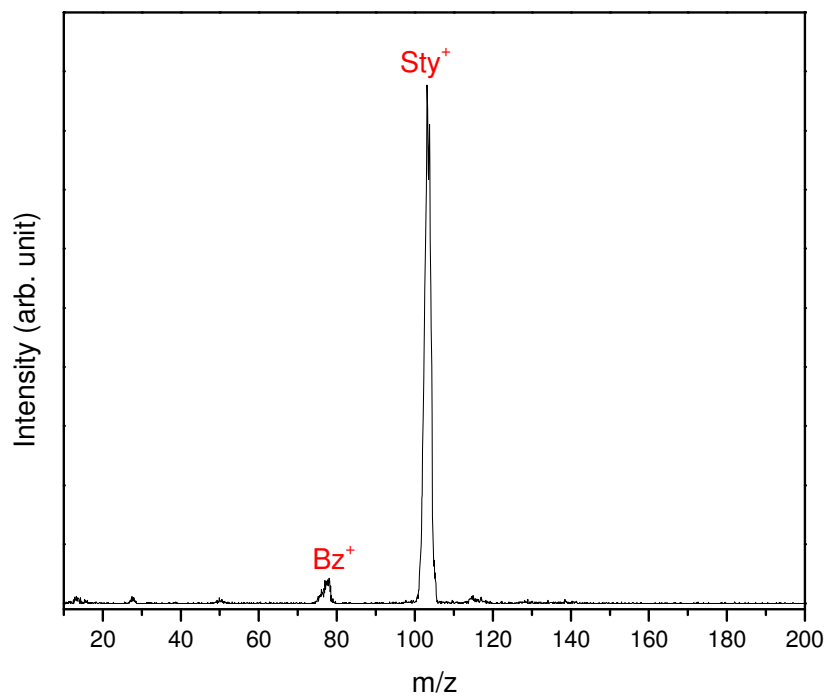
Figure 42. Mass spectra obtained upon injection of mass selected styrene radical cation $(C_8H_6)^{\bullet+}$ into the drift cell at 298 K. The cell field was 6 Vcm^{-1}, the injection energy (IE) was 14 eV (lab), and the cell pressure was 1 Torr He.
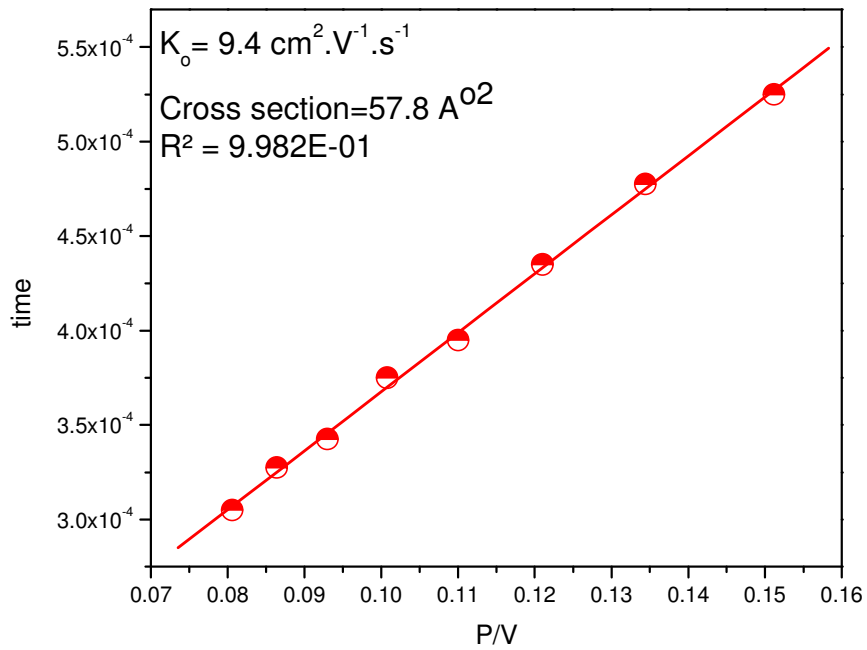
Figure 43. . Plot of arrival time vs. P/V for $C_8D_8^+$; 20 μs ion pulse into a drift cell filled with 2.419 Torr He at different cell voltages (16-30 V).
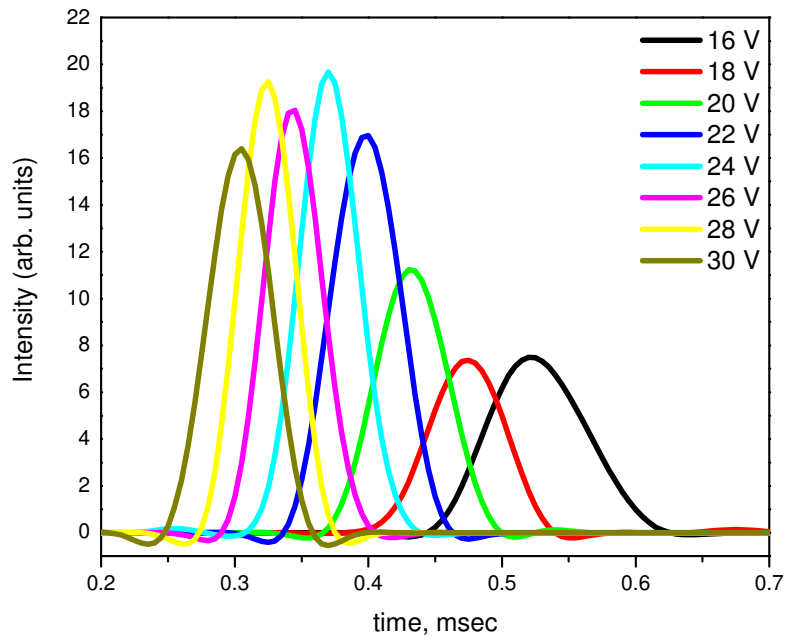
Figure 44. The arrival time distribution (ATDs) of injecting $C_8D_8^+$; 20 μs ion pulse into a drift cell filled with 2.419 Torr He at different cell voltages (30-16 V). The earlier ATD corresponds to drift cell voltage of 30V and the later ATD corresponds to drift cell voltage of 16 V.
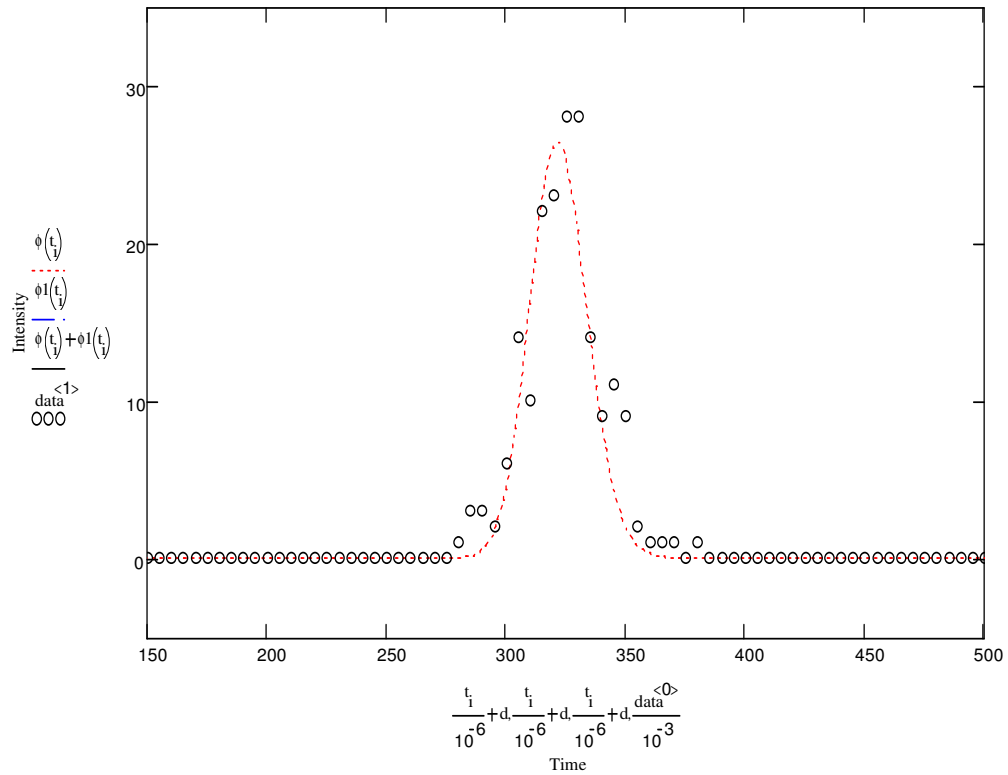
Figure 45. Arrival Time Distribution of mass selected $C_8H_8^{+\bullet}$ ion into the drift cell containing 2.419 Torr He, at 301 K. (o) measured values, (⋯⋯) Theoretical fit of the ATD.

4.5 Conclusions

In this chapter, we studied the ion-molecule reactions of acetylene with different ions in order to understand the formation of complex organics in different ionizing environments. The reactions of benzene radical cations with acetylene produce styrene-type and naphthalene-type cations at high temperatures. The second order rate constant of this reaction was found to be in the order of 10^{-14} cm^3.s^{-1} with a barrier of 3.5 kcal.mol^{-1}. Under low temperature regime, benzene radical cation acts as a catalyst to initiate the formation of higher complex hydrocarbons through the associative charge transfer to the acetylene clusters, $(C_2H_2)_n^+$, n= 6-10. The observed reactions can explain the formation of complex organics under different conditions in space.

To further investigate the possible mechanisms of formation of PAHs in space, phenylium ion was reacted with acetylene, in order to prove the experimental assumptions of formation of phenylium ions in the HACA proposed mechanism. The obtained results are consistent with the theoretical predictions. The rate of reaction in this case was four orders of magnitudes faster than the measured benzene/acetylene one, which again provides a conclusive evidence of the formation of phenylium ions to trigger the reactions of benzene with acetylene. Phenylium cation was reacted with benzene and the product is consistent with that reported in the literature. Also, the reactions rate in this case was found to be close to the collision rate and the main product was the biphenyl cation. The proposed structures of the addition of the acetylene molecules to benzene and phenylium cation calculated by the DFT (B3LYP/6-31-G**) method suggests that the additions are occurred according to Bittner-Howard mechanism.

Formation of PAHs from the reactions of acetylene with different cations was expanded to the reactions with phenylacetylene cation and styrene radical cation. In both cases, only one acetylene molecule was added to the cation to form the naphthalene-type isomer, with the exception of more additions of acetylene molecules to the phenylacetylene cation under high temperatures. The reaction rate was measured to be slower than that of the phenylium cation but faster than that of benzene cation in case of phenylacetylene. However, the reaction rate was almost the same in the styrene/acetylene reactions compared with benzene radical cation reactions with acetylene.

Chapter 5 Formation of Polyaromatic nitrogen-containing compounds in the gas phase

In this chapter, we present examples of formation of PANHs in the gas phase via the ion-molecules reactions of acetylene with different heterocyclic precursors. Reactions of pyridine cation, benzonitrile cation and pyrimidine radical cations are presented to afford the formation of fused aromatic rings with incorporated nitrogen atom. Kinetics, CID, ion mobility measurements and DFT calculations were utilized to elucidate the structure of the formed adduct ions.

5.1 Gas phase sequential reactions of pyridine cation with acetylene

5.1.1 Introduction

Pyridine is considered as one of the well known prototype aromatic nitrogen heterocyclic compounds. Pyridine and its derivatives are widely spread in nature, mainly, as enzymes and alkaloids.[210] Pyridine and similar heterocylces are the core of the compositions of biological molecules and it could be a source of prebiotic materials that had been transported by comets and meteoroids to the earth and was a source of nutrients for life.[211] Pyridine and its derivatives are important in chemical industry and they are produced mainly from coal.[212] Their importance in ion-molecule reactions is crucial for the formation of complex organics in the gas phase as well as the condensed ones and has recently received a great attention in science.[73,213-214] Formation of pyridine and pyrimidine from the reactions of acetylene and nitriles have been studied in absence [215] and presence

of catalysts such as Co and Ru[216-217] in the condensed phase chemistry. Observations of complex organics such as PAHs and PANHs in space have been reported.[13,17-18,58,218-223] Those observations of PAHs and PANHs have raised many questions about the fundamentals of the ion-molecule reactions and their capabilities of formation of complex organics and the possible mechanisms of such formation.[17,224-225] The presence of acetylene and hydrogen cyanide in Titan's atmosphere[32] in ionizing environments could lead to the formation of heterocyclic organic complexes. We have reported the formation of complex organics, mainly PAHs, such as styrene-type, naphthalene-type and polymerized cations via the reactions of benzene cation with acetylene under a wide range of temperatures as a prototype example of formation of PAHs in space.[145] Also, the reactions of (benzene/pyridine)$^{\bullet+}$ as a model of PAHs and nitrogen heterocylces interactions in ionizing environment have been reported as well.[73] The experimental and theoretical results suggest that the adduct (benzene.pyridine)$^{\bullet+}$ is covalent one with binding energy of >33 kcal.mol^{-1}, the covalently C-N bonded $(C_6H_5-NC_5H_6)^{\bullet+}$ dimer adduct was evidentially confirmed by collisional induced dissociation (CID), reactivity and mobility measurements were conducted by the drift cell technique. These reactions may represent a general class of addition reactions that can form complex hydrocarbon species in ionizing environments and in space. Simulations of nitrogen rich atmosphere, such as Titan's atmosphere, suggest that the nitrogen will be incorporated easily in the aromatic ring [60] and predict that this process is barrierless and exothermic.

In this work, we present evidence by ion mobility, collisional dissociation and ab initio calculations of formation of PANHs in the gas phase through reacting pyridine cation

with acetylene via ion-molecule and intracluster reactions. These experiments are mimicking the reaction conditions in Titan's atmosphere to get an insight of possible pathways of formation of heterocyclic organic complexes.

5.1.2 Experimental section

The molecular ions ($C_5H_5N^+$ or $C_5D_5N^+$) were generated by electron impact (EI) ionization of the corresponding molecular clusters formed by expanding 4.8 bar of ultra pure He seeded with 0.2 % pyridine or d-pyridine through a 200 µm diameter pulsed nozzle (General Valve, Series 9), in pulses of 150-300 µs duration at repetition rate of 50-100 Hz, into a source chamber (10^{-8} mbar). In the mixed clusters experiments, He seeded with <3% C_2H_2 expanded over pyridine/d-pyridine bubbler cooled at 194.6 K (liquid nitrogen temperature), and introduced to the source chamber. The molecular ions or the cluster ions of interest were mass selected by a quadrupole mass filter and the beam is chopped into small pulses (5-15 µs pulses) and injected into the drift cell (the length of drift cell is 5 cm) filled with pure He or C_2H_2/He mixtures. A constant pressure was maintained in the drift cell utilizing two flow controllers (MKS # 1479A). Arrival time distributions (ATDs) of the different ions were measured by monitoring the signals corresponding to each ion as a function of time after injection into the drift cell.

5.1.3 Results and Discussions

5.1.3.1 Reactions of $C_5H_5N^+$($C_5D_5N^+$) with C_2H_2

Figure 46 displays different mass spectra collected upon injection of $C_5H_5N^+$ into different pressures of neutral acetylene/He mixtures. At low pressure of acetylene, (15

mTorr C_2H_2 in 1 Torr He), as shown in Figure 46 (a), the reaction between $C_5H_5N^+$ and C_2H_2 proceeds according to the following equations:

$$C_5H_5N^+ + C_2H_2 \longrightarrow C_5H_5N.C_2H_2^+ \qquad (5.1)$$

$$\longrightarrow C_5H_4N^+ + H^\bullet \qquad (5.2)$$

$$H^\bullet + C_2H_2 \longrightarrow C_2H^\bullet + H_2 \qquad (5.3)$$
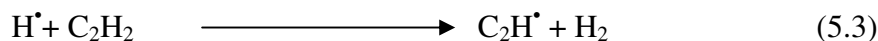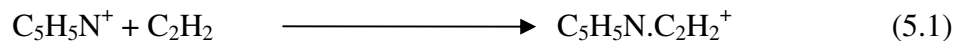
when the $C_5H_5N^+$ ions are injected into the drift cell containing pure He, only $C_5H_5N^+$ ions are observed. However, in the presence of acetylene neutral in the drift cell in presence or absence of He, $C_5H_4N^+$ ions are detected confirming the occurrence of equation (5.2) as observed previously.[226-229] Elimination of the hydrogen from pyridine cation was predicted to be from the o-position on the pyridine ring.[230] Figure 47 shows the formation of $C_5H_4N^+$ in presence of C_2H_2 in the drift cell. This reaction, (5.2), produces $H^\bullet$ radical which could further react with a C_2H_2 molecule to produces molecular hydrogen and $C_2H^\bullet$ radical as shown in equation (5.3), which could initiate a series of radical reactions with neutral acetylene molecules. Equation (5.1) was predicted theoretically for the addition of C_2H_2 to $C_5H_5N^+$ to be a barrierless and exothermic reaction [60] and the experimental results are completely consistent with the theoretical predictions. The sequential addition of acetylene molecules to $C_5H_5N^+$ increases as the acetylene pressure increases in the drift cell (480 mTorr C_2H_2 mixed with 1 Torr He) as shown in Figure 46 (e). This trend of addition occurs even at higher pressures of acetylene (up to 1.1 Torr C_2H_2 as shown on Figure 48 (c)) to generate the series of $C_5H_5N.(C_2H_2)_n^+$ cations where n=1-5. These ions are corresponding to the formula $C_nH_nN^+$ where n=5, 7, 9, 11, 13 and 15. We observed that for $C_nH_nN^+$ where n=9, a hydrogen loss from this species which will generate $C_9H_8N^+$ will

lead to ring closure as expected from the theoretical predictions.[60] The observation of the $C_9H_9N^+$ and $C_9H_8N^+$ cations, (m/z=131 and m/z=130 respectively), in all the mass spectra in Figure 46 and Figure 48 confirm their formation even at very low acetylene pressures. The lowest pressure was as low as 100 mTorr C_2H_2. Another evidence of the formation of these covalent adducts is the thermal stability studies done by injecting $C_5H_5N^+$ into the drift cell containing 1.10 Torr C_2H_2 at different temperatures as shown in Figure 49. The addition of acetylene molecules to the pyridine cations was observed to be up to n=5 at temperature range 50-100 ^{o}C, upon increasing the temperature to higher values, the addition of only two acetylene molecules to the pyridine cations is observed suggesting the covalent character for the $C_7H_7N^+$, $C_9H_9N^+$ and $C_9H_8N^+$ cations, and the last two ones are corresponding to the diprotonated isoquinoline and protonated isoquinoline isomers respectively.

$C_9H_8N^+$ cation could also be produced from the following reactions;
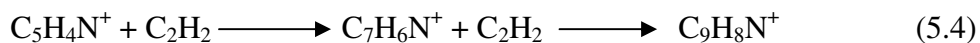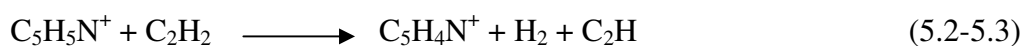
$$C_5H_5N^+ + C_2H_2 \longrightarrow C_5H_4N^+ + H_2 + C_2H \tag{5.2-5.3}$$

$$C_5H_4N^+ + C_2H_2 \longrightarrow C_7H_6N^+ + C_2H_2 \longrightarrow C_9H_8N^+ \tag{5.4}$$

Kinetics studies were carried out to measure the reaction rate coefficient of addition of acetylene molecules to $C_5D_5N^+$ cations. The drift cell was filled with ~0.02 Torr acetylene diluted with 0.3 Torr He at 304.15 K. Arrival time distributions (ATDs) of the various ions were measured by monitoring the signals corresponding to each ion as a function of time after injection into the cell (residence time). Residence time was varied between 60 and 300 μs by changing the field applied on the cell, as shown in Figure 50. The time-resolved studies allow the identification of primary and secondary reaction

products, and the measurement of rate coefficients. Pseudo first-order rate constant for the decay of the $C_5D_5N^+$ reactant ions was obtained from time-resolved experiments using the relation ln $I/\Sigma I = -kt$. Hence, we obtained k_1 from plots of ln $I/\Sigma I$ vs. t, where I is the integrated intensity of the reactant ion peak and ΣI is the sum of intensities of the reactant and all product ion peaks including secondary products, and t is the mean drift time (taken as the center of the arrival time distribution) of the reactant. Second-order rate coefficients, k_2, were obtained from $k_2 = k_1/[N]$ where N is the number density (molecules.cm^{-3}) of the neutral C_2H_2 reactant in the cell. The overall rate of the disappearance of the $C_5D_5N^+$ (m/z=84), and the generations of the first adduct $C_7D_5NH^{\bullet+}$ (m/z=109) and the second adduct $C_7D_5NH_2^+$ (m/z=110) as shown in the following equations:

$$C_5D_5N^+ + C_2H_2 \longrightarrow C_7D_5NH^{\bullet+} + H^\bullet \qquad (5.5)$$

$$\longrightarrow C_7D_5NH_2^+ \qquad (5.6)$$
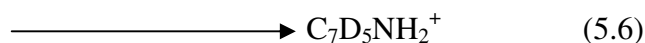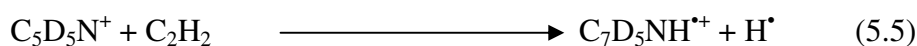
Second order reaction coefficient was measured at various temperatures and pressures and the results are summarized in Table 15.

Figure 51 shows the normalized intensities of reactants and products of the reactions (5.5) and (5.6) as a function of time. The rate coefficient for the overall reaction to form products is on the order of 5.0×10^{-11} cm^3.s^{-1}; which is about two orders of magnitude smaller than the collision rate ($\sim\times10^{-9}$ cm^3.s^{-1}).

139

Table 15. Second order rate constants of the reactions of pyridine cation with acetylene

$P(C_2H_2)$ Torr	$P(He)$ Torr	T K	k_2 cm^3.s^{-1}
0.0166	0.32	303.85	9.54×10^{-11}
0.0158	0.32	303.35	6.01×10^{-11}
0.0174	0.32	303.25	1.41×10^{-10}
0.0141	0.32	302.75	3.92×10^{-11}
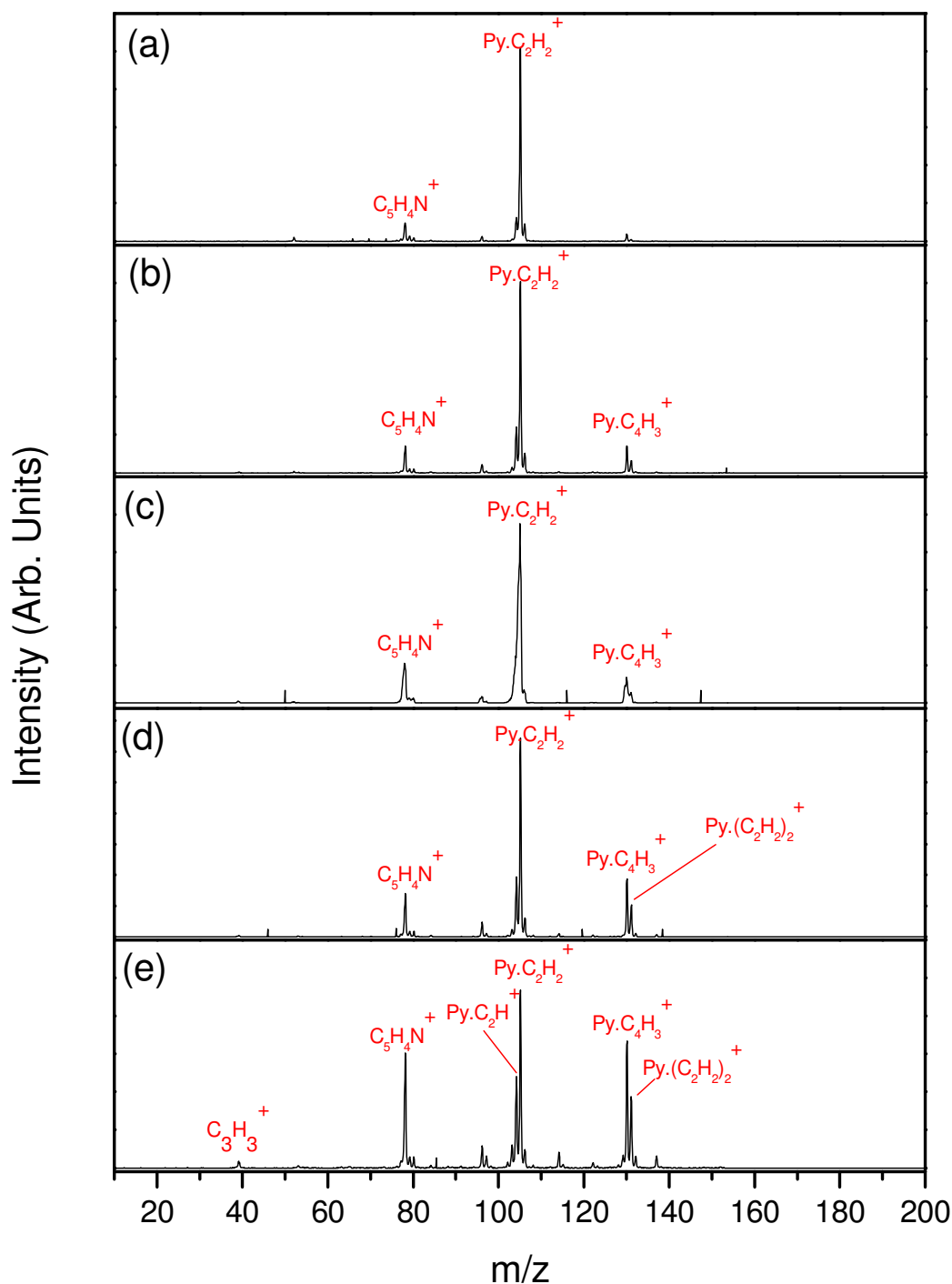
Figure 46. Mass spectrum of $C_5H_5N^+$ after injection into the drift cell. The injection energy is 26 eV (Lab frame), drift cell temperature is 30 ^{o}C and the cell voltage is 20 V. The cell pressure is (a) 1 Torr (15 mTorr C_2H_2), (b) 1.1 Torr (100 mTorr C_2H_2), (c) 1.09 Torr (135 mTorrC_2H_2), (d) 1.18 Torr (200 mTorr C_2H_2) and (e) 1.02 Torr (480 mTorr C_2H_2).
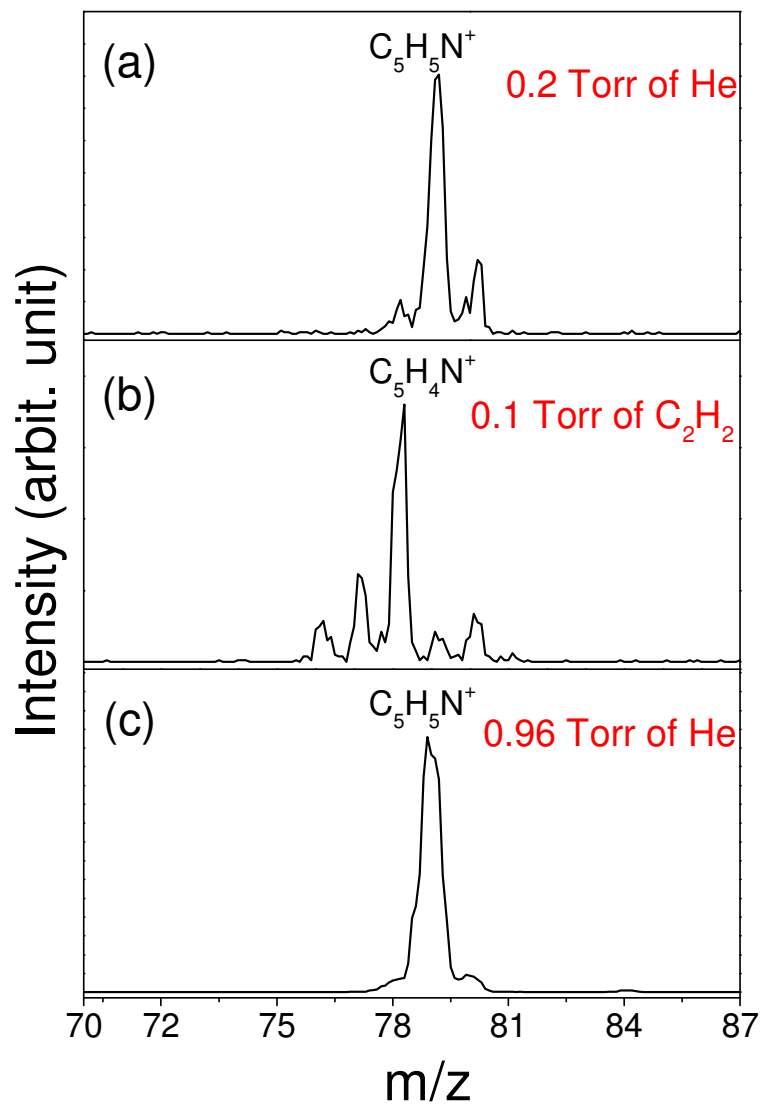
Figure 47. Injected mass selected Pyridine (mass = 79) in He, C_2H_2 and He. The Carrier gas is He at 60 psi, the injection energy is 24 eV, the temperature is 29 $^{\circ}$C and the cell voltage is 25 V.
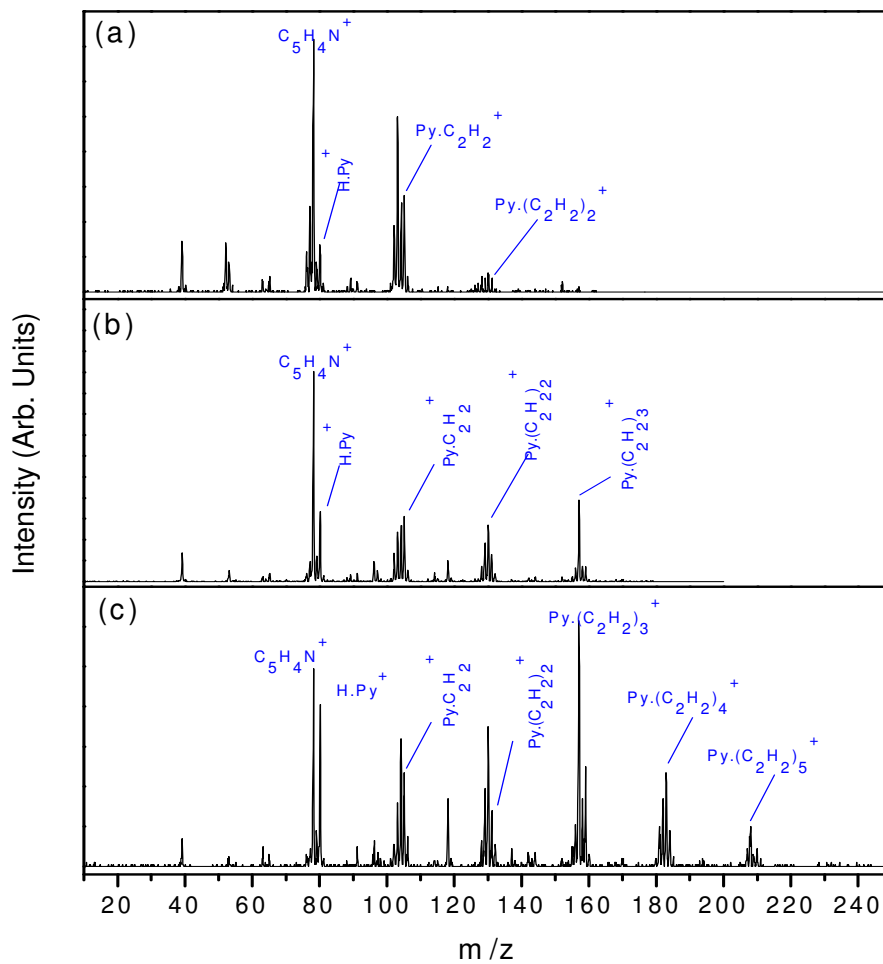
Figure 48. Mass spectrum of $C_5H_5N^+$ after injection into the drift cell. The injection energy is 24 eV (Lab frame), drift cell temperature is 29 ^{o}C and the cell voltage is 25 V. The cell pressure is (a) 0.1 Torr C_2H_2, (b) 0.5 Torr C_2H_2 and (c) 1.0 Torr C_2H_2.
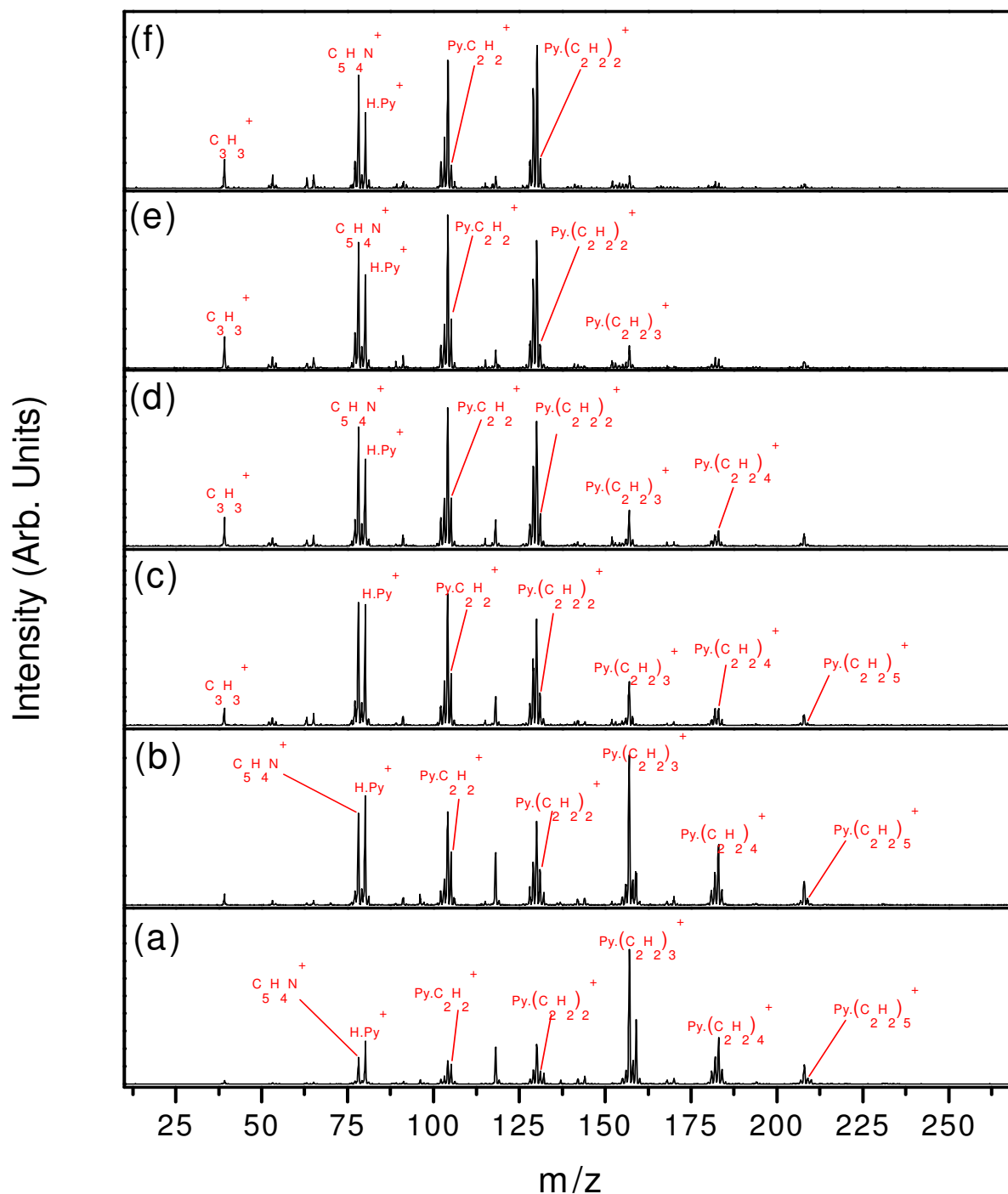
Figure 49. Mass spectrum of $C_5H_5N^+$ after injection into the drift cell. The injection energy is 30 eV (Lab frame), the cell voltage is 25 V. The cell pressure is 1.1 Torr C_2H_2. Drift cell temperatures are: (a) 50 ^oC, (b) 100 ^oC, (c) 200 ^oC, (d) 250 ^oC, (e) 300 ^oC and (f) 350 ^oC respectively.
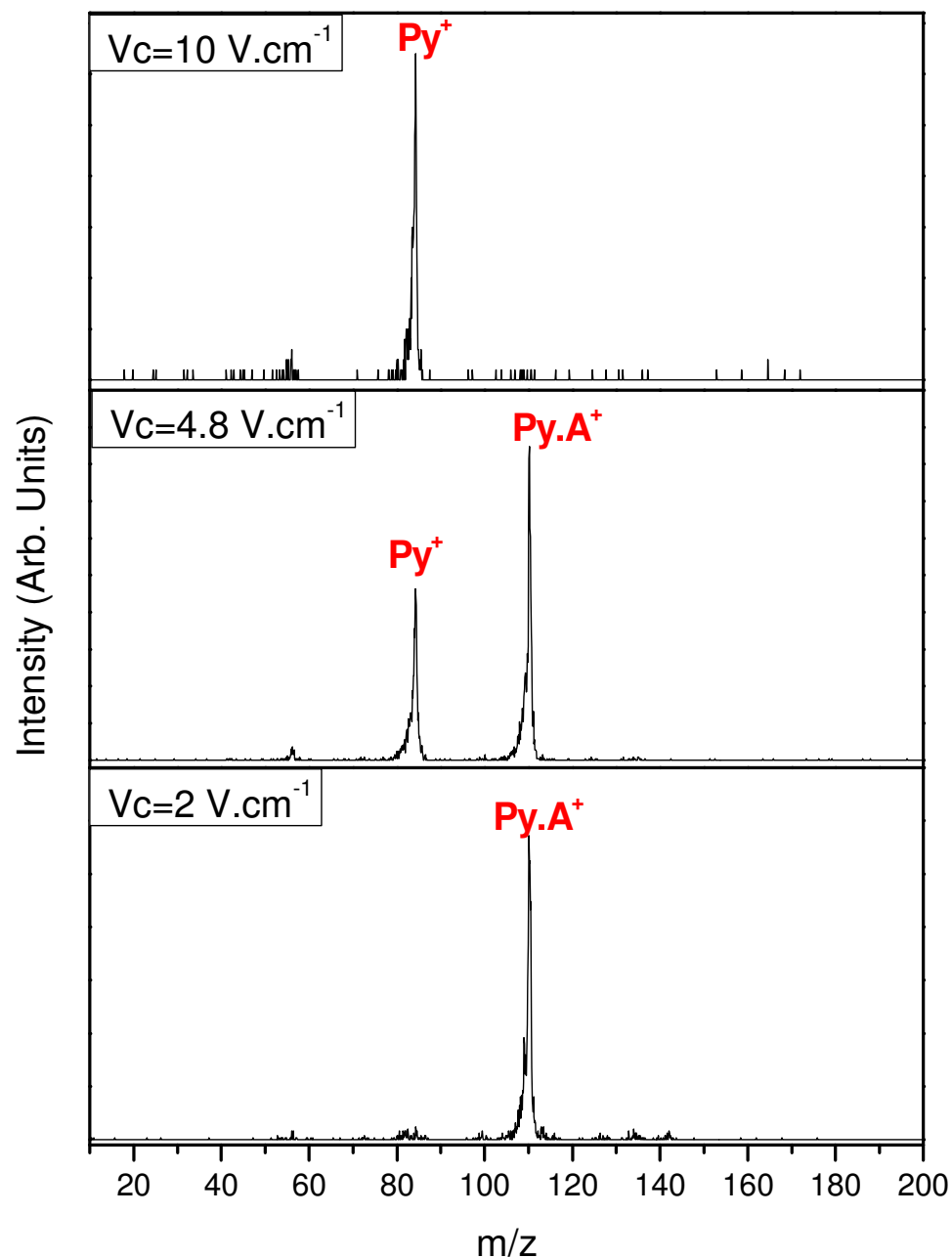
Figure 50. Mass spectra obtained upon injection of mass selected pyridine cation $(C_5D_5N)^+$ into cell containing purified acetylene using different cell fields. The cell was held at 30 ºC, the injection energy (IE) was 19 eV (lab), and the cell pressure was 18 mTorr acetylene and 320 mTorr helium.
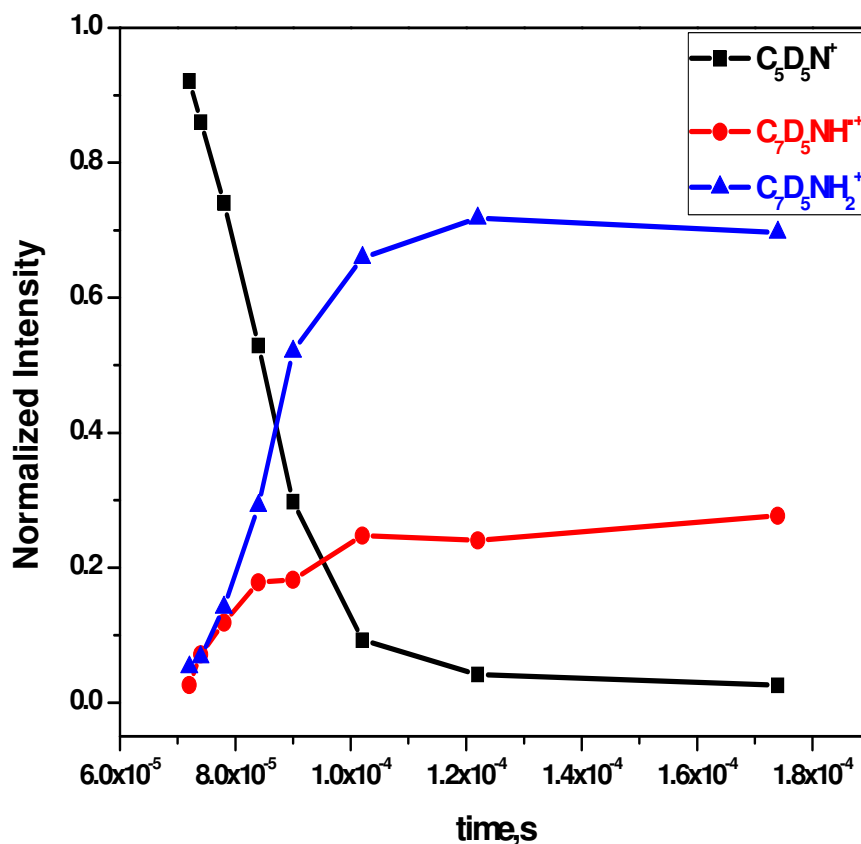
Figure 51. Normalized intensities of ion signals (integrated ATD peaks) as a function of reaction time after injection of $C_5D_5N^+$ ions into the mobility cell with a mixture of 0.02 Torr and 0.3 Torr of C_2H_2 and He, respectively, T = 31 ºC, and injection energy (IE) =15.3 eV (Lab frame). The intensities are normalized to the sum of the reactant and all product ions.

5.1.3.2 Mobility Measurements

Ion mobility measurements were carried out by injecting an ion pulse (10-50 µs) into the drift cell. ATDs were collected at different P/V values, where P is the pressure of buffer gas in the drift cell in Torr and V is the drift voltage in volts, by varying the V while keeping P fixed. The plot of the mean arrival time (assuming Gaussian peak shape) versus P/V gives a straight line, and the reduced mobility could be estimated from the slope using the relation [231]

$$t = (z^2 \times 273.15/T \times 760)*(P/V) + t_o$$

where, t is the mean arrival time, z is the drift cell length, T is the cell temperature in Kelvin, K_o is the reduced mobility and t_o is the time that the ions spend outside the drift cell. Structure determination was performed by measuring the reduced mobilities of the ions and comparing the resulting values with those mobilities with different structures calculated using the MOBCAL program. [144]

Ion mobility spectrometry (IMS) is an analytical technique that separates different ionic species depending on their collision cross section. [93,232] The formation of pyridine-acetylene mixed clusters were carried out by flowing a mixture of acetylene/He (~1%) over cooled pyridine (pyridine bubbler cooled by dry ice at 195.2 K to lower the amount of pyridine vapor in the seed gas as described in the experimental section) by supersonic adiabatic expansion and ionizing the formed clusters using electron impact ionization (EI). A typical mass spectrum of the pyridine-acetylene cluster ions is shown in Figure 52. From this figure, we observe the acetylene clusters (m/z= 52, 78, 104, and 130 amu), pyridine-(acetylene)$_n$ binary clusters, where n= 1-4 corresponding to masses (m/z=110, 136, 162

and 188 amu) respectively, protonated pyridine dimer (m/z=169 amu) and acetylene.(pyridine)$_2$ cluster ion (m/z=194 amu). The observed peak for the $C_9D_5H_3N^+$ ion, (m/z=135), could represent the cyclic nitrogen-containing hydrocarbon compound (isomer of quinoline). The mobility and collision cross sections of pyridine, protonated pyridine and the protonated pyridine dimer were measured previously in our group and their values are 11.8±0.6, 11.8±0.6 and 6.9±0.3 cm^2.V^{-1}.s^{-1} and 46±2, 45±2 and 78±3 A^{o2} respectively.[73] Our interest is to study the mobility of the binary clusters of pyridine-acetylene. The intensity of the acetylene-(pyridine)$_2$ (m/z=194) peak is enhanced suggesting extra stability of this ion. This strong magic number behavior is observed under different experimental conditions as shown in Figure 53, where the neutral clusters of pyridine and acetylene were ionized by EI ionization and detected in vacuum. Structural information on the product ions can be obtained by measuring the ion mobility of the cluster ion. The experimentally measured mobilities and collision cross-sections at different temperatures are compared to theoretical values obtained for the $C_5H_5N.(C_2H_2)_n^+$ cation, where n=1 and 2 as well as the $(C_5H_5N)_2C_2H_2^+$ cation. The structures used in the theoretical calculations are presented in Figure 57. The measured and calculated ion mobilities of $C_5D_5N.C_2H_2^+$ and $C_5D_5N.(C_2H_2)_2^+$ and $(C_5D_5N)_2C_2H_2^+$ cluster ions as well as their corresponding cross sections are included in Table **16**. At 173 K, there is an excellent agreement between the measured mobilities of $C_5H_5N.C_2H_2^+$ cluster ion with the theoretically calculated ones, where the measured values are 11.2±0.7 cm^2.V^{-1}.s^{-1} while the calculated ones are 11.10 cm^2.V^{-1}.s^{-1}. At higher temperatures the average measured mobilities is 9.2±0.4 cm^2.V^{-1}.s^{-1} while the calculated ones have an average of 9.6±0.01

$cm^2.V^{-1}.s^{-1}$. The measured and calculated cross sections of $C_5H_5N.C_2H_2^+$ are also in good consistency as the average measured cross sections is 58.8 ± 1.7 $\mathring{A}^2$ and 63.7 ± 0.4 $\mathring{A}^2$ at high and low temperatures respectively. The corresponding average calculated cross sections is 56.6 ± 1.6 $\mathring{A}^2$ and 64.2 ± 0.02 $\mathring{A}^2$ at high and low temperatures respectively. ATDs of the $C_5D_5N.C_2H_2^+$ cluster ion are shown in Figure 54, injected in 50 μs ion pulses into the drift cell containing 3.344 Torr He at different cell voltages (40-22 V) with injection energy of 18.9 eV. This consistency between the calculated and measured values of the mobility and average collision cross sections gives a good indication that the acetylene molecules adds to the nitrogen atom of the pyridine ring as shown in the proposed structure in Figure 57, suggesting that the proposed structure is the actual one. For the $C_5H_5N.(C_2H_2)_2^+$ cation, the average measured mobilities at high temperatures is 7.7 ± 0.1 $cm^2.V^{-1}.s^{-1}$, while the average calculated mobilities at high temperatures is 7.9 ± 0.01 $cm^2.V^{-1}.s^{-1}$ showing excellent agreement between the measured and calculated mobilities. The average corresponding calculated cross section is 67 ± 0.3 $\mathring{A}^2$ is in excellent agreement with the average measured cross sections 70 ± 0.9 $\mathring{A}^2$. At low temperatures, the average measured mobilities are 10.1 $cm^2.V^{-1}.s^{-1}$ and the corresponding measured cross sections is 70.6 $\mathring{A}^2$. The corresponding average mobilities and collision cross sections are 9.4 $cm^2.V^{-1}.s^{-1}$ and 75.8 $\mathring{A}^2$ respectively.

These excellent agreements between the calculated and measured mobilities and collision cross sections continue with the $(C_5H_5N)_2.C_2H_2^+$ cation which shows a high stability in all mass spectra of the pyridine/acetylene clusters. At high temperatures, the average measured and calculated mobilities are 6.4 ± 0.2 $cm^2.V^{-1}.s^{-1}$ and 6.5 ± 0.1 $cm^2.V^{-1}.s^{-1}$ respectively. The corresponding average measured and calculated collision cross sections

at high temperatures are 84 ± 3 Å^2 and 83 ± 0.2 Å^2 respectively. At low temperatures, the average measured and calculated mobilities are 7.9 ± 0.2 cm^2.V^{-1}.s^{-1} and 7.8 ± 0.1 cm^2.V^{-1}.s^{-1} respectively. Their corresponding average measured and calculated collision cross sections are 90 ± 3 Å^2 and 91 ± 0.1Å^2 respectively. Figure 55 and Figure 56 represent the ATDs of the later ions, respectively. These excellent agreements of the measured and calculated results of the mobilities and collision cross sections of these specific ions suggest that the proposed structures of these cations are the most probable ones, where the addition of all acetylene molecules are carried out on the N-atom in the pyridine ring, even though these suggested structures are not the lowest energy possible structures from the energy point of view.
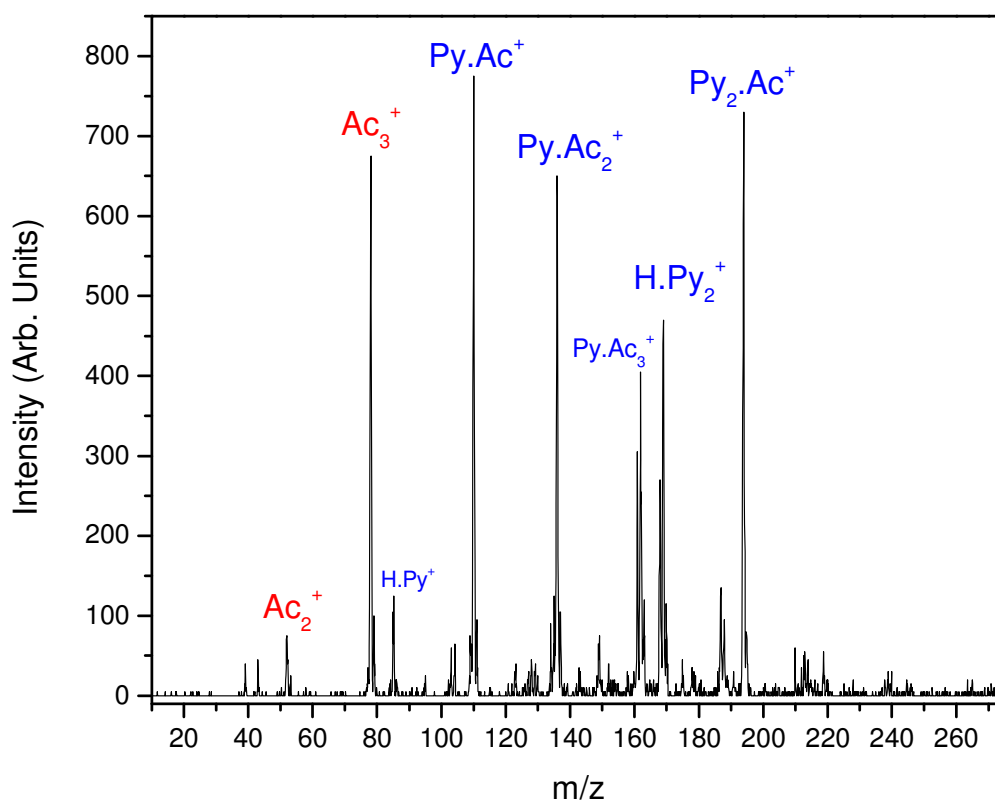
Figure 52. Mass spectrum of expanded d-pyridine/acetylene/helium mixture. A mixture of ≈5 psi acetylene and 60 psi helium was passed over pyridine at -78 ºC (dry ice temp.). Resulting heterogeneous clusters was injected (IE = 13.4 eV) into mobility cell containing 0.5 Torr He. The cell field was 6.48 V/cm and cell temperature was 303.2 K.
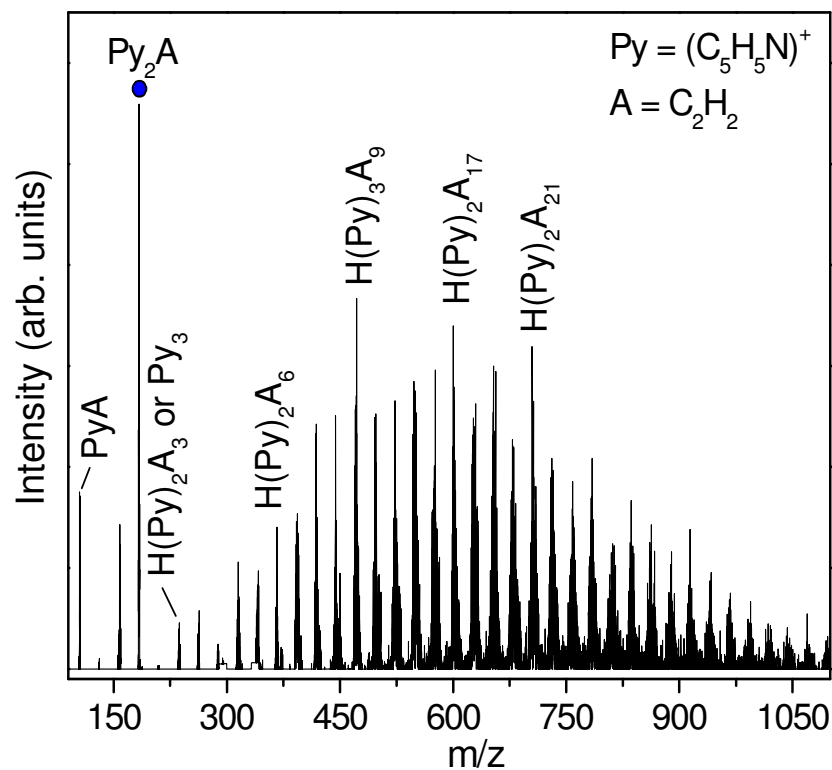
Figure 53. Mass spectrum of expanded pyridine/acetylene/helium mixture. A mixture of ~3 psi acetylene and 60 psi helium was passed over pyridine at 273 K. The resulting binary clusters were ionized by electron impact ionization.

Table 16. Measured and calculated ion mobilities and collision cross sections of $(C_5D_5N)_m.(C_2H_2)_n^+$, binary clusters where m=1,2 and n=1,2 at different experimental conditions.

Cluster	Temp (c)	Pres (Torr)	K cm^2/V.s	X section A^{o2}(exp)	K cm^2/V.s (calc)	X section A^{o2}(calc)
110	30.5	3.191	9.07	59.59	9.62	56.3
110	32.7	2.167	9.13	58.99	9.59	56.18
110	32.7	2.162	9.56	56.33	9.59	58.18
110	29.65	3.139	8.95	60.48	9.62	56.31
110	33.7	3.344	9.16	58.7	9.59	56.14
110	-98.5	2.472	11.27	63.29	11.11	64.18
110	-98.75	3.055	11.2	63.68	11.11	64.21
110	-98.45	1.736	11.13	64.02	11.11	64.17
136	30.5	3.19	7.6	70.88	7.99	67.43
136	31.3	3.17	7.67	70.14	7.98	67.4
136	30.85	2.332	7.81	68.93	7.99	67.42
136	-99.85	2.528	10.1	70.59	9.42	75.76
194	31.7	3.06	6.21	86.2	6.5	82.37
194	24	2.021	6.58	82.4	6.56	82.69
194	24	2.021	6.38	84.99	6.56	82.69

194	25.8	2.029	6.28	86.11	6.55	82.64
194	25.8	2.029	6.7	80.71	6.55	82.64
194	-99.85	2.531	8.18	86.8	7.76	91.57
194	-99.85	2.882	7.75	91.61	7.76	91.57
194	-98.45	1.736	7.76	91.13	7.74	91.4
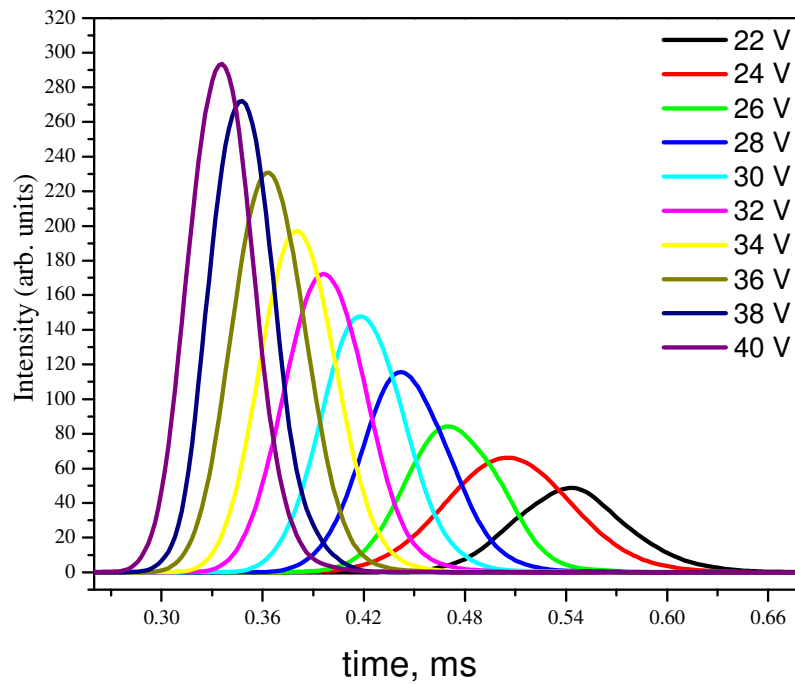
Figure 54. The arrival time distributions (ATDs) of injecting $C_5D_5N.C_2H_2^+$ (50 μs ion pulses) into the drift cell filled with 3.344 Torr He at different cell voltages (40-22 V). Injection energy is 18.9 eV (lab frame). The earlier ATD corresponds to drift cell voltage of 40V and the later ATD corresponds to drift cell voltage of 22 V.
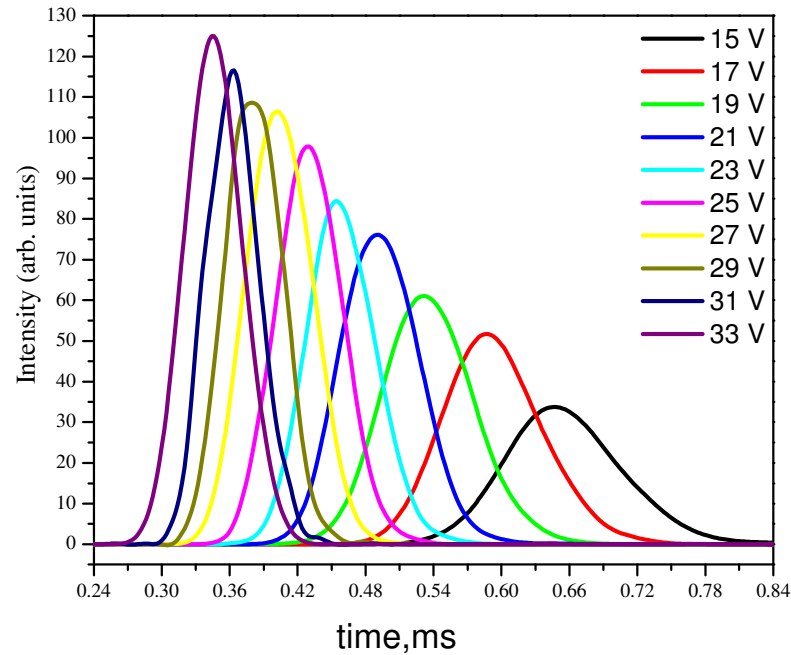
Figure 55. The arrival time distributions (ATDs) of injecting $C_5D_5N.(C_2H_2)_2^+$ (50 μs ion pulses) into the drift cell filled with 2.332 Torr He at different cell voltages (33-15 V). Injection energy is 18.4 eV (lab frame). The earlier ATD corresponds to drift cell voltage of 33V and the later ATD corresponds to drift cell voltage of 15 V.
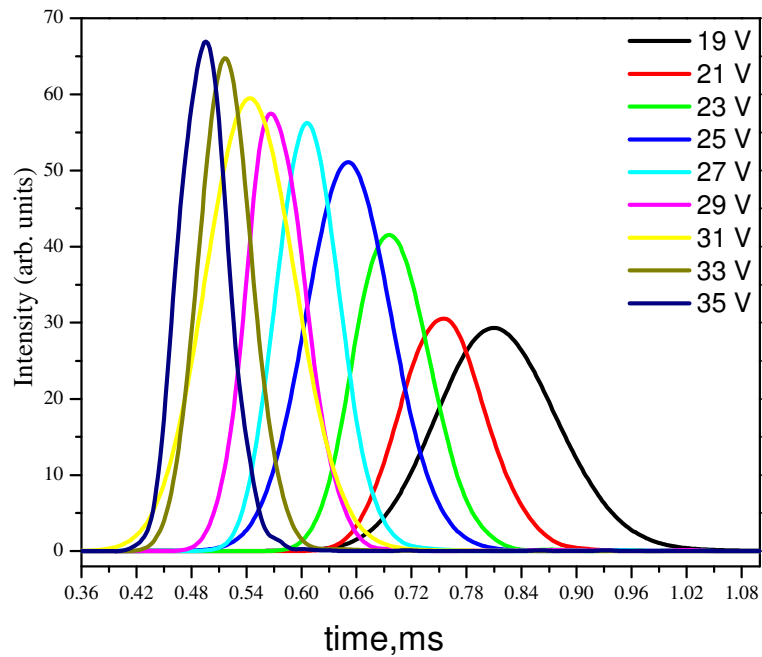
Figure 56. The arrival time distributions (ATDs) of injecting $(C_5D_5N)_2.C_2H_2^+$ (50 µs ion pulses) into the drift cell filled with 3.062 Torr He at different cell voltages (35-19 V). Injection energy is 20.4 eV (lab frame). The earlier ATD corresponds to drift cell voltage of 35V and the later ATD corresponds to drift cell voltage of 19 V.

Figure 57. Proposed Structures of $C_5D_5N.C_2H_2^+$ (m/z=110), $C_5D_5N.(C_2H_2)_2^+$ (m/z=136), and $(C_5D_5N)_2C_2H_2^+$ (m/z=194).

5.1.3.3 Collisional Induced Dissociation Studies (CID)

Collisional activation technique is widely used to study the possible fragmentation of specific ions, where the ions are accelerated into an inert gas, (He in our case). High energy collisions of the ions with neutral molecules result in electronic, vibrational and rotational excitations of the injected ions. The excited ions could reach a threshold where they suffer dissociations.[221] For further understanding of the mechanism of addition of acetylene molecules to the pyridine cation, collisional induced dissociation experiments were carried out on the $C_5D_5N.C_2H_2^+$ and $(C_5D_5N)_2.C_2H_2^+$ cations to investigate their fragmentation patterns upon injection of these cluster ions with high injection energies (IE) into the drift cell filled with He. Using an (IE) of 43eV, the observed fragmentation of $C_5D_5N.C_2H_2^+$ ion, (m/z= 110), are $(C_5D_5N)^+$ which is corresponding to m/z= 84, as shown in Figure 58, suggesting that the addition of acetylene molecules to be on the nitrogen of the pyridine cation as suggested theoretically.[60] In order to confirm this theoretical prediction, the fragmentation patterns of $(C_5D_5N)_2.C_2H_2^+$ (m/z=194) was also studied as shown in Figure 59. At high injection energies (62 eV), the main fragment was $C_5D_5N.C_2H_2^+$ cation, which corresponds to m/z= 110. Which confirm that the addition of the acetylene was to the nitrogen atom in the pyridine ring and no observations of $C_7HD_5N^+$ cation. In either case the absence of $C_5D_4N^+$ cation which should be observed if the addition was carried out on one of the carbons of the pyridine ring confirm our proposed mechanism. From the results of the mobility measurements and the CID studies, it is conclusive that the addition of acetylene molecules to the pyridine cations is made to the N-atom of the aromatic ring. These results are consistent with the previous theoretical

studies on adducts of selected ions with pyridines, indicating that the reaction site of pyridine is the N atom of the aromatic ring.[210,233-235] The mechanism of addition of acetylene to the pyridine has been investigated. Mainly, through the radical mechanism[236] and the ionic mechanism.[60] According to the radical mechanism, the addition of acetylene to pyridine ring will be on the ortho position corresponding to the N atom of the ring. This prediction agrees with the theoretically calculated structures, which give the most stable isomers adding to the same positions in this work and in Jiao et al [214] as well (will be discussed in the following section). While the ionic mechanism predicts that the addition is made directly to the N atom of the aromatic ring as found in this work. Upon formation of the neutral clusters, acetylene molecules attracted towards the N atom of pyridine due to its dipole moment,[237] leading to strong interaction, which could explain this mode of addition.
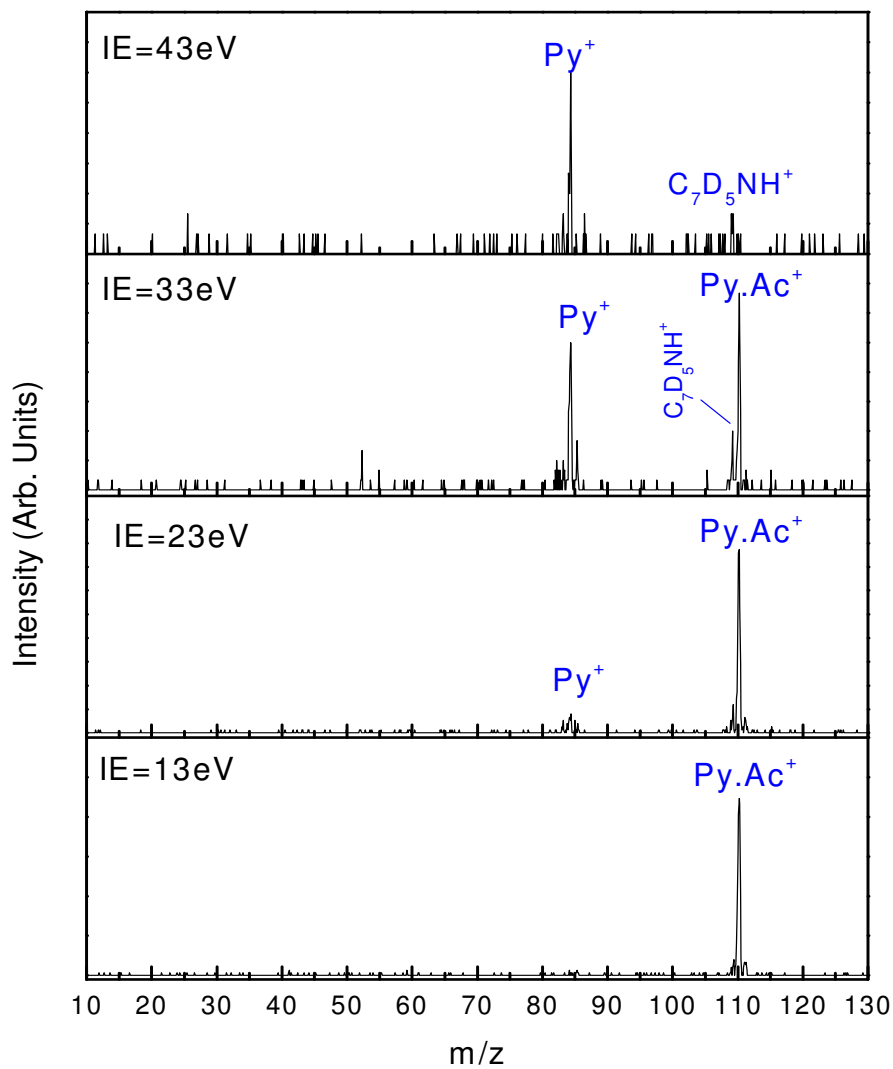
Figure 58. Mass spectra of the $C_5D_5N.C_2H_2^+$ cluster injected into the drift cell using different injection energies (lab). Drift cell voltage, temperature, and pressure were 40V, 303 K, and 0.7 Torr Helium respectively.
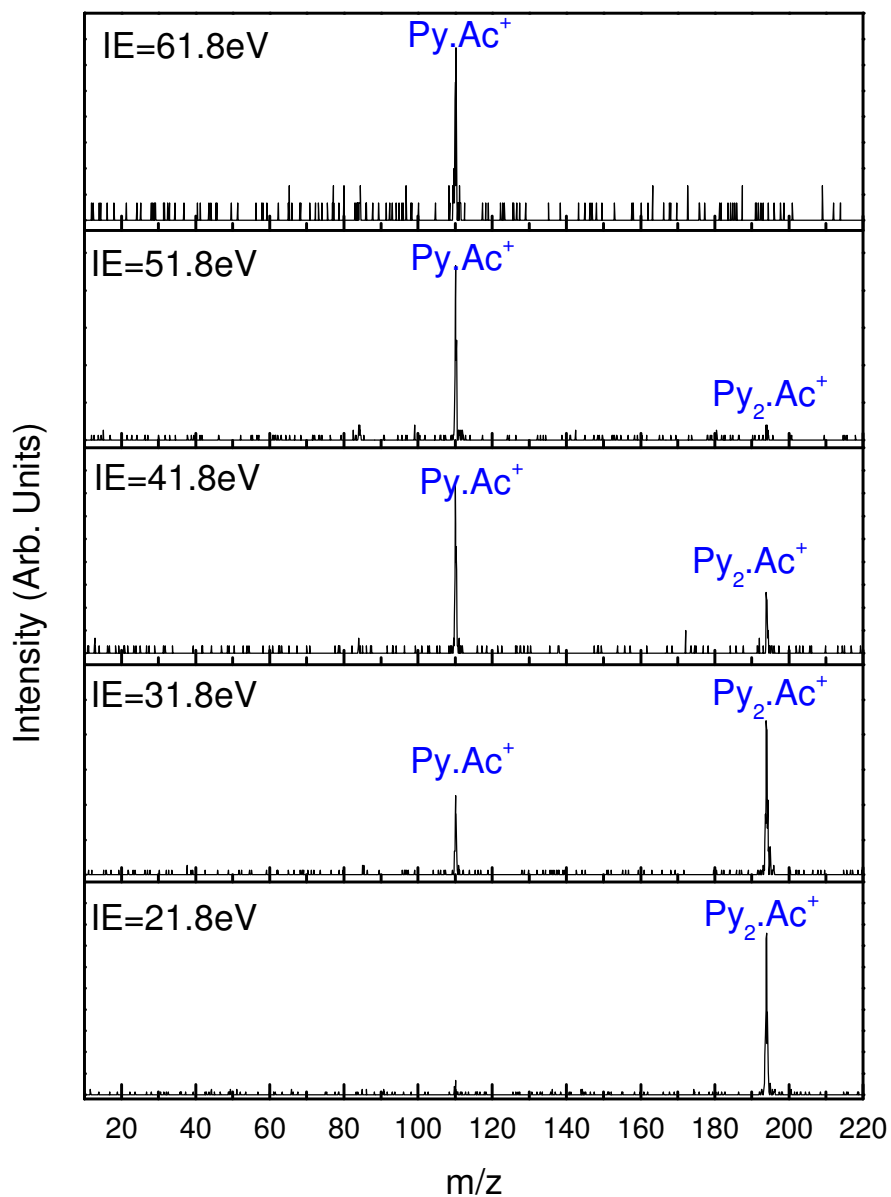
Figure 59. Mass spectra of the $(C_5D_5N)_2C_2H_2^+$ (m/z = 194) cluster injected into the drift cell using different injection energies (lab). Drift cell voltage, temperature, and pressure were 31V, 305 K, and 0.4 Torr Helium respectively.

5.1.3.4 Theoretical Calculations
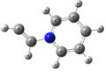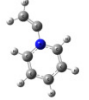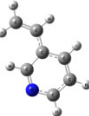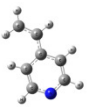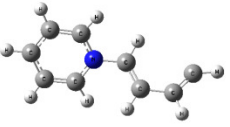
The ab initio calculations examined several $((C_5H_5N)_m.(C_2H_2)_n)^+$ adducts where n,m=1,2, and were optimized at B3LYP/6-31+g** level of theory. The calculations were carried out using Gaussian G03 RevD.03.[238] The optimized structures were confirmed to be minima by vibrational frequency analysis. The ab initio calculations examined several possible structures of the $C_5H_5N.C_2H_2^+$, $C_5H_5N.(C_2H_2)_2^+$ and $(C_5H_5N)_2.C_2H_2^+$ as shown in Table 17. For the $C_5H_5N.C_2H_2^+$ cluster ion, five isomers were studied to obtain the most stable structure of this cluster ion. These isomers were computed as a function of the point of attachment of acetylene to the pyridine cation; two isomers are representing the addition of acetylene molecule on the nitrogen atom; pyac1 and pyac2, and three isomers corresponding to the addition of acetylene onto the ortho, meta and para positions on the pyridine ring pyac3, pyac4 and pyac5 respectively.
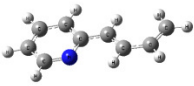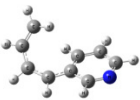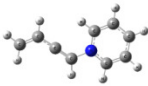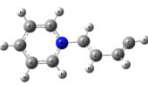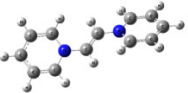
The most stable isomer of $C_5H_5N.C_2H_2^+$ is (Pyac3) as shown in Table 17, with binding energy of 61 kcal.mol^{-1} assuming the interaction of $C_5H_5N^+$ with acetylene. This result in agreement with condensation studies of pyridine with $C_4H_4^+$ ions reported previously.[214] The (Pyac1) conformer is higher in energy by15 kcal/mol than (Pyac3) with binding energy of ~46 Kcal.mol which is in the same range of C-N bond energy reported for the hetero-aromatic adducts.[73] Mobility measurements and CID experiments suggests that this is the most probable isomer for the pyridine cation reacted with acetylene as discussed previously.

Different isomers representing the addition of the second acetylene molecule to $C_5H_5N.C_2H_2^+$ were also studied at the same level of theory. The lowest energy isomer of

this addition is (Py2ac2) where the addition follows the Bittner-Howard mechanism on the ortho-position of the pyridine ring with the highest binding energy. The proposed structure of the $C_5H_5N(C_2H_2)_2^+$, isomer (Py2ac1), has higher relative energy (29 kcal.mol^{-1}).

Table 17. Theoretical Calculation Results of the reactions of pyridine cations, $C_5H_5N^+$ with acetylene

Name	Structure	Rel. Energy kcal/mol	K cm^2.V^{-1}.S^{-1}	Xsection A^{o2}	B.E. kcal/mol
Pyac1		15.22	9.60	56.20	-45.99
Pyac2		18.07	9.64	56.00	-43.15
Pyac3		0	9.63	56.04	-61.21
Pyac4		4.56	9.63	56.05	-56.66
Pyac5		12.72	9.60	56.20	-48.49
Py2ac1		28.95	7.99	67.43	-47.04

Py2ac2		0	8.04	67.06	-60.76
Py2ac3		12.02	8.21	65.61	-53.29
Py2ac4		10.7	8.03	67.10	-62.78
Py2ac5		25.9	7.84	68.76	N/A
Py2ac6		28.95	7.94	67.86	N/A
Ac2py1		0	6.5	82.36	-48.2

| Ac2py2 | | 4.14 | 6.59 | 80.78 | -43.8 |
| | | | | | |

5.2 Benzonitrile$^+$ /C$_2$H$_2$ System

5.2.1 Introduction

Polycyclic aromatic hydrocarbons PAHs present in Earth in the form of atmospheric aerosols,[3] soot[63-64,239] and volatile particles,[240] are also believed to play an important role in interstellar chemistry and in the atmospheric chemistry of planets and their moons in our solar system.[5] Detection of small aromatic molecules such as benzene, which is the basic building block toward complex PAHs formation, in the low-temperature atmospheres of solar planet including Titan's one suggest that the synthesis of PAHs proceeds in these environments. The presence of high abundance of nitrogen in Titan's atmosphere suggested that the haze layer of the Titan's composed of PANHs as well as the PAHs. Incorporation of nitrogen atom in the process of PAHs formation was predicted to be feasible for the formation of PANHs by Ricca et al.[60] The authors utilized density functional B3LYP method of calculations and the 6-31+G* basis set to compute potential energy profiles for reaction sequences analogous to the Hydrogen-Abstraction–C$_2$H$_2$-Addition (HACA) mechanism of PAH growth, but with HCN replacing C$_2$H$_2$ at certain reaction steps. They found that the presence of a nitrogen atom increases the barrier heights relative to the pure hydrocarbon species to about 15 kcal.mol^{-1} and concluded that the calculated barriers are probably too high to allow reactions to occur in the atmosphere of Titan unless the reaction rates are enhanced by vibrational energy of the aromatic

molecule, although the presence of a nitrogen atom in the aromatic ring promotes the formation of an additional ring.

We extended our investigation of PANHs formation from different cationic precursor through reaction with acetylene. In this part, we investigated the ion-molecule reactions of benzonitrile radical cation with acetylene under different experimental conditions, *for the first time*, to confirm the theoretical predictions. The addition of acetylene neutral molecule to the benzonitrile radical cation was calculated to be barrierless and exothermic reaction by ~51 kcal.mol^{-1}. Theoretically, this addition was followed by ring closure to form isoquinoline radical cation with a barrier of 7 kcal.mol^{-1}, and the ring closure produces energy of 6.7 kcal/mol in order to incorporate nitrogen atom in aromatic ring.

5.2.2 Reactions of Benzonitrile cation with acetylene

Figure 60 displays a set of mass spectra obtained by injection of benzonitrile radical cation into He (panel (a)), 8 mTorr purified C_2H_2 in He, (Panel (b), 10 mTorr purified C_2H_2, (panel (c)) and 12 mTorr purified C_2H_2 in He as shown in panel (d). The addition of two acetylene molecules to the benzonitrile cation corresponding to the formation of $C_9H_7N^+$ adduct (m/z=129) and $C_{11}H_9N+$ adduct (m/z=155) was observed. We obtained the same results by increasing the pressure of acetylene to 100 mTorr as shown in Figure 61, the addition of acetylene molecules can be expressed in the following two equations;

$$C_7H_5N^+ + C_2H_2 \longrightarrow C_9H_7N^+ \qquad (5.7)$$

$$C_9H_7N^+ + C_2H_2 \longrightarrow C_{11}H_9N^+ \qquad (5.8)$$

Figure 62 displays the injection of benzonitrile radical cation into higher concentrations of acetylene, 500 mTorr as shown in Figure 62 (d), the depletion of $C_7H_5N^{\bullet+}$ peak is apparent under these conditions and the main adduct formation is the $C_{11}H_9N^{\bullet+}$.

Pseudo first-order rate constants were calculated using $\ln\frac{I}{\Sigma I} = -kt$, where I is the integrated intensity of the reactant ion mobility peak and ΣI is the sum of the intensities of the reactants and all product ions peak including the secondary products and t is the mean drift time, taken as the center of the of the reactant ion. k is obtained from plotting $lnI/\Sigma I$ versus t, where we varied the reaction time by varying the drift cell voltage, and the pseudo first-order rate coefficients k_1 were obtained from the slope of the plot.

Second-order rate constants k_2 were obtained from $k_2 = k_1/$ [N], where N is the number density (molecules.cm^{-3}) of the neutral reactant C_2H_2 calculated from the equilibrium pressure of the reactant over a reservoir in which its vapor is mixed with He carrier gas at known temperature. Figure 63 displays voltage studies of injection of benzonitrile radical cation into acetylene/He mixture, the applied field on the drift cell ranged from 2 V.cm^{-1} to 18 V.cm^{-1}. We have inspected the ATDs, Figure 64, of the product ions to establish whether or not the $C_7H_5N^+$ ion and the formed adducts $C_9H_7N^+$ and $C_{11}H_9N^+$ are in equilibrium. If in equilibrium, the ATDs peaks of the ions should overlap, since equilibrium populations interchange from one form to another and drift coupled together in the cell. However, Figure 64 shows that the ATDs peaks of $C_7H_5N^+$, the $C_9H_7N^+$ and $C_{11}H_9N^+$ adducts do not overlap, indicating that they are not in

equilibrium and that at least, the first C_2H_2 molecule adds irreversibly to $C_7H_5N^+$ under our experimental conditions.

The overall second order rate constant of the benzonitrile cation with acetylene are tabulated in Table 18, and the integrated arrival time distribution of the product ions are presented in Figure 65 (left). The average overall second rate constant of these reactions is 4.2×10^{-11} molecule. cm^3. s^{-1}, which is two orders of magnitude less than the collision rate ($\sim \times 10^{-9}$ molecule. $cm^3.s^{-1}$). Arrhenius plot is represented in Figure 66 which shows negative activation energy for these reactions.
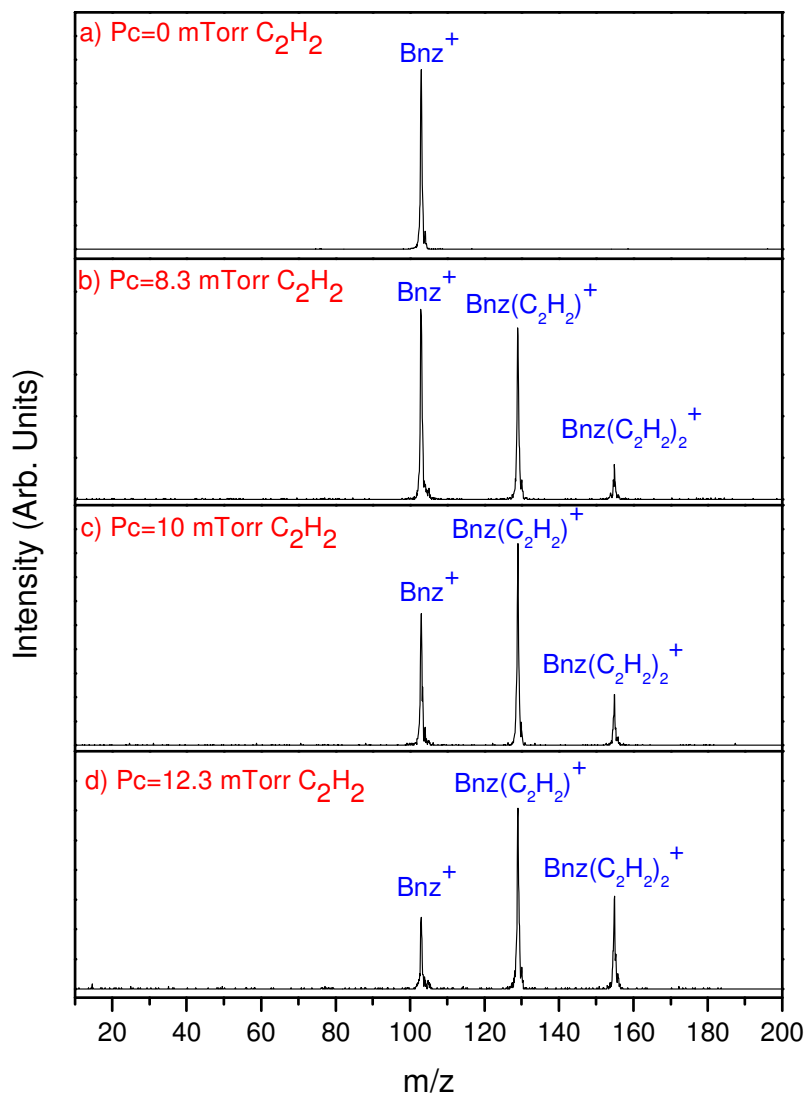
Figure 60. Mass spectrum of $C_7H_5N^+$ after injection into the drift cell. The injection energy is 13.9 eV (Lab frame). Cell voltage is 30 V. Drift cell temperatures is 26 °C. Drift cell pressure is a) 0 mTorr , b) 8.3 mTorr, c) 10 mTorr and d) 12.3 mTorr purified C_2H_2 respectively.
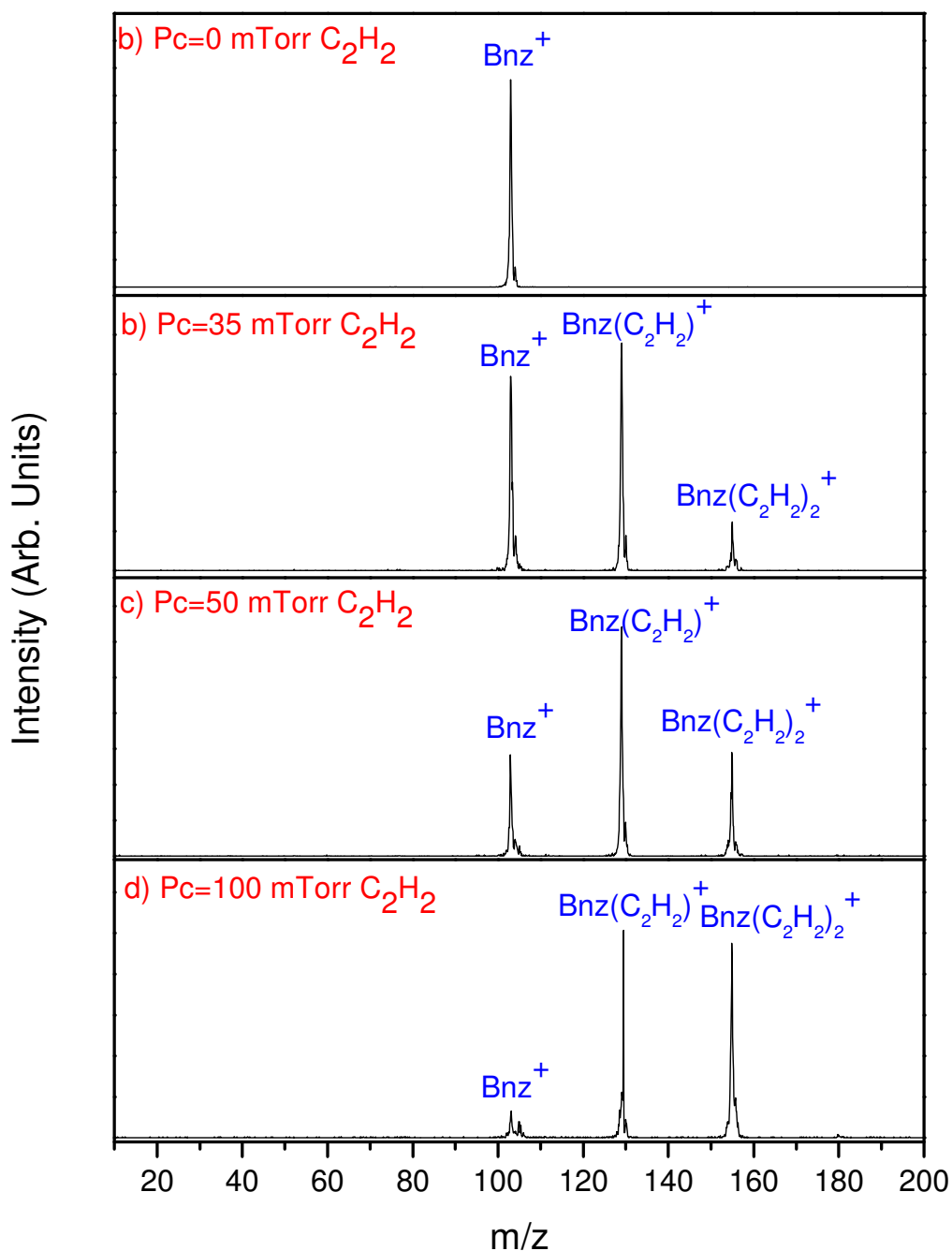
Figure 61. Mass spectrum of $C_7H_5N^+$ after injection into the drift cell. The injection energy is 13.9 eV (Lab frame). Cell voltage is 30 V. Drift cell temperatures is 26 $^{\circ}$C. Drift cell pressure is a) 0 mTorr , b) 35 mTorr, c) 50 mTorr and d) 100 mTorr purified C_2H_2 respectively.
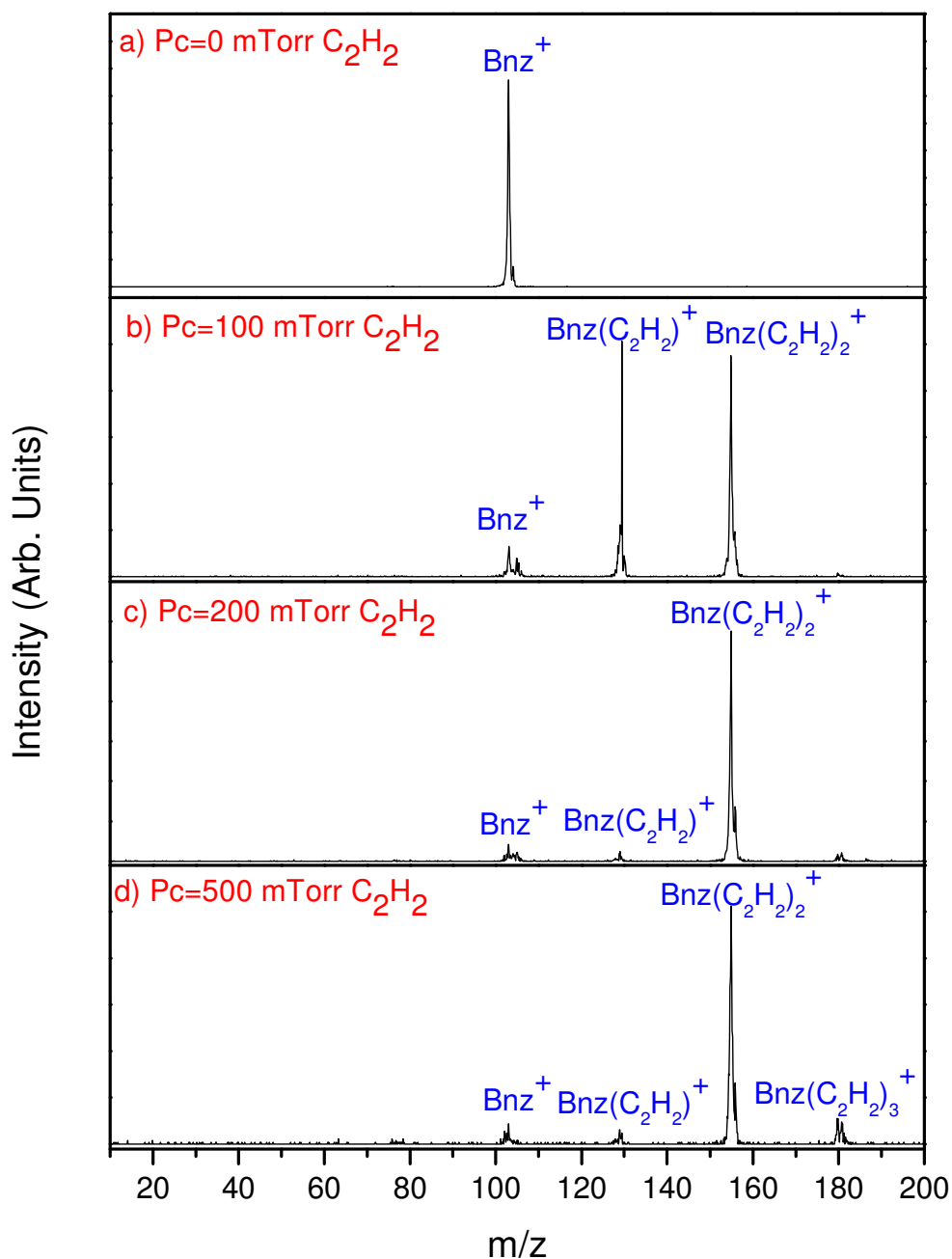
Figure 62. Mass spectrum of $C_7H_5N^+$ after injection into the drift cell. The injection energy is 13.9 eV (Lab frame). Cell voltage is 30 V. Drift cell temperatures is 26 ^{o}C. Drift cell pressure is a) 0 mTorr , b) 100 mTorr, c) 200 mTorr and d) 500 mTorr purified C_2H_2 respectively.
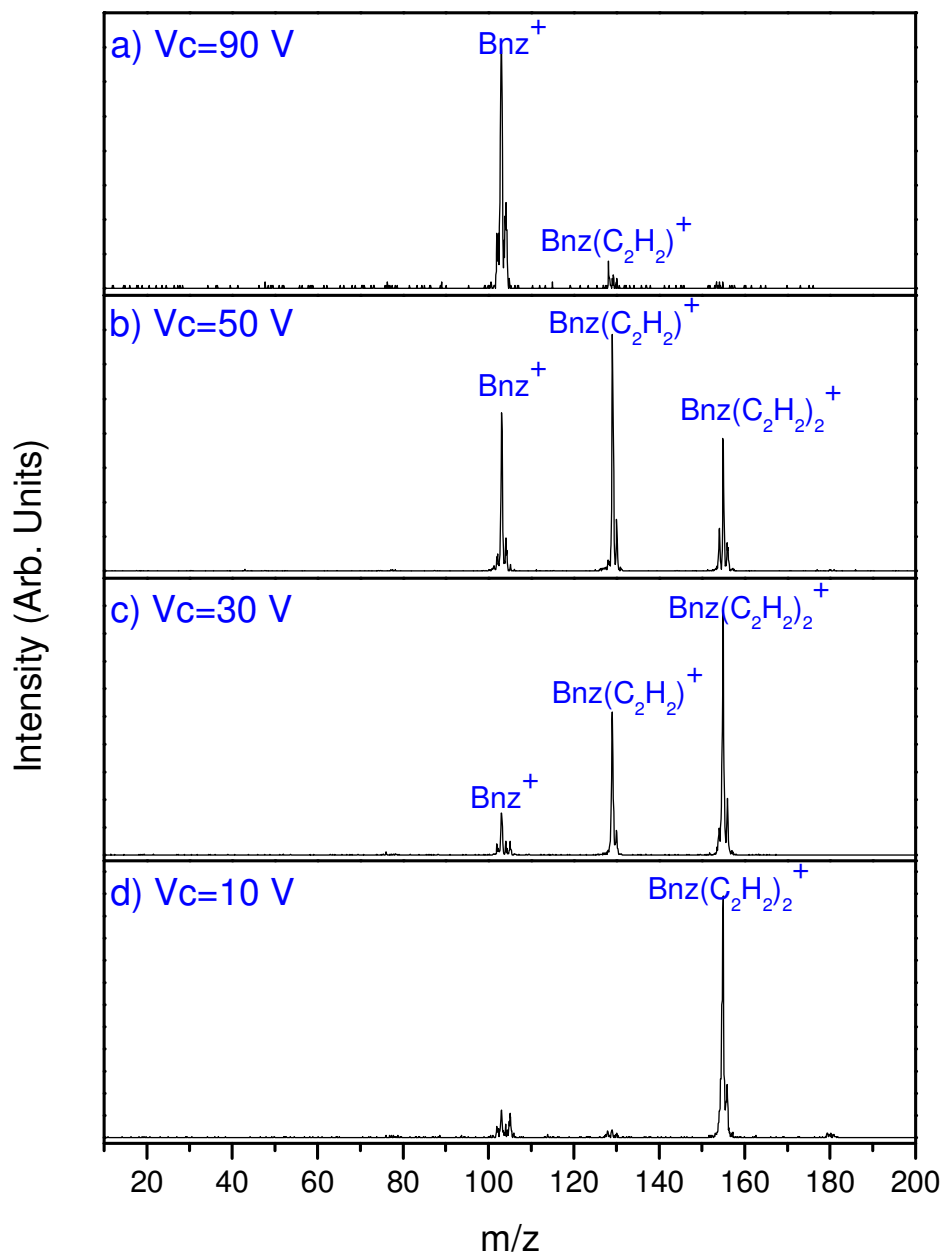
Figure 63. Mass spectrum of $C_7H_5N^+$ after injection into the drift cell. The injection energy is 14 eV (Lab frame). Drift cell temperatures is 27 ^{o}C. Drift cell pressure is 100mT C_2H_2&495 mTorr He. Cell voltage is a)90, b)50, c)30 and d)10 V respectively.
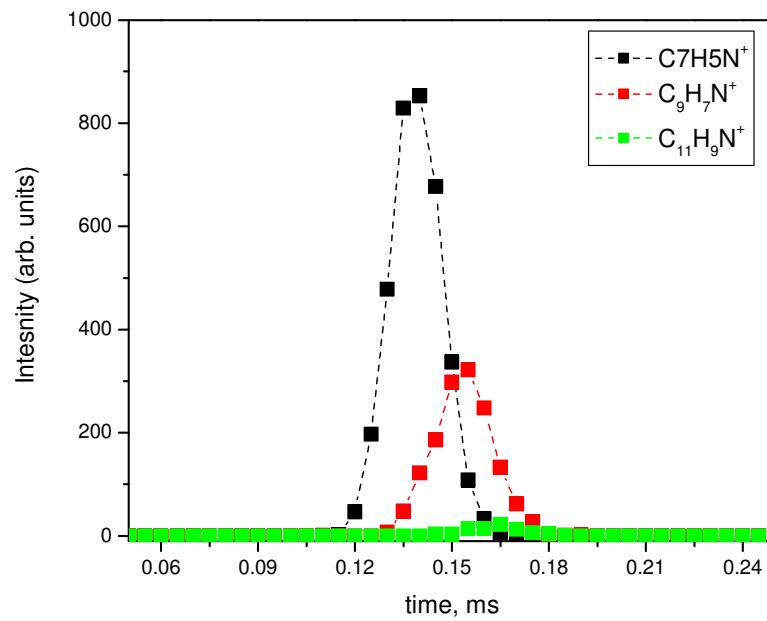
Figure 64. Arrival time distributions (ATDs) of the ions observed following the injection of $C_7H_5N^{+\bullet}$ ions into C_2H_2/He at 304 K, $P(C_2H_2)$ = 5 mtorr, $P(He)$ = 515 mtorr, injection energy (lab) = 13.9 eV, cell field = 4 V/cm.
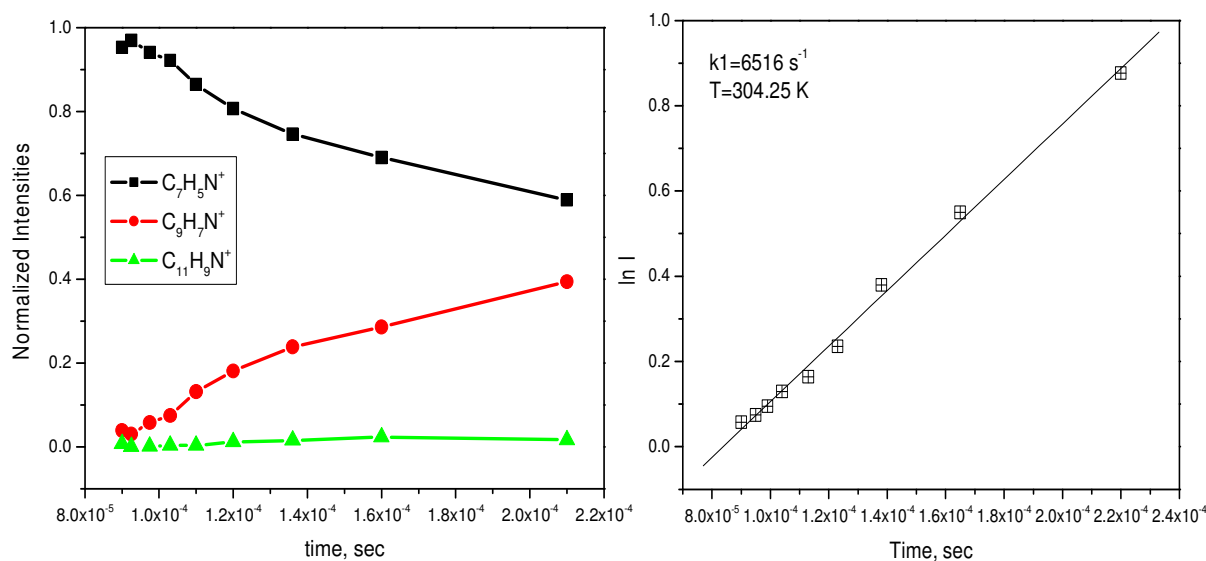
Figure 65. (Left) Integrated arrival time distributions of the reactant and product ions as a function of reaction time following the injection of benzonitrile cation $C_7H_5N^+$ into the drift cell containing 515 mTorr (5 mTorr acetylene, balance is He) at 304.3 K. Injection energy 13.9 eV (lab frame). Drift cell filed varied between 10-2 V.cm^{-1}. (Right) Pseudo first-order rate constant of the reactions of benzonitrile cation with acetylene under the same experimental conditions, $k1$= 6.561×10^3 s^{-1}.

Table 18. Second order rate constant of the reactions of benzonitrile cation with acetylene.

P acetylene mTorr	P He mTorr	T ^{o}C	T k	k_2 cm^3.s^{-1}	ln k_2	1000/T
5	500	26.6	299.75	3.70×10^{-11}	-24.0201	3.336113
5.39	539	70.65	343.8	3.98×10^{-11}	-23.9472	2.908668
5.85	588	140.4	413.55	2.48×10^{-11}	-24.4202	2.418087
6.3	630	210.55	483.7	1.40×10^{-11}	-24.992	2.067397
6.69	669	279.5	552.65	2.07×10^{-11}	-24.6009	1.809463
5.1	511	31.1	304.25	3.90×10^{-11}	-23.9675	3.286771
4.8	5.11	0.5	273.65	7.80×10^{-11}	-23.2743	3.654303
4.58	511	-28.5	244.65	8.70×10^{-11}	-23.1651	4.087472
4.24	424	-60.7	212.45	2.11×10^{-11}	-24.5817	4.70699
4.06	510	-82	191.15	5.30×10^{-11}	-23.6607	5.231494
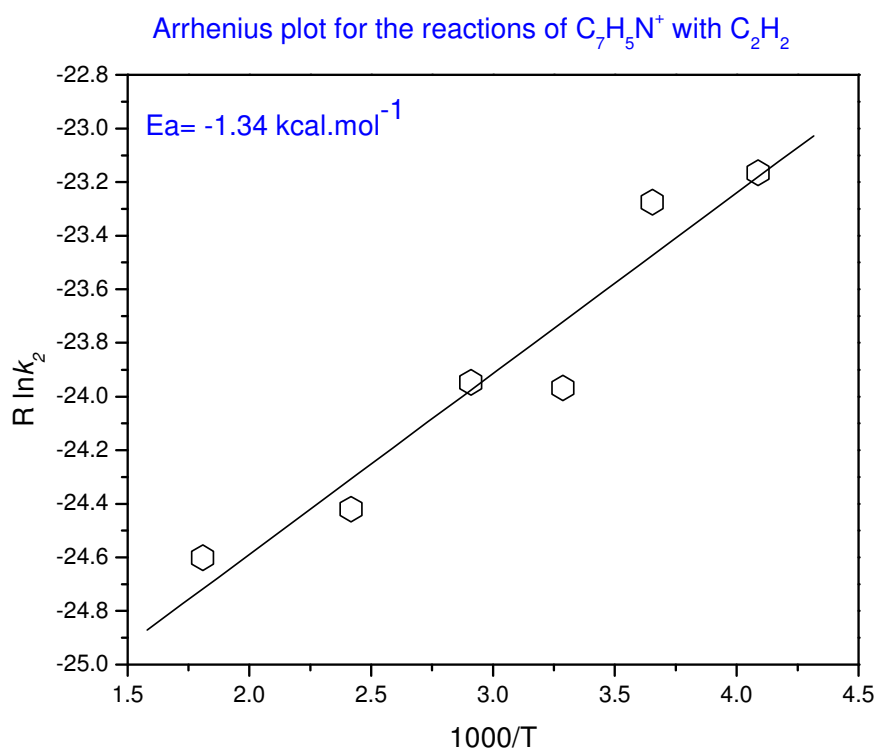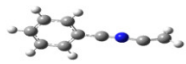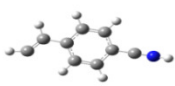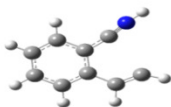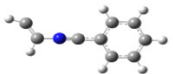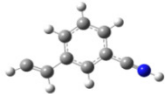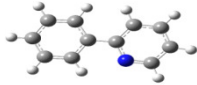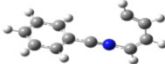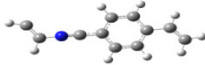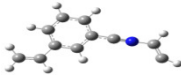
Figure 66. Arrhenius plot of the reactions of $C_7H_5N^+$ with C_2H_2, obtained by plotting the measured second order rate coefficient as a function of inverse temperature.

Table 19 summarizes different calculated possible isomers of the addition of acetylene to benzonitrile cations. Calculations were carried out at the B3LYP/6-31+G** level of theory. The lowest energy possible structure of the addition of C_2H_2 to $C_7H_5N^+$ was isomer (Bzac1) where the addition of the acetylene were carried out on the terminal nitrogen atom in the nitrile group and not on the aromatic ring as predicted theoretically.[60] Addition of the second acetylene molecule could lead to the formation of 2-phenyl-pyridine via ring closure, isomer (Bz2ac1). Other possible isomers were calculated as well and were summarized in Table 19.

Table 19. Theoretical Calculation Results of the reactions of benzonitrile cations, $C_7H_5N^+$ with acetylene

$C_7H_5N^+ + C_2H_2$				
Isomer	Structure	Method/Basis Set	Relative E	B.E. kcal.mol^{-1}
Bnzac1		B3LYP/6-31+G**	0	-44.5
Bnzac2		B3LYP/6-31+G**	7.4	-37.2
Bnzac3		B3LYP/6-31+G**	8.3	-36.2
Bnzac4		B3LYP/6-31+G**	8.8	-35.6

Bnzac5		B3LYP/6-31+G**	10.4	-34.1
$C_7H_5N^+ +2\ C_2H_2$				
Bz2ac1		B3LYP/6-31+G**	0	-152.6
Bz2ac2		B3LYP/6-31+G**	65.1	-87.5
Bz2ac3		B3LYP/6-31+G**	70.7	-81.9
Bz2ac4		B3LYP/6-31+G**	73.3	-79.3

5.3 Pyrimidine radical cations

Reactions of pyrimidine radical cation with acetylene are, *for the first time,* presented in this section. Additions of up to two acetylene molecules were observed as the condensation products accompanied with hydrogen elimination. This could be a general trend in the reactions of N-containing heterocyclic compounds as this type of condensation-elimination reactions were reported also in the reactions of pyridine cation with acetylene. Kinetic measurements of the condensation reactions are measured and DFT calculations preformed for different possible isomers are reported.

Also, reactions of benzene radical cation with pyrimidine are reported as an example of the ionic interactions between aromatic hydrocarbons and heterocyclic compounds. Ion mobility measurements, CID and DFT calculations of the possible products of these interactions are reported as well.

5.3.1 Pyrimidine radical cation reactions with acetylene

5.3.1.1 Results and Discussion

Pyrimidine radical cations were generated through the expansion of He gas seeded with pyrimidine vapor through a pulsed nozzle. The formed clusters were ionized by the EI ionization and pyrimidine radical cation, $C_4H_4N_2^+$, was mass selected by the first quadrupole mass filter of the IMS system and introduced into the drift cell. Mobility measurements of pyrimidine radical cation were measured in He, the average measured mobility and collision cross section values are 11.86 $cm^2.V^{-1}.s^{-1}$ and 45.89 $Å^2$ respectively.

Meanwhile, the average calculated mobilities and collision cross section are 11.97 $cm^2.V^{-1}.s^{-1}$ and 45.61 $Å^2$ respectively which are in good agreement with the calculated results.

Figure 67 represent the injection of pyrimidine radical cation into the drift cell containing different amounts of acetylene. Figure 67 bottom panel represents the injected pyrimidine radical cation into He, no observations of fragmentations under these experimental conditions. The measured mobility of pyrimidine radical cation was carried under these conditions will be discussed in the following section. In presence of small amount of acetylene pressure, 0.04 mTorr, observation of the first adduct of acetylene added to the pyrimidine radical cation according to the following equation;

$$C_4H_4N_2^{\bullet+} + C_2H_2 \longrightarrow C_6H_6N_2^{\bullet+} \qquad (5.9)$$
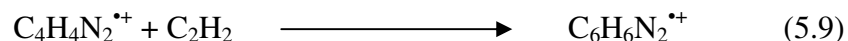
Further increase in acetylene pressure, leads to the observation of the second adduct as the following equation,

$$C_6H_6N_2^{\bullet+} + C_2H_2 \longrightarrow C_8H_7N_2^{+} + H^{\bullet} \qquad (5.10)$$
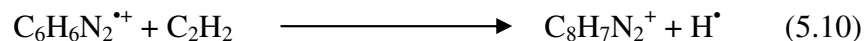
These adducts formation is a function of acetylene pressure. No further addition of acetylene to the pyrimidine radical cations were observed by increasing acetylene pressure, maximum pressure applied was 1273 mTorr purified C_2H_2. Interestingly, at high acetylene pressure in the drift cell, 294 mTorr and higher, a peak corresponding to m/z=78 was observed. This peak may be corresponding to $(C_2H_2)_3^{+}$, and this could be produced from clustering of acetylene trimer in the presence of pyrimidine radical cation followed by a charge transfer to the formed acetylene trimer as in the following equation,

$$C_4H_4N_2^{\bullet+} + 3(C_2H_2) \longrightarrow C_4H_4N_2^{\bullet} + (C_2H_2)_3^{+} \qquad (5.11)$$

184
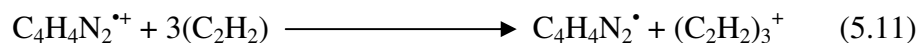
To further investigate on the formed adducts either they covalent or van der Waal's compounds, Pyrimidine radical cations were injected into 300 mTorr purified acetylene (total pressure in the drift cell was 1002 mTorr, balance was He), drift cell temperature varied from 322 K to 494 K as shown in Figure 68 and the adducts formed show a good stability at these high temperatures which is an indication of their covalent character.

Kinetics studies were carried out to measure the reaction rate coefficient of addition of acetylene molecules to $C_4H_4N_2^{\bullet+}$ cations. The drift cell was filled with ~0.04 mTorr acetylene diluted with 1.559 Torr He at 301.2 K. Arrival time distributions (ATDs) of the various ions were measured by monitoring the signals corresponding to each ion as a function of time after injection into the cell (residence time). Residence time was varied between 100 and 200 μs by changing the field applied on the cell, as shown in Figure 69. The time-resolved studies allow the identification of primary and secondary reaction products, and the measurement of rate coefficients. Pseudo first-order rate constant for the decay of the $C_4H_4N_2^{\bullet+}$ reactant ions was obtained from time-resolved experiments using the relation ln $I/\Sigma I = -kt$. Hence, we obtained k_1 from plots of ln $I/\Sigma I$ *vs. t*, where I is the integrated intensity of the reactant ion peak and ΣI is the sum of intensities of the reactant and all product ion peaks including secondary products, and t is the mean drift time (taken as the center of the arrival time distribution) of the reactant. Second-order rate coefficients, k_2, were obtained from $k_2 = k_1/[N]$ where N is the number density (molecules.cm^{-3}) of the neutral C_2H_2 reactant in the cell Figure 70 shows the normalized intensities of reactants and products of the reactions (5.9) and (5.10) as a function of time. The rate coefficient for

the overall reaction to form products is on the order of 2.9×10^{-9} cm^3.s^{-1}; which is in the

order of collision rate ($\sim \times 10^{-9}$ cm^3.s^{-1}).
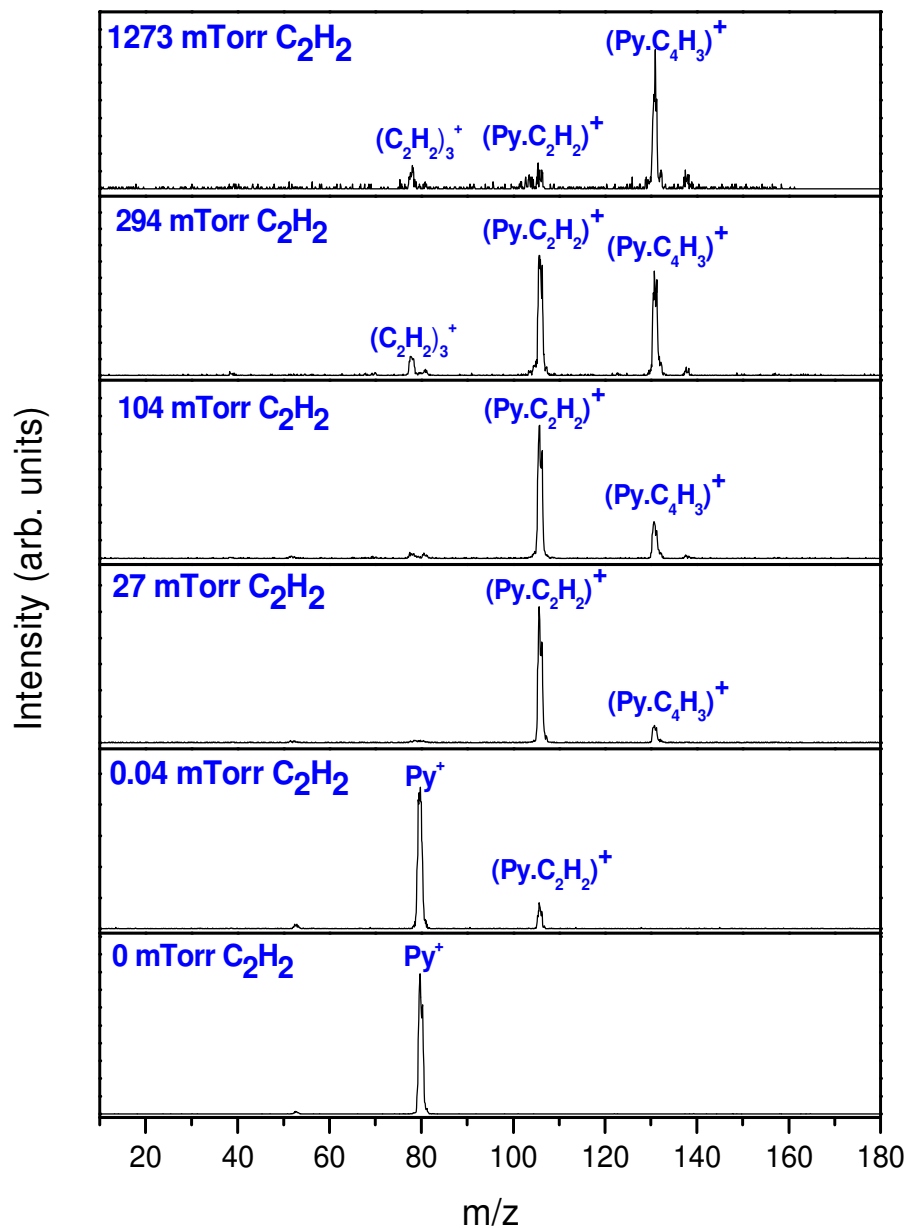
Figure 67. Injected mass selected Pyrimidine radical cation into the drift cell. Cell temperature was 304.2 K. Cell voltage was 6.2 V.cm^{-1}. Injection energy was 17.4 eV (lab). Acetylene pressure inside the drift cell was: 0, 0.04 mTorr, 27 mTorr, 104 mTorr, 294 mTorr and 1273 mTorr from bottom panel to the top one respectively.
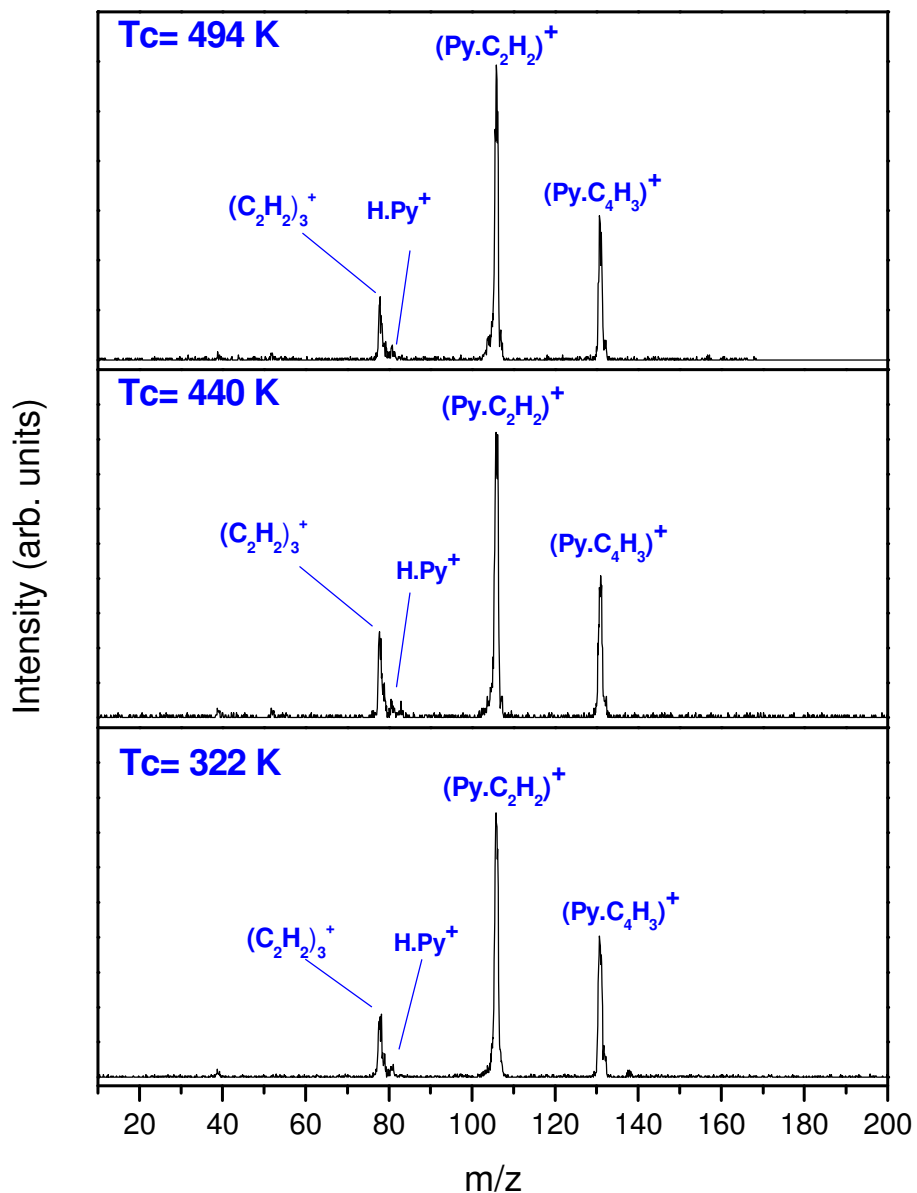
Figure 68. Injected mass selected Pyrimidine radical cation into the drift cell. Cell voltage was 6.2 V.cm^{-1}. Injection energy was 17.4 eV (lab). Pressure inside the drift cell was 1002 mTorr (300 mTorr purified C_2H_2), Temperature of the drift cell was 322 K, 440 K and 494 K from bottom panel to the top one respectively.
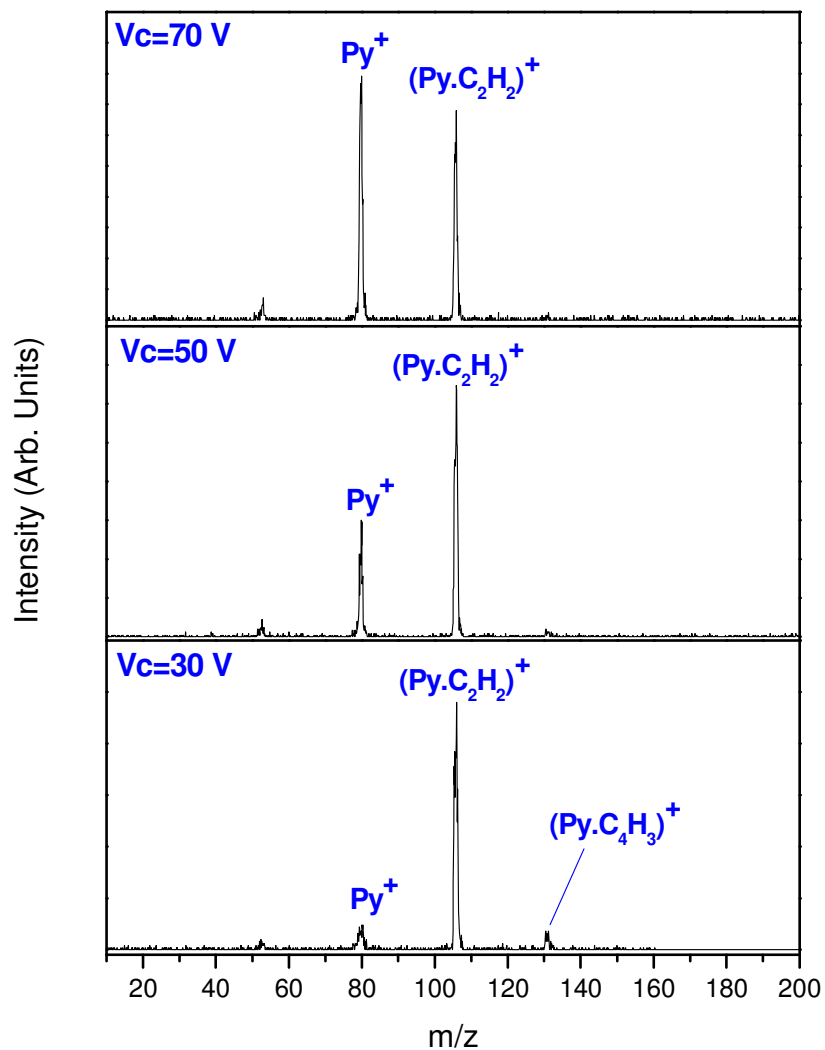
Figure 69. Injected mass selected pyrimidine radical cation into the drift cell. Injection energy was 19 eV (lab). Pressure inside the drift cell was 1559 mTorr (0.04 mTorr purified C_2H_2), Temperature of the drift cell was 301.2 K. Cell voltage was 14 V.cm^{-1}, 10 V.cm^{-1} and 6 V.cm^{-1} from top panel to the bottom one respectively.
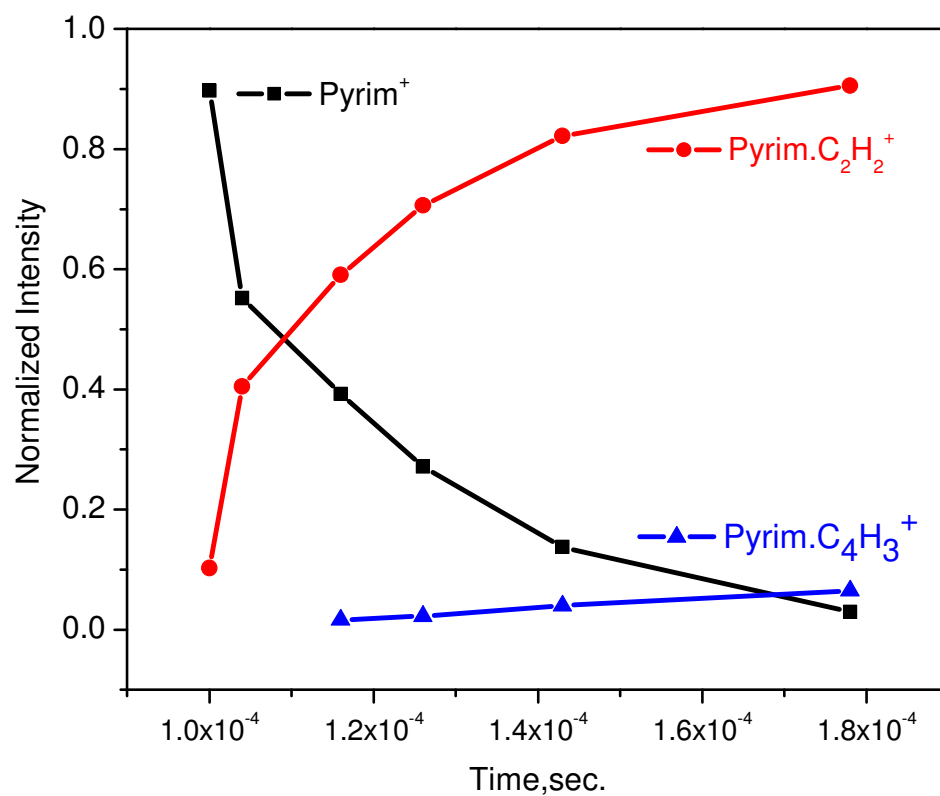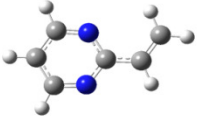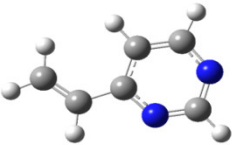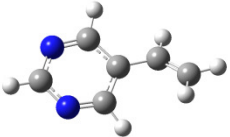
Figure 70. Integrated arrival time distribution of the reactant and product ions as a function of reaction time following the injection of $C_4H_4N_2^{\bullet+}$ into the drift cell containing 0.04 mTorr acetylene, and formation of $C_6H_6N_2^{\bullet+}$ and $C_8H_7N_2^{\bullet+}$ respectively, at 301 K.

Several possible isomers of the addition of C_2H_2 to pyrimidine radical cation in order to form $C_6H_6N_2^{.+}$ radical cation are calculated utilizing the DFT calculations at the UB3LYP/6-311+G** level of theory are performed and summarized in Table 20. (Pa1) was the lowest energy structure where the addition of the acetylene molecule to the pyrimidine carried out to the o-position for the N-atom, (same observation was determined in reacting pyridine cation with acetylene (section 2.3.4)). Addition of acetylene to the N-atom of the pyrimidine ring, isomer (Pa4), was 16 Kcal.mol^{-1} higher in energy than the lowest possible isomer.

Possible isomers of the reaction of C_2H with $C_6H_6N_2^{.+}$ radical cation are calculated utilizing the DFT calculations at the UB3LYP/6-311+G** level of theory are performed and summarized in Table 21. All possible C_2H additions are made to the (Pa1) isomer given in Table 20. Addition of the C_2H to C1 or C2 on the o-position of the pyrimidine molecule, C1 being the covalently bonded carbon to the ring and C2 is the terminal carbon, lead to the formation of (P2a2) isomer and (P2a1) isomer respectively. These two isomers found to be the most stable isomers of this reaction, provided that isomer (P2a1) is more stable by 17 Kcal.mol^{-1} than isomer (P2a2).

Table 20. Proposed possible structures of the addition of C_2H_2 to $C_4H_4N_2^{\cdot+}$ radical cation

Isomer	Structure	Method	Basis Set	Relative E kcal.mol^{-1}	B.E. kcal.mol^{-1}
Pa1		UB3LYP	6-311+G**	0	-52.2
Pa2		UB3LYP	6-311+G**	4.7	-47.4
Pa3		UB3LYP	6-311+G**	6.3	-45.9
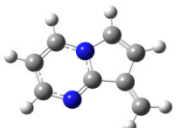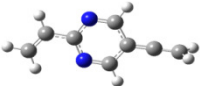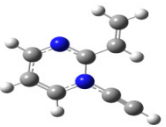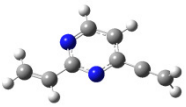
Pa4		UB3LYP	6-311+G**	15.9	-36.3

Table 21. Proposed possible structures of the addition of C_2H to $C_6H_6N_2{}^{\cdot+}$ radical cation

Isomer	Structure	Method	Basis Set	Relative E kcal.mol^{-1}
P2a1		UB3LYP	6-311+G**	0
P2a2		UB3LYP	6-311+G**	17
P2a3		UB3LYP	6-311+G**	68
P2a4		UB3LYP	6-311+G**	69.8
P2a5		UB3LYP	6-311+G**	87.5

At low temperatures, sequential association reactions of several acetylene molecules onto the $C_4H_4N^+$ radical cation are observed as shown in Figure 71. At 255 K, association of C_2H_2 and C_4H_3 onto the pyrimidine radical cation to form the $C_6H_6N_2^+$ and $C_8H_7N_2^+$ ions respectively was observed. By lowering the temperature to 163 K, acetylene adds to the $C_8H_7N_2^+$ cation to form the $C_{10}H_9N_2^+$ cations. At the lowest temperature, 127 K, the association of acetylene onto the formed acetylene-pyrimidine clusters reached up to $C_{14}H_{13}N_2^+$.
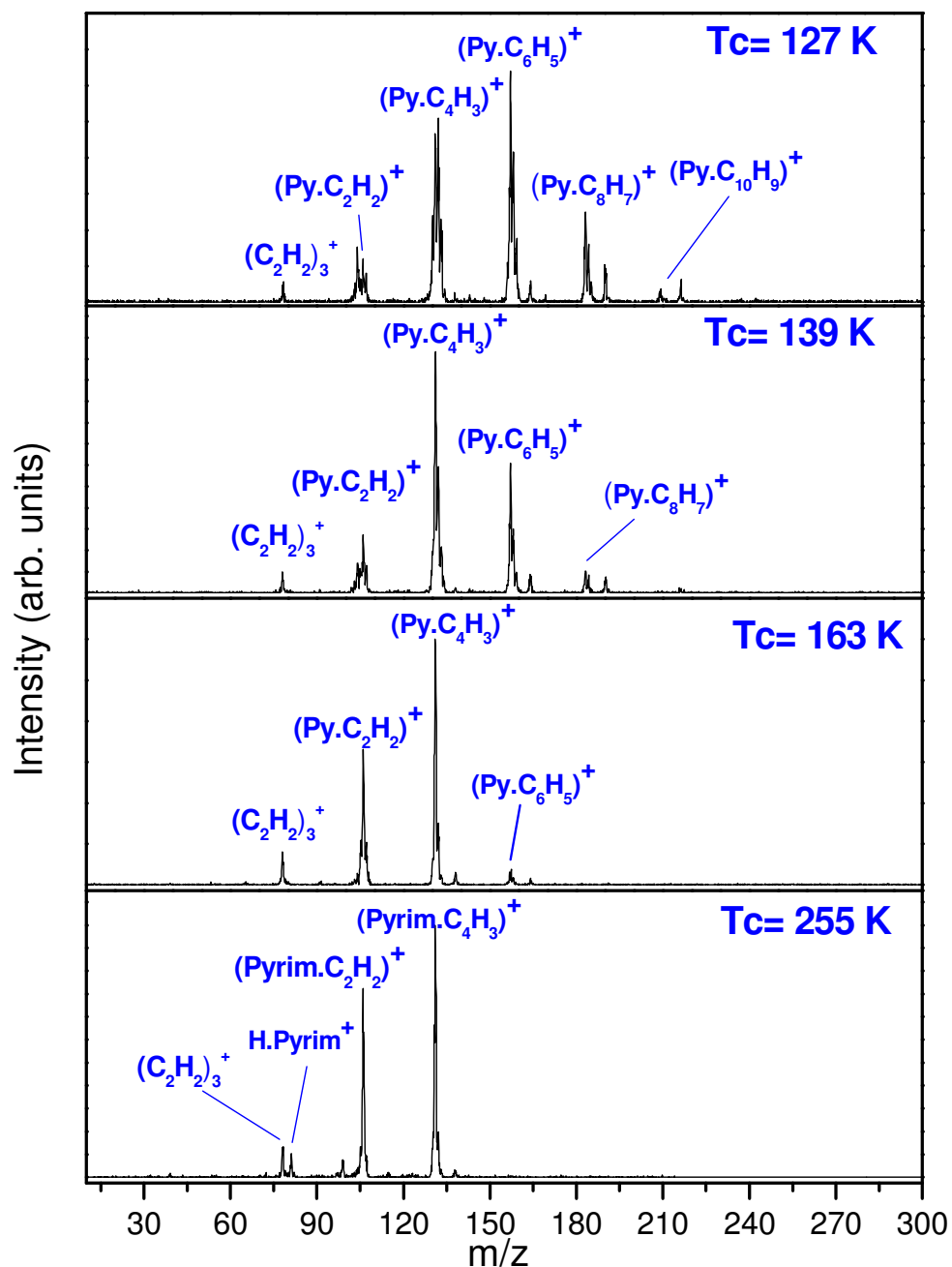
Figure 71. Injected mass selected Pyrimidine radical cation into the drift cell. Cell voltage was 6.2 V.cm^{-1}. Injection energy was 17.3 eV (lab). Pressure inside the drift cell was 971 mTorr (320 mTorr purified C_2H_2), Temperature of the drift cell was 255 K, 163 K and 139 K and 127 K from bottom panel to the top one respectively.

5.3.2 Benzene radical cation reactions with Pyrimidine

5.3.2.1 Ion-molecule reactions

Benzene, $C_6H_6^{\bullet+}$, ions are generated by electron impact ionization (EI=50-75eV) of the clusters formed by supersonic adiabatic expansion of $C_6H_6^{\bullet+}$/He mixture (2% $C_6H_6^{\bullet+}$) and they are mass selected and injected into a drift cell containing He/pyrimidine. Figure 72 represents the injection of d-benzene radical cation into (a) He, (b) pyrimidine and (c) Pyrimidine/He. Injection of $C_6H_6^{\cdot+}$ into pure pyrimidine in the drift cell, as shown in Figure 72 (b), produces the following products as shown in Scheme 1;
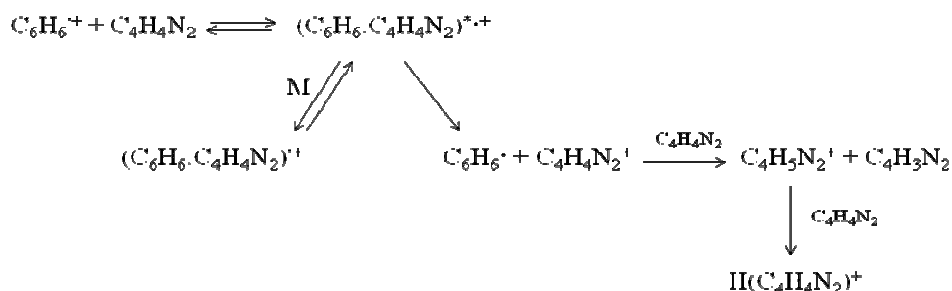
Scheme 1. Reactions of $C_6H_6^{\cdot+}$ with Pyrimidine.

The major reaction products of the reaction of $C_6H_6^{\cdot+}$ with pyrimidine is the adduct $(C_6H_6.C_4H_4N_2)^{\cdot+}$ and minor products resulting from the charge transfer from $C_6H_6^{\cdot+}$ to $C_4H_4N_2$ was observed. This channel followed by a proton transfer from a neutral pyrimidine molecule to form the protonated pyrimidine, $H.C_4H_4N_2^+$ and followed by a subsequent association to form $H.(C_4H_4N_2)_2^{\cdot+}$. In the presence of He, (third body effect),

the major product is the association adduct, $(C_6H_6.C_4H_4N_2)^{.+}$, which was stabilized by He as shown in scheme1.
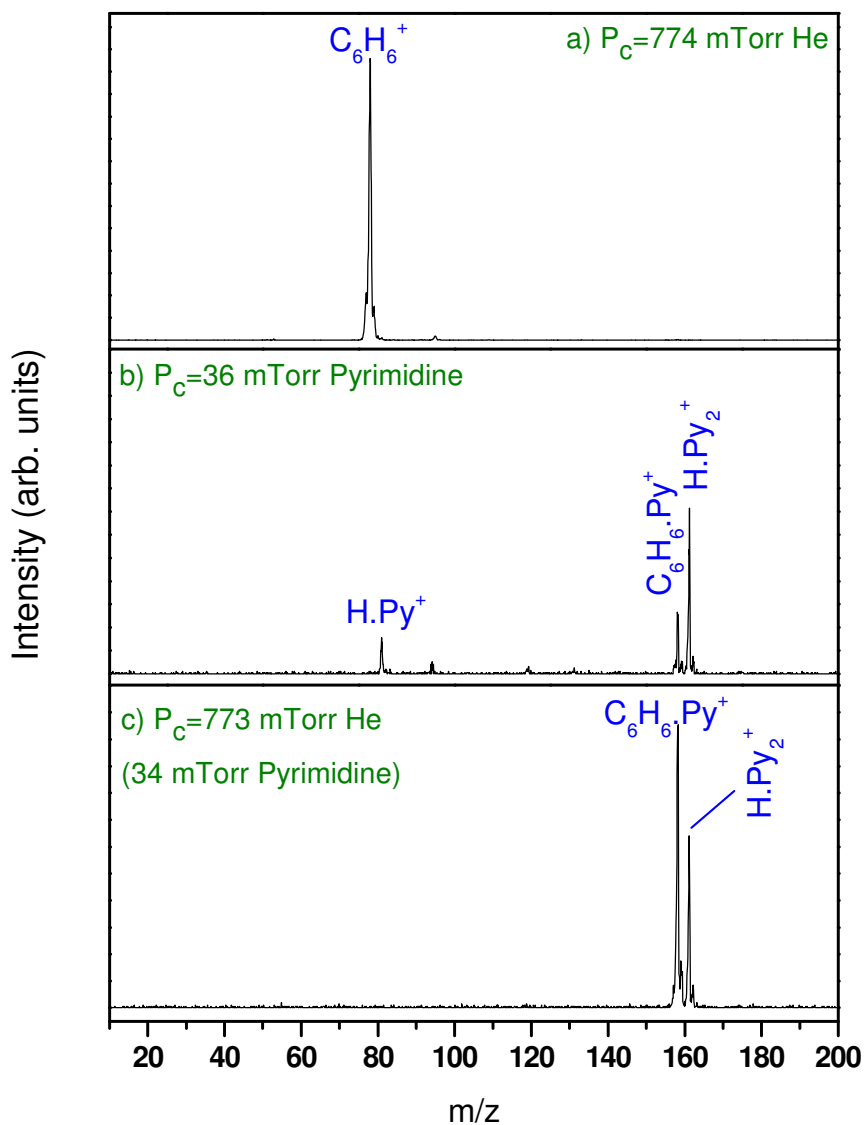
Figure 72. Mass spectrum of $C_6H_6^{\bullet+}$ injected into the drift cell. The injection energy is 15.6 eV (Lab frame), drift cell temperature is 298.2 K and the cell voltage is 21 V. The cell pressure is (a) 774 mTorr He, (b) 36 mTorr pyrimidine and (c) 773 mTorr (34 mTorr pyrimidine).

5.3.2.2 Collisional Dissociation of $(C_6H_6 \cdot C_4H_4N_2)^{\cdot+}$ adduct

Collisional dissociation of the $(C_6H_6 \cdot C_4H_4N_2)^{\cdot+}$ adduct was studied by generating the adduct formed by supersonic jet expansion of the neutral clusters of C_6D_6 and pyrimidine. The formed adduct then ionized by the EI ionization and mass selected by the first quadrupole mass filter of the ion-mobility system. The adduct were then injected into He at injection energies 10-40 eV (lab frame), and the resulting mass spectrum identified the major dissociation products are $H \cdot (C_4H_4N_2)^+$ and $(C_4H_4N_2)_2^+$ with minor products of $C_6D_6^{\cdot+}$ and $H \cdot C_4H_4N_2^+$ as shown in Figure 73. Figure 74 shows the effect of the injection energy on the dissociation products of the $(C_6H_6 \cdot C_4H_4N_2)^{\cdot+}$ adduct in 0.831 Torr He. The dissociation products suggest that the formed adduct either a noncovalent $(C_6H_6 \cdot C_4H_4N_2)^{\cdot+}$ or a covalent one bonded by a single C-N covalent bond, as there were no fragments contain more carbon atoms than the monomer reactants which suggests that no fused ring were formed.

The mass spectra given in Figure 73 and the effect of injection energy given in Figure 74 suggest that the lowest collision energy for dissociation is about 30 eV, and the main products are $H \cdot (C_4H_4N_2)_2^+$, $C_6D_6^+$ and $H \cdot C_4H_4N_2^+$ corresponding to a complex with a covalent C-N bond as mentioned earlier. The possible structures of the formed adduct will be discussed in the next section. These results confirm the assumption of formation of pyrimidine radical cation was carried out through a charge transfer from the $C_6D_6^{\cdot+}$ to $C_4H_4N_2$ and no proton transfer take place in this case, as there were no observations of $D \cdot C_4H_4N_2^+$, as shown in Scheme 1.

5.3.2.3 Thermal stability of $(C_6H_6.C_4H_4N_2)^{.+}$ adduct

Thermal stability of the $(C_6H_6.C_4H_4N_2)^{.+}$ adduct has been tested as shown in Figure 75. At 300 K, the major peaks detected were corresponding to the adduct $(C_6H_6.C_4H_4N_2)^{.+}$ and the $H.(C_4H_4N_2)_2^{+}$ as shown in Figure 75 top panel. Increasing the temperature to 372 K leads to a great reduction in the intensity of the $H.(C_4H_4N_2)_2^{+}$ with no change in the stability, hence, the intensity of the adduct $(C_6H_6.C_4H_4N_2)^{.+}$. Raising the drift cell temperature to 472 K leads to complete dissociation of the $H.(C_4H_4N_2)_2^{+}$ and the $(C_6H_6.C_4H_4N_2)^{.+}$ shows a great thermal stability with a little fragmentations <1% o produce $H.C_4H_4N_2^{+}$, $D.C_4H_4N_2$ and $C_6D_6^{.+}$ cations respectively. These thermal stability behavior of the formed adduct provides evidence for its covalent character.
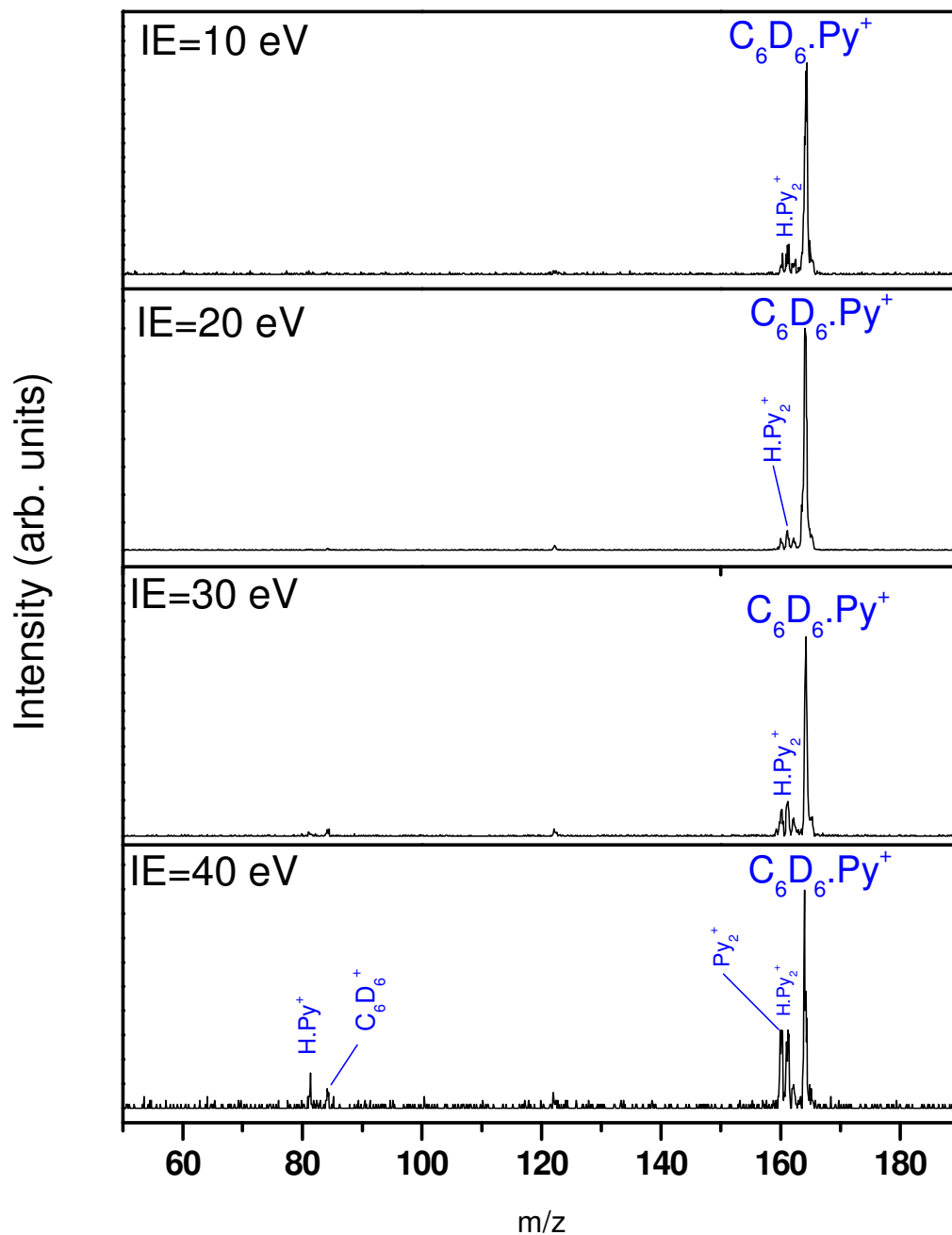
Figure 73. Mass spectrum of $C_6H_6.C_4H_4N_2^{\bullet+}$ injected into the drift cell at 300.2 K and the cell voltage is 24 V. The cell pressure is 831 mTorr He. The injection energy was 10, 20, 30 and 40 eV (Lab frame) from top panel to the bottom one respectively.
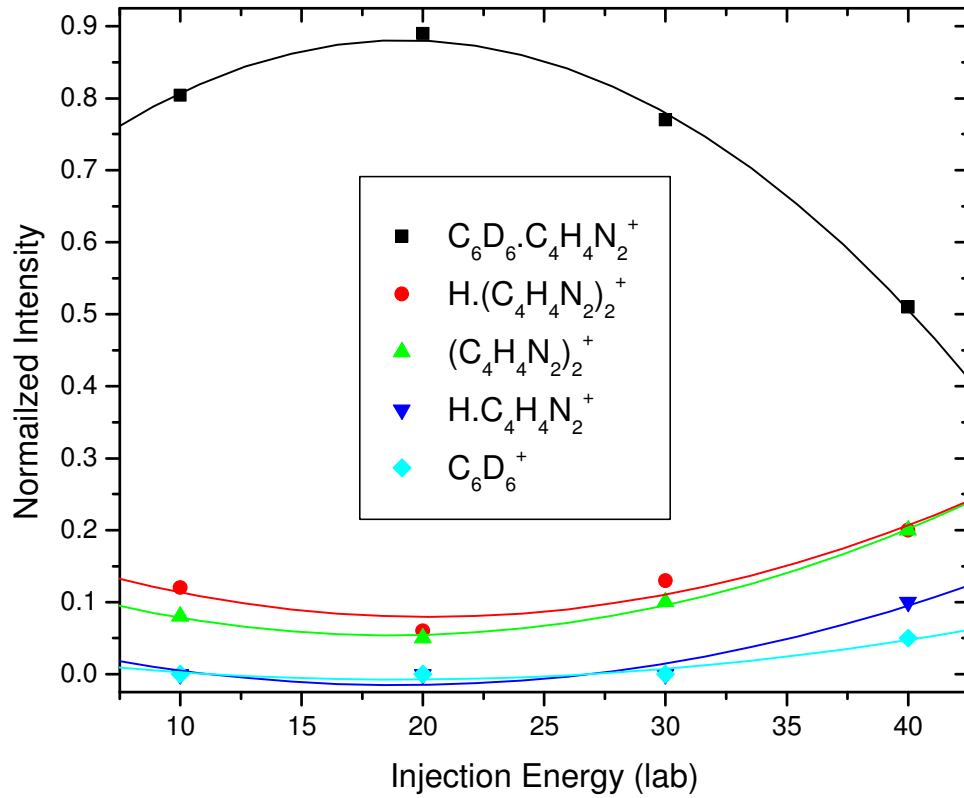
Figure 74. Effect of injection energy on the Collisional dissociation of the $C_6D_6.C_4H_4N_2^{.+}$ adduct injected into 0.831 Torr He.
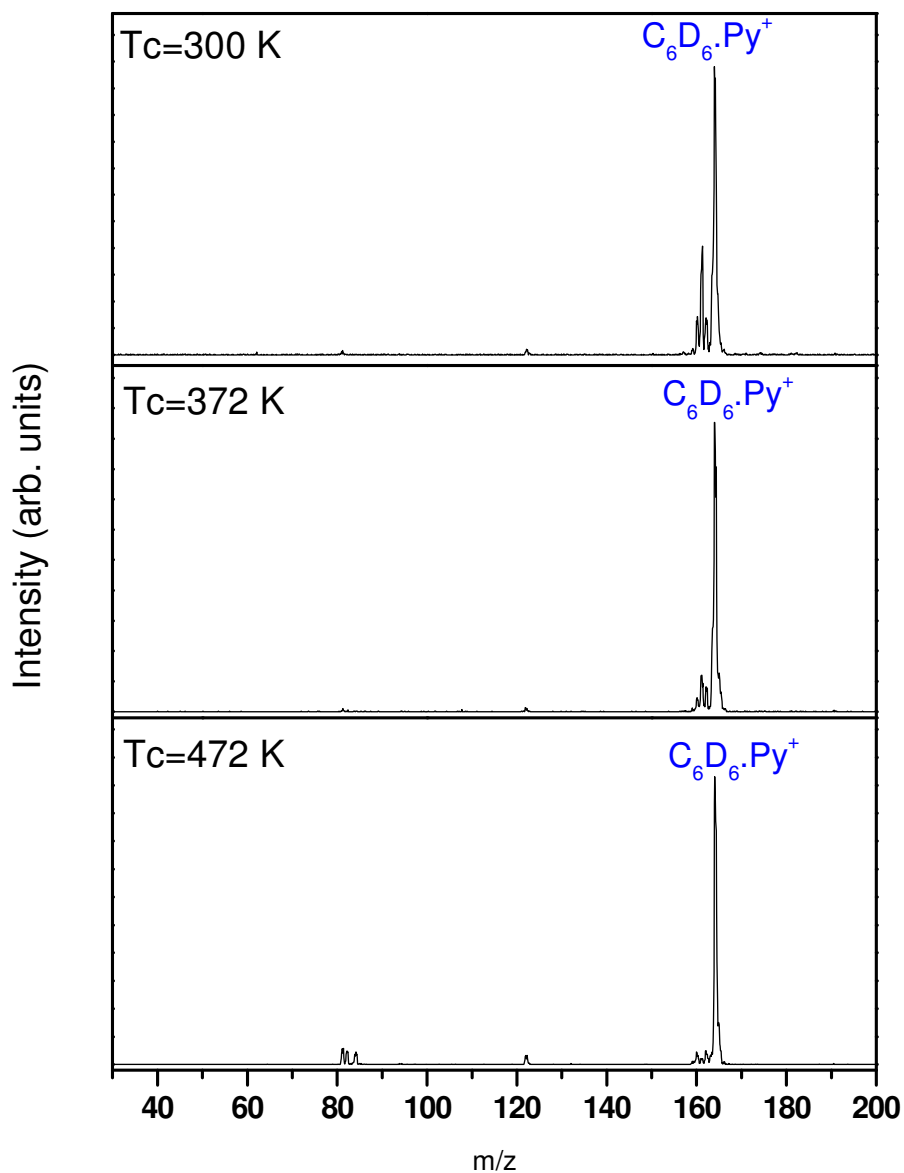
Figure 75. Mass spectrum of $C_6H_6.C_4H_4N_2^{\bullet+}$ injected into the drift cell and the cell voltage is 24 V. The cell pressure is 817 mTorr He. The injection energy was 19.6 eV (Lab frame). Drift cell temperature was 300 K, 372 K and 472 K from top panel to the bottom one respectively.

5.3.2.4   Mobility   measurements   and   structural   determination   of   the $(C_6H_6.C_4H_4N_2)^{.+}$adduct

The reduced mobilities measured in helium and their corresponding collision cross sections of the $(C_6H_6.C_4H_4N_2)^{.+}$ adduct are tabulated in Table 22. The ATDs of the $(C_6H_6.C_4H_4N_2)^{.+}$ adduct at 299 K at different applied potential (21-31 V) across the drift cell is represented in Figure 76. Mobility measurements provide structural information of the $(C_6H_6.C_4H_4N_2)^{.+}$ adduct based on its collision cross section which depends on the geometric shape of the ion. Theoretical calculations of the possible structural isomers of the ion are thereupon used to compute the average collision cross section at different temperatures and compared with the measured ones. The average measured mobilities of the $(C_6H_6.C_4H_4N_2)^{.+}$ adducts was 7.8 ± 0.2 cm^2.V^{-1}.cm^{-1} and the average measured collision cross section was 69.64 ± 2 Å^2. The measured mobilities and collisional cross section could be compared with the calculated mobilities of the different possible isomers given in Table 23.

Table 22. Measured mobility and collision cross section of the $(C_6H_6.C_4H_4N_2)^{.+}$ adduct

Temp. K	Pressure He (Torr)	K_o cm^2.V^{-1}.s^{-1} measured	Ω Å^2 measured
302	2.670	7.8	69.18
299	3.018	7.6	71.58
299	2.743	7.9	68.24
299	3.011	7.8	69.56
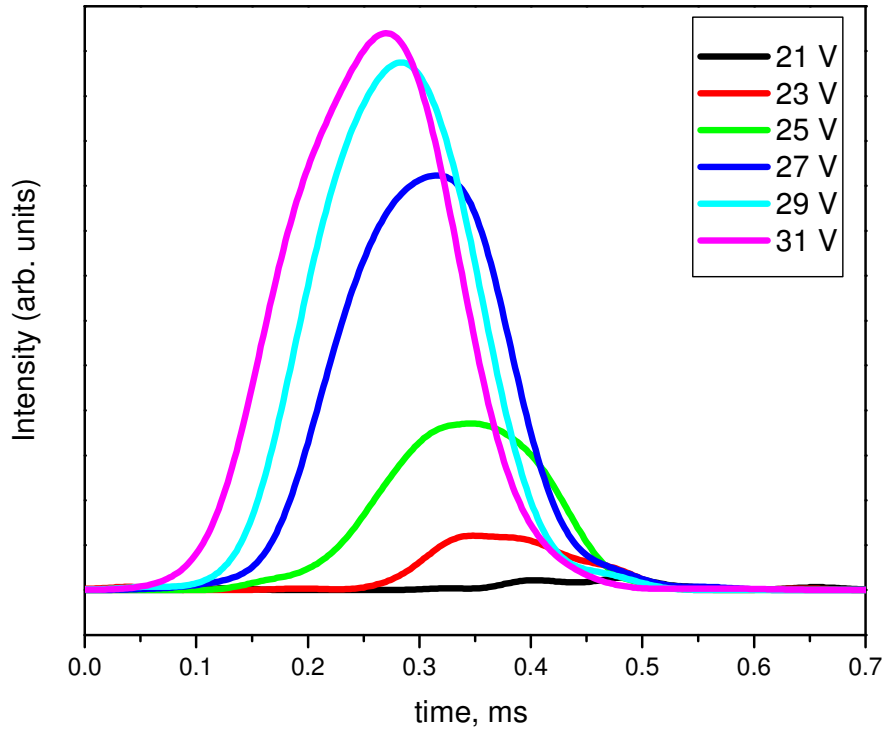
Figure 76. The arrival time distributions (ATDs) of injecting $(C_6H_6.C_4H_4N_2)^{.+}$ (40 μs ion pulses) into the drift cell filled with 3.008 Torr He at different cell voltages (31-21 V). Injection energy is 12 eV (lab frame). The earlier ATD corresponds to drift cell voltage of 31V and the later ATD corresponds to drift cell voltage of 21 V.
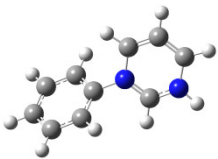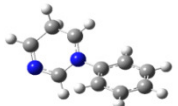
5.3.2.5 Theoretical Calculations of the possible isomers of $(C_6H_6.C_4H_4N_2)^{.+}$ adduct
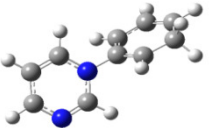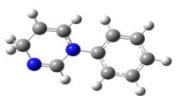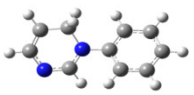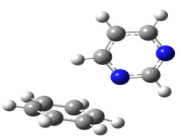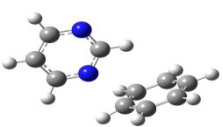
Several possible isomers of the $(C_6H_6.C_4H_4N_2)^{.+}$ adduct have been optimized by the ab initio calculations at the UB3LYP/6-311+G** level. Table 23 represents the optimized structures for the covalent bonded and van der Waal's complexes assuming the interaction of $C_6H_6^{.+}$ and pyrimidine. Table 23 shows the calculated dissociation energies of all isomers. The lowest energy isomer is the covalently bonded isomer (Pb1) which contains a covalent C-N bond with a proton transferred from $C_6H_6^{.+}$ to the second nitrogen of the pyrimidine. The other covalently bonded isomers (Pb2-Pb7) have higher energies by (1.5-21 kcal.mol^{-1}) with respect to isomer Pb1. The calculated cross section of the covalent isomers (average value is 71.8±1.0 Å^2) in good agreement with the measured cross section of the $(C_6H_6.C_4H_4N_2)^{.+}$ adduct. Meanwhile, the calculated cross section of the van der Waal's isomers (Pb8 and Pb9) were slightly higher than the measured one (the average calculated cross section of both isomers was 74±0.1 Å^2), indicating that the covalent isomers are the most probable isomers in this case.

The binding energy of the Pb1 isomer was calculated to be ~45 kcal.mol-1 which is in agreements with the reported value of the hetero-aromatic adducts >33 kcal.mo^{-1}.[73] However, the perpendicular van der Waals' isomers have binding energies of 22.8 Kcal.mo-1 and this could be attributed to the strong dipole moment on the pyrimidine (1.26 D). The structures of the noncovalent isomers suggest the electrostatic interactions are dominant. The C-N bond length in the non-covalent isomer is 2.1 Å while in the covalent isomers is in the range (1.52-1.62 Å). The distorted geometries of the benzene and pyrimidine rings which lead to the propeller-like twisted geometries of the planes of the

two rings could be explained by the repulsion forces between the ortho hydrogens of benzene and pyrimidine rings leading to the decrease in the C-N bond energies of the covalent isomers.

Table 23. Proposed structures of different isomers of $(C_6H_6.C_4H_4N_2)^{.+}$ adduct and their calculated binding energies, mobilities and collisional cross sections.

Isomer	Structure	Method/Basis Set	Relative E	B. E. kcal.mol^{-1}	K_o	$\Omega^{(1,1)}$
Pb1		UB3LYP/6-311+G**	0	-44.8	7.45	72.53
Pb2		UB3LYP/6-311+G**	1.5	-28.9	7.64	70.77
Pb3		UB3LYP/6-311+G**	3.4	-27	7.45	72.53
Pb4		UB3LYP/6-311+G**	5	-25.4	7.63	70.88

Pb5		UB3LYP/6-311+G**	5.8	-24.6	7.54	71.72
Pb6		UB3LYP/6-311+G**	15.9	-28.9	7.56	71.48
Pb7		UB3LYP/6-311+G**	20.18	-24.59	7.43	72.74
Pb8		UB3LYP/6-311+G**	22.8	-21.9	7.29	74.1
Pb9		UB3LYP/6-311+G**	22.9	-21.8	7.32	73.89

5.4 Conclusions

In this chapter, we examined several ion molecule reactions of N-containing cations with acetylene in order to investigate the possible mechanisms of formation of PANHs in different environments utilizing the IMS technique. Interactions of pyridine cation with acetylene via the ion-molecule reactions lead to condensation products of up to 5 acetylene molecules onto the pyridine cation. These products were thermally tested and the most stable compounds were those corresponding to $(C_5H_5N.(C_2H_2)_2)^+$ at 623 K. Moreover, condensation reactions with H-elimination were also determined. These reactions lead to the formation of $C_9H_8N^+$, and this adduct is protonated isoquinoline isomer, which has a fused nitrogen atom in the aromatic ring. This is the first experimental report on formation of N-containing fused aromatic ring from the reactions of pyridine cation with acetylene. Kinetic measurements were conducted and the second order rate coefficient was determined to be two orders of magnitudes less than the collision rate. Also, intracluster reactions of mixed pyridine/acetylene lead to the formation of different hetero aromatic compounds. Ion mobility measurements, CID and ab initio calculations provided the most probable structures of product ions.

Interactions of acetylene with hetero aromatic compounds were expanded to the pyrimidine radical cations. Condensation reactions were determined and they were limited to the addition of C_4H_3 with no further additions. These reactions are fast reactions and estimated to be near the collision rate. The predicted structures were cyclic with fused N-atom and this could explain the limitation of the addition of acetylene to pyrimidine radical cation to only two molecules with H-elimination.

Benzonitrile cations reactions with acetylene were investigated as well. These interactions lead to the formation of isoquinoline and 2-phenyl-pyridine isomers through the addition of one and two acetylene molecules to benzonitrile cation respectively. The reactions of acetylene with benzonitrile cation were determined to be two orders of magnitudes slower than the collision rate.

Interactions of benzene radical cation with pyrimidine were studied as an example of the ionic interactions of aromatic compounds with heterocylces. The formed adduct $(C_6H_6.C_4H_4N_2)^{.+}$ was believed to be covalent one through the formation of C-N covalent bond with binding energy of ~45 Kcal.mol^{-1} calculated theoretically. Ion mobility measurements, CID and ab initio calculations confirmed this finding.

Chapter 6 Formation of polyaromatic hydrocarbons over Pd and Pd supported nanocatalysts

6.1 Introduction

Acetylene polymerization is one of the possible mechanisms of formation of poly aromatic hydrocarbons, PAHs, which are the main constituents of soot. The formation of PAHs and soot was believed to proceed through radical and ionic mechanisms.[29,78,219,241-242]

The best theory to explain the formation of soot is the one described by Haynes and Wagner[243] in which they propose the formation of first aromatic species from acetylene, followed by the addition of other aliphatic and aromatic moieties to structure higher PAHs. The formed PAHs are considered as soot nuclei that lead to further growth to high molecular mass of soot in the range of 500-2000 amu.

Formation of PAHs is the milestone in soot formation, and it was believed that the PAHs formation follow the HACA route as mentioned earlier in the previous chapters.[59,244] Acetylene pyrolysis has been a subject of a great number of studies.[202-203,245-257] Thermal cyclization of acetylene was discovered on 1886.[78] This process require high temperatures >400 ^{o}C.[79] The presence of transition metal catalysts[81-82] and supported metal catalysts on TiO$_2$, VO$_2$ [258] and MgO[83] had changed the high energy demand for this process. Theoretical studies of the cyclotrimerization of acetylene on supported size-selected Pd clusters showed that the production of benzene can be efficient at room temperature.[80,85] In those studies, the cyclotrimerization of acetylene on size selected Ag, Rh and Pd atoms and

also on clusters such as Pd$_n$, where n is in the range of (1≤n≤30) supported on metal oxide substrate, e.g. MgO(100) and MgO(111), have been conducted. The production of benzene was observed on Pd and Rh atoms, while Pd$_6$ clusters were the highest selective clusters to produce butadiene, Pd$_{20}$ clusters was the best selective for butane and Ag atoms were inert for such processes. It was reported that Pd catalyzes acetylene polymerization rather than C-C bond cleavage; this could explain why the all reported products from those studies have even number of carbon atoms. These findings suggest that this class of reactions is strongly dependent on the structure of the catalyst. Upon the interaction with the MgO substrate, the free Pd atom is believed to be activated by charge transfer from the defect sites of the substrate upon deposition. DFT calculations support this activation of Pd atom which is inserted in an F center on the MgO substrate. The interaction of the Pd atom and the F center is strong (3.4 eV).[85] As a result, the Pd atom can be catalytically active.

Materials in the nanoscale exhibit unique properties than those in the bulk one. These properties depend mainly on the size, shape and surface of the material in the nanoscale which will influence the number of surface atoms and their intrinsic properties.[259] Due to the high surface to volume ratio and quantum confinement of the materials in the nanoscale, their catalytic properties are enhanced dramatically. Therefore, tailoring and designing of catalysts on the nanoscale have been subject to enormous research.[84,260-270] Investigations into the reactions of acetylene on Pd have been attractive research in the field of catalysis.[263,271-274] These reactions include, cross coupling reactions,[260,263] selective hydrogenation[261,268,273-276] and acetylene polymerization.[80,258,276-283] There are several methods used to prepare nanoparticles including; physical and chemical ones. In this study,

we have prepared Pd and Pd supported nanocatalysts utilizing the LVCC technique.[284-289] The main advantage of the LVCC technique is overthrow of the high temperatures needed in nanoparticle syntheses. Furthermore, the use of mixtures of reactive/inert gases can manipulate the chemical composition of the catalysts.[287,290]

In this chapter, we present the self polymerization of acetylene and formation of PAHs from the catalytic processes over Pd nanocatalysts and Pd nanocatalysts supported on MgO and CeO_2 utilizing the flow tube reactor.

6.2 Experimental

Pd rod (3.1 mm diam., 99.9+%) was purchased from Aldrich. Pd powder (-22 mesh, 99.995%) was purchased from Alfa Aesar, CeO_2 powder (<5 micron, 99.9% metal basis) purchased from Aldrich and MgO (-325 mesh, 99+% metal basis) was purchased from Sigma Aldrich. All chemicals were used as received. The X-ray diffraction patterns were measured with X'Pert Philips Materials Research Diffractometer using the Cu KαR radiation. TEM images were obtained using a JEOL JEM-1230 electron microscope operated at 120 kV equipped with a Gatan Ultrascan 4000SP 4k× 4k CCD camera. GC-MS analyses were performed on Varian Saturn 2000 GC/MS/MS gas chromatograph where ionization of the formed products was carried out by EI ionization and the GC was equipped with ion-trap electron multiplier detector.

Pd nanoparticles were prepared by laser ablation of Pd rod utilizing the second harmonic, 532 nm, of the Nd:YAG laser. Laser power was 133 mJ/pulse under He. Top plate of the LVCC chamber kept at 233 K and the bottom plate temperature was 363 K.

Pd powder was mixed with CeO_2 and MgO in order to prepare 5% Pd/CeO_2 and 5%Pd/MgO, (wt %), respectively. The mixed powder was pressed in a pellet and irradiated with laser ablation as described before in section 2.4 in the experimental setup. All catalysts were of the same weight, (10 mg), throughout the course of experiments, and were introduced into a quartz tube where purified acetylene was flowing over the catalysts at different temperatures. The formed hydrocarbons were collected with hexanes (Fischer Chemicals, certified ACS, 99.9%) and were transferred to the Varian GC/MS/MS for further analyses. All mass scans run in the range of 20-400 amu.

6.3 Results and Discussions

Figure 77 represents the XRD of Pd nanoparticles prepared by the LVCC technique and the TEM images of the Pd sample. Pd NPs are in the (111), (200) and (220) facets,[291] the closet-packed (111) is the most active surface for the acetylene polymerization.[292] Pd particle size was in the range of 10-50 nm. Figure 78 represents the XRD and TEM of 5% Pd/CeO$_2$ prepared by the LVCC, Pd average particle size was 20 nm. Figure 79 represents the XRD and TEM image of 5% Pd/MgO prepared by the LVCC, Pd average particle size was in the same range, 20 nm. Figure 80 represents the PAHs produced from the flow of purified acetylene in a quartz tube at different temperatures. Temperatures range from 27 ^{o}C to 600 ^{o}C. No polymerization occurs at low temperatures. It is clear that the acetylene self polymerize at 400 ^{o}C and higher temperatures produce several complex organics. The main species detected at 400 ^{o}C are; C$_7$H$_8$, C$_8$H$_8$, C$_9$H$_{10}$, C$_{10}$H$_8$, C$_{13}$H$_{10}$ and C$_{14}$H$_{10}$ which correspond to mass; 92, 104, 118, 128 and 178 respectively. Meanwhile, at 600 ^{o}C, the peak corresponding to C$_8$H$_8$ disappeared, and the formation of C$_{10}$H$_8$ was greatly enhanced. New peaks also were detected that correspond to C$_{11}$H$_{10}$ and C$_{12}$H$_{10}$ species.

The observed products were typical to those observed for acetylene pyrolysis by Badger et al.[79] carried out at 700 ^{o}C. The tendency of higher molecular masses at high temperatures, 600 ^{o}C, can be assumed due to further transformation at higher temperatures. The choice of the upper temperature limit to 600 ^{o}C was made because above this temperature decomposition of the formed PAHs will occur leading to formation of carbon, carbon fibers and hydrogen.[256,278] It was reported that the activation energy required for the C-H activation in the temperature range 410-480 ^{o}C was estimated to be 45-50 kcal.mol^{-1}

which is independent of acetylene pressure.[256-257] The PAHs formed upon acetylene pyrolysis are consistent with the previous results that lead to the formation of benzene and consequently, react with C_2H_2 to form higher PAHs products.[79,202-203,243,247,250-257,292-301]

Figure 81 represents the polymerization of acetylene over Pd Powder and Pd nanoparticles prepared by LVCC technique under different experimental conditions. In all cases the flow of acetylene was constant and maintained at 100 ccm/min, after passing through a purifying cell (acetylene passed over concentrated sulfuric acid, 5 N sodium hydroxide and passed over a drying cartridge made of 1:1, dry rite : phosphorus pentaoxide). These experiments were compared with a blank run at 600 ^{o}C, Figure 81 (top panel), and the observed PAHs are typical to those observed previously in Figure 80. The main constituent in the blank experiment was $C_{10}H_8$ (naphthalene isomer) and the highest observed mass corresponds to the $C_{14}H_{10}$.

In case of Pd powder, the experiment was carried out at 400 ^{o}C, the observed acetylene polymerization products were; C_7H_6, C_8H_8, C_9H_8, $C_{10}H_8$, $C_{13}H_{10}$ and $C_{14}H_{10}$ which are typical products of the acetylene self polymerization at the same temperature, see Figure 80 panel (e). These observations indicate that the Pd powder does not contribute to the formation of PAHs in this case other than the self polymerization of acetylene at 400 ^{o}C. In the case of Pd nanoparticles at 400 ^{o}C, it is clear that the presence of a distinctive peak appeared at 5.7 minutes (retention time) corresponds to C_8H_{10}. This new peak could be produced through the following reaction;

$$C_7H_8 + CH_4 \longrightarrow C_8H_{10} + H_2 \qquad (6.1)$$
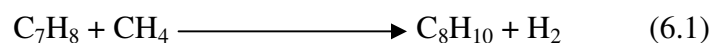
The presence of methane under these conditions was explained before,[302] and Pd NPs could activate this reaction on their surface.

At a higher temperature, 600 $^{\circ}$C, the peak corresponding to the C_8H_{10} disappeared, as shown in Figure 81 (c), and another interesting peak appeared at 15.4 minutes, corresponding to $C_{16}H_{10}$.

The disappearance of C_8H_{10} and the appearance of $C_{16}H_{10}$ could be attributed to further transformation due to the high temperature and the catalytic activity of Pd NPs. It is clear that these two products are not present in the blank experiments, which supports the role of Pd in the formation of these adducts.

Figure 82 represent the GC-MS results for the flow of purified acetylene in a quartz tube containing glass wool, 10 mg Pd NPs, 10 mg 5% Pd/CeO_2 and 5% Pd/MgO catalysts from top to bottom respectively. The temperature of the tube furnace was set at 600 $^{\circ}$C for the entire course of the experiments. In the presence of the catalysts, Figure 82 panel (b), (c), and (d), the formation of the higher PAHs, $C_{16}H_{10}$ was supported by the peak corresponding to m/z= 202. This peak appears at retention time 15.7 minute and it appears to be more intense in the presence of Pd NPs and Pd supported on CeO_2, but its intensity is lower in the case of Pd supported on MgO. The intensity of the $C_{16}H_{10}$ is mainly dependent on the metal particle size and has weak dependence on the support material.[273] Formation of $C_{16}H_{10}$ was evident as one of the products resulted from the ion molecule reactions of naphthylium ions with benzene leading to growth of larger hydrocarbons through C-C bond formation, equation (6.2).[74] Another possible route of the formation of $C_{16}H_{10}$ (pyrene isomer) is via acetylene addition through reaction of phenanthrene molecule

($C_{14}H_9$) with acetylene molecule. This reaction was predicted theoretically to be exothermic reaction with -257 kJ.mol^{-1} (at the B3LYP level).[301] Or, it could be a result of condensation of two acetylene molecules with $C_{12}H_7$, this mechanism involve first addition of one acetylene molecule to the $C_{12}H_7$ and this was calculated to be exothermic with -449 kJ.mol^{-1} with a small barrier 18 kJ.mol-1 (at the B3LYP level), the addition of the second acetylene molecule was predicted to follow the Bittner-Howard mechanism with a barrier of 23 kJ.mol^{-1}.[301] An alternative mechanism of formation of $C_{16}H_{10}$ is through aromatic condensation of C_6H_6 with $C_{10}H_7$ as shown in the following equation

$$C_6H_6 + C_{10}H_7 \longrightarrow C_{16}H_{10} + H_2 + H \qquad (6.2)$$
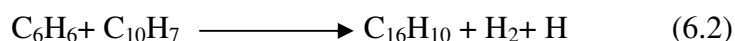
This reaction was calculated to be endothermic by 24 kJ.mol^{-1} (B3LYP) while the highest barrier of the reaction path was estimated to be 85 kJ.mol^{-1}.[301]
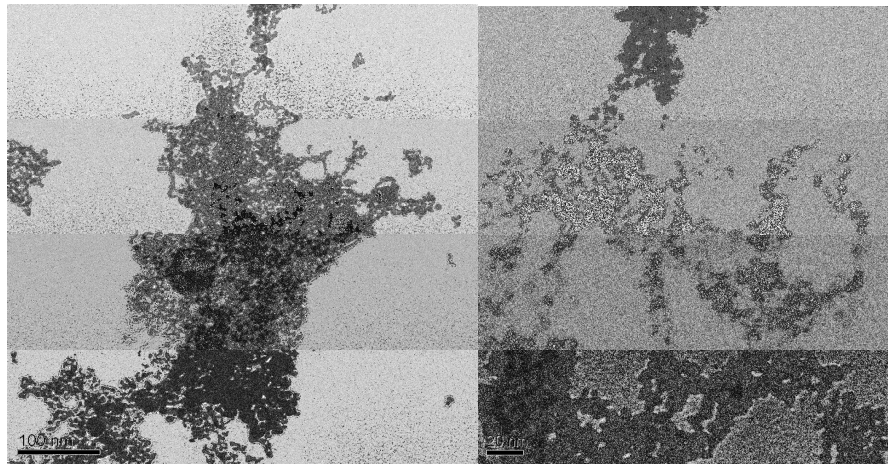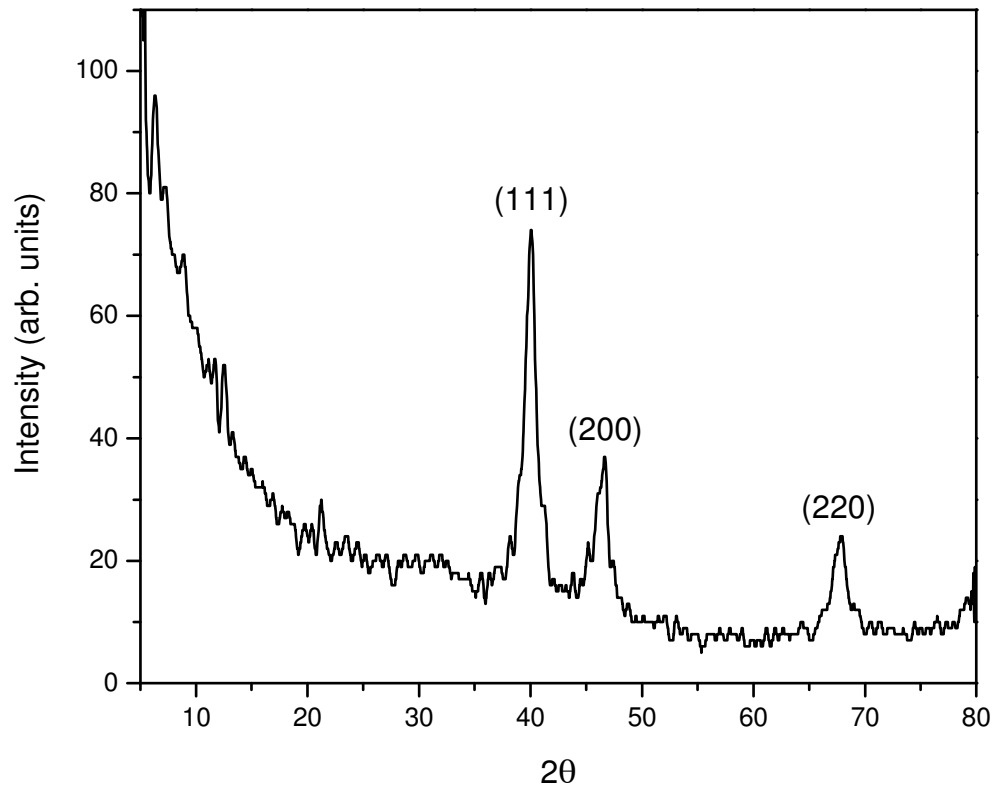
Figure 77. XRD of Pd nanoparticles prepared by LVCC and TEM images of Pd NPs prepared by LVCC.
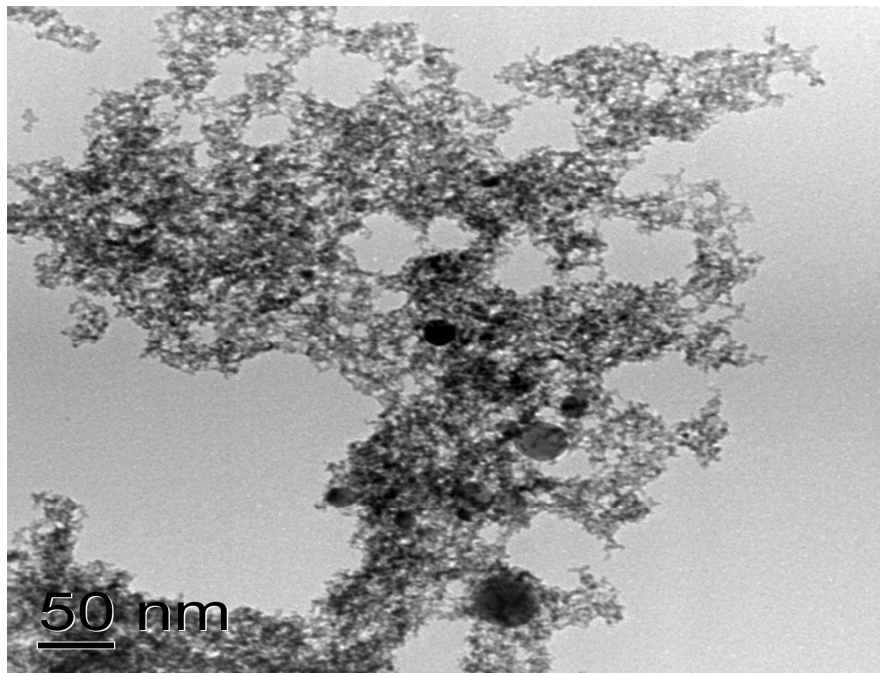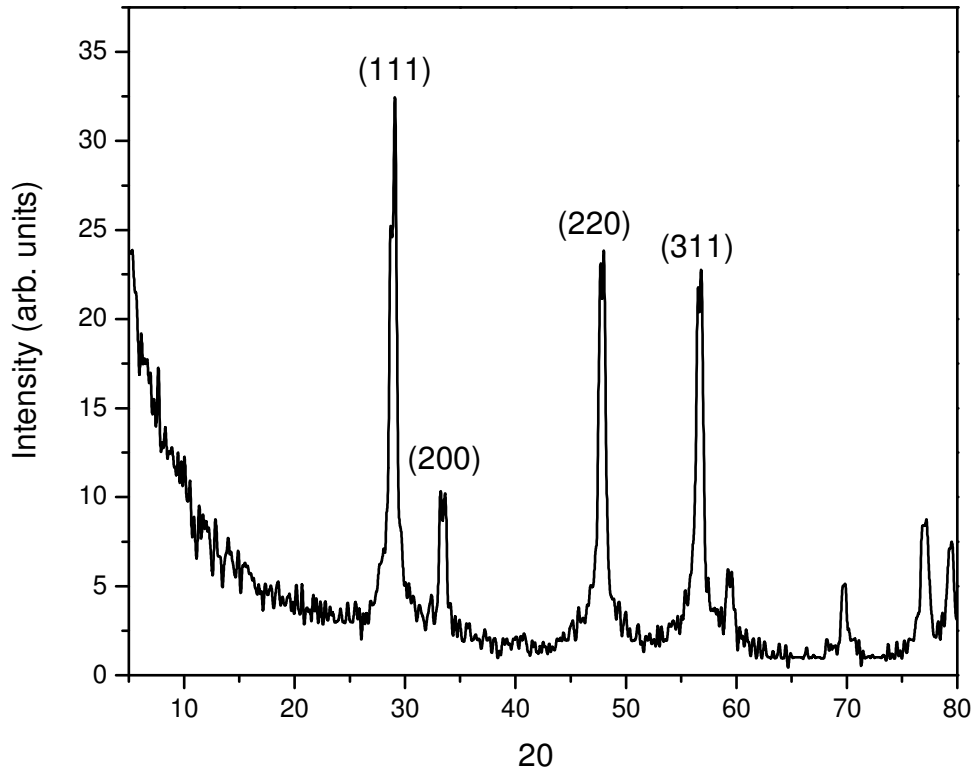
Figure 78. XRD of 5% Pd/CeO$_2$ prepared by LVCC and TEM image of 5% Pd/CeO$_2$ prepared by LVCC
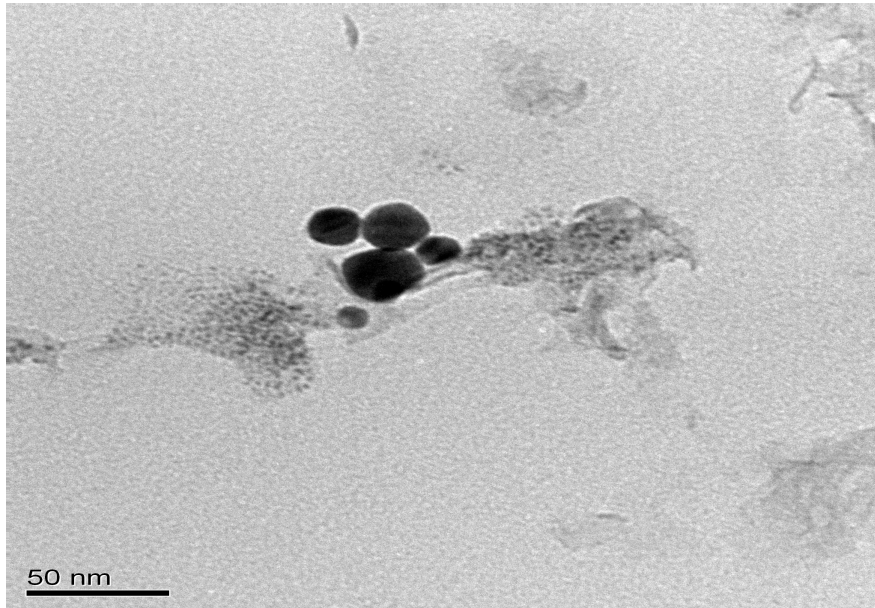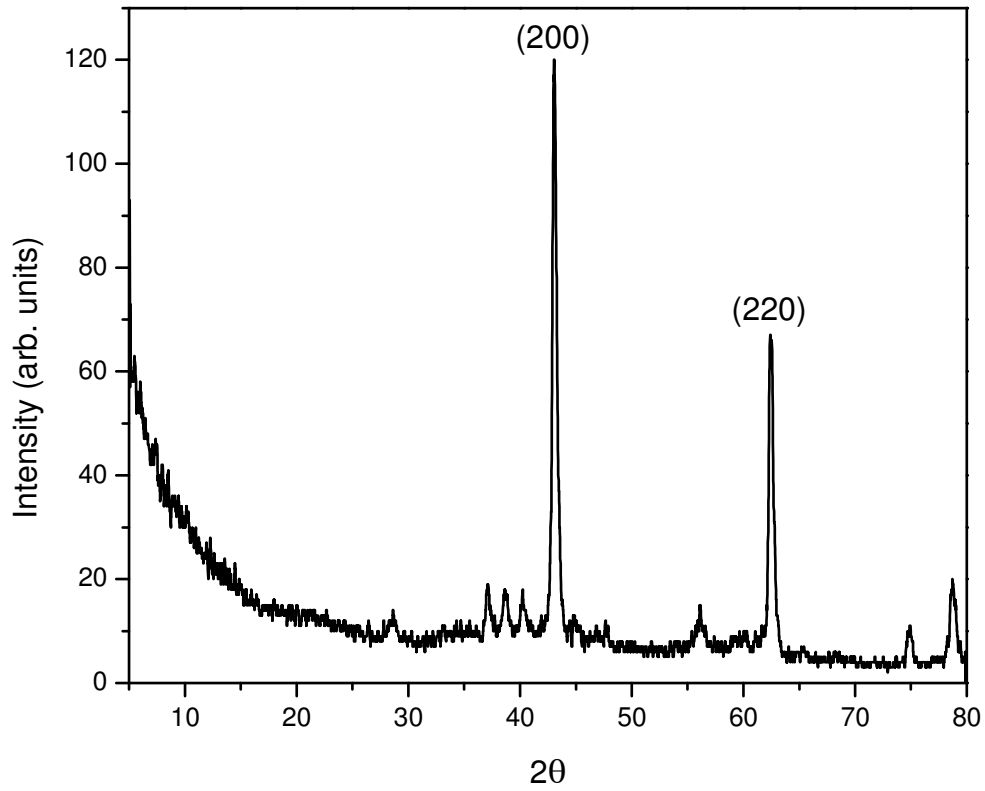
Figure 79. XRD of 5% Pd/MgO prepared by LVCC and TEM image of 5% Pd/MgO prepared by LVCC
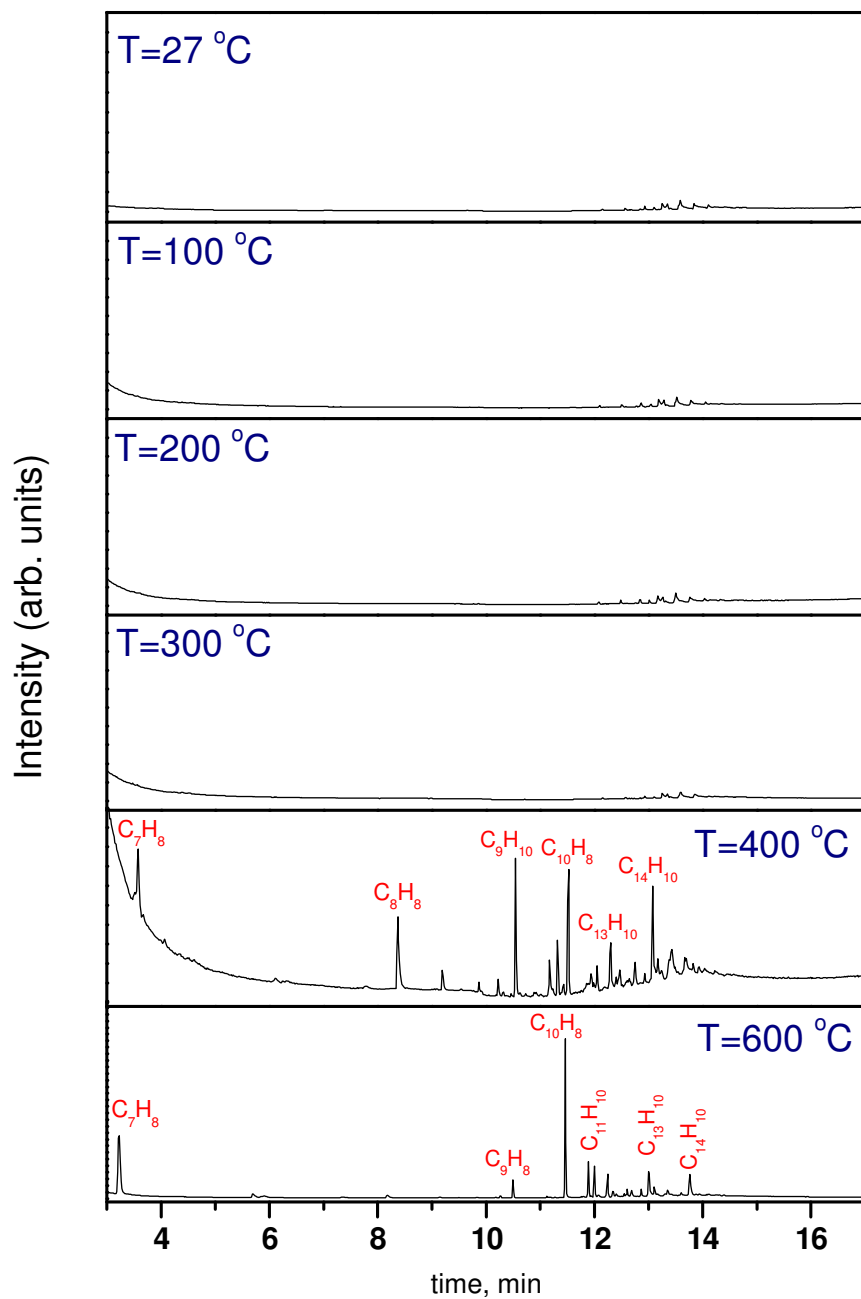
Figure 80. Flow of purified C_2H_2 (100ccm), in a quartz tube at different temperatures; 27 ^{o}C, 100 ^{o}C, 200 ^{o}C, 300 ^{o}C, 400 ^{o}C and 600 ^{o}C. Hexane was used as a solvent to collect the formed products.
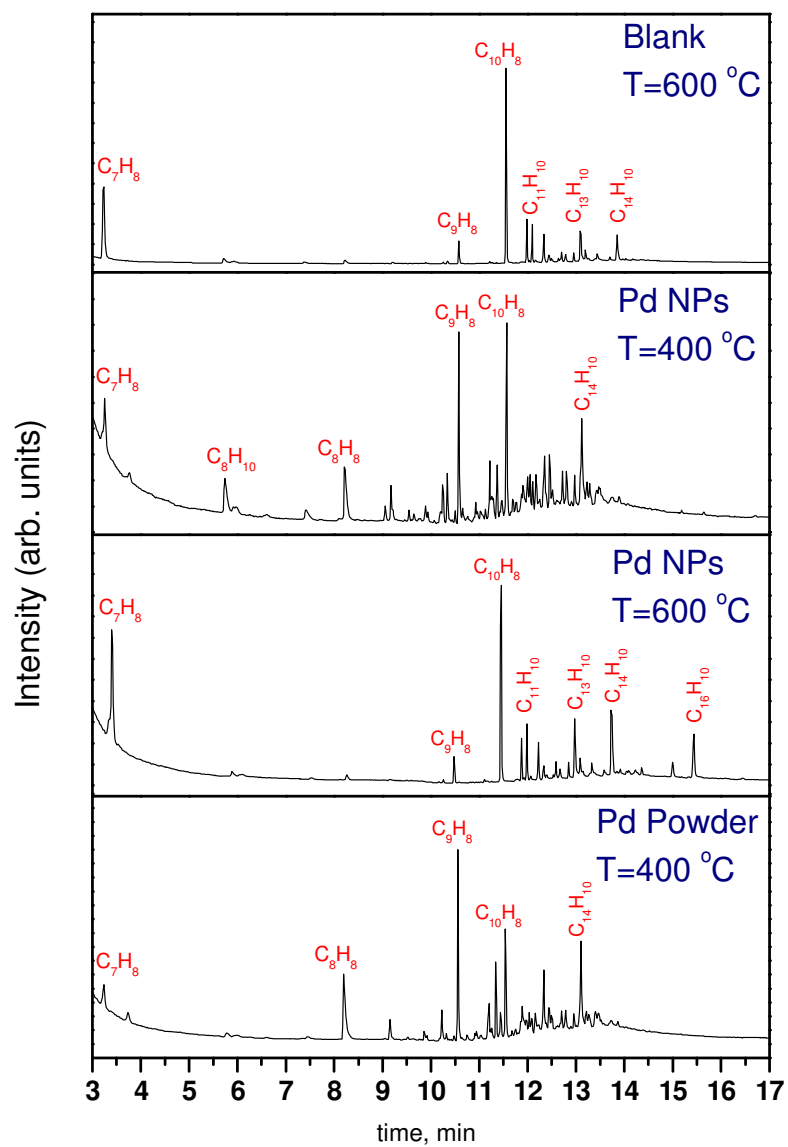
Figure 81. Flow of Purified C_2H_2 over Pd powder and Pd NPs; Panels from top to bottom are as the following: Blank, T= 600 $^{\circ}$C; Pd NPs, T=400 $^{\circ}$C; Pd NPs, T=600 $^{\circ}$C; and Pd Powder, T= 400 $^{\circ}$C, respectively
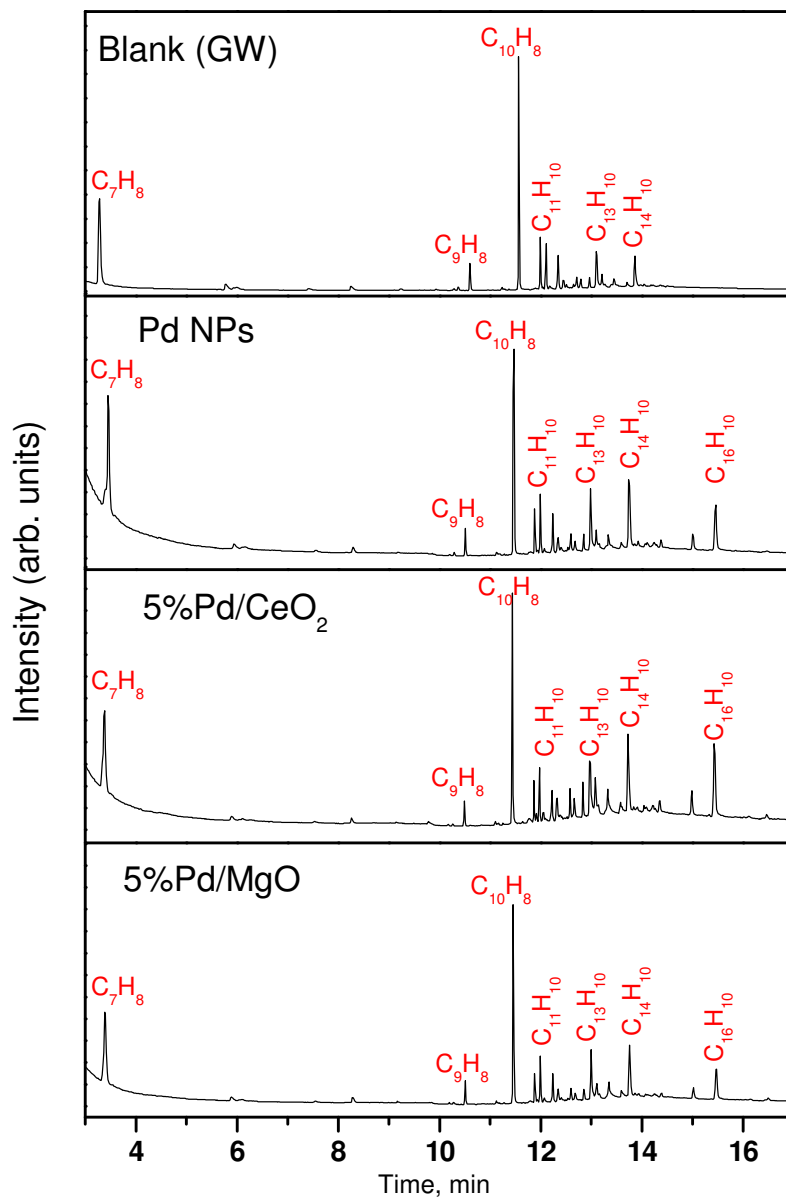
Figure 82. Flow of purified C_2H_2 over; Pd Nps, 5% Pd/CeO_2 and 5% Pd/Mgo from top to bottom respectively. Catalyst load is 10 mg for all runs. Temperature= 600 ^{o}C.

6.4 Conclusions

In this chapter, we studied the self polymerization of acetylene at different temperatures (28 ^{o}C-600 ^{o}C), and polymerization of acetylene over Pd nanocatalyst and supported Pd nanocatalyst over MgO and CeO$_2$, in order to understand the possible mechanisms of formation of PAHs over nanoparticle surfaces. These studies will eventually, help to explore the possible ways of formation of PAHs in different environments such as space and on surfaces of dust grains and on the surface of carbonaceous materials in space.

The self polymerization of acetylene produces C$_7$H$_6$, C$_8$H$_8$, C$_9$H$_8$, C$_{10}$H$_8$, C$_{13}$H$_{10}$ and C$_{14}$H$_{10}$ species at 400 ^{o}C and higher temperatures. No polymerization products were observed below 400 ^{o}C.

Polymerization of purified acetylene over Pd and supported Pd nanocatalysts results in the production of different hydrocarbon species in addition to the products produced from the self catalysis process of acetylene. Note worthy was the formation of C$_{10}$H$_8$ (naphthalene isomer) species were greatly enhanced in the presence of all types of catalysts. The new products observed in the presence of the catalysts and supported catalysts were temperature dependent. At 400 ^{o}C, formation of C$_8$H$_{10}$ species was observed. These species could form through the reactions of C$_7$H$_8$ (toluene isomer) with methane. The presence of methane in such conditions could be explained by the self polymerization process of acetylene. However, at 600 ^{o}C, observation of C$_{16}$H$_{10}$ (pyrene isomer) was predominant over all types of catalysts, with higher intensities in the case of Pd and 5% Pd/CeO$_2$. Formation of the pyrene isomer in these experiments could be

explained through different possible routes. It could be produced from the reaction of naphthylium radical with benzene that could be produced from polymerization of acetylene over Pd. Another possible pathway for the formation of $C_{16}H_{10}$ is the reaction of acetylene molecule with $C_{14}H_9$. Also, $C_{16}H_{10}$ could be produced from the reaction of $C_{12}H_7$ with two acetylene molecules. These three pathways are possible routes and more investigations are required in order to determine the most favored one.

Literature Cited

(1)   Homann, K.-H. *Angewandte Chemie International Edition* **1998**, *37*, 2434.

(2)   Saha, B.; Irle, S.; Morokuma, K. *Journal of Chemical Physics* **2010**, *132*, 224303.

(3)   Todd Gouin, D. W., Stephen Hummel, Ben Meyer, Andrew Culley *Atmospheric Pollution Research* **2010**, *1*, 7.

(4)   Delitsky, M. L.; McKay, C. P. *Icarus* **2010**, *207*, 477.

(5)   Sittler Jr, E. C.; Ali, A.; Cooper, J. F.; Hartle, R. E.; Johnson, R. E.; Coates, A. J.; Young, D. T. *Planetary and Space Science* **2009**, *57*, 1547.

(6)   Bruce, J. H.; et al. *The Astrophysical Journal* **2009**, *694*, 1147.

(7)   Bezard, B. *Philosophical Transactions of the Royal Society a-Mathematical Physical and Engineering Sciences* **2009**, *367*, 683.

(8)   Speck, A.; Barlow, M.; Wesson, R.; Clayton, G.; Volk, K. *Iau: Organic Matter in Space* **2008**, *251*, 195.

(9)   Waite, J. H., Jr.; Young, D. T.; Cravens, T. E.; Coates, A. J.; Crary, F. J.; Magee, B.; Westlake, J. *Science* **2007**, *316*, 870.

(10)   Petrie, S.; Bohme, D. K. *Mass Spectrometry Reviews* **2007**, *26*, 258.

(11)   Waite, J. H., Jr.; Combi, M. R.; Ip, W.-H.; Cravens, T. E.; McNutt, R. L., Jr.; Kasprzak, W.; Yelle, R.; Luhmann, J.; Niemann, H.; Gell, D.; Magee, B.; Fletcher, G.; Lunine, J.; Tseng, W.-L. *Science* **2006**, *311*, 1419.

(12)   Peeters, Z.; Botta, O.; Charnley, S. B.; Kisiel, Z.; Kuan, Y. J.; Ehrenfreund, P. *Astronomy & Astrophysics* **2005**, *433*, 583.

(13)   Kunde, V. G.; Flasar, F. M.; Jennings, D. E.; Bezard, B.; Strobel, D. F.; Conrath, B. J.; Nixon, C. A.; Bjoraker, G. L.; Romani, P. N.; Achterberg, R. K.; Simon-Miller, A. A.; Irwin, P.; Brasunas, J. C.; Pearl, J. C.; Smith, M. D.; Orton, G. S.; Gierasch, P. J.; Spilker, L. J.; Carbon, R. C.; Mamoutkine, A. A.; Calcutt, S. B.; Read, P. L.; Taylor, F. W.; Fouchet, T.; Parrish, P.; Barucci, A.; Courtin, R.; Coustenis, A.; Gautier, D.; Lellouch, E.; Marten, A.; Prange, R.; Biraud, Y.; Ferrari, C.; Owen, T. C.; Abbas, M. M.; Samuelson, R. E.; Raulin, F.; Ade, P.; Cesarsky, C. J.; Grossman, K. U.; Coradini, A. *Science* **2004**, *305*, 1582.

(14)   Shemansky, D. E.; Stewart, A. I. F.; West, R. A.; Esposito, L. W.; Hallett, J. T.; Liu, X. *Science* **2005**, *308*, 978.

(15)   Winnewisser, G.; Kramer, C. *Space Science Reviews* **1999**, *90*, 181.

(16)   Ehrenfreund, P.; et al. *Reports on Progress in Physics* **2002**, *65*, 1427.

(17)   Mattioda, A. L.; Rutter, L.; Parkhill, J.; Head-Gordon, M.; Lee, T. J.; Allamandola, L. J. *Astrophysical Journal* **2008**, *680*, 1243.

(18)   Matteson, D. S.; Lunine, J. I.; Stevenson, D. J.; Yung, Y. L. *Science* **1984**, *223*, 1131.

(19)   Sloan, G. C.; Matsuura, M.; Zijlstra, A. A.; Lagadec, E.; Groenewegen, M. A. T.; Wood, P. R.; Szyszka, C.; Bernard-Salas, J.; van Loon, J. T. *Science* **2009**, *323*, 353.

(20)   Frenklach, M.; Feigelson, E. D. *Astrophys. J.* **1989**, *341*, 372.

(21)   Cernicharo, J.; Heras, A. M.; Tielens, A. G. G. M.; Pardo, J. R.; Herpin, F.; Guelin, M.; Waters, L. B. F. M. *Astrophys. J.* **2001**, *546*, L123.

(22)   Scott, G. B. I.; Fairley, D. A.; Freeman, C. G.; McEwan, M. J.; Adams, N. G.; Babcock, L. M. *The Journal of Physical Chemistry A* **1997**, *101*, 4973.

(23)   Woods, P. M.; Millar, T. J.; Zijlstra, A. A. *Astrophysical Journal* **2002**, *574*, L167.

(24)   Woods, P. M.; Schöier, F. L.; Nyman, L.-A.; Olofsson, H. *Astron. Astrophys.* **2003**, *402*, 617.

(25)   Woods, P. M.; Millar, T. J.; Herbst, E.; Zijlstra, A. A. *A&A* **2003**, *402*, 189.

(26)   Anicich, V. G.; McEwan, M. J. *Planetary and Space Science* **1997**, *45*, 897.

(27)   Brooke, T. Y.; Tokunaga, A. T.; Weaver, H. A.; Crovisier, J.; Bockelee-Morvan, D.; Crisp, D. *Nature* **1996**, *383*, 606.

(28)   Salama, F.; Bakes, E. L. O.; Allamandola, L. J.; Tielens, A. G. G. M. *Astrophysical Journal* **1996**, *458*.

(29)   Salama, F.; Joblin, C.; Allamandola, L. J. *Planetary and Space Science* **1995**, *43*, 1165.

(30)   Menor-Salvan, C.; Ruiz-Bermejo, M.; Osuna-Esteban, S.; Munoz-Caro, G.; Veintemillas-Verdaguer, S. *Chemistry & Biodiversity* **2008**, *5*, 2729.

(31)   El-Shall, M. S. *Accounts of Chemical Research* **2008**, *41*, 783.

(32)   Anicich, V. G.; Wilson, P.; McEwan, M. J. *Journal of the American Society for Mass Spectrometry* **2004**, *15*, 1148.

(33)   Chretien, S.; Salahub, D. R. *Journal of Chemical Physics* **2003**, *119*, 12291.

(34)   Paul, M. W.; et al. *The Astrophysical Journal Letters* **2002**, *574*, L167.

(35)   D'Anna, A.; D'Alessio, A.; Kent, J. *Combustion and Flame* **2001**, *125*, 1196.

(36)   Richter, H.; Howard, J. B. *Progress in Energy and Combustion Science* **2000**, *26*, 565.

(37)   Appel, J.; Bockhorn, H.; Frenklach, M. *Combustion and Flame* **2000**, *121*, 122.

(38)   Nguyen, H. M. T.; Sumathi, R.; Nguyen, M. T. *Journal of Physical Chemistry A* **1999**, *103*, 5015.

(39)   Wang, H.; Frenklach, M. *Combustion and Flame* **1997**, *110*, 173.

(40)   Coolbaugh, M. T.; Whitney, S. G.; Vaidyanathan, G.; Garvey, J. F. *The Journal of Physical Chemistry* **1992**, *96*, 9139.

(41)   Benson, S. W. *International Journal of Chemical Kinetics* **1992**, *24*, 217.

(42)   Bauschlicher, C. W.; Langhoff, S. R.; Taylor, P. R. *Chemical Physics Letters* **1990**, *171*, 42.

(43)   Knight, J. S.; Freeman, C. G.; McEwan, M. J.; Anicich, V. G.; Huntress, W. T., Jr. *Journal of Physical Chemistry* **1987**, *91*, 3898.

(44)   Jameson, C. J.; Fowler, P. W. *Journal of Chemical Physics* **1986**, *85*, 3432.

(45)   Suzuki, I. H.; Maeda, K. *Adv. Mass Spectrom.* **1978**, *7A*, 182.

(46)   Suzuki, I. H.; Maeda, K. *Shitsuryo Bunseki* **1977**, *25*, 223.

(47)   Moruzzi, J. L.; Parkes, D. A.; Fletcher, J.; Lecoat, Y. *Vacuum* **1974**, *24*, 589.

(48)   Buttrill, S. E. *Journal of the American Chemical Society* **1970**, *92*, 3560.

(49)   Myher, J. J.; Harrison, A. G. *Canadian Journal of Chemistry* **1968**, *46*, 1755.

(50)   Derwish, G. A. W.; Galli, A.; Giardini.A; Volpi, G. G. *Journal of the American Chemical Society* **1965**, *87*, 1159.

(51)   Ono, Y.; Ng, C. Y. *Journal of the American Chemical Society* **1982**, *104*, 4752.

(52)   Goebbert, D. J.; Liu, X. P.; Wenthold, P. G. *Journal of the American Society for Mass Spectrometry* **2004**, *15*, 114.

(53)   Coolbaugh, M. T.; Whitney, S. G.; Vaidyanathan, G.; Garvey, J. F. *Journal of Physical Chemistry* **1992**, *96*, 9139.

(54)   Momoh, P. O.; Abrash, S. A.; Mabrouki, R.; El-Shall, M. S. *Journal of the American Chemical Society* **2006**, *128*, 12408.

(55)   Shinohara, H.; Sato, H.; Washida, N. *The Journal of Physical Chemistry* **1990**, *94*, 6718.

(56)   Momoh, P. O.; El-Shall, M. S. *Chemical Physics Letters* **2007**, *436*, 25.

(57)   Ibrahim, Y. M.; Mautner, M. M. N.; Alshraeh, E. H.; El-Shall, M. S.; Scheiner, S. *Journal of the American Chemical Society* **2005**, *127*, 7053.

(58)   Chyba, C.; Sagan, C. *Nature* **1992**, *355*, 125.

(59)   Bauschlicher, C. W.; Ricca, A.; Rosi, M. *Chemical Physics Letters* **2002**, *355*, 159.

(60)   Ricca, A.; Bauschlicher, C. W.; Rosi, M. *Chemical Physics Letters* **2001**, *347*, 473.

(61)   Landera, A.; Mebel, A. M. *Faraday Discussions* **2010**, *147*, 479.

(62)   Shukla, B.; Koshi, M. *Physical Chemistry Chemical Physics* **2009**, *12*, 2427.

(63)   Raj, A.; Celnik, M.; Shirley, R.; Sander, M.; Patterson, R.; West, R.; Kraft, M. *Combustion and Flame* **2009**, *156*, 896.

(64)   Mai Lan Nguyen, Y. B. a. A. G. *Journal of Atmospheric Chemistry* **2009**, *62*, 139.

(65)   Jager, C.; et al. *The Astrophysical Journal* **2009**, *696*, 706.

(66)   Gu, X. B.; Kaiser, R. I. *Accounts of Chemical Research* **2009**, *42*, 290.

(67)   Shukla, M.; Susa, A.; Miyoshi, A.; Koshi, M. *Journal of Physical Chemistry A* **2008**, *112*, 2362.

(68)   Hildebrandt, B.; Reiß, G.; Ganter, C. *Journal of Organometallic Chemistry* **2010**, *695*, 474.

(69)   Partha P. Bera; Timothy J. Lee; Schaefer, H. F. *Journal of Chemical Physics* **2009**, *131*, 8.

(70)   Fondren, L. D.; Adams, N. G.; Stavish, L. *The Journal of Physical Chemistry A* **2008**, *113*, 592.

(71)   Li, Y.; Liu, H.-l.; Huang, X.-r.; Wang, D.-q.; Sun, C.-c.; Tang, A.-c. *The Journal of Physical Chemistry A* **2008**, *112*, 8188.

(72)   Gerbaux, P.; Haverbeke, Y. V.; Flammang, R. *Journal of the American Society for Mass Spectrometry* **2003**, *14*, 241.

(73)   El-Shall, M. S.; Ibrahim, Y. M.; Alsharaeh, E. H.; Meot-Ner, M.; Watson, S. P. *Journal of the American Chemical Society* **2009**, *131*, 10066.

(74)   Ascenzi, D.; Aysina, J.; Tosi, P.; Maranzana, A.; Tonachini, G. *Journal of Chemical Physics* **2010**, *133*, 9.

(75)   Zabka, J.; Polasek, M.; Ascenzi, D.; Tosi, P.; RoithovaÌ , J.; Schroder, D. *The Journal of Physical Chemistry A* **2009**, *113*, 11153.

(76)   Ascenzi, D.; Cont, N.; Guella, G.; Franceschi, P.; Tosi, P. *The Journal of Physical Chemistry A* **2007**, *111*, 12513.

(77)   Bohme, D. K.; Wlodek, S.; Zimmerman, J. A.; Eyler, J. R. *International Journal of Mass Spectrometry and Ion Processes* **1991**, *109*, 31.

(78)   Berthelot, M. a. C. R. H. *C. R. Hebd. Seances Acad. Sci* **1866**, *62*.

(79)   G. M. Badger, G. E. L. a. I. M. N. *Journal of the Chemical Society* **1960**.

(80)   Gilb, S.; Arenz, M.; Heiz, U. *Low Temperature Physics* **2006**, *32*, 1097.

(81)   Saito, S.; Yamamoto, Y. *Chemical Reviews* **2000**, *100*, 2901.

(82)   Schore, N. E. *Chemical Reviews* **1988**, *88*, 1081.

(83)   Judai, K.; Worz, A. S.; Abbet, S.; Antonietti, J.-M.; Heiz, U.; Vitto, A. D.; Giordano, L.; Pacchioni, G. *Physical Chemistry Chemical Physics* **2005**, *7*, 955.

(84)   Boudjahem, A.-G.; Monteverdi, S.; Mercy, M.; Bettahar, M. M. *Applied Catalysis A: General* **2003**, *250*, 49.

(85)   Abbet, S.; Sanchez, A.; Heiz, U.; Schneider, W. D.; Ferrari, A. M.; Pacchioni, G.; Rosch, N. *Journal of the American Chemical Society* **2000**, *122*, 3453.

(86)   Shvartsburg, A. A.; Jarrold, M. F. *Chemical Physics Letters* **1996**, *261*, 86.

(87)   Bernstein., E. R. *Atomic and Molecular Clusters* **1990**, *68*, 551.

(88)   Kemper, P. R.; Bowers, M. T. *Journal of the American Society for Mass Spectrometry* **1990**, *1*, 197.

(89)   ABB Automation Inc., A. D., Extrel **2003**.

(90)   Ibrahim, Y.; Alsharaeh, E.; Mabrouki, R.; Momoh, P.; Xie, E.; El-Shall, M. S. *The Journal of Physical Chemistry A* **2008**, *112*, 1112.

(91)   Vonhelden, G.; Hsu, M. T.; Gotts, N.; Bowers, M. T. *Journal of Physical Chemistry* **1993**, *97*, 8182.

(92)   Wyttenbach, T.; vonHelden, G.; Batka, J. J.; Carlat, D.; Bowers, M. T. *Journal of the American Society for Mass Spectrometry* **1997**, *8*, 275.

(93)   Revercomb, H. E.; Mason, E. A. *Analytical Chemistry* **1975**, *47*, 970.

(94)   Mesleh, M. F.; Hunter, J. M.; Shvartsburg, A. A.; Schatz, G. C.; Jarrold, M. F. *Journal of Physical Chemistry* **1996**, *100*, 16082.

(95)   Floyd, G. R.; Prince, R. H.; Duley, W. W. *Journal of the Royal Astronomical Society of Canada* **1973**, *67*, 299.

(96)   Henning, T.; Salama, F. *Science* **1998**, *282*, 2204.

(97)   Lewis, J. S. *Physics and Chemistry of the Solar System*; Academic Press, New York, 1997.

(98)   O'D. Alexander, C. M.; Boss, A. P.; Carlson, R. W. *Science* **2001**, *293*, 64.

(99)   Fegley, B. *Space Science Reviews* **1999**, *90*, 239.

(100)   Niemann, H. B.; Atreya, S. K.; Bauer, S. J.; Carignan, G. R.; Demick, J. E.; Frost, R. L.; Gautier, D.; Haberman, J. A.; Harpold, D. N.; Hunten, D. M.; Israel, G.; Lunine, J. I.; Kasprzak, W. T.; Owen, T. C.; Paulkovich, M.; Raulin, F.; Raaen, E.; Way, S. H. *Nature* **2005**, *438*, 779.

(101)   Hansen, N.; Miller, J. A.; Kasper, T.; Kohse-Hoinghaus, K.; Westmoreland, P. R.; Wang, J.; Cool, T. A. *Proceedings of the Combustion Institute* **2009**, *32*, 623.

(102)   Ma, Y. P.; Xue, W.; Wang, Z. C.; Ge, M. F.; He, S. G. *Journal of Physical Chemistry A* **2008**, *112*, 3731.

(103)   Paul, M. W.; Karen, W. *The Astrophysical Journal Letters* **2007**, *655*, L49.

(104)   Wilson, E. H.; Atreya, S. K.; Coustenis, A. *Journal of Geophysical Research-Planets* **2003**, *108*.

(105)   D'Anna, A.; D'Alessio, A.; Kent, J. *Combustion Science and Technology* **2002**, *174*, 279.

(106)   Li, Y. Y.; Tian, Z. Y.; Zhang, L. D.; Yuan, T.; Zhang, K. W.; Yang, B.; Qi, F. *Proceedings of the Combustion Institute* **2009**, *32*, 647.

(107)   Lebonnois, S. *Planetary and Space Science* **2005**, *53*, 486.

(108)   Ausloos, P.; Lias, S. G.; Editors *NATO Advanced Science Institutes Series, Series C: Mathematical and Physical Sciences, Vol. 193: Structure/Reactivity and Thermochemistry of Ions*, 1987.

(109)   Cernicharo, J.; Heras, M.; Tielens, A. G. G. M.; Pardo, J. R.; Herpin, F.; Guelin, M.; Waters, L. B. F. M. *Astrophys. J.* **2001**, *546*, L123.

(110)   Murray, J. M.; et al. *The Astrophysical Journal* **1999**, *513*, 287.

(111)   Tielens, A. G. G. M., Hony, S., van Kerckhoven, C., & Peeters, E. *The Universe as Seen by ISO. Eds. P. Cox & M. F. Kessler. ESA-SP* **1999**, *427*.

(112)   Hudgins, D. M. *Polycyclic Aromatic Compounds* **2002**, *22*.

(113)   Kaneda, H.; et al. *The Astrophysical Journal Letters* **2005**, *632*, L83.

(114)   Lin, Y.; et al. *The Astrophysical Journal* **2005**, *628*, 604.

(115)   Ruiterkamp, R.; Peeters, Z.; Moore, M. H.; Hudson, R. L.; Ehrenfreund, P. *A&A* **2005**, *440*, 391.

(116)   Duley, W. W. *Faraday Discussions* **2006**, *133*, 415.

(117)   Jose, C.; et al. *The Astrophysical Journal Letters* **2001**, *546*, L123.

(118)   Sonnentrucker, P.; et al. *The Astrophysical Journal Letters* **2007**, *671*, L37.

(119)   Fuente, A.; et al. *The Astrophysical Journal Letters* **2005**, *619*, L155.

(120)   Lambert, D. L.; Sheffer, Y.; Federman, S. R. *Astrophysical Journal* **1995**, *438*, 740.

(121)   Feuchtgruber, H.; et al. *The Astrophysical Journal Letters* **2000**, *535*, L111.

(122)   Betz, A. L. *Astrophysical Journal* **1981**, *244*, L103.

(123)   Pithawalla, Y. M. S.; Mautner, M.; Gao, J. L.; El-Shall, M. S.; Baranov, V. I.; Bohme, D. K. *J. Phys. Chem. A* **2001**, *105*, 3908.

(124)   Saha, B.; Irle, S.; Morokuma, K. *Journal of Chemical Physics*, *132*.

(125)   Shukla, B.; Koshi, M. *Physical Chemistry Chemical Physics*, *12*, 2427.

(126)   Schmitt, R. J.; Ross, D. S.; Buttrill, S. E., Jr. *Journal of the American Chemical Society* **1981**, *103*, 5265.

(127)   Liu, S.; Jarrold, M. F.; Bowers, M. T. *Journal of Physical Chemistry* **1985**, *89*, 3127.

(128)   Holman, R. W., 1988.

(129)   Holman, R. W.; Warner, C. D.; Hayes, R. N.; Gross, M. L. *Journal of the American Chemical Society* **1990**, *112*, 3362.

(130)   Bauschlicher, C. W.; Langhoff, S. R. *Molecular Physics* **1999**, *96*, 471.

(131)   Herbst, E.; Le Page, V. *Astronomy and Astrophysics* **1999**, *344*, 310.

(132)   Bauschlicher Jr, C. W.; Ricca, A. *Chemical Physics Letters* **2000**, *326*, 283.

(133)   Kaiser, R. I.; Vereecken, L.; Peeters, J.; Bettinger, H. F.; Schleyer, P. V.; Schaefer, H. F. *Astronomy & Astrophysics* **2003**, *406*, 385.

(134)   Sorrilha, A.; Santos, L. S.; Gozzo, F. C.; Sparrapan, R.; Augusti, R.; Eberlin, M. N. *Journal of Physical Chemistry A* **2004**, *108*, 7009.

(135)   Bohm, H.; Jander, H. *Oxidation Communications* **2005**, *28*, 17.

(136)   Kubicki, J. D. *Environmental Science & Technology* **2006**, *40*, 2298.

(137)   Kunioshi, N.; Komori, S.; Fukutani, S. *Combustion and Flame* **2006**, *147*, 1.

(138)   Woon, D. E. *Chemical Physics* **2006**, *331*, 67.

(139)   Wang, H.; Frenklach, M. *The Journal of Physical Chemistry* **1994**, *98*, 11465.

(140)   Bittner, J. D.; Howard, J. B. *Symposium (International) on Combustion* **1981**, *18*, 1105.

(141)   Morrison, J. D.; Stanney, K.; Tedder, J. M. *J. Chem. Soc., Perkin Trans. 2* **1981**, 838.

(142)   Bohme, D. K.; Wlodek, S.; Zimmerman, J. A.; Eyler, J. R. *International Journal of Mass Spectrometry and Ion Processes* **1991**, *109*, 31.

(143)   Pithawalla, Y. B.; Meot-Ner, M.; Gao, J.; El Shall, M. S.; Baranov, V. I.; Bohme, D. K. *Journal of Physical Chemistry A* **2001**, *105*, 3908.

(144)   Mesleh, M. F.; Hunter, J. M.; Shvartsburg, A. A.; Schatz, G. C.; Jarrold, M. F. *The Journal of Physical Chemistry* **1996**, *100*, 16082.

(145)   Momoh, P. O.; Soliman, A.-R.; Meot-Ner, M.; Ricca, A.; El-Shall, M. S. *Journal of the American Chemical Society* **2008**, *130*, 12848.

(146)   McMahon, R. J.; McCarthy, M. C.; Gottlieb, C. A.; Dudek, J. B.; Stanton, J. F.; Thaddeus, P. *Astrophys. J.* **2003**, *590*, L61.

(147)   Duncan, F. J.; Trotman-Dickenson, A. F. *J. Chem. Soc.* **1962**, *null*, 4672.

(148)   Fahr, A.; Stein, S. E. *Symp. (Int.) Combust., [Proc.]* **1989**, *22n*, 1023.

(149)   Herzler, J.; Frank, P. *Berichte Der Bunsen-Gesellschaft-Physical Chemistry Chemical Physics* **1992**, *96*, 1333.

(150)   Wang, R.; Cadman, P. *Combust. Flame* **1998**, *112*, 359.

(151)   Yu, T.; Lin, M. C. *J. Phys. Chem.* **1995**, *99*, 8599.

(152)   Yu, T.; Lin, M. C. *Combust. Flame* **1995**, *100*, 169.

(153)   Richter, H.; Mazyar, O. A.; Sumathi, R.; Green, W. H.; Howard, J. B.; Bozzelli, J. W. *Journal of Physical Chemistry A* **2001**, *105*, 1561.

(154) Park, J.; Nam, G. J.; Tokmakov, I. V.; Lin, M. C. *J. Phys. Chem. A* **2006**, *110*, 8729.

(155) Tokmakov, I. V.; Park, J.; Lin, M. C. *ChemPhysChem* **2005**, *6*, 2075.

(156) Tokmakov, I. V.; Lin, M. C. *J. Phys. Chem. A* **2004**, *108*, 9697.

(157) Tokmakov, I. V.; Lin, M. C. *Journal of the American Chemical Society* **2003**, *125*, 11397.

(158) Anicich, V. G.; Huntress, W. T.; McEwan, M. J. *The Journal of Physical Chemistry* **1986**, *90*, 2446.

(159) Eyler, J. R.; Campana, J. E. *International Journal of Mass Spectrometry and Ion Processes* **1984**, *55*, 171.

(160) Tasaka, M.; Ogata, M.; Ichikawa, H. *Journal of the American Chemical Society* **1981**, *103*, 1885.

(161) Lifshitz, C.; Gibson, D.; Levsen, K. *International Journal of Mass Spectrometry and Ion Physics* **1980**, *35*, 365.

(162) Knight, J. A. *Radiation Research* **1976**, *65*, 423.

(163) Rylander, P. N.; Meyerson, S. *Journal of Chemical Physics* **1957**, *27*, 1116.

(164) Meyerson, S.; Rylander, P. N. *Journal of the American Chemical Society* **1957**, *79*, 1058.

(165) Mallard, W. G.; Fahr, A.; Stein, S. E. *Chem. Phys. Processes Combust.* **1984**, 92/1.

(166) Anicich, V. G.; Wilson, P.; McEwan, M. J. *Journal of the American Society for Mass Spectrometry* **2003**, *14*, 900.

(167)   Anicich, V. G.; Wilson, P. F.; McEwan, M. J. *Journal of the American Society for Mass Spectrometry* **2006**, *17*, 544.

(168)   Hassan, J.; Sevignon, M.; Gozzi, C.; Schulz, E.; Lemaire, M. *Chem. Rev.* **2002**, *102*, 1359.

(169)   Hseuh, H. H.; Hsu, M. Y.; Wu, T. L.; Liu, R. S. *Journal of Organic Chemistry* **2009**, *74*, 8448.

(170)   Harvey, R. G. *Current Organic Chemistry* **2004**, *8*, 303.

(171)   Hagen, S.; Hopf, H. *Carbon Rich Compounds I* **1998**, *196*, 45.

(172)   Ascenzi, D.; Cont, N.; Guella, G.; Franceschi, P.; Tosi, P. *Journal of Physical Chemistry A* **2007**, *111*, 12513.

(173)   LaVerne, J. A.; Araos, M. S. *J. Phys. Chem. A* **2002**, *106*, 11408.

(174)   Lifshitz, C.; Reuben, B. G. *Isr. J. Chem.* **1969**, *7*, 149.

(175)   Wexler, S.; Clow, R. P. *J. Am. Chem. Soc.* **1968**, *90*, 3940.

(176)   Park, J.; Burova, S.; Rodgers, A. S.; Lin, M. C. *J. Phys. Chem. A* **1999**, *103*, 9036.

(177)   Park, J.; Burova, S.; Rodgers, A. S.; Lin, M. C. *Chem. Phys. Processes Combust.* **1999**, 308.

(178)   Rusyniak, M. J.; Ibrahim, Y. M.; Wright, D. L.; Khanna, S. N.; El-Shall, M. S. *Journal of the American Chemical Society* **2003**, *125*, 12001.

(179)   Lifshitz, C.; Reuben, B. G. *The Journal of Chemical Physics* **1969**, *50*, 951.

(180)   Bennett, C. J.; Morales, S. B.; Le Picard, S. D.; Canosa, A.; Sims, I. R.; Shih, Y. H.; Chang, A. H. H.; Gu, X. B.; Zhang, F. T.; Kaiser, R. I. *Physical Chemistry Chemical Physics* **2010**, *12*, 8737.

(181)   ZÌŒabka, J.; PolaÌ sÌŒek, M.; Ascenzi, D.; Tosi, P.; RoithovaÌ , J.; SchroÌˆder, D. *The Journal of Physical Chemistry A* **2009**, *113*, 11153.

(182)   Wahlund, J. E.; Galand, M.; Müller-Wodarg, I.; Cui, J.; Yelle, R. V.; Crary, F. J.; Mandt, K.; Magee, B.; Waite Jr, J. H.; Young, D. T.; Coates, A. J.; Garnier, P.; Ågren, K.; André, M.; Eriksson, A. I.; Cravens, T. E.; Vuitton, V.; Gurnett, D. A.; Kurth, W. S. *Planetary and Space Science* **2009**, *57*, 1857.

(183)   Reddy, V. S.; Mahapatra, S. *Journal of Chemical Physics* **2009**, *130*.

(184)   Norinaga, K.; Deutschmann, O.; Saegusa, N.; Hayashi, J. *Journal of Analytical and Applied Pyrolysis* **2009**, *86*, 148.

(185)   Mebel, A. M.; Kislov, V. V.; Kaiser, R. I. *Journal of the American Chemical Society* **2008**, *130*, 13618.

(186)   Landera, A.; Mebel, A. M.; Kaiser, R. I. *Chemical Physics Letters* **2008**, *459*, 54.

(187)   Bohm, H.; Braun-Unkhoff, M. *Combustion and Flame* **2008**, *153*, 84.

(188)   Pino, T.; Douin, S.; Boudin, N.; Brechignac, P. *Journal of Physical Chemistry A* **2007**, *111*, 13358.

(189)   Nam, G.; Tokmakov, I. V.; Park, J.; Lin, M. C. *Proceedings of the Combustion Institute* **2007**, *31*, 249.

(190)   Kanuru, V. K.; Kyriakou, G.; Beaumont, S. K.; Papageorgiou, A. C.; Watson, D. J.; Lambert, R. M. *Journal of the American Chemical Society* **2010**, *132*, 8081.

(191)   Gil, W.; Lis, T.; Trzeciak, A. M.; Ziolkowski, J. J. *Inorganica Chimica Acta* **2006**, *359*, 2835.

(192)   Han, W. S.; Lee, S. W. *Organometallics* **2005**, *24*, 997.

(193)   Noyce, D. S.; Schiavel.Md *Journal of the American Chemical Society* **1968**, *90*, 1020.

(194)   Jiang, C. F.; Blacque, O.; Berke, H. *Organometallics*, *29*, 125.

(195)   McEnally, C. S.; Pfefferle, L. D. *Combustion Science and Technology* **1997**, *128*, 257.

(196)   Dyakov, Y. A.; Ni, C. K.; Lin, S. H.; Lee, Y. T.; Mebel, A. M. *Physical Chemistry Chemical Physics* **2006**, *8*, 1404.

(197)   Dyakov, Y. A.; Mebel, A. M.; Lin, S. H.; Lee, Y. T.; Ni, C. K. *Journal of the Chinese Chemical Society* **2006**, *53*, 161.

(198)   van der Hart, W. J. *International Journal of Mass Spectrometry* **2002**, *214*, 269.

(199)   Schroeter, K.; Schroder, D.; Schwarz, C. *Journal of Physical Chemistry A* **1999**, *103*, 4174.

(200)   Schroeter, K.; Schroder, D.; Schwarz, H. *The Journal of Physical Chemistry A* **1999**, *103*, 4174.

(201)   Friedrichs, G.; Goos, E.; Gripp, J.; Nicken, H.; Schonborn, J. B.; Vogel, H.; Temps, F. *Zeitschrift Fur Physikalische Chemie-International Journal of Research in Physical Chemistry & Chemical Physics* **2009**, *223*, 387.

(202)   Wu, C. H.; Singh, H. J.; Kern, R. D. *International Journal of Chemical Kinetics* **1987**, *19*, 975.

(203)   Fields, E. K.; Meyerson, S. *Tetrahedron Letters* **1967**, *8*, 571.

(204)   Mayo, F. R. *J. Am. Chem. Soc.* **1968**, *90*, 1289.

(205)   Chong, Y. K.; Rizzardo, E.; Solomon, D. H. *J. Am. Chem. Soc.* **1983**, *105*, 7761.

(206)   Kothe, T.; Fischer, H. *J. Polym. Sci., Part A* **2001**, *39*, 4009.

(207)   Alsharaeh, E. H.; Ibrahim, Y. M.; El-Shall, M. S. *Journal of the American Chemical Society* **2005**, *127*, 6164.

(208)   Zhang, F.; Gu, X.; Guo, Y.; Kaiser, R. I. *The Journal of Organic Chemistry* **2007**, *72*, 7597.

(209)   Wilkins, C. L.; Gross, M. L. *Journal of the American Chemical Society* **1971**, *93*, 895.

(210)   Rodgers, M. T.; Stanley, J. R.; Amunugama, R. *Journal of the American Chemical Society* **2000**, *122*, 10969.

(211)   Fondren, L. D.; McLain, J.; Jackson, D. M.; Adams, N. G.; Babcock, L. M. *International Journal of Mass Spectrometry* **2007**, *265*, 60.

(212)   Padoley, K. V.; Mudliar, S. N.; Pandey, R. A. *Bioresource Technology* **2008**, *99*, 4029.

(213)   Shengjun, Y.; Xiang, Z.; Lei, Z.; Cuihong, W.; Yinlong, G. *Rapid Communications in Mass Spectrometry* **2007**, *21*, 1739.

(214)   Jiao, C. Q.; Boatz, J. A.; DeJoseph Jr, C. A.; Garscadden, A. *International Journal of Mass Spectrometry* **2009**, *288*, 22.

(215)   Cairns, T. L.; Sauer, J. C.; Wilkinson, W. K. *Journal of the American Chemical Society* **1952**, *74*, 3989.

(216)   Dazinger, G.; Torres-Rodrigues, M.; Kirchner, K.; Calhorda, M. J.; Costa, P. J. *Journal of Organometallic Chemistry* **2006**, *691*, 4434.

(217)   Wakatsuki, Y.; Yamazaki, H. *Tetrahedron Letters* **1973**, *14*, 3383.

(218)   Mumma, M. J.; DiSanti, M. A.; Russo, N. D.; Fomenkova, M.; Magee-Sauer, K.; Kaminski, C. D.; Xie, D. X. *Science* **1996**, *272*, 1310.

(219)   Smyth, K. C.; Miller, J. H. *Science* **1987**, *236*, 1540.

(220)   Broadfoot, A. L.; Herbert, F.; Holberg, J. B.; Hunten, D. M.; Kumar, S.; Sandel, B. R.; Shemansky, D. E.; Smith, G. R.; Yelle, R. V.; Strobel, D. F.; Moos, H. W.; Donahue, T. M.; Atreya, S. K.; Bertaux, J. L.; Blamont, J. E.; McConnell, J. C.; Dessler, A. J.; Linick, S.; Springer, R. *Science* **1986**, *233*, 74.

(221)   Comita, P. B.; Brauman, J. I. *Science* **1985**, *227*, 863.

(222)   Hayatsu, R.; Scott, R. G.; Studier, M. H.; Lewis, R. S.; Anders, E. *Science* **1980**, *209*, 1515.

(223)   David, E. W.; Jin-Young, P. *The Astrophysical Journal* **2004**, *607*, 342.

(224)   Bernstein, M. P.; Mattioda, A. L.; Sandford, S. A.; Hudgins, D. M. *Astrophysical Journal* **2005**, *626*, 909.

(225) Bohme, D. K. *Chem. Rev.* **1992**, *92*, 1487.

(226) Arakawa, R.; Yoshikawa, Y. *Bulletin of the Chemical Society of Japan* **1987**, *60*, 49.

(227) Lifshitz, C.; Gibson, D.; Levsen, K.; Dotan, I. *International Journal of Mass Spectrometry and Ion Physics* **1981**, *40*, 157.

(228) Dickinson, R. J.; Williams, D. H. *Journal of the Chemical Society, Perkin Transactions 2* **1972**, 1363.

(229) Jiao, C. Q.; DeJoseph, J. C. A.; Lee, R.; Garscadden, A. *International Journal of Mass Spectrometry* **2006**, *257*, 34.

(230) Kim, J. K.; Anicich, V. G.; Huntress, W. T. *Journal of Physical Chemistry* **1977**, *81*, 1798.

(231) Mason, E. A.; McDaniel, E. W. **1988**.

(232) Becker, C.; Fernandez-Lima, F. A.; Russell, D. H. *Spectroscopy* **2009**, *24*, 38.

(233) Pullman, A.; Berthier, G.; Savinelli, R. *Journal of Computational Chemistry* **1997**, *18*, 2012.

(234) Wang, F.; Ma, S.; Wong, P.; Cooks, R. G.; Gozzo, F. C.; Eberlin, M. N. *International Journal of Mass Spectrometry* **1998**, *179-180*, 195.

(235) Sparrapan, R.; Mendes, M. A.; Eberlin, M. N. *International Journal of Mass Spectrometry* **1999**, *182-183*, 369.

(236) Ricca, A.; Bauschlicher, C. W.; Bakes, E. L. O. *Icarus* **2001**, *154*, 516.

(237) Yang, Y.-S.; Hsu, W.-Y.; Lee, H.-F.; Huang, Y.-C.; Yeh, C.-S.; Hu, C.-H. *The Journal of Physical Chemistry A* **1999**, *103*, 11287.

(238) Gaussian 03, R. D.; M. J. Frisch, G. W. T., H. B. Schlegel, G. E. Scuseria, ; M. A. Robb, J. R. C., J. A. Montgomery, Jr., T. Vreven, ; K. N. Kudin, J. C. B., J. M. Millam, S. S. Iyengar, J. Tomasi, ; V. Barone, B. M., M. Cossi, G. Scalmani, N. Rega, ; G. A. Petersson, H. N., M. Hada, M. Ehara, K. Toyota, ; R. Fukuda, J. H., M. Ishida, T. Nakajima, Y. Honda, O. Kitao, ; H. Nakai, M. K., X. Li, J. E. Knox, H. P. Hratchian, J. B. Cross, ; V. Bakken, C. A., J. Jaramillo, R. Gomperts, R. E. Stratmann, ; O. Yazyev, A. J. A., R. Cammi, C. Pomelli, J. W. Ochterski, ; P. Y. Ayala, K. M., G. A. Voth, P. Salvador, J. J. Dannenberg, ; V. G. Zakrzewski, S. D., A. D. Daniels, M. C. Strain, ; O. Farkas, D. K. M., A. D. Rabuck, K. Raghavachari, ; J. B. Foresman, J. V. O., Q. Cui, A. G. Baboul, S. Clifford, ; J. Cioslowski, B. B. S., G. Liu, A. Liashenko, P. Piskorz, ; I. Komaromi, R. L. M., D. J. Fox, T. Keith, M. A. Al-Laham, ; C. Y. Peng, A. N., M. Challacombe, P. M. W. Gill, ; B. Johnson, W. C., M. W. Wong, C. Gonzalez, and J. A. Pople, ; Gaussian, I., Wallingford CT, 2004. **2003**.

(239) Indarto, A. *Environmental Engineering Science* **2009**, *26*, 1685.

(240) Kamphus, M.; Braun-Unkhoff, M.; Kohse-Hoinghaus, K. *Combustion and Flame* **2008**, *152*, 28.

(241) Calcote, H. F.; Olson, D. B.; Keil, D. G. *Energy & Fuels* **1988**, *2*, 494.

(242) Keil, H. F. C. a. D. G. *Pure and Applied Chemistry* **1990**, *62*, 815.

(243) Haynes, B. S.; Wagner, H. G. *Progress in Energy and Combustion Science* **1981**, *7*, 229.

(244)   Frenklach, M. *Physical Chemistry Chemical Physics* **2002**, *4*, 2028.

(245)   Mendiara, T.; Domene, M. P.; Millera, A.; Bilbao, R.; Alzueta, M. U. *Journal of Analytical and Applied Pyrolysis* **2005**, *74*, 486.

(246)   Dimitrijevic, S. T.; Paterson, S.; Pacey, P. D. *Journal of Analytical and Applied Pyrolysis* **2000**, *53*, 107.

(247)   Kiefer, J. H.; Von Drasek, W. A. *International Journal of Chemical Kinetics* **1990**, *22*, 747.

(248)   Colket Iii, M. B.; Seery, D. J.; Palmer, H. B. *Combustion and Flame* **1989**, *75*, 343.

(249)   Chanmugathas, C.; Heicklen, J. *International Journal of Chemical Kinetics* **1987**, *19*, 659.

(250)   Frenklach, M.; Taki, S.; Durgaprasad, M. B.; Matula, R. A. *Combustion and Flame* **1983**, *54*, 81.

(251)   Ogura, H. *Bulletin of the Chemical Society of Japan* **1977**, *50*, 1044.

(252)   Back, M. H. *Can. J. Chem.* **1971**, *49*, 2199.

(253)   Cullis, C. F.; Franklin, N. H. *Proceedings of the Royal Society of London. Series A. Mathematical and Physical Sciences* **1964**, *280*, 139.

(254)   Hou, K. C.; Anderson, R. C. *The Journal of Physical Chemistry* **1963**, *67*, 1579.

(255)   Cullis, C. F.; Nettleton, M. A. *Transactions of the Faraday Society* **1963**, *59*, 361.

(256)   Cullis, C. F.; Minkoff, G. J.; Nettleton, M. A. *Transactions of the Faraday Society* **1962**, *58*, 1117.

(257)   Minkoff, G. J. *Can. J. Chem.* **1958**, *36*, 131.

(258)   Ma, Y.-P.; Xue, W.; Wang, Z.-C.; Ge, M.-F.; He, S.-G. *The Journal of Physical Chemistry A* **2008**, *112*, 3731.

(259)   Alivisatos, A. P. *The Journal of Physical Chemistry* **1996**, *100*, 13226.

(260)   Siamaki, A. R.; Khder, A. E. R. S.; Abdelsayed, V.; El-Shall, M. S.; Gupton, B. F. *Journal of Catalysis* **2011**, *279*, 1.

(261)   Mei, D. H.; Neurock, M.; Smith, C. M. *Journal of Catalysis* **2009**, *268*, 181.

(262)   Jiang, L. C.; Gu, H. Z.; Xu, X. Z.; Yan, X. H. *Journal of Molecular Catalysis a-Chemical* **2009**, *310*, 144.

(263)   Demel, J.; Cejka, J.; Stepnicka, P. *Chemicke Listy* **2009**, *103*, 145.

(264)   Glaspell, G.; Hassan, H. M. A.; Elzatahry, A.; Abdalsayed, V.; El-Shall, M. S. *Topics in Catalysis* **2008**, *47*, 22.

(265)   Yoshimura, Y.; Toba, M.; Matsui, T.; Harada, M.; Ichihashi, Y.; Bando, K. K.; Yasuda, H.; Ishihara, H.; Morita, Y.; Kameoka, T. *Applied Catalysis a-General* **2007**, *322*, 152.

(266)   Batchu, V. R.; Barange, D. K.; Kumar, D.; Sreekanth, B. R.; Vyas, K.; Reddy, E. A.; Pal, M. *Chemical Communications* **2007**, 1966.

(267)   Ahn, I. Y.; Lee, J. H.; Kum, S. S.; Moon, S. H. *Catalysis Today* **2007**, *123*, 151.

(268) Stacchiola, D.; Calaza, F.; Zheng, T.; Tysoe, W. I. *Journal of Molecular Catalysis a-Chemical* **2005**, *228*, 35.

(269) Mittendorfer, F.; Thomazeau, C.; Raybaud, P.; Toulhoat, H. *Journal of Physical Chemistry B* **2003**, *107*, 12287.

(270) Barnes, R.; Abdelrehim, I. M.; Madey, T. E. *Topics in Catalysis* **2001**, *14*, 53.

(271) Tang, C. M.; Zeng, Y.; Yang, X. G.; Lei, Y. C.; Wang, G. Y. *Journal of Molecular Catalysis a-Chemical* **2009**, *314*, 15.

(272) Sawoo, S.; Srimani, D.; Dutta, P.; Lahiri, R.; Sarkar, A. *Tetrahedron* **2009**, *65*, 4367.

(273) Binder, A.; Seipenbusch, M.; Muhler, M.; Kasper, G. *Journal of Catalysis* **2009**, *268*, 150.

(274) Semagina, N.; Renken, A.; Kiwi-Minsker, L. *Journal of Physical Chemistry C* **2007**, *111*, 13933.

(275) Ruta, M.; Semagina, N.; Kiwi-Minsker, L. *The Journal of Physical Chemistry C* **2008**, *112*, 13635.

(276) Stacchiola, D.; Molero, H.; Tysoe, W. T. *Catalysis Today* **2001**, *65*, 3.

(277) Gath, K. K.; Kumar, D.; Yi, C. W.; Chen, M. S.; Goodman, D. W. *Abstracts of Papers of the American Chemical Society* **2007**, *234*, 333.

(278) Chiang, H. L.; Ho, Y. S.; Lin, K. H.; Leu, C. H. *Journal of Alloys and Compounds* **2007**, *434*, 846.

(279)   Uemura, T.; Kitaura, R.; Ohta, Y.; Nagaoka, M.; Kitagawa, S. *Angewandte Chemie* **2006**, *118*, 4218.

(280)   Xu, X.; Pacey, P. D. *Physical Chemistry Chemical Physics* **2005**, *7*, 326.

(281)   Martinez, M.; Michelin, M. D.; Rivalta, I.; Russo, N.; Sicilia, E. *Inorganic Chemistry* **2005**, *44*, 9807.

(282)   Judai, K.; Abbet, S.; Wörz, A. S.; Ferrari, A. M.; Giordano, L.; Pacchioni, G.; Heiz, U. *Journal of Molecular Catalysis A: Chemical* **2003**, *199*, 103.

(283)   Jungwirthova, I.; Kesmodel, L. L. *Journal of Physical Chemistry B* **2001**, *105*, 674.

(284)   Abdelsayed, V.; Glaspell, G.; Nguyen, M.; Howe, J. M.; El-Shall, M. S. *Faraday Discussions* **2008**

 138, 163.

(285)   Abdelsayed, V.; Saoud, K. M.; El-Shall, M. S. *Journal of Nanoparticle Research* **2006**, *8*, 519.

(286)   Abdelsayed, V.; El-Shall, M. S.; Seto, T. *Journal of Nanoparticle Research* **2006**, *8*, 361.

(287)   El-Shall, M. S.; Abdelsayed, V.; Pithawalla, Y. B.; Alsharaeh, E.; Deevi, S. C. *The Journal of Physical Chemistry B* **2003**, *107*, 2882.

(288)   Pithawalla, Y. B.; Deevi, S. C.; El-Shall, M. S. *Materials Science and Engineering a-Structural Materials Properties Microstructure and Processing* **2002**, *329*, 92.

(289)   Pithawalla, Y. B.; El-Shall, M. S.; Deevi, S. C.; Strom, V.; Rao, K. V. *The Journal of Physical Chemistry B* **2001**, *105*, 2085.

(290)   Li, S. T.; El-Shall, M. S. *Applied Surface Science* **1998**, *127*, 330.

(291)   Haglund, J.; Fernandez-Guillermet, F.; Grimvll, G.; Korling, M. *Phys. Rev. B: Condens. Matter.* **1993**, *48*, 11685.

(292)   Rucker, T. G.; Logan, M. A.; Gentle, T. M.; Muetterties, E. L.; Somorjai, G. A. *The Journal of Physical Chemistry* **1986**, *90*, 2703.

(293)   Beck, W. H.; Mackie, J. C. *Journal of the Chemical Society, Faraday Transactions 1: Physical Chemistry in Condensed Phases* **1975**, *71*, 1363.

(294)   Tanzawa, T.; Gardiner, W. C. *The Journal of Physical Chemistry* **1980**, *84*, 236.

(295)   Duran, R. P.; Amorebieta, V. T.; Colussi, A. J. *Journal of the American Chemical Society* **1987**, *109*, 3154.

(296)   Kiefer, J. H.; Mitchell, K. I. *Energy & Fuels* **1988**, *2*, 458.

(297)   Durán, R. P.; Amorebieta, V. T.; Colussi, A. J. *International Journal of Chemical Kinetics* **1989**, *21*, 947.

(298)   Schlund, R.; Schrock, R. R.; Crowe, W. E. *Journal of the American Chemical Society* **1989**, *111*, 8004.

(299)   Hidaka, Y.; Hattori, K.; Okuno, T.; Inami, K.; Abe, T.; Koike, T. *Combustion and Flame* **1996**, *107*, 401.

(300)   Xu, X.; Pacey, P. D. *Physical Chemistry Chemical Physics* **2001**, *3*, 2836.

(301)   Unterreiner, B. V.; Sierka, M.; Ahlrichs, R. *Physical Chemistry Chemical Physics* **2004**, *6*, 4377.

(302)   Alter, W.; Borgmann, D.; Stadelmann, M.; Worn, M.; Wedler, G. *Journal of the American Chemical Society* **1994**, *116*, 10041.

VITA

Abdel Rhaman Ibrahim Mohamed Soliman was born on April, 24th, 1975, in Giza governorate, Egypt. He earned his Bachelor degree in Chemistry from Cairo University in Egypt on 1997 with honor grade.

Abdel Rahman then joined the national research center in Cairo, Egypt, where he joined the physical chemistry department and gained his master degree on 2005. He joined El-Shall's research group on August 2006 to pursue his PhD in physical chemistry.

Education:

Virginia Commonwealth University, Department of Chemistry, College of Humanities and Sciences, Richmond, VA. USA, *Ph.D.* Thesis Title:"*Growth Mechanisms of Complex Organics in the Gas Phase and on Metal Nanoparticles Generated by A Laser Vaporization Process"* **May, 2011**. **Advisor: Prof. Dr. M. Samy El-Shall.**

Cairo University, Faculty of Science, Department of Chemistry, Egypt. **M.Sc. in Physical Chemistry. Awarded on October 2005,** M.Sc. Thesis entitled *"Microbial Corrosion Control in Injection water in Petroleum Production"*. Advisor: **Prof. Dr. M. Saber Al-Basiouny, Prof. Dr. Abdel Ghany A. El-Hosary.**

Cairo University, Faculty of Science, Department of Chemistry, Egypt. B. Sc. in Chemistry, May 1997. General Estimation of "Very good with Honor" GPA: 3.4/4.

Research Interests:

- Gas phase ion-molecule reactions.

- Poly aromatic hydrocarbons (PAHs) and Poly aromatic nitrogen-containing hydrocarbons (PANHs) formation mechanisms in the gas phase, utilizing the Mass Selected-Ion Mobility Spectrometry-Mass Spectrometry (MS-IMS-MS).

- Electrospary Ionization-Ion Mobility Spectrometry-Quadruple Mass Spectrometer (ESI-IMS-QMS) development. Design, Instrumentation and applications of new mass spectrometry technique.

- Metal-Ion Clusters formation and detection using Reflectron-Time of Flight mass spectrometer (R-TOF-MS).

- Formation of PAHs and PANHs via polymerization of small hydrocarbons over metal and metal supported nanocatalysts. New techniques in catalysis.

EXPERIENCE:

➢ August 2010-present, Graduate Research Assistant, Altria Fellow, Chemistry Department, College of Humanities and Sciences, Virginia Commonwealth University. Richmond, VA.

➢ May 2010-Angust 2010: Graduate Research Assistant, Chemistry Department, College of Humanities and Sciences, Virginia Commonwealth University. Richmond, VA.

➢ Jan. 2010-May 2010: Graduate Teaching Assistant, Chemistry Department, College of Humanities and Sciences, Virginia Commonwealth University. Richmond, VA. Courses: *CHEZ 101*

➢ May 2008-December 2009: Graduate Research Assistant, Altria Fellow, Chemistry Department, College of Humanities and Sciences, Virginia Commonwealth University. Richmond, VA.

➢ August 2006-May 2008: Graduate Teaching Assistant, Chemistry Department, College of Humanities and Sciences, Virginia Commonwealth University. Richmond, VA. Courses: *CHEM 100, CHEM 101, CHEM 102, CHEZ 101*

➢ November 2005-August 2006: Graduate Research Assistant, Electrochemistry and Corrosion Lab, Physical Chemistry Department, National Research Centre, Cairo, Egypt.

➢ August 2000-November 2005: Graduate Assistant Researcher, Electrochemistry and Corrosion Lab, Physical Chemistry Department, National Research Centre, Cairo, Egypt.

➢ February 1999-August 2000: Quality Control Chemist, Gas lab, Ras Shukir dist. Red Sea, Egypt. Gulf of Suez Petroleum Co (GUPCO).

➢ April 1998-February 1999: Graduate Assistant Researcher, Phytochemistry lab, Organic Chemistry Department, National Research Centre, Cairo, Egypt.

Honors:
- ✓ Altria (Philip Morris) Scholarship, Chemistry Dept., Virginia Commonwealth University, August, 2010-May, 2011

- ✓ Altria (Philip Morris) Scholarship, Chemistry Dept., Virginia Commonwealth University August-December 2009.

- ✓ Distinguished Scholar, Cairo University, Department of Chemistry, EGYPT, (1993--1997).

- ✓ The Egyptian Academy of Science Scholarship May, 1998-August, 1999.

Affiliations:
- o American Chemical Society.

- o Egyptian Corrosion Society.

Publications:

Momoh, O. Paul; Soliman, Abdel-Rahman; Meot-Ner, Michael; Ricca, Alessandra; El-Shall, M. Samy *Formation of Complex Organics From Acetylene Catalyzed by ionized Benzene*. *J. Am. Chem. Soc.* **2008**, *130*, 12848.

Soliman, Abdel-Rahman; Hamid, Ahmed; Momoh, Paul; El-Shall, M. Samy. *New pathways for the formation of complex organics by gas phase and intracluster ion-molecule reactions.* 238th ACS National Meeting, Washington, DC, United States, August 16-20, 2009.

Hamid, Ahmed; Soliman, Abdel-Rahman; El-Shall, M. Samy. *Gas phase hydration of organic ions: Phenylium and benzonitrile cations.* 238th ACS National Meeting, Washington, DC, United States, August 16-20, 2009.

Soliman, Abdel-Rahman; El-Shall, M. Samy. *Gas phase sequential reactions of pyridine and pyrimidine radical cations with acetylene: Evidence for nitrogen-containing*

covalent cyclic adducts. 240th ACS National Meeting & Exposition August 22-26, 2010,

Boston, Massachusetts